PRICES SUBJECT TO CHANGE

FINAL REPORT

SPACEBORNE SYNTHETIC APERTURE RADAR

PILOT STUDY

APRIL 11, 1974

CONTRACT NO. NAS 5-21951

PRESENTED TO:

NATIONAL AERONAUTICS AND SPACE ADMINISTRATION

GODDARD SPACE FLIGHT CENTER

GREENBELT, MARYLAND

BY:

WESTINGHOUSE ELECTRIC CORPORATION

SYSTEMS DEVELOPMENT DIVISION

BALTIMORE, MARYLAND

FINAL REPORT

SPACEBORNE SYNTHETIC APERTURE RADAR

PILOT STUDY

APRIL 11, 1974

CONTRACT NO. NAS 5-21951

PRESENTED TO:

NATIONAL AERONAUTICS AND SPACE ADMINISTRATION

GODDARD SPACE FLIGHT CENTER

GREENBELT, MARYLAND

BY:

WESTINGHOUSE ELECTRIC CORPORATION

SYSTEMS DEVELOPMENT DIVISION

BALTIMORE, MARYLAND

ERRATA SHEET

FOR

FINAL REPORT

SPACEBORNE SYNTHETIC APERTURE RADAR

PILOT STUDY

1. Page 3-16, line 24: Change the word "varified" to "verified".

2. Page 3-17, line 5: Change "X-band" to "K-band".

3. Page 3-39, Figure 3.2.3.3-7: Change "V = 7.6 itm/sec." to "V = 7.6 Km/sec."

4. Page 3-43, after line 9, before the equation, insert the following paragraph:

$$T = \frac{150W}{4\ kW \cdot 3.7\ KHz}$$

$$= 10.1\ us$$

"The PRF varies somewhat with depression angle in this configuration. Maximum transmitter efficiency occurs when the tube is always operated at peak power; if the pulsewidth is held constant to simplify transmitter/stalo design, average power will then vary a slight amount as a function of depression angle.

If the antenna azimuth aperture is 27 ft., the PRF must become 3.0 KHz at steep depression angles and 2.0 KHz at shallower depression angles. For a 4.5 kW peak power tube,".

5. Page 3-50, Table 3.2.3.4-2: Below the words "Total RF" the words "Spectral Amplitude Weighting" should appear.

6. Page 3-53, line 12: Change "Appendix B" to "Appendix D".

7. Page 3-55, Figure 3.2.3.4-5: The Y-axis ordinate should read "Final S/N (dB)" instead of "Final Sin (dB)".

8. Page 3-74: Replace Figure 3.2.3.6-3 with the following figure.

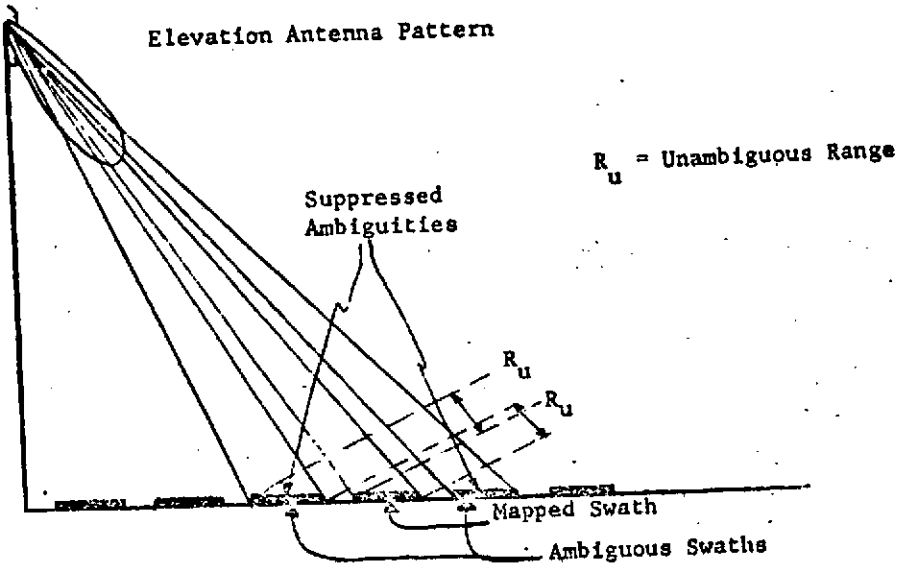

9. Page 3-85, line 10: Change the word "back" to "both".

10. Insert Figure 3.2.3.6-10 (Illustrated on the third errata sheet) after page 3-86.

11. Page 3-96, line 11: Immediately before the word "may", insert the words "the received swath".

12. Page 3-105, change the third equation from "cos θ_n m/sec" to "cos θ_n Km/sec".

13. Page 3-128, line 11: Change "62.4 megabits/sec." to "78 megabits/sec."

14. Page 3-132, line 7: Change "= (40 km)" to " = (40 km)[1]" and add the following footnote at the bottom of the page: "System design is for 50 not 40 km."

15. Page 3-134, change the third equation from "1.25 $\frac{4000m}{30m}$ " to "1.25 = $\frac{4000m}{30m}$".

16. Page 3-149, line 13: Change the words "on top of" to "around".

17. Page 3-181, delete line 18.

18. Page 3-193, in Table 3.3.5-6, change "44.5 dBi" to "44.5 dBi[1]" and add the following footnote at the bottom of the page: "[1]Includes losses such as spillover and feedline."

19. Page 3-194, in Table 3.3.5-7 change "Gain (one way)" to "Gain (one way)[1]" and add the following footnote at the bottom of the page: "[1]Includes losses such as spillover and feedline."

v-b

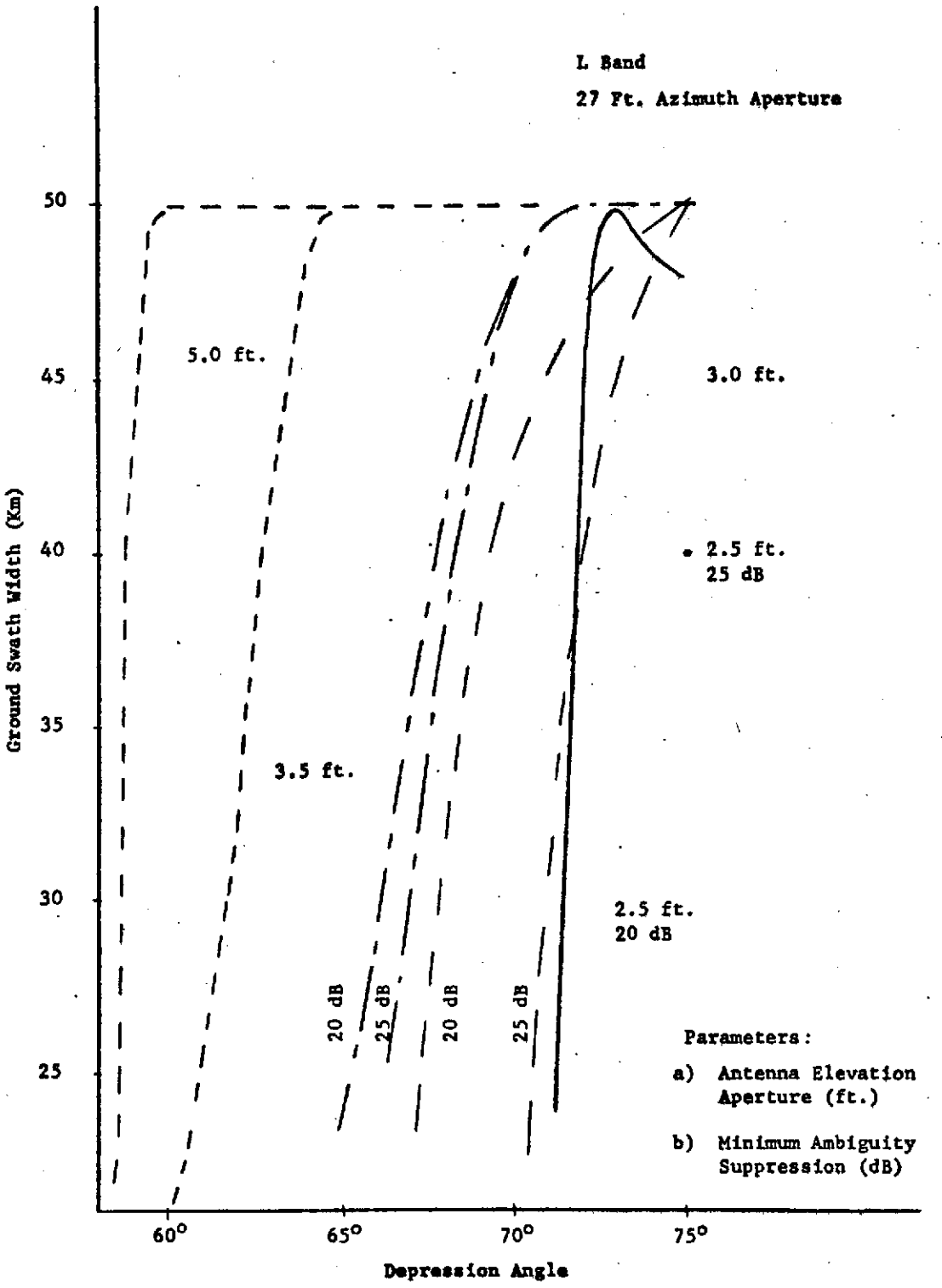

Figure 3.2.3.6-10. Ground Swath Width vs. Depression Angle

w-c

20. Page 3-202, Table 3.3.5-9: Change the rate from "~13 MHz" to "~25 MHz" for Configuration #1 and change "27 MHz" to "25 MHz" for Configuration #2.

21. Page 5-7, line 1: change the words "25% over-sample:" to "25% over-sample:[1]" and add the following footnote at the bottom of the page: "[1]The slowdown factors, A/D ratios used in this section are nominal values, and while not exactly the same as the values in the previous section, are adequate for preliminary design purposes."

22. On page C-2, change equation [4] from "$r_a \frac{r_{rs}}{\sin \phi_i}$" to "$r_a \frac{v_{rs}}{\sin \phi_i}$".

w.d

TABLE OF CONTENTS

		Page
1.0	INTRODUCTION	1-1
2.0	PROGRAM SUMMARY	1-1
3.0	SYSTEMS ANALYSES	3-1
3.1	Radar Rationale and Design Summary	3-1
3.1.1	Radar Rationale	3-2
3.1.2	Design Summary	3-6
3.2	Systems Requirements	3-10
3.2.1	System Guidelines	3-10
3.2.2	Radar As An Earth Resource Sensor	3-13
3.2.3	Development of Radar Parameters	3-26
3.3	Proposed Configurations	3-112
3.3.1	Configuration Summary	3-112
3.3.2	Radar Parameters	3-114
3.3.3	Functional Block Diagrams	3-122
3.3.4	Parametric Verification	3-128
3.3.5	Subsystem Specifications	3-144
4.0	MECHANICAL DESIGN	4-1
4.1	Requirements	4-1
4.2	Summary of System Mechanical/Thermal Characteristics	4-1
4.3	Electronic Packaging	4-2
4.3.1	Radar Electronics	4-2
4.4	Thermal Analysis	4-12
4.4.1	Radar Electronics	4-12
4.5	Antenna	4-22
4.5.1	General Description	4-22
4.5.2	Spacecraft Connections	4-35
4.6	Potential Mechanical Problem Areas	4-38

TABLE OF CONTENTS (Cont'd)

		Page
5.0	GROUND SUPPORT EQUIPMENT RADAR CALIBRATION	5-1
5.1	Ground Support Equipment	5-1
5.1.1	Introduction	5-1
5.1.2	Overall System Description	5-1
5.1.3	Data Management	5-14
5.2	Ground Data Reduction	5-32
5.2.1	Introduction	5-32
5.2.2	Processor Requirements	5-33
5.2.3	Basic SAR Principles	5-34
5.2.4	Processor Configuration	5-44
5.2.5	Detailed Processor Design	5-54
5.3	Radar Calibration	5-75
5.3.1	Reflectivity Determination	5-75
5.3.2	Calibration Technique	5-79

APPENDICES

Appendix A	Derivation of Backscatter Equation	A-1
Appendix B	Calculation of Signal and Noise Levels in Radars Using Pulse Compression and Synthetic Aperture	B-1
Appendix C	Derivation of Backscatter Equation	C-1
Appendix D	Signal/Noise and Depression Angle Relationships	D-1
Appendix E	Gain Variation Over Sloped Earth	E-1
Appendix F	Azimuth Ambiguity Calculation	F-1
Appendix G	Antenna Switching	G-1
Appendix H	Locking Device Weight	H-1
Appendix J	Hinge Stress Calculations	J-1

TABLE OF CONTENTS (Cont'd)

		Page
ppendix K	Hinge Post Stress Calculations	K-1
ppendix L	Weight Calculations for Hinge	L-1
ppendix M	Weight Calculations for Hinge Posts	M-1
ppendix N	Honeycomb Structure Stress Calculations	N-1

LIST OF TABLES

Table No.		Page
3.1.1-1	Desired Radar Capability	3-5
3.1.2-1	Spaceborne Synthetic Aperture Radar	3-7
3.1.2-2	Processing Flexibility	3-8
3.2.1-1	System Guidelines	3-11
3.2.2-1	Applications of Remote Sensing Radar	3-21
3.2.3.4-1	Configuration Parameters	3-41
3.2.3.4-2	System Losses	3-50
3.2.3.5-1	System Multilook Capability	3-68
3.2.3.6-1	Swath Width Parameters	3-84
3.2.3.7-1	Antenna Pointing and Stability Requirements	3-95
3.2.3.7-2	System Performance vs. Orbit Parameters	3-100
3.2.3.7-3	Ground Range Offset of Near Swath Edge	3-101
3.3.2-1	Preliminary Radar Parameters - Configuration #1	3-116
3.3.2-2	Preliminary Radar Parameters - Configuration #2	3-119
3.3.5-1	Transmitter Requirements	3-146
3.3.5-2	Transmitter Fidelity Specifications	3-147
3.3.5-3	TWT Characteristics	3-158
3.3.5-4	Antenna Specifications - Configuration #1	3-186
3.3.5-5	Antenna Specifications - Configuration #2	3-190
3.3.5-6	Configuration #1 - Antenna Characteristics	3-193
3.3.5-7	Configuration #2 - Antenna Characteristics	3-194
3.3.5-8	Preliminary STALO/Synchronizer/System Controller Specification	3-196
3.3.5-9	Receiver Specifications	3-202
4.3.1-1	Physical Properties Summary	4-3
4.3.2-1	Configuration #1 Structure Summary	4-10
4.3.2-2	Configuration #2 Structure Summary	4-11
4.4.1-1	SSAR Power Dissipation	4-16
4.4.1-2	SSAR Base Plate Temperatures	4-20
5.1.2-1	Baseline Design Parameters	5-6
5.1.2-2	Processing - Output Parameters	5-11
5.1.3.5-1	SSAR Input Data Tape Recorder Specifications	5-22
5.1.3.5-2	SSAR Input Data Tape Recorder Proposed Design	5-26
5.1.3.6-1	Recorder Specifications	5-31
5.2.2-1	Baseline System Requirements	5-33
5.2.2-2	Baseline Processor Parameters	5-34
5.2.3-1	Basic SAR Equations for Sidelooking Radar	5-36
5.2.5-1	Comparison of X-Band Options for Memory Requirements	5-71
5.2.5-2	PDSP Utilization	5-73

LIST OF ILLUSTRATIONS

Figure No.		Page
3.2.3.3-1	Resolution Definition	3-29
3.2.3.3-2	Pulse Weighting	3-31
3.2.3.3-3	Slant and Ground Range Resolution	3-32
3.2.3.3-4	Bandwidth vs. Depression Angle	3-34
3.2.3.3-5	Ground Range Resolution vs. Depression Angle	3-34
3.2.3.3-6	Doppler Bandwidths	3-37
3.2.3.3-7	Azimuth Integration Time vs. Depression Angle	3-39
3.2.3.3-8	Synthetic Aperture Length vs. Depression Angle	3-39
3.2.3.4-1	Spherical Earth Geometry	3-51
3.2.3.4-2	Slant Range to Earth vs. Depression Angle	3-52
3.2.3.4-3	Correlator Bandwidth vs. Depression Angle	3-52
3.2.3.4-4	Single Look S/N vs. Depression Angle	3-54
3.2.3.4-5	S/N vs. Depression Angle	3-55
3.2.3.4-6	S/N vs. Backscatter Coefficient σ_o	3-57
3.2.3.5-1	Azimuth Multilook	3-60
3.2.3.5-2	Overlapping Multilook	3-61
3.2.3.5-3	Range Multilook	3-62
3.2.3.5-4	Contract Accuracy Improvement with Multilook	3-63
3.2.3.5-5a	Map Film Density with No Multilook	3-64
3.2.3.5-5b	Map Film Density with Multilook	3-64
3.2.3.5-6	Doppler Spectra	3-66
3.2.3.6-1	Two-Way Antenna Elevation Patterns	3-70
3.2.3.6-2	Swath Width Calculation	3-71
3.2.3.6-3	Location of Range Ambiguities	3-74
3.2.3.6-4	Range Ambiguity Suppression vs. Depression Angle	3-76
3.2.3.6-5	Azimuth Ambiguities	3-77
3.2.3.6-6	Doppler Spectra	3-78
3.2.3.6-7	Azimuth Ambiguity Suppression vs. PRF	3-79
3.2.3.6-8	Swath Width vs. Depression Angle	3-82
3.2.3.6-9	Swath Width vs. Depression Angle	3-83
3.2.3.7-1	Deterministic Antenna Motion Requirement	3-89
3.2.3.7-2	Non-Deterministic Antenna Motion Requirement	3-91
3.2.3.7-3	Angle Modulation Spectra	3-92
3.2.3.7-4	Received Swath Illumination	3-96
3.2.3.7-5	Range Gate Drift	3-97
3.2.3.8-1	Earth Rotation Effect	3-103
3.2.3.8-2	Vector Velocities	3-103
3.2.3.8-3	Range Drift	
3.2.3.9-1	Orbit Geometry	3-108
3.2.3.9-2	Path Increment vs. Orbit Altitude	3-110
3.2.3.9-3	Period and Inclination vs. Altitude	3-111
3.3.3-1	Spaceborne Synthetic Aperture Radar (SSAR) - Configuration #1	3-123

LIST OF ILLUSTRATIONS

Figure No.		Page
3.3.3-2	Spaceborne Synthetic Aperture Radar (SSAR) Configuration #2	3-124
3.3.4-1	Pre-A/D Ground Range Resolution	3-129
3.3.4-2	Ground Range Resolution	3-130
3.3.4-3	Slant Range/Ground Range	3-131
3.3.4-4	Target Separation	3-132
3.3.4-5	Number of Cells and Data Bits for Real Time Readout	3-134
3.3.4-6	SSAR Reliability Block Diagram	3-137
3.3.5-1	Transmitter Leakage or "OFF" Noise	3-148
3.3.5-2	Matched Filter Discrete Target Response	3-150
3.3.5-3	SSAR STALO/Transmitter Noise Specification	3-152
3.3.5-4	Block Diagram - TWT Electronics	3-162
3.3.5-5	Amplifier Chain - Module	3-166
3.3.5-6	Paschen's Curve	3-171
3.3.5-7	Transmitter Weight Power Trade-Off	3-184
3.3.5-8	Two-Way Azimuth Antenna Pattern	3-187
3.3.5-9	Two-Way Antenna Elevation Patterns	3-188
3.3.5-10	Functional Block Diagrams	3-197
3.3.5-11	Range Swath Timing	3-205
4.3.1-1	Configuration #1 Layout	4-5
4.3.1-2	Configuration #2 Layout	4-6
4.4.1-1	Polar Sun Synchronous Orbit	4-13
4.4.1-2	SSAR Thermal Model	4-15
4.4.1-3	Transmitter Tube Interface Temperature	4-19
4.4.1-4	Maximum and Minimum Base Plate Temperatures (^{o}C)	4-21
4.5.1-1	Thermal Expansion Graphite Composite Laminate	4-24
4.5.1-2a	SSAR Antenna Configuration #1	4-30
4.5.1-2b	Stowed Dimensions Configuration #1	4-31
4.5.1-3a	SSAR Antenna Configuration #2	4-33
4.5.1-3b	Stowed Dimensions Configuration #2	4-34
4.5.2-1	Antenna Hinge	4-36
4.5.2-2	Locking Device	4-37
5.1.1-1	SSAR Processing Block Diagram	5-2
5.1.1-2	SSAR Operational Flow Diagram	5-3
5.1.3-1	Library Layout	5-15
5.1.3-2	Processing Equipment Layout	5-16
5.1.3.5-1	Codes for Digital Recording	5-24
5.1.3.5-2	Design Chart for Space-Multiplexed PCM Recording	5-28
5.2.3-1	Doppler Frequency Spread Geometry	5-35
5.2.3-2	Geometry from which Doppler Frequency and FM Slope are Calculated	5-38

LIST OF ILLUSTRATIONS

'igure No.		Page
5.2.3-3	SAR Geometrics	5-41
5.2.4-1	Simplified Sequential Correlator	5-45
5.2.4-2	Batch Processing	
5.2.4-3	Time vs. Frequency Histories of Ground Return	5-47
5.2.4-4	Corner Turning	
5.2.4-5	Input Storage for Continuous Block Processing	5-48
5.2.4-6	Batch Correlation of Chirp Waveforms	5-49
5.2.4-7	Single-Stage Time Correlator Example	5-49
5.2.4-8	Two-Stage Time Correlation Concept	5-51
5.2.4-9	Related Fourier Analysis Concepts	5-52
5.2.4-10	Triangular Memory	5-53
5.2.5-1	SSAR L-Band Processor	5-56
5.2.5-2	Corner Turn Buffer	5-58
5.2.5-3	L-Band Processor Memory Requirements	5-60
5.2.5-4	Triangle Memory	5-62
5.2.5-5	Multilook L-Band	5-63
5.2.5-6	Map Reference Generator	5-64
5.2.5-7	SSAR X-Band Processor	5-66
5.2.5-8	Memory Tradeoff for X-Band	5-67
5.2.5-9	Line-by-Line Correlator	5-69
5.3.1-1	Beam Edge Shift	5-78
5.3.2-1	Calibration Signal Injection	5-81
5.3.2-2	Calibration Pulses	5-82
5.3.2-3	Possible Calibration Sequences	5-83
5.3.2-4	Delay Device	5-87
5.3.2-5	Calibration Pulse Generator	5-89

1.0 INTRODUCTION

The Systems Development Division of the Westinghouse Electric Corporation has completed the level of effort, specified in NASA contract NAS 5-21951, to perform a pilot study of a spaceborne sidelooking radar.

The final report covers the that effort in detail and documents the results of trade studies conducted to determine parameters of and configurations for candidate systems. No hardware was planned for this phase.

Section 2 is a summary of the effort. Copies of viewgraphs used in the final report oral presentation have previously been provided.

Section 3 contains the results of the system trade studies and gives the electrical parameters for the proposed subsystems.

Section 4 is devoted to the mechanical aspects of the study. Packaging, thermal control and dynamics of the proposed design are presented.

Section 5 contains the details of the data processor. A system is described that allows the data from a pass over the U. S. to be in hard copy form within two hours.

Section 6 contains the proposed schedule, Work Breakdown Structure, and cost estimate. This section is under separate cover per direction of the NASA Project Officer.

2.0 PROGRAM SUMMARY

The primary emphasis during this study was placed on doing trades to optimize a sidelooking radar for space use, e.g., high

quality, scientific imagery. Initially, certain boundaries and ground rules were established between Westinghouse and the NASA EOS project office. These constraints were set up so that the radar might be compatible with the design concepts of the EOS satellite. The proposed systems are well within the imposed limitations of power, weight, volume and data link capacity.

The approach taken to develop the parameters and, thus, the critical subsystem specifications, was to conduct a literature search on the user requirements and also to contact recognized authorities on user requirements to determine their real needs. It became quickly apparent that the system frequency was critical as was polarization, resolution and number of looks per resolution cell.

In summary, our proposed system has the following base characteristics:

- Synthetic aperture techniques to provide the high resolution in azimuth.
- Pulse compression to limit peak powers.
- Flexible digital processor for diverse user needs.
- Minimum spacecraft hardware to enhance reliability.
- Scientific quality imagery through ambiguity suppression and multilook.
- Dual polarization
- Dual frequency

Because of the requirement and necessity to keep the development cost as low as possible by utilizing existing hardware designs, two frequencies, X and L band, were chosen. This resulted in a trade study of antenna depression angles, swath width, etc. The dual polarization capability was determined to be feasible based on an existing antenna. The processor was chosen to be all digital based on on-going work at Westinghouse and for the full flexibility required for the diverse user needs, i.e., multiple processing with different parameters of azimuth and range resolution, area of interest, and number of looks.

The mechanical effort centered about a layout of subsystem components into a NASA-suggested volume, performance of a preliminary mechanical design, and the thermal and dynamic analyses to determine component temperatures and expected stress levels during the launch and orbital phases. These analyses show that the packaging concept, including the thermal control, was adequate and well within the state-of-the-art.

Considerable effort was expended in the preliminary design of the rather complex processor required for the SAR data. In addition, the task of data management was addressed.

Certain assumptions were made for development of the budgetary cost data. A schedule was generated based on a radar-equipped satellite launch in 1978. It was assumed that there would be a thermal structural model, one prototype and one flight system. The ground station consists of that equipment to process the SAR data and produce hard copy only.

Based on the preliminary system design, it was assumed that the system could meet the reliability requirement with no redundancy and that the quality of the parts would compare to those used on other spacecraft programs at Westinghouse.

3.0 SYSTEMS ANALYSES

3.1 Radar Rationale and Design Summary

The function of the satellite borne radar is to provide maps and map imagery to be used for such earth resource applications as agricultural crop identification, geologic lineament and fault detection, and urban land use planning.

The satellite radar has the capability of mapping the entire United States in four to six months regardless of inclement weather; however, the imagery must have a high degree of resolution to be meaningful. The diverse uses require maximum resolutions on the order of 30m. Attaining this resolution at the satellite altitude is not feasible without signal processing as opposed to simply relying on the track and cross-track dimension as determined by the antenna resolution and transmitted pulse width respectively.

Linear FM signal processing techniques enable achievement of ground resolution two to three orders of magnitude greater than the basic antenna size and pulse width allow, as well as enhanced Signal to Noise (S/N) ratio.

The increase in crosstrack or range resolution is achieved by transmitting a pulse whose frequency is dispersed in a linear FM fashion. Upon reception, this pulse is compressed by passing it through a dispersive delay line whose time delay is a function of frequency. All frequency components of the pulse then occur at the same time and the pulse is compressed to a fraction of its transmitted length thus achieving a high resolution.

The along track or azimuth resolution improvement is achieved using the linear FM caused by increasing and decreasing doppler as the

S/C approaches and recedes from the target. The target return exists as long as it is illuminated by the real antenna pattern. Subsequent signal processing and compression results in a relatively short duration signal and high resolution as if the target were illuminated by a much narrower antenna beam resulting from a larger azimuth antenna aperture than exists. Such a system is called a Synthetic Aperture Radar (SAR).

3.1.1 Radar Rationale

The key note of the Westinghouse design approach is that the maps and imagery obtained are to be used for scientific evaluation of earth resources and, therefore, must be of highest obtainable quality compatible with the diverse users requirements.

Historically, radar imagery was primarily used for target identification only with heavy reliance placed upon man-made or regular geometric features for identification. Thus, even with poor or noisy quality imagery, these features "stand out" among random or noisy clutter. These techniques are not satisfactory when the imagery is to be used for crop identification, moisture content through backscatter coefficient evaluation, etc., because here, nature's intrinsic randomness is of interest.

Imagery of the required quality can be achieved through the design approach in several areas: ambiguity or false target control, adequate Signal to Noise (S/N) Ratio, Multilook Capability, and definitive subsystem specifications to insure overall system performance.

Ambiguities arise in several ways (see section 3.2.3) which are a fundamental factor in the radar design. As such, a specified tolerance should be placed on them as they form a numerical constraint and key

trade-off or design criterion.[1]

S/N ratios as low as -3 dB have been used satisfactorily for military target identification. The S/N ratio of interest for many earth resources applications is power returned from a clutter cell of low reflectivity like 3" green grass (σ^{o} = -20 dB) to the intrinsic system noise. Specifying S/N of +3 to +10 dB for this type of background should allow backscatter determination and geological lineament determination against poor reflectors.

As every subsystem in the radar can introduce noise or sidelobes, tight coordinated subsystem specifications are necessary to hold their contribution to -30 dB or 1/1000 of the primary target response. Thus, preliminary specifications detailing not only with major functional requirements, but also the error tolerance allocated to each one were developed (section 3.3.5). These specifications are necessary in order that itemized estimates may be prepared for such parameters as weight and power consumption in order to develop a credible system design. A realistic appraisal was made and the supporting documentation is given in section 3.3.5.

Finally, map quality may be enhanced through the use of multilook techniques. Examination of a target from a fixed aspect angle for a limited period of time can result in image degradation. This condition may be alleviated by "looking" at the target from several aspect angles in azimuth or by averaging several range cells together (section 3.2.3.5). Basically, the less resolution required, the more looks can be obtained.

---

[1] Appendix E

User's resolution requirements vary from 30m to 900m or more. The proposed radar designs have a base 30m maximum resolution (9 azimuth looks) which can be reduced during ground processing depending upon a particular user's requirement. As the resolution requirements are reduced, the maximum number of looks possible commensurate with ambiguity requirements are taken. Table 3.1.2-2 shows possible resolution/looks processing flexibility. The multilook addition also results in a S/N improvement.

Several system parameters or features are of dominant interest. These include: swath width, polarization, frequency, altitude, depression angle, image quality, reliability, power consumption, weight, ambiguities,[1] and antenna dimensional envelope. These parameters and others are given in Tables 3.3.2-1 and 3.3.2-2. Some of these were customer directed, (section 3.2.1), others, the radar investigators had some latitude in selecting. There is, however, a tight interrelationship between swath width ambiguities, depression angle for given antenna dimensions, frequency, etc. A realistic design approach requires examination of the actual azimuth and elevation antenna patterns as they illuminate a non-flat earth, PRF selection commensurate with swath width, desired ambiguities, etc.

A design study must take into account these variables and is not amenable in an efficient manner to standard equations or "cook book" approaches because of the complex parametric interrelationship and graphical data inputs such as the antenna pattern and integration filter shapes.

---

[1] ambiguities are false targets which degrade map quality. They are more fully explained in section 3.2.3.6.

General system requirements indicated a system configuration should have the capabilities shown in Table 3.1.1-1.

Table 3.1.1-1 Desired Radar Capability

Resolution	30 - 900m
Polarization	like/cross
Frequency	X, L band
Depression Angle	55^{o} - 75^{o}
Antenna Envelope	13.5 x 2.5 x 1 ft. 27.0 x 2.5 x 1 ft.
Reliability	Operating life 500 hrs. with 95% probability of success.
Weight	$\leq$ 500 lbs.
Power Consumption	$\leq$ 4 kW

As mentioned, because of the tight parametric interrelationship, it is difficult to extrapolate indefinitely from a general set of tradeoff curves. Further, the specified antenna dimensions, commensurate with various launch vehicle capabilities, indicated one or two "point" or baseline configurations around which tradeoffs may be made.

The L-band requirements dictated the use of the 27 ft. antenna in order to attain the required ambiguity level. Simultaneous X and L dual frequency was then achieved in Configuration #2 with single polarization at each frequency, although a dual X band polarization option with L band is possible.

Dual transmit/receive X band polarization using the smaller antenna dimension was studied in Configuration #1.

The key features of the point or baseline designs are:

- SAR for enhanced azimuth resolution
- Pulse compression for higher average power
- Flexible processing for multiple resolutions/looks
- Ground signal processing for minimum spacecraft hardware
- High image quality through ambiguity restraints and multilook
- Dual polarization
- Dual frequency band

3.1.2 Design Summary

A summary of the radar and system parameters are given in Table 3.1.2-1. Some of these parameters such as image quality, altitude ground resolution, frequency, signal to noise, noise figure, and antenna dimensions were used as a design criterion. Swath width was then traded against ambiguity level over the depression angle range. The 50 km swath width and -25 dB ambiguities were selected as being the widest swath with reasonable ambiguity levels. Basically then, the design rationale was to maximize swath width and minimize power consumption given a fixed antenna size, desired ambiguity level, S/N over the swath and resolution. This was done on the basis of 20% overall transmitter/HVPS, modulator efficiency and within the data link capacity of 2 each, 140 megabits/sec channels.

Both configurations utilize TWT X band transmitter to attain the required ambiguity control by minimizing phase and amplitude deviations. The tube selected is a tapered design from well-established space-qualified TWTs commensurate with a low risk, high reliability requirements.

Table 3.1.2-1 Spaceborne Synthetic Aperture Radar

System Parameters		
Satellite		
Altitude	914 km	
Orbit Period	103 min.	
Operating Period/Orbit	10 min (over continental U.S.)	
Expected Satellite Life	4 - 6 months.	
Mapped Area	Continental U.S., Hawaii, Alaska	
Radar	**Configuration #1**	**Configuration #2**
Base Ground Resolution[1]		
Range	30m	30m
Azimuth	30m (9 looks)	30m (7 looks)
Swath Width	50 km (27 n.mi)	50 km (27 n.mi)
Ambiguities		
Azimuth	-25 dB	-25 dB
Range	-25 dB	-25 dB
Frequency	9.3-9.5 GHz	9.3-9.5 GHz and 1.7 GHz
Polarizations	HH, HV or VV, VH	HH (both freqs.)[2]
Signal to Noise (σ^o = -20 dB)	+3 to 10 dB	+3 to 10 dB
Depression Angle	55° to 75°	75°
Noise Figure	1.7 dB	1.7 dB
Antenna Dimensions	4.1 x .76 x .3m (13.5 x 2.5 x 1 ft.)	8.25 x .76 x .3m (27 x 2.5 x 1 ft.)
Weight	119 kg (262 lbs.)	176 kg (387 lbs.)
Power Consumption	1140 watts	1250 watts
Volume (Electronics)	.106 m^3 (3.75 ft^3)	.15 m^3 (5.1 ft^3)

[1] See processing flexibility table.

[2] Dual X band polarization option with single polarization L band possible.

Table 3.1.2-2 Processing Flexibility

(X Band 13.5 ft. aperture)

Resolution	Range Looks	Azimuth Looks	Total Looks
30m	1	9	9
60m	2	18	36
90m	3	27	81

The L band configuration is solid state for reliability and low risk considerations. Both transmitters utilize Westinghouse's expertise in these specialized areas.[1, 2]

Low noise receiver front ends (1.7 dB receiver overall NF) enables the minimized transmitter power requirements. X band paramps and L band transistor amplifiers are used.

Range pulse compression is necessary to obtain the average power compatible with PRF, pulse width, etc. Dispersive surface wave lines for expansion and compression are used. Both lines are placed on board the S/C such that they be in the same environment and maintain their "matched" properties. The savings in ground based processing complexity and hardware is substantial. Digital data conversion of complex video is utilized. This is followed by a small amount of data conditioning ("range slowdown") to reduce the data rate prior to the High Speed Data Processor (HSDP) for parallel/serial data conversion and formatting. The A/D converter sampling may be drifted in range to compensate for the earth's rotation. The stalo/synchronizer/system controller has been

---

Band Transistor Amplifier Dishes Out 1 KW, Microwaves, December, 1972.

ransmitter Contract End Item Report, Jan. 1973, Aeronautical System ivision, WPAFB, Contract #F33657-71-C-0786.

optimized for maximum reliability by reducing the number of crystal oscillators by deriving all timing and microwave sources from one primary source using frequency multipliers and dividers.

The antennas utilize a Westinghouse proprietary feed to allow both vertical and horizontal polarization. A pair of waveguides are coupled to a common aperture through a combination of polarization sensitive grids.

The antenna is positioned to obtain a compact launch profile and then repositioned when in orbit. The antenna reflector is constructed of the new, lightweight graphite/epoxy composite material to allow an approximately 40 percent savings in weight and to minimize thermal distortions in the reflector face. A conductive layer is deposited on the inner face of the reflector for electrical conductivity. The remaining parts of the assembly, including the feed, are constructed of aluminum.

The Statement of Work (SOW)refers to tasks (a) through (g). Task (a), Radar Configuration, which concerns synthesis and study of various radar configurations to meet the needs of earth resources applications are discussed primarily in sections 3.2 and 3.3; Task (b), Radar System Parameters, which concerns study of various salient parameters, is primarily covered in section 3.2.3; Task (c) Hardware Design Considerations, which asks for a review of available components for applicability to orbital operation along with transmitter reliability is discussed in section 3.3.5.1.3 and 3.3.4.3. The practicability of building and deploying the antenna is discussed in section 3.3.5.2. Performance requirements of the A/D converter and digital hardware are shown in

section 3.3.5.4. Cost and Schedule data appears in Section 6. Task (d), Auxiliary Equipment Study for radar calibration is given in section 5.3. Data interface requirements are shown in section 3.3.5.4.

3.2 Systems Requirements

3.2.1 System Guidelines

The radar system designs are heavily dependent upon such satellite parameters as altitude and velocity as well as such features as area to be mapped and polarization desired. A number of subjective parameters influence image quality. These include signal to noise (S/N) ratio and ambiguity levels.

System requirements are given in Table 3.2.1-1. The satellite altitude is significant in that S/N, swath width, Multiple Time Around Echo (MTAE) and depression angle are affected. The 914 km altitude indicated was selected by the customer and also preferred by EOSPDG.[1.] The orbit characteristic affects mapped area as well as the on time/orbit. The eccentricity, earth oblateness and local relief displacement affect the transmit/receive time. The "on-time/orbit" is a rough estimate of the time the satellite is above the continental United States (i.e. "the lower 48"). As there is no desire for on-board data storage all data must be transmitted to the ground over the available two 100 MHz channels. It is desired to map the continental U.S. during the operating life of the radar/satellite. The ability to do this depends upon satellite orbit trajectory over the operating life. This reliability or operating life requirement is discussed in section 3.3.4.3. Possible techniques to cover specific areas of interest which might be missed include slight

1. Earth Observatory Satellite Payload Discussion Group (EOSPDG) Final Report, October 1973, NASA, Washington, D.C.

Table 3.2.1-1

System Guidelines

Satellite Altitude (716 or 914 Km)	914 Km preferred*
Orbit Characteristic	polar, circular, sun-synchronous*
Orbit Period	100 min.*
On Time/Orbit	~ 10 min.*
Data Link Capacity	2-100 MHz channels*
Reliability	500 hrs. operating time with 95% prob. of success*
Mapped Area	United States
Antenna Size	27' x 2.5' x 1' (8.2 x .76 x .31m)* & 13.5' x 2.5' x 1' (4.1 x .76 x .31m)*
Frequency	X band (8.5 - 9.5 GHz) L band (1.7 GHz)
Dual Polarization	HH, HV & VV, VH
S/N	+ 3-10 dB on 3" grass
Ground Resolution	≥30m*
Swath Width	50 Km (27 nm)
Ambiguous Responses	-25 db
Prime Power	≤ 4 KW*
Depression Angle	50° to 60°

* Customer directed

variations in antenna depression angle depending upon orbit, or use of a fixed position antenna and roll the spacecraft a slight amount.

The antenna azimuth aperture determines the return doppler spectrum which then is of significant interest in evaluating azimuth ambiguities, number of azimuth looks, PRF, etc. The elevation aperture is of concern in that it defines the elevation beam shape and thus the signal strength variation over the swath. Further, in an ambiguous range operation the signal return from contiguous terrain to the swath width of interest impact on PRF and as such is a definitive parameter. Two maximum antenna azimuth apertures of 13.5 and 27 ft. were suggested commensurate with available launch vehicle sizes. Two frequency bands were suggested, X and L. These frequencies were also suggested by EOSPDG.[2.] Simultaneous mapping with each polarization or frequency should take place such that the diverse backscatter characteristic may be directly compared. Such a capability was recommended by EOSPDG and others.[3.]

The signal-to-noise requirement of +3 to +10 db on 3" grass should result in instrumentation quality imagery. More specifically this stems from a desire to detect the background with some positive S/N. It would be desirable for desert backgrounds to have at least +3 db S/N such that, for example, hydrologists may readily detect land drainage features. Generally low reflectivity backgrounds do allow the use of

---

2. Ibid.
3. Section 3.2.2

of coarser 60-100m resolution cells under which conditions the S/N can be increased over what it would be for 30m resolution. The resolution in both azimuth and range can be degraded simply by changing ground processing parameters. Another parameter which affects image quality is the number of independent looks in range and azimuth. As the resolution requirements decrease the number of looks can and should be increased. The more the number of looks, the less the image graininess and better the image quality. Westinghouse has taken full advantage of this effect in both range and azimuth, (section 3.2.3.5).

An additional factor directly contributing to image quality is ambiguous responses. These responses result from such system imperfections as: linear distortion in amplitude or phase of system elements, improper selection of PRF after consideration of swath width and antenna patterns, video limiting or nonlinear distortion, etc. Inadequate suppression of these responses result in the appearance of false targets and poor map background. More than 25 db suppression is desirable; however, attaining a 50 km swath width and other requirements impact on the ambiguity specification. This is fully discussed with tradeoffs in section 3.2.3.6.

A prime power drain of less than 4 KW was indicated. Present requirements are about 1200 w.

3.2.2 Radar as an Earth Resource Sensor

Introduction

Since World War II much effort has been expended in applying radar concepts and equipment to ground mapping. In the mid-sixties, images

were first made available to scientists for study and evaluation. Much has been written covering the entire spectrum of radar imaging, systems, system parameters, ground parameters, geoscience uses, data processing and image interpretation. Here, interest lies in geoscience uses, the system, and its parameters.

The major portion of the literature is expectedly general, often lacking information about the radar system and its parameters. As is usual in an emerging field of study, there is much repetition and duplication. Almost exclusively, Ka-band radars in the form of the Westinghouse AN/APQ-97 have been used for imaging. Some imaging has been accomplished using X-band while there exists little or no L-band imagery.

Current Research and Development

The University of Kansas, in Lawrence, Kansas, is most actively engaged in radar remote sensing research. The early work was in K-band and some X-band imagery interpretation and evaluation. Effort has been directed toward developing computerized systems for data acquisition, handling, and processing for image enhancement and interpretation. Research is deeply involved in a continuing study (22)* which covers radar and ground parameter investigation, usage studies in agriculture, hydrology, geology, etc., and differentiation of crop types, surface types, moisture content, etc.

---

*Due to repeated use, references are listed in a tabular bibliography at the end of the article.

Ohio State University became involved very early in radar ground return characteristics performing parametric measurements of backscatter coefficients for controlled surfaces. Recently developed at the University of Michigan, Ann Arbor, is a quickly convertible X- and L-band radar.(20). Work continues there on the design and implementation of a multiplexing system which would allow simultaneous X- and L-band imagery in a single flight.

General Geoscience Uses

Radar has ably proved itself in the field of geoscience remote sensing. Radar is often weather independent. Huge areas can be mapped on a single pass making radar a valuable tool for temporal studies and regional mapping. The output can be a magnetic recording or a continuous photographic image as opposed to photography's mosaics. Many uses for radar imagery have been tried or postulated (see Table 3.2.2-1). In forestation uses include type discrimination, growth status determination, insect attack warnings, fire protection in placing ranger stations and fire breaks location. (23). Hydrological uses include finding water run-offs and soil moisture content. In urban planning, land uses and non-uses, regions and districts by housing or building type are typical uses. Transportation uses include traffic flow and congestion and sight investigation for future transportation systems for minimal trouble with geology and congestion. (23)

Radar Parameters

Frequency: K-band

The radar parameters affecting ground return are wavelength or frequency, resolution, look direction and angle of depression, polarization,

and power. Presumably because of its availability, Ka-band radar has been used in the majority of imaging studies. As a tool for regional investigations, multipolarization K-band radars have, to an acceptable degree of accuracy, determined broadband uses, crop types, vegetation communities and urban land uses. [8] In agriculture, Moore[4] has cited adequate results using radar imagery in determining 1) field boundaries; 2) crop types within fields and total acreage of a given crop; 3) progress of field preparation and planting; 4) progress in harvest; 5) in some cases the extent of irrigation in fields known to be bare. A European Study [23] cites evidence from Kansas that sufficient discrimination at .86 centimeter wavelength was found between groups of, a) sugar beets, b) maize, and c) sorghum, lucerne, emerging wheat, weeds, bare ground. Similar data from Holland discriminated between, a) sugar beets; b) barley, flax, wheat, and lucerne; and c) potatoes and peas. In both cases the crops within each group were poorly discriminated. In vegetation mapping, Moore and Simonett [4] suggest possible uses in 1) preparation of small scale regional or reconnaissance vegetation maps of vegetable type expecially when there are pronounced structural differences between plant communities; 2) delineation of vegetable zones which vary with altitude; 3) tracing burn patterns from previous forest fires; 4) delineating altitudinal timber lines; 5) identification of species by inference in areas characterized by "monospecific" stands; 6) discrimination of structural subtypes in cut-over, burned and regrowth forest. To an extent, these possibilities were varified by successful vegetation mapping of Horsefly Mountain, Oregon using dual-polarization K-band

radar imagery. [5] W. P. Waite [17] suggests that Ka band imaging radar can be used in relative or qualitative moisture determination under conditions of defoliation (in winter) or if the vegetation is essentially dry or leafless.

X-band radar has been found extremely useful in geology.[11,19] In many cases radar shows land formations better than do aerial photographs. Lineaments often show on radar images where none were apparent on photographs; however, the radar missed none of those shown on the photograph (15, pg. 25-40, figure 40). Joint system and sometimes rock outcrops are quite evident. Some penetration of dry sand has been detected with a possible use in determining underlying structure. K-band radar has also found use in polar ice mapping, distinguishing between ice types. This is especially useful considering the cloud cover and lighting problems in the Arctic.

Frequency: X-band

X-band radars have seen much less use in geoscience imaging than have K-band radars. Indications are that capabilities will not be degraded. Due to the longer wavelength, penetration may be greater than with K-band. Lineaments and joint systems are found to be quite prominent in X-band. [3] A study in Holland using 3.3 centimeters wavelength radar found quite good distinction among the groups: a) potatoes; b) potatoes with dead leaves; and c) sugar beets, lucerne, wheat. As with K-band, distinguishing attributes shown among members within each group defied separation. Comparisons of K- and X-band results in this field tends to indicate a possible influence of frequency on crop type determination.

Frequency: Low Frequency (L and P band)

Lower frequencies are postulated for more study. The use in penetrating to forest floors or at least below the tree crowns would yield valuable information.[23] Because of its penetrating capabilities and the moisture dependence of penetration, quantitative moisture measurements may be possible.[4,17,22] However, the full value of long-wavelength imaging systems (L or P bands) will be realized only when they produce imagery which is collected simultaneously with X- or K-band imagery.[9]

Look Direction and Polarization

Look direction and polarization are also influences in image evaluation. Multipolarization radars have been praised to a great extent. HH and HV (horizontal send, horizontal and vertical receive) polarizations are needed in multifrequency radars for full crop identification.[4,15] The use of cross-polarized images has particular value in identifying lithologies.[2] Cross polarization enhanced a number of lava-alluvium contacts not as evident on like-polarized images. Some lithologic contacts are well defined on cross-polarized images allowing separation of lava flows of different ages, weathering, and roughness. In conjunction with look direction, lineaments and joint systems are extremely dependent on look direction.[11] These act as corner reflectors and for full coverage in uncharted regions, four orthogonal look directions are suggested.

Linear cultural features are dependent on look direction. However, this dependence is somewhat compensated by use of dual polarized images.

A. J. Lewis [13] used a semitrained, relatively inexperienced group of student observers to interpret radar images. With a 99.9% confidence level the objects correctly located in the HH polarization images were: 1) powerlines and railroads traversing land when aligned parallel to the flight path; 2) bridges, channel markers and other high return features traversing water regardless of orientation of the features with respect to the flight path. HV polarization images gave better detection of railroads and powerlines not parallel to the flight path.

Resolution

Resolution is a basic parameter involved in image utility. Dellwig [2] has found low resolution (15 meters range and 208 meters azimuth) X-band imagery quite valuable in turning up otherwise unnoticed lineaments. For an orbiting radar, [1,7] 30 to 60 meters is the highest resolution considered for use in mapping and field discrimination. Lower resolutions 150-200 meters is suggested for oceanic fishing activity, finding boundaries of moist and dry ground after rainfall (if possible) and lineaments and joint system detection. For polar ice studies, 250 meters may suffice while kilometer resolutions could be used for measurements of ocean properties, and 70 kilometers (at 1-2 centimeters) may be used to determine precipitation. See Table 3.2.2-1.

Radar Systems for Geoscience Use

Moore has suggested possible systems for use in geoscience remote sensing. The improvements suggested are: 1) panchromatic illumination, analogous to the broad-band visible light spectrum, which would reduce speckling caused by monochromatic illumination: 2) multispectral sensing - using several center frequencies which could be processed

to give a radar "color" image, [10] 3) squint-mode techniques to reduce the number of passes needed to achieve multiple looks and possibly give stereo height indication, 4) calibration of the radar to make available comparisons with data-bank information. To keep the bandwidth within reason, Moore suggests using higher resolution and averaging resolution cells effectively increasing the bandwidth. The frequencies chosen for the system are 16, 35, and 94 GHz. The first is already in use and the latter two are windows in atmospheric absorption. Thomann recommends an alternative to the 94 GHz frequency.[16] He chooses L-band because of its possible utility in vegetation and soil penetration, X-band for its proven earth science usefulness, weather independence, high resolution and high quality synthetic aperture systems, and 35 GHz panchromatic and dual-polarization K_a-band for its proven and postulated usefulness.

The following table of remote sensing radar uses is a modified form of a table taken from the European Space Research Organization study of SLAR remote sensing radars.[23] Abbreviations used are:

Resolution - Low: Greater than 30 meters; Med: 10 to 30 meters; High: Less than 10 meters

Status - Pres: Presently in use; Exist: Could be implemented using present technology; Dev: Research and development are indicated before it could be implemented.

Present Frequency Band: Radar frequency band in current or past use.

Postulated Band: Frequency band postulated for possible study or use. Where K, X, L is listed, same indication exists that polypanchromatic radar may be valuable.

Table 3.2.2-1. Applications of Remote Sensing Radar

Ref	Application	Resolution	Status	Present Frequency Band(s)	Postulated Band(s)
1	Lithological Studies	High	Dev.	Ka,X	K,X,L
2	Lineation Plotting	Med	Pres.	Ka, X	
3	Fracture trace analysis	High	Exist		
4	Plate tectonic studies	Low	Dev		
5	Medium and small-scale geological mapping	Med	Exist	Ka	
6	Location of civil engrg. construction materials	High	Pres.		
7	Volcano damage assessment	High	Exist		
8	Earthquake damage assessment	High	Exist		
9	Physiographic and geomorphological analysis and mapping particularly in areas of low angle slopes	Med	Pres	Ka	K,X,L
10	Micro-glacial land forms	High	Exist		
11	Sedimentation studies	Med	Pres	Ka	
12	River basin morphological	High	Pres	Ka	
13	Broad studies soil pattern classification	High	Dev	Ka	K,X,L
14	Soil moisture	Med	Dev	Ka	L
15	Soil erosion	Med	Exist		
16	Detection of surface run-off	High	Dev		
17	Floodwater monitoring	High	Pres	Ka	
18	Inventory of wetlands and lakes	Med	Pres		

Table 3.2.2-1. Applications of Remote Sensing Radar (Cont'd)

Ref	Application	Resolution	Status	Present Frequency Band(s)	Postulated Band(s)
19	Snow storage	Med	Exist		
20	Glacial studies	High	Exist	Ka,X	
21	Land use patterns	Low	Pres		
22	Vegetation mapping	High	Dev	Ka	Ka,L
23	General reconnaissance of forestry	Low	Exist		
24	Forest surveys and mapping	Med	Dev		K,X,L
25	Stratification of forest	High	Exist		K,X,L
26	Forest protection	Med	Dev		
27	Shifting cultivation with forest fallow in the Tropics	High	Exist		
28	Crop growth and moisture stress	Med	Dev	Ka	K,X,L
29	Crop recognition and inventories	High	Dev	Ka	
30	Timeliness of agricultural operations	Med	Dev	Ka	
31	Agricultural systems	Med	Exist	Ka	
32	Epidemiology of pests and diseases	High	Dev		
33	Field boundaries and patterns	High	Dev	Ka	K,X,L
34	Map updating of cultural features	High	Pres	Ka	
35	Urban Planning	High	Exist		

Table 3.2.2-1. Applications of Remote Sensing Radar (Cont'd)

Ref.	Application	Resolution	Status	Present Freq. Band(s)	Postulated Band(s)
36	Initial route planning studies	High	Exist		
37	Traffic counts on main roads	High	Dev		
38	Detection of crashed aircraft	High	Pres	Ka	
39	Surface winds (sea state)	Low	Dev		
40	Ocean currents (sea state)	Low	Dev		
41	Salinity	Low	Dev		
42	Sea ice	Med	Pres		
43	Iceberg detection	Med	Pres		
44	Gross organic surfactants	Med	Exist		
45	Oil slick detection	Med	Pres		

References

(1) Ellermeier, R. O., Simonett, D. S., "Imaging Radars On Spacecraft As A Tool For Studying Earth," University of Kansas, Lawrence, CRES Tech. Report 61-6, 1965.

(2) Dellwig, L. F., Moore, R. K., "The Geological Value of Simultaneously Produced Like- and Cross-polarized Radar Imagery," j. Geophys Res., vol. 71, pp. 3997-3601, July 15, 1966.

(3) Dellwig, L. F., Kirk, Walters, "Potential of Low-Resolution Radar Imagery," J. Geophys Res., vol. 71, pp. 4995-4998, 1966.

(4) Moore, R. K., Simonett, D. S., "Radar Remote Sensing In Biology," Bioscience, vol. 17, pp. 384-390, June 1967.

(5) Morain, S. A., Simonett, D. S., "K-band Radar In Vegetation Mapping," Photogrammets Eng., vol. 33, pp. 730-740, July 1967.

(6) MacDonald, H. G., Brennan, Dellwig, L.F., "Geologic Evaluation By Radar Imagery of NASA Sedimentary Test Site," IEEE Trans., vol. GE-5, no. 3, pp. 72-78, Dec., 1967.

(7) Moore, R. K., Simonett, O. S., "Potential Research and Earth Resources Studies With Orbiting Radars," AIAA paper 67-767, 1967.

(8) Nunnally, N. R., "Radar As A Tool For Regional Investigations," Interagency Report NASA-67, Jan., 1969.

(9) Rouse, Jr. J. W., MacDonald, H. C., Waite, W. P., "Geoscience Applications of Radar Sensors," IEEE Trans., vol. GE-7, No. 1, pp. 2-18, Jan. 1969.

(10) Moore, R. K., Waite, W. P., Rouse, J. W., "Panchromatic and Poly-panchromatic Radar, "Proc. IEEE, vol. 57, pp. 590-593, April 1969.

(11) MacDonald, H. D., "Geologic Evaluation of Radar Imagery from Darien Province, Panama," Modern Geology, vol. 1, 1969, or University of Kansas CRES Tech. Report No. 133-6.

(12) MacDonald, H.C., Kirk, Dellwig, L. F., "Influence of Radar Look-Direction on the Detection of Selected Geological Features," Proc. of 6th Annual Symposium on Remote Sensing of the Environment, pg. 637, 1969.

(13) Lewis, A. J., MacDonald, H. C., Simonett, D. S., "Detection of Linear Cultural Features with Multipolarized Radar Imagery," Proc. of 6th Annual Symposium on Remote Sensing of the Environment, 1969.

(14) Dellwig, L. F., "A Geoscience Evaluation of Multifrequency Radar Imagery of the Pisgah Crater Area, California," Modern Geology, vol. 1, pp. 173-186, 1970.

(15) Moore, R. K., "Ground Echo," in M. I. Skolnik, Radar Handbook, New York: McGraw-Hill, chapter 25, pp. 25-41, 1970.

(16) Thomann, G.D., Dickey, F. M., "Geoscience Radar Systems," University of Kansas CRES Tech. Report 177-18, May, 1971.

(17) Waite, W. P., MacDonald, H. C., "Vegetation Penetration with K-Band Imaging Radars," IEEE Trans., vol. GE-9, No. 3, pp. 147-154, July 1971.

(18) Moore, R. K., Thomann, G. C., "Imaging Radars for Geoscience Use," IEEE Transactions, vol. GE-9, No. 3, pp. 155-169, July 1971.

(19) Wing, R. S., "Structural Analysis from Radar Imagery: Eastern Panamanian Isthmus," Modern Geology, vol. 2, No. 1, 1971, or University of Kansas CRES Tech. Report 133-15.

(20) Porcello, L. J., Rendleman, R. A., "Multispectral Imaging Radar," 4th Annual Earth Resources Program Review, vol. II, 37-1, January, 1972.

(21) Morain, S. A., "The Status of Parametric Studies in Radar Agriculture," 4th Annual Earth Resources Program Review, vol. II, 37-1, January 1972.

(22) "Radar Studies Related to Earth Resources Program," Quarterly Progress Report, University of Kansas CRES Tech. Memo 177-28.

(23) Roberts, E. H., "Side-looking Radar Systems and Their Potential Applications to Earth Resources Surveys," ESRO (European Space Research Organization), vol. 3, June 1972, (Elliot-Automation Space and Advanced Mil. Systems, LTD, Chamberly, England, Aug. 1972).

3.2.3 Development of Radar Parameters

This section discusses how the various radar system parameters, such as frequency, resolution, power, PRF, bandwidth, etc., were derived. To determine these, radar performance parameters such as signal/noise ratio, swath width, and ambiguity suppression will be calculated. All parameters were derived under the system constraints and guidelines discussed in section 3.2.1. The purpose of this section is not to propose a specific system configuration (see section 3.3) but is rather to show what radar parameters are required to achieve given system performance.

3.2.3.1 Frequency

It would be desirable from the user viewpoint to observe the earth at all microwave frequencies (UHF -K_a band). Only certain frequencies can be implemented, of course, and the frequency of broadest user interest appears to be X-band.[1] (User requirements are also discussed in section 3.2.2). This is also a desirable frequency from the standpoint of ready accessability of components such as transmitter tubes, low noise receiver front ends, and antenna components. Little or no hardware development would be required. The atmospheric attenuation at X band is not significant. Further, ground swath width is more readily maximized while maintaining a given range ambiguity suppression at X band than at other frequencies. X band thus appears as a very attractive operating frequency from both engineering and user viewpoints and will be the prime radar frequency.

---

1. Earth Observatory Satellite Payload Discussion Group (EOSPDG) Final Report, October, 1973, NASA, Washington, D.C.

Specifically, 9.5 GHz lies in a band that would potentially be approved for use.

At frequencies higher than X, namely K_u-K_a, components are also readily available, ground backscatter can be somewhat stronger than at X band, and antenna gain for a given size antenna in greater than at X band. Atmospheric loss can be much greater at K_a, though, and on the whole more transmitter power at K_a band than at X may then be necessary to achieve a given signal/noise ratio. The K_u and X transmitter powers required are nearly identical. Due to the difficulty of power dissipation problems in satellites, this is a definite drawback for K_a band operation. Specifically, radar frequencies near the water vapor absorption frequency of 22.5 GHz must be avoided. Also, achievable ground swath width at K band is less than that at X. For these reasons X band is a better frequency choice than K band.

Users have also indicated interest in observations at a frequency below X band to complement the X band data (section 3.2.2).[1] L band appears to be the best choice for this alternate. It provides some degree of foilage penetration and as such would yield observations of a different nature from the X band data (no foilage penetration), as is desired. Observations taken at a slightly higher frequency, S band, would be too similar to those of X band to be useful. The foilage penetration property is of interest to most users, and L band does satisfy some specific user requests. At lower frequencies, UHF, foilage penetration is even greater. With the antenna dimensions required with a satellite, however, the resultant elevation beamwidth

1. EOSPDG Final Report, October, 1973

is so broad at UHF that acceptable ambiguity suppression becomes impossible to achieve. The UHF problem is further complicated by frequency allocation difficulties. The L band choice then is the best low-frequency alternate to X band. Specifically, 1.7 GHz lies in a band that would potentially be approved for use.

3.2.3.2 Polarization

Users have indicated definite interest in observing the earth at different polarizations simultaneously with a single frequency (section 3.2.2).[1] The value of this technique has been documented.[2] User interest is almost exclusively centered on comparing like and cross polarized imagery; that is, transmit with horizontal polarization (H) and receive on both horizontal and vertical (V) polarization. These are known as HH and HV. If transmission is with vertical polarization, the pair is VV and VH. A choice between these two will be provided by mechanizing the transmitter to transmit on either H or V and by mechanizing two receiver channels, one for H and one for V. The double polarization scheme does then increase satellite receiver hardware. Also, two processor channels must be mechanized on the ground. Providing all four polarizations simultaneously, in addition to requiring four channels, would complicate processing since the processor receives samples of a given polarization pair only in every other interpulse period. Since little user interest exists in having all four present simultaneously, this will not be mechanized.

1. EOSPDG Final Report, October, 1973
2. R. K. Moore, "Ground Echo" in M.I. Skolnik, Radar Handbook, McGraw-Hill, 1970, Chapter 25.

3.2.3.3 Resolution

Many different users desire different resolutions (section 3.2.2.).[1] Resolutions varying from 10m to 1000m were indicated as being desirable for different uses. As a guideline, 30m was given as a design goal resolution; this will be taken as the requirement for the work below. At the processor output, 30m resolution cells may be degraded to any other desired resolution by sloughing cells together. Although it is not required, square resolution cells (30m in both range and azimuth) will be provided.

The 30m resolution referred to here is the 4 dB width of the resolution cell, as shown in figure 3.2.3.3-1. Also, consecutive resolution cells are spaced by a maximum of 30m. To insure that point objects separated by 30m can be distinguished on the map, the processor output will be over-sampled by 25% (sample at 24m, not 30m) in both range and azimuth.

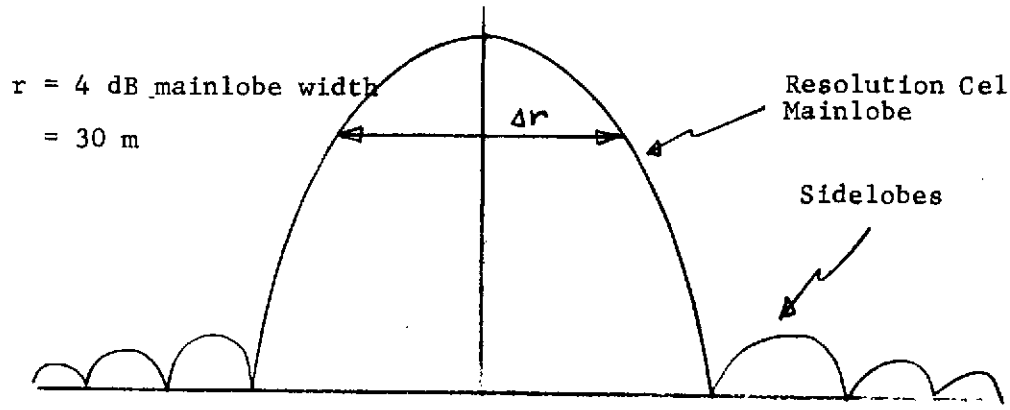

Figure 3.2.3.3-1
Resolution Definition

---

1. EOSPDG Final Report, October, 1973.

3.2.3.3.1 Range Resolution

Achieving a high range resolution and a large average power simultaneously requires use of a linear frequency modulated or chirped pulse. The transmitter/ stalo generates an expanded pulse of width T and with linear FM bandwidth ΔF. Upon reception, this expanded pulse is compressed to a pulse of τ width, where

$$\tau = 1/\Delta F$$

ΔF is also called the range bandwidth. This compressed pulsewidth is related to range resolution by

$$r = \frac{c\tau}{2}$$

where c = speed of light

$= 3 \cdot 10^8$ m/sec

The compressed pulse is of form SIN X/X with its attendent -13.4 dB peak sidelobe level. If unsuppressed, these sidelobes can appear as false targets in range on the map. They may be suppressed to any desired level by spectral amplitude weighting in the compression device. In addition to suppressing sidelobes, the weighting also broadens the mainlobe. This effect is shown in figure 3.2.3.3-2. Specifically, if sidelobes are suppressed to -30 dB peak level below mainlobe, the mainlobe will be broadened by 30%. This assumes a Taylor weighting function. Further, phase and amplitude errors throughout the system will degrade resolution (broaden mainlobe) somewhat; a 5% allowance will be made for these errors. The

range bandwidth ΔF must then be commensurate with a resolution 35% better than the net desired resolution:

$$\Delta F = \frac{1.35}{\tau}$$

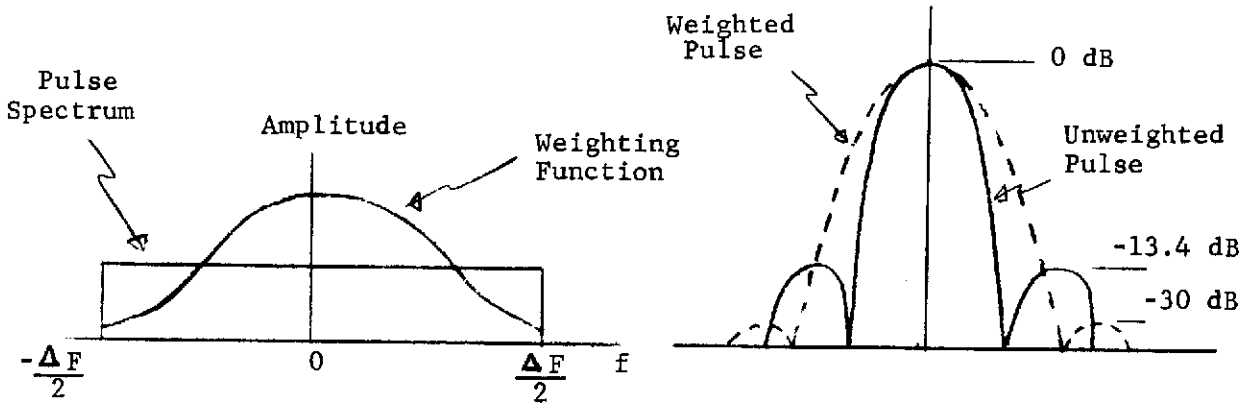

(a) Spectral Amplitude Weighting (b) Weighting Effects

Figure 3.2.3.3-2

Pulse Weighting

The resolution given by

$$r = \frac{c\tau}{2}$$

is the slant range resolution; the 30m resolution is a ground resolution, however. The difference between the two is depicted in figure 3.2.3.3-3.

From it,

$$r_g = \frac{r_s}{\cos\phi} = \frac{c\tau}{2\cos\phi}$$

where ϕ = depression angle

combining these equations,

$$\Delta F = \frac{1.35\ c}{2\cos\phi\ r_g}$$

$$= \frac{6.75\ \text{MHz}}{\cos\phi}$$

for r_g = 30m. This bandwidth is plotted in figure 3.2.3.3-4 as a function of depression angle. These would be the bandwidths required to yield 30m resolution commensurate with -30 dB peak sidelobe level. In

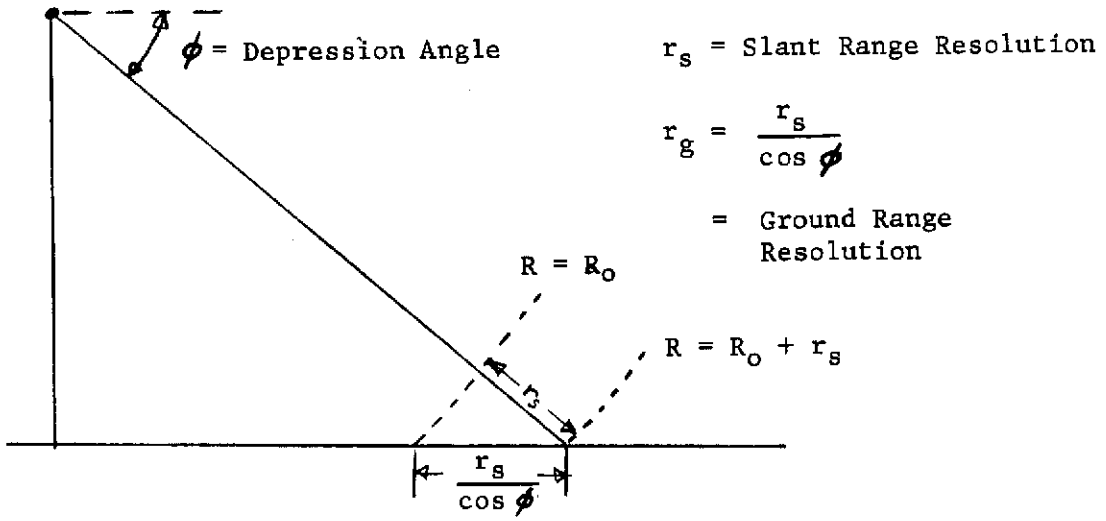

Figure 3.2.3.3-3

Slant and Ground Range Resolution

practice, only one bandwidth ΔF may be mechanized. Ground resolution will then be a function of depression angle. For example, if 60°

depression angle were taken as the reference for 30m resolution, then

$$\Delta F = 13.5 \text{ MHz}$$

and ground resolution will vary as in figure 3.2.3.3-5. Further, if 75° were taken as the reference, then

$$\Delta F = 26.0 \text{ MHz}$$

and ground range resolution will vary as in figure 3.2.3.3-5.

In conclusion, the required range bandwidth to achieve 30m ground range resolution and -30 dB peak sidelobe level lies in the interval

$$13.5 \text{ MHz} < \Delta F < 26 \text{ MHz}$$

for the depression angles of interest. At some depression angles resolution is better than 30m; if constant 30m resolution is desired here, the pulses may be sloughed as need be.

In section 3.2.3.4.2, the expanded pulsewidth T is derived to have values

$$10 \ \mu s < T < 16.7 \ \mu s$$

The product of expanded pulsewidth T and doppler bandwidth ΔF is the range signal time-bandwidth product TBP.

$$\begin{aligned} TBP &= T\Delta F \\ &= (16.7 \ \mu s)\ (26 \text{ MHz}) \\ &= 435 \end{aligned}$$

This is the largest TBP that would be encountered, and 250 is the smallest; generating and compressing signals of this TBP are well

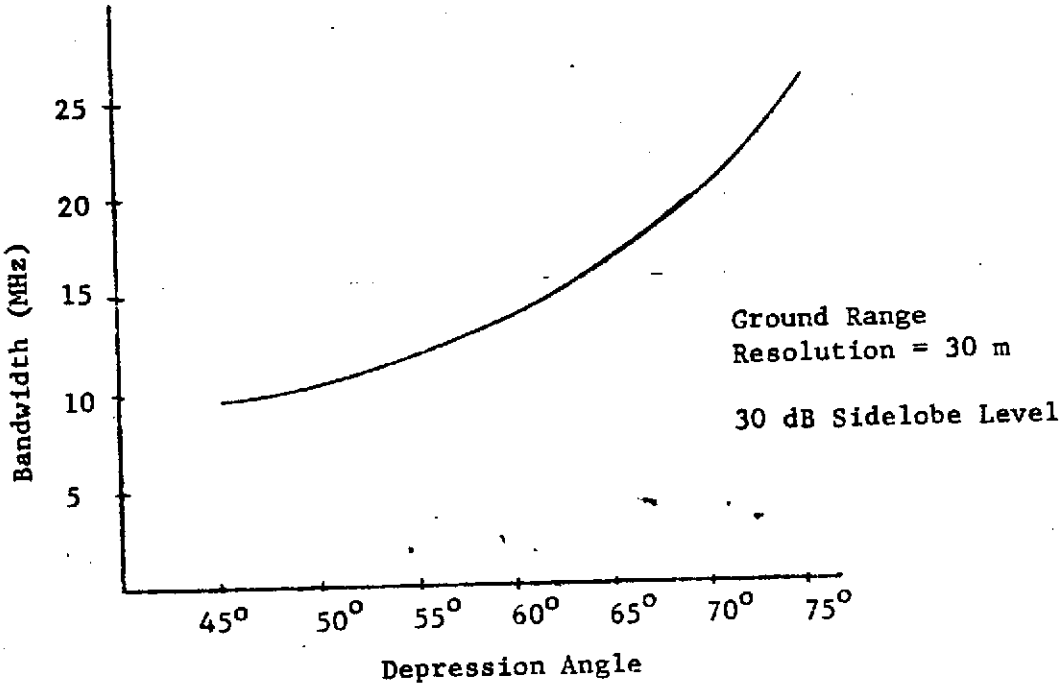

Figure 3.2.3.3-4. Bandwidth vs. Depression Angle

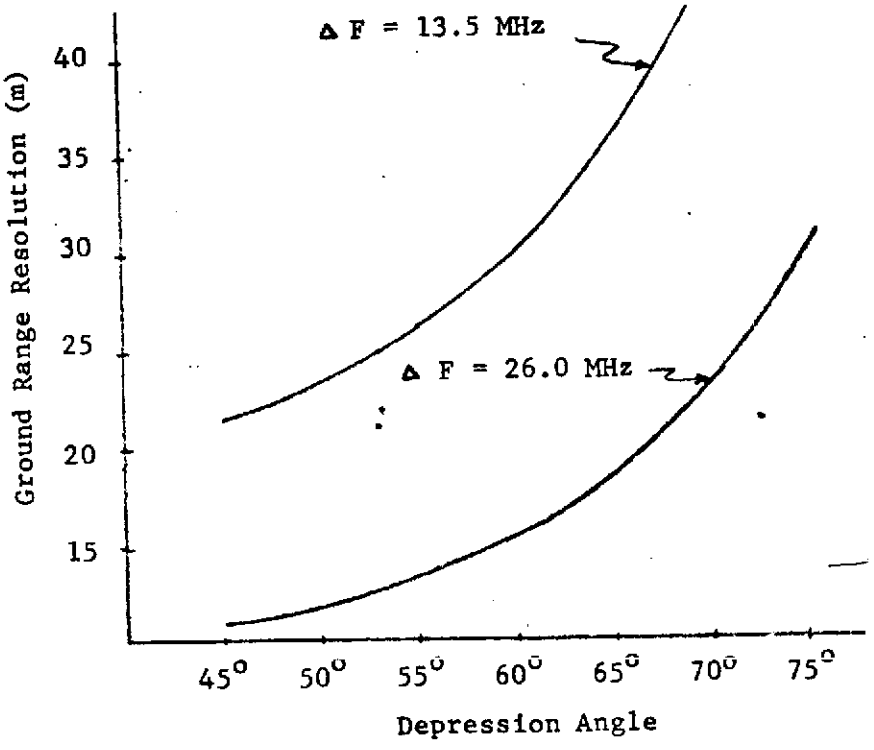

Figure 3.2.3.3-5. Ground Range Resolution vs. Depression Angle

within the state-of the-art.

Nothing prohibits designing the radar for ground range resolutions of 10-20m. For 10m resolution, the required chirp bandwidth would be on the order of 40 MHz $\lesssim \Delta F \lesssim$ 88 MHz depending upon depression angle. For 20m resolution, 27 MHz $\lesssim \Delta F \lesssim$ 52 MHz. These bandwidths are all readily mechanized, but limitations on achievable TBP may preclude use of bandwidths greater than about 45 MHz.

3.2.3.3.2 Azimuth Resolution

Synthetic aperture techniques must be used to achieve 30m azimuth resolution. Real beam mapping would provide resolutions of only

$$r = R\theta$$
$$\approx 1000 \text{ km} \cdot \frac{3\text{cm}}{8\text{m}}$$
$$\approx 5 \text{ km}$$

Unfocussed processing[1] would yield only

$$r = 1/2 \sqrt{\lambda R}$$
$$\approx \sqrt{3\text{cm} \cdot 1000 \text{ km}} \Big/ 2$$
$$\approx 100 \text{ m}$$

Hence synthetic aperture must be used for 30m azimuth resolution.

As in the case of range compression, a given bandwidth ΔF must be collected and stored in the processor. This azimuth bandwidth is the bandwidth of the linear FM due to a target's doppler frequency change as the satellite flies past it. The required bandwidth for a given azimuth resolution is

$$\Delta F = \frac{v}{r}$$

where v = satellite velocity

= 7.6 km/sec

This velocity was calculated for a 914 km satellite altitude with a 100 min. orbit period.

The compressed azimuth response again has a sin x/x response with -13.4 dB peak sidelobe level. As in the case of range compressed pulses, these sidelobes can cause false targets on the map in azimuth and must be suppressed. Spectral amplitude weighting is used again, and a weighting that suppresses peak sidelobe level to -30 dB will broaden the mainlobe by 30% (see figure 3.2.3.3-2). Allowance must be made for resolution degradation due to phase and amplitude errors. A larger allowance, 10%, must be made for azimuth than for range since atmospheric anomalies can induce phase and amplitude errors over the azimuth signal history. The collected azimuth bandwidth ΔF must then be commensurate with a resolution 40% better than the desired resolution to account for these degradations:

$$\Delta F = 1.4 \frac{v}{r}$$

For 30m azimuth resolution, then,

$$\Delta F = 1.4 \quad \frac{7.6 \text{ km/sec}}{30\text{m}}$$

$$= 355 \text{ Hz}$$

This is the doppler bandwidth required for processing 30m azimuth resolution with -30 dB peak sidelobe level. The doppler bandwidth available for processing defined by the antenna azimuth pattern is

$$\Delta F_o \approx 0.7 \frac{2v}{\lambda} \frac{\lambda}{d}$$

$$= 0.7 \frac{2 \cdot 7.6 \text{ km/sec}}{8\text{m}}$$

1. L. J. Cutrona, "Synthetic Aperture Radar," in MI.I. Skolnik, Radar Handbook, McGraw-Hill, 1970, p. 23-5.

$\approx$1.4 KHz (4 dB bandwidth)

This is shown in figure 3.2.3.3-6. The available doppler bandwidth thus greatly exceeds the required bandwidth. These conclusions apply to both X and L band systems.

The integration time T is the time required to collect a doppler bandwidth ΔF. The doppler frequency time rate of change, df/dt, for the linear FM is

$$\frac{df}{dt} = \frac{2v^2}{\lambda R}$$

The required integration time is then

$$T = \frac{\lambda R}{2v^2} \Delta F$$

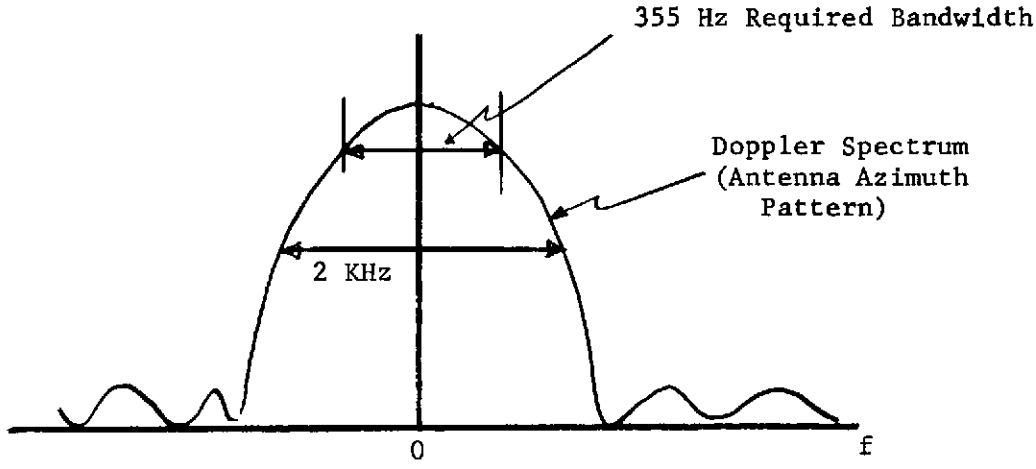

Figure 3.2.3.3-6

Doppler Bandwidths

This is plotted in figure 3.2.3.3-7 as a function of depression angle. Range was calculated as a function of depression angle using spherical earth geometry. Required integration time for X band operation is approximately 0.1 sec over the depression angels of interest; for L band operation the time increases to 0.5 - 0.7 sec.

The distant L that the satellite travels during an integration time is the synthetic aperture length:

$$L = VT$$

where V = satellite velocity

$= 7.6$ Km/sec

This is plotted as a function of depression angle in figure 3.2.3.3-8.

The product of integration time and doppler bandwidth is the azimuth signal time-bandwidth product TBP:

$$TBP = T\Delta F$$

$\approx$ (0.1 sec) (3.55 Hz)

= 35.5 X Band

$\approx$ (.5 sec) (355 Hz)

= 180 L Band

As TBP increases, the complexity of a digital processor also increases; the L band processor must be more complex than the X band processor. This is discussed in section 5.2.

Since the available doppler bandwidth, approximately 1.4 KHz, exceeds the required bandwidth for 30m resolution, 355 Hz, azimuth resolution better than 30m may be processed if desired. The optimum azimuth resolution achievable is

$$r_{AZ} = 30\text{m} \frac{355 \text{ Hz}}{1.4 \text{ KHz}} = 7.5\text{m}$$

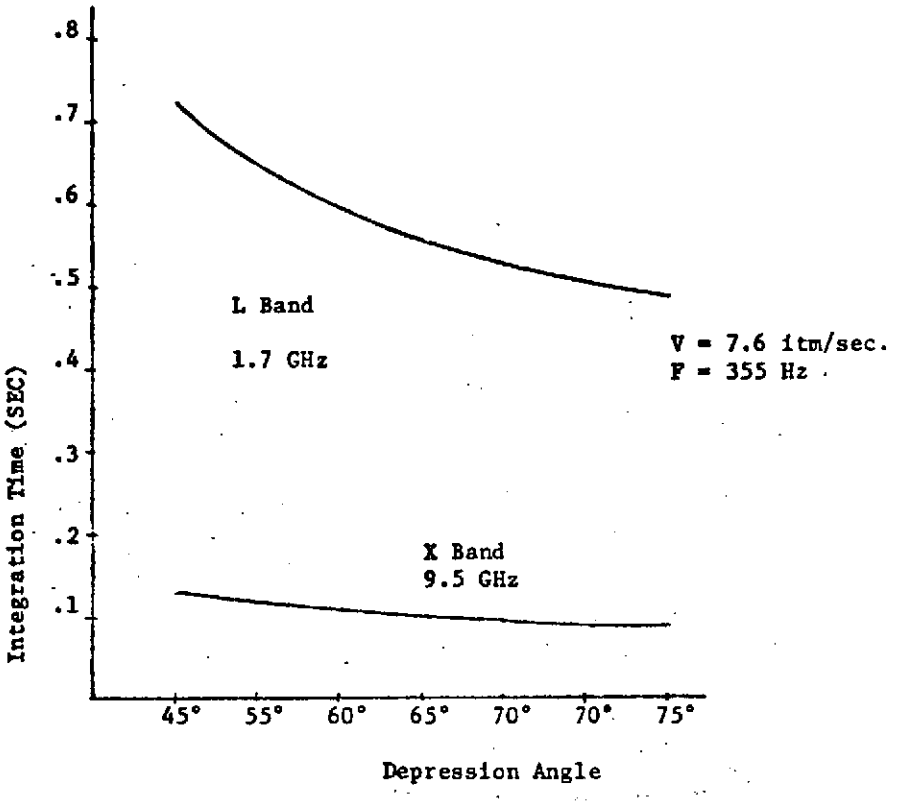

Figure 3.2.3.3-7. Azimuth Integration Time vs. Depression Angle

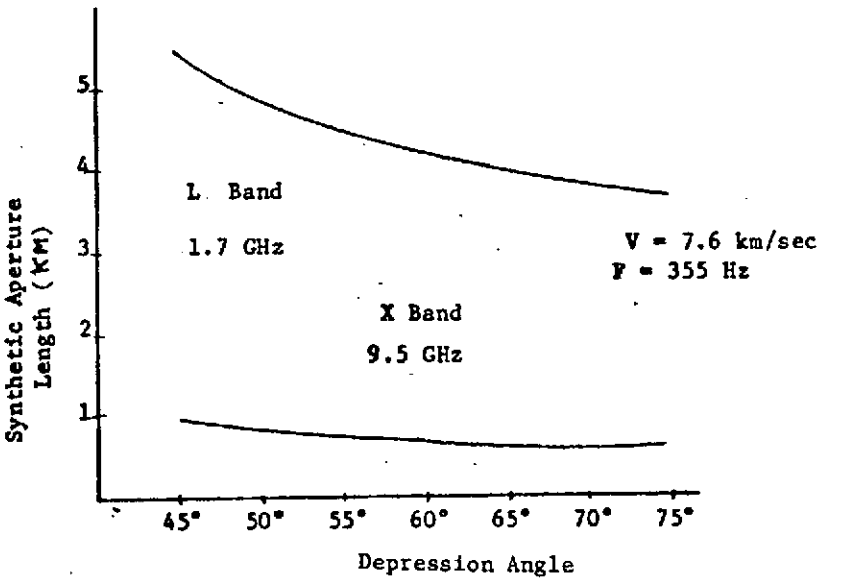

Figure 3.2.3.3-8. Synthetic Aperture Length vs. Depression Angle

Thus, 10m or 20m azimuth resolution could be achieved by changing ground processor algorithms. By processing for better azimuth resolution, the map smoothing effects of azimuth multilook are reduced or even lost (section 3.2.3.5).

3.2.3.4 Signal/Noise Ratio

Providing imagery that is of earth resources exploitation quality requires signal/noise (S/N) ratios of 3-10 dB on a low reflectivity background such as 3" grass (section 3.1). This is in accordance with previous Westinghouse experience with the APQ-97 earth resources radar. These S/N ratios will insure that various terrain types, such as agricultural fields, may be readily identified and distinguished from one another. With S/N ratios of 0-3 dB or below, distinguishing terrain types and features from each other and from noise can become very difficult or even impossible. The S/N of interest is, of course, that of area targets, not point targets.

This section will make three sample S/N calculations: one for an X band radar with a 13.5 ft. antenna azimuth aperture, one for an X band radar with a 27 ft. antenna azimuth aperture, and one for an L band radar with a 27 ft. antenna azimuth aperture. These systems are listed in Table 3.2.3.4-1.

The S/N calculation must include the effects of multilook (section 3.2.3.5). In the analysis below, S/N will be first calculated for single look operation, and the effects of multilook will then be added.

3.2.3.4.1 Signal/Noise Equation

The S/N equation for any synthetic aperture radar, for a single look, is

$$\frac{S}{N} = \frac{P_{ave}\, G^2\, \lambda^2\, \sigma}{(4\pi)^3\, kT_o\, \Delta f\, \overline{NF}\, L\, R^4}$$

TABLE 3.2.3.4-1

CONFIGURATION PARAMETERS

f_o GHz	cm	A_{AZ} ft	A_{EL} ft	P_{ave} w	P_{pk} kw	T us	PRF KHz	G dB
9.5	3.16	13.5	2.5	150	4.0	10.1	3.7	44.9
9.5	3.16	27.0	2.5	150	4.5	11.1,16,7	3.0,2.0	47.9
1.7	17.6	27.0	2.5	25	0.75	11.1	3.0	32.0

A_{AZ} = antenna azimuth aperture

A_{EL} = elevation aperture

Antenna gain G includes spillover losses.

Where P_{ave} = average transmitter power

G = one-way peak antenna gain

λ = transmitted wavelength

σ = target cross-sectional area (area targets)

kT_o = -204.4 dBw

Δf = correlator bandwidth

$\overline{NF}$ = system noise figure

L = system losses

R = slant range to target

This relation is derived in Appendix A.

3.2.3.4.2 Average Transmitter Power

In satellite operation average power must be minimized consistent with detection requirements. This relaxes requirements on satellite prime power generating capacity and eases the thermal energy dissipation problem. Peak transmitter power must also be minimized to avoid the large voltages associated with large peak powers and to increase transmitter reliability. Average and peak transmitter power are related by

$$P_{ave} = P_{pk} \quad Tf_R$$

T = transmitted pulsewidth

f_R = PRF

The PRF was chosen almost solely on the basis of maximizing swath width as a function of depression angle while maintaining a given ambiguity suppression (section 3.2.3.6).

Initial analysis showed that the X band radars (both 13.5 ft. and 27 ft. azimuth aperture radars) require 150w average power to achieve the detection goals. As a net transmitter efficiency of 20%, transmitter prime power consumption is 750w, which is an acceptable value. A peak power of 5 KW or less will pose no high voltage or special reliability problems.

If the antenna azimuth aperture is 13.5 ft, the PRF must be 3.7 KHz to avoid ambiguity problems (section 3.2.3.6). For a peak power of 4.0 KW peak power tube,

$$T_1 = \frac{150}{4.5 \text{ KW} \cdot 3.0 \text{ KHz}}$$

$$= 11.1 \text{ us}$$

and

$$\frac{150\text{W}}{}$$

$$= 4.5 \text{ KW} \cdot 2 \text{ KHz}$$

$$= 16.7 \text{ us}$$

A change in pulsewidth was required here to maintain acceptable average power.

For the L band radar, only 25W average power is required to meet detection goals. For a 27 ft. antenna azimuth aperture, the PRF must be 3.0 KHz. With a peak power of 750W,

$$T = \frac{25\text{W}}{750\text{W} \cdot 3.0 \text{ KHz}}$$

$$= 11.1 \text{ us}$$

In conclusion, this section has demonstrated that sets of average powers, peak powers, pulsewidths, and PRF's with acceptable and mechanizable values can be found. The average and peak powers are low enough to be compatible with satellite operation, and the average

power yields the desired S/N ratios as will be demonstrated shortly. The PRF's were determined on the basis of maximizing swath width while maintaining a given ambiguity suppression; this is fully discussed in section 3.2.3.6. These values are summarized in Table 3.2.3.4-1.

3.2.3.4.3 Wavelength

The X band radar frequency is 9.5 GHz. The wavelength is then

$$\lambda = \frac{c}{f}$$

$$= \frac{3 \cdot 10^8 \text{ m/sec}}{9.5 \text{ GHz}}$$

$$= 3.16 \text{ cm}$$

$$= 0.103 \text{ ft.}$$

The L band radar frequency is 1.7 GHz, with a corresponding wavelength of $\lambda = 17.6$ cm

$$= 0.578 \text{ ft.}$$

3.2.3.4.4 Antenna Gain

The maximum allowed antenna size is 27 ft. in azimuth by 2.5 ft. in elevaiton. The peak one-way gain is then

$$G = 4\pi \frac{A}{\lambda^2}$$

$$= 4\pi \frac{27 \text{ ft.} \cdot 2.5 \text{ ft}}{(.103 \text{ ft.})^2}$$

$$= 49.0 \text{ ft.} \quad \text{X band}$$

$$= 4\pi \frac{27 \text{ ft.} \cdot 2.5 \text{ ft.}}{(0.578 \text{ ft.})^2}$$

$$= 34.1 \text{ dB} \quad \text{L band}$$

If the azimuth aperture is reduced to 13.5 ft. for the X band radar,

$$G = 46.0 \text{ dB}$$

The apertures were not intentionally weighted. The relatively narrow

elevation aperture does not, however, intercept the entire feed horn beam; this results in a spillover loss. Further, the feed horn beam may or may not uniformly illuminate the aperture. As the weighting becomes more uniform, spillover loss increases. In the X band radars, spillover loss was minimized by not uniformly weighting the elevation aperture with the feed horn beam. Spillover loss was then 1.1 dB, and the weighted two-way elevation pattern had -32 dB peak sidelobe level instead of -26 dB. In the L band radar, where S/N is not critical and narrow elevation beamwidth is (section 3.2.3.6), the feed horn beam uniformly illuminated the elevation aperture with a resultant 2.1 dB spillover loss. The net peak one-way gains are then

G = 47.9 dB X Band, 27 ft.

G = 32.0 dB L Band, 27 ft.

G = 44.9 dB X Band, 13.5 ft.

These values are summarized in Table 3.2.3.4-1.

Antenna gain patterns are given in section 3.3.5.2.2.

3.2.3.4.5 Target Cross-Sectional Area

The cross-sectional area σ of interest here is for area targets, not point targets:

$$\sigma = \sigma_o A$$

$$= \sigma_o \, r_R \, r_{AZ}$$

$$= \sigma_o \frac{c \tau}{2 \cos \phi} r_{AZ}$$

where

σ_o = equivalent target cross-section per unit area

A = area of resolution cell

At X-band σ_o for 3" grass, a terrain type of very low backscatter is -20 dB at 75° depression angle, and it decreases to -25 dB at 45° depression angle.[1] At L band, σ_o is -5 dB for 3" grass at 75° depression angle.[2] This data indicates that the altitude line is much wider at L band than at X; this greater L band σ_o accounts for the fact that the L band transmitter requires much less power than the X band transmitter. If the L band radar operated at shallower depression angles than 75°, where σ_o is approximately -25 dB for 3" grass, it would require more power than the X band radar. Due to ambiguity constraints, however, the L band radar operates at 75° depression angle only (section 3.2.3.6). The only terrain types that backscatter less energy than 3" grass are deserts, bodies of water, and concrete or asphalt roads and runways.

The range and azimuth resolutions used to determine the resolution cell area are not the 30m final resolutions, but instead are the unweighted resolutions (spectral amplitude weighting does not improve S/N):

$$r_R = \frac{C/2}{\Delta F_R} \quad \frac{1}{\cos \phi}$$

$$r_{AZ} = \frac{V}{\Delta F_{AZ}}$$

For X and L band radars (section 3.2.3.3.2)

$$r_{AZ} = \frac{7.6 \text{ km/sec}}{355 \text{ Hz}}$$

$$= 21.4 \text{ m}$$

1. Private communications with R.K. Moore, University of Kansas.

2. R. K. Moore, "Ground Echo" in M.I. Skolnik, Radar Handbook, MdGraw-Hill, 1970, p.25-30.

Range resolution, as discussed in section 3.2.3.3.1, can assume many values depending upon the design. For example, if the chirp bandwidths were 26 MHz, unweighted range resolution would be 22.2m at 75° depression angle and would improve at shallower depression angles. Pulses could be sloughed, however, to yield 22.2m over all depression angles. Further, if the bandwidth were 13.5 MHz, unweighted resolution would be 22.2m at 60° depression angle. It would degrade at steeper depression angles. To simplify this analysis, range resolution will be taken as

$$r_R = 22.2\text{m}$$

over all depression angles. Actual variations from this assumption do not alter any detection conclusions reached here.

3.2.3.4.6 Noise Figure

A very low noise paramp will be used at the receiver front end for both L and X band radars. The overall system noise figure will then be 1.7 dB. Without this or any other paramp, noise figure would be 5-6 dB. This additional 4 dB loss could have been compensated only by increasing transmitter power, which is distinctly disadvantageous.

3.2.3.4.7 System Losses

System Losses consist of RF, atmospheric, and weighting losses. No field degradation loss was alloted since only a single system is involved here. Beamshape loss is negligible for a single look (see section 3.2.3.5).

The RF losses consist of contributions from antenna feed lines, waveguide, circulator, and receiver protector. These losses are itemized in Table 3.2.3.4-2. The total RF losses are:

RF = 2.8 dB, X Band, 13.5 ft. Antenna

RF = 4.0 dB, X Band, 27 ft. Antenna

RF = 1.4 dB, L Band, 27 ft. Antenna

Weighting losses arise when spectral amplitude weighting is applied to range and azimuth signals to suppress compressed response sidelobes (see sections 3.2.3.3.1 and 3.2.3.3.2). Each signal will be weighted for 30 dB sidelobe suppression; this corresponds to a 1 dB S/N loss in range and azimuth for a 2 dB total weighting loss.[1]

Several atmospheric conditions were studied to compile an atmospheric loss value. Normal (clear sky) gaseous absorption for the satellite geometry was calculated from atmospheric data to be 0.25 dB at X band and completely negligible at L band.[2] Cloud attenuation is a function of cloud temperature, density and size.[3] From this data, cloud attenuation is calculated to be on the order of 0.4 - 1.0 dB at X-band and from 0 - 0.2 dB at L band. Rainfall contributes additional loss. Assuming a two-way radar signal path through rainfall of 5 km, X-band loss for light rainfall (1 mm/hr) will be about 0.1 dB, and L-band loss will be negligible.[1] For moderate rainfall (4 mm/hr), this loss increases to about 0.25 dB at X band.

A 1.0 dB X band and 0.2 dB L band atmospheric loss will then account for normal gaseous absorption, reasonably heavy cloud cover, and light rainfall. These will be taken as the nominal atmospheric losses.

---

1. E. C. Farnett, T. B. Howard, and G. H. Stevens, "Pulse Compression Radar", in MI.I. Skolnik, Radar Handbook, McGraw-Hill, 1970, p.20-31.
2. B. R. Dean, E. J. Dutton, and B. D. Warner, "Weather Effects on Radar," in MI.I. Skolnik, Radar Handbook, McGraw Hill, 1970, p.24-18.
3. Ibid, p.24-22.

Actually, rainfall must become quite severe (16 mm/hr) before moderate degradation of map imagery occurs (3 dB or greater S/N loss); an additional 1 dB or so loss for moderate to heavy rainfall is barely noticeable with high S/N imagery such as is provided by these systems.

The net system losses are then:

L = 7.0 dB X band, 27 ft. antenna

L = 3.6 dB L band, 27 ft. antenna

L = 5.8 dB X band, 13.5 ft. antenna

Losses are summarized in Table 3.2.3.4-2.

3.2.3.4.8 Range

The slant range to the target, the earth in this case, is a function of antenna depression angle. Range was calculated for a spherical earth using the geometry of figure 3.2.3.4.-1. In this figure,

R_E = mean earth radius = 6371 km

H = satellite altitude = 914 km

$\emptyset$ = depression angle

1. Skolnik, M. I., Introduction to Radar Systems, McGraw-Hill, 1962, p.544.

TABLE 3.2.3.4-2

SYSTEM LOSSES

LOSS	SYSTEM		
	X BAND 13.5 ft.Aperture	X BAND 27 ft.Aperture	L BAND 27 ft.Aperture
Antenna Feed Line (two-way)	0.8 dB	1.6 dB	0
Waveguide (two-way)	0.6 dB	1.0 dB	0
Circulator (two-way)	0.8 dB	0.8 dB	0.8 dB
Receiver Protector	0.6 dB	0.6 dB	0.6 dB
Total RF	2.8 dB	4.0 dB	1.4 dB
Range	1.0 dB	1.0 dB	1.0 dB
Azimuth	1.0 dB	1.0 dB	1.0 dB
Atmosphere	1.0 dB	1.0 dB	0.2 dB
Total	5.8 dB	7.0 dB	3.6 dB

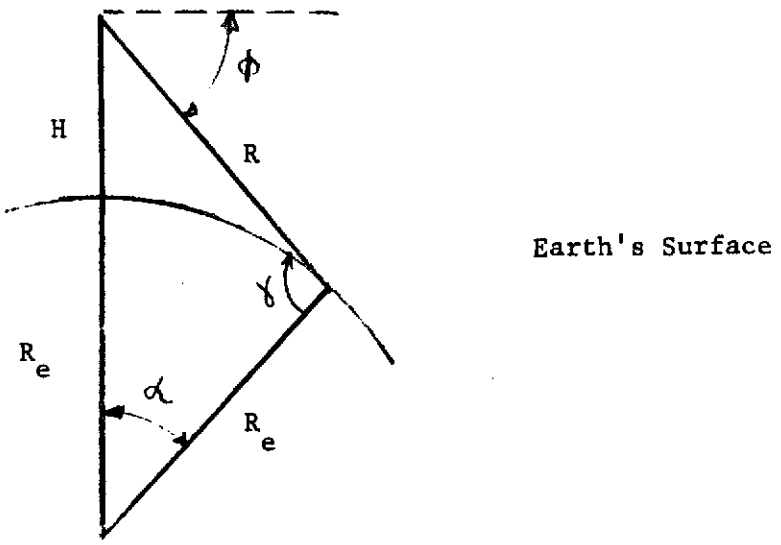

Figure 3.2.3.4-1

Spherical Earth Geometry

Then

$$\frac{\sin \gamma}{R_E + H} = \frac{\cos \phi}{R_E}$$

$$\text{Sin } \gamma = (1 + H/R_E) \cos \phi$$

$$\frac{\text{Sin} \alpha}{R} = \frac{\cos \phi}{R_E}$$

and $R = R_E \sin \alpha / \cos \phi$

Range as a function of depression angle is given in figure 3.2.3.4-2.

3.2.3.4.9 Correltor Bandwidth

The correlator bandwidth is the inverse of the coherent azimuth integration time:

$$\Delta f = \frac{1}{T} = \frac{2V r_{AZ}}{\lambda R}$$

where V = satellite velocity = 7.6 km/sec

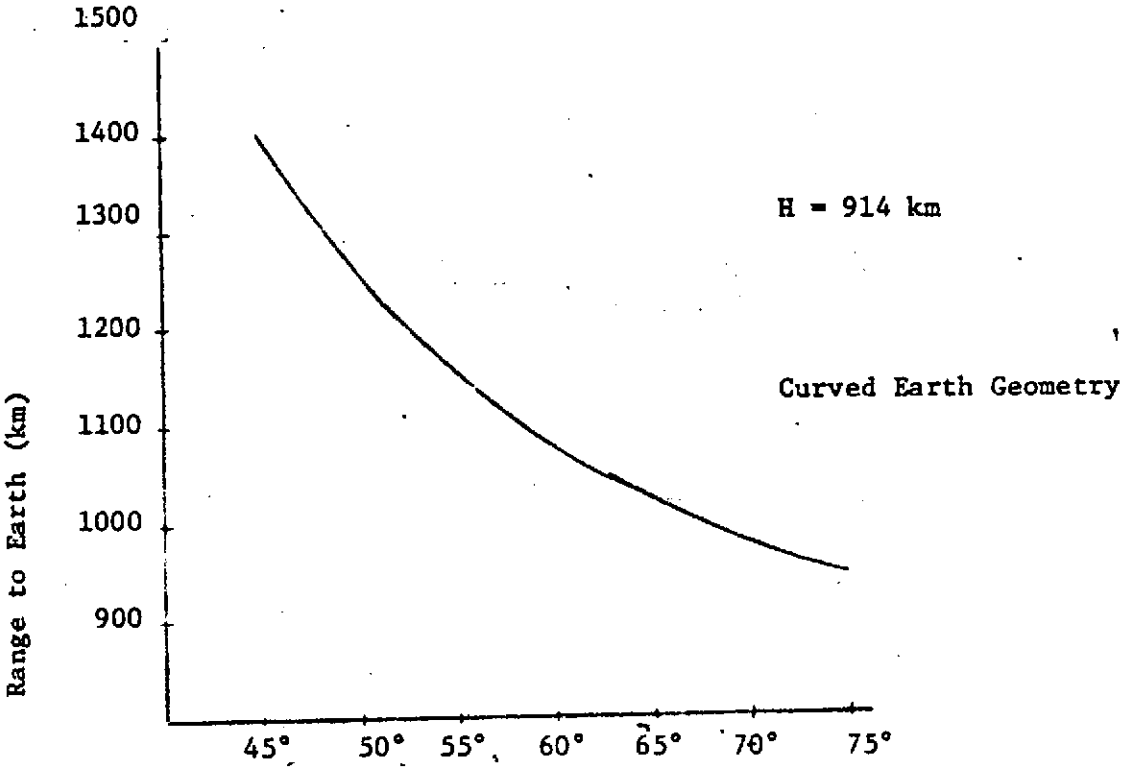

Figure 3.2.3.4-2. Slant Range To Earth Vs. Depression Angle

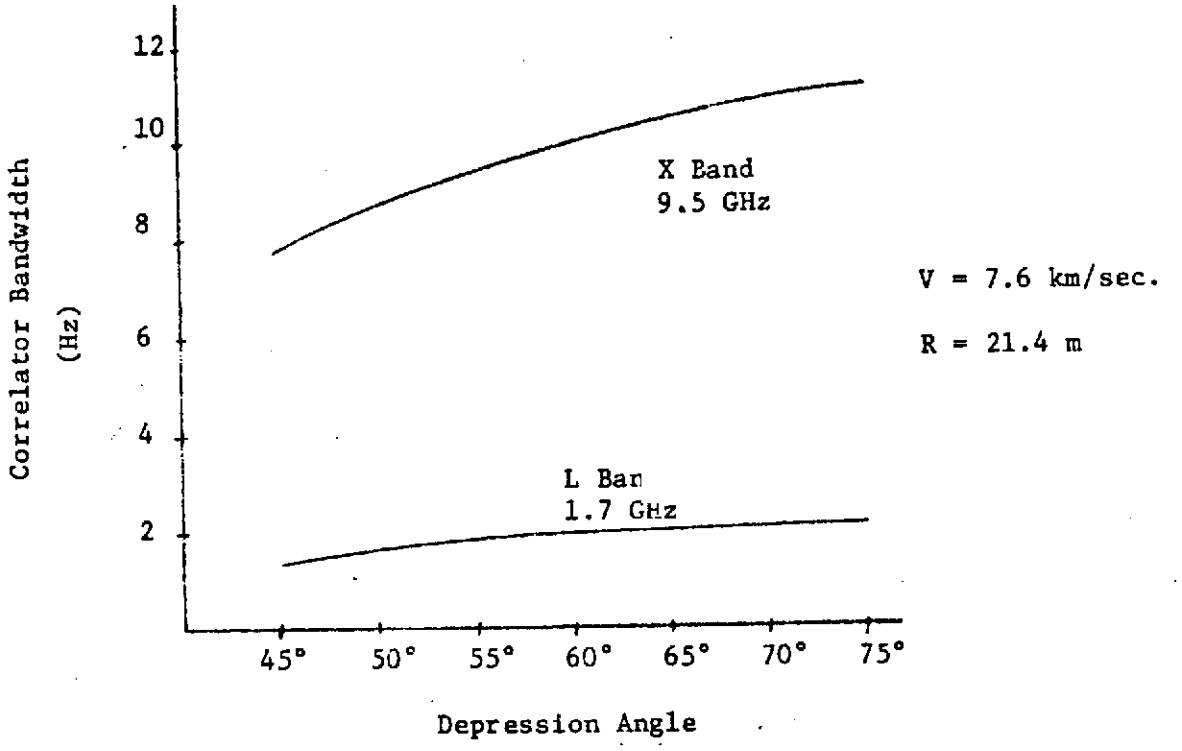

Figure 3.2.3.4-3. Correlator Bandwidth Versus Depression Angle

r_{AZ} = unweighted azimuth resolution

= 21.4m (section 3.2.3.4.5)

The coherent integration times were calculated in section 3.2.3.3.2 and are plotted in figure 3.2.3.3-7. The correlator bandwidths derived from them are plotted in figure 3.2.3.4-3.

3.2.3.4.10 Net Single Look S/N

When the expressions for target cross-sectional area of section 3.2.3.4.5 and for correlator bandwidth of section 3.2.3.4.9 are inserted into the S/N equation of 3.2.3.4.1

$$S/N = \frac{P_{ave}\, G^2 \lambda^2 \sigma}{(4\pi)^3\, kT_o\, \Delta f\, \overline{NF}\, L\, R^4}$$

$$\sigma = \sigma_o\, r_R\, r_{AZ}$$

$$\Delta f = \frac{2V\, r_{AZ}}{\lambda R}$$

$$S/N = \frac{P_{ave}\, G^2 \lambda^3\, r_R\, \sigma_o}{2(4\pi)3\, KT_o\, V\, \overline{NF}\, L\, R^3}$$

Note that S/N is an inverse function of R^3 now, and not R^4. S/N is a function of depression angle in that R is a function of depression angle. Also, although it was not assumed here, r_R may be a function of depression angle. Some of the relationships between S/N ratio and depression angle are discussed in Appendix B.

Figure 3.2.3.4-4 is a plot of S/N as a function of depression angle for the three radar systems discussed here. The parameters derived here in section 3.2.3.4 were used in the calculation. Specifically, this is single look, cneter of swath S/N ratio. The S/N at swath edge is discussed in section 3.2.3.6.

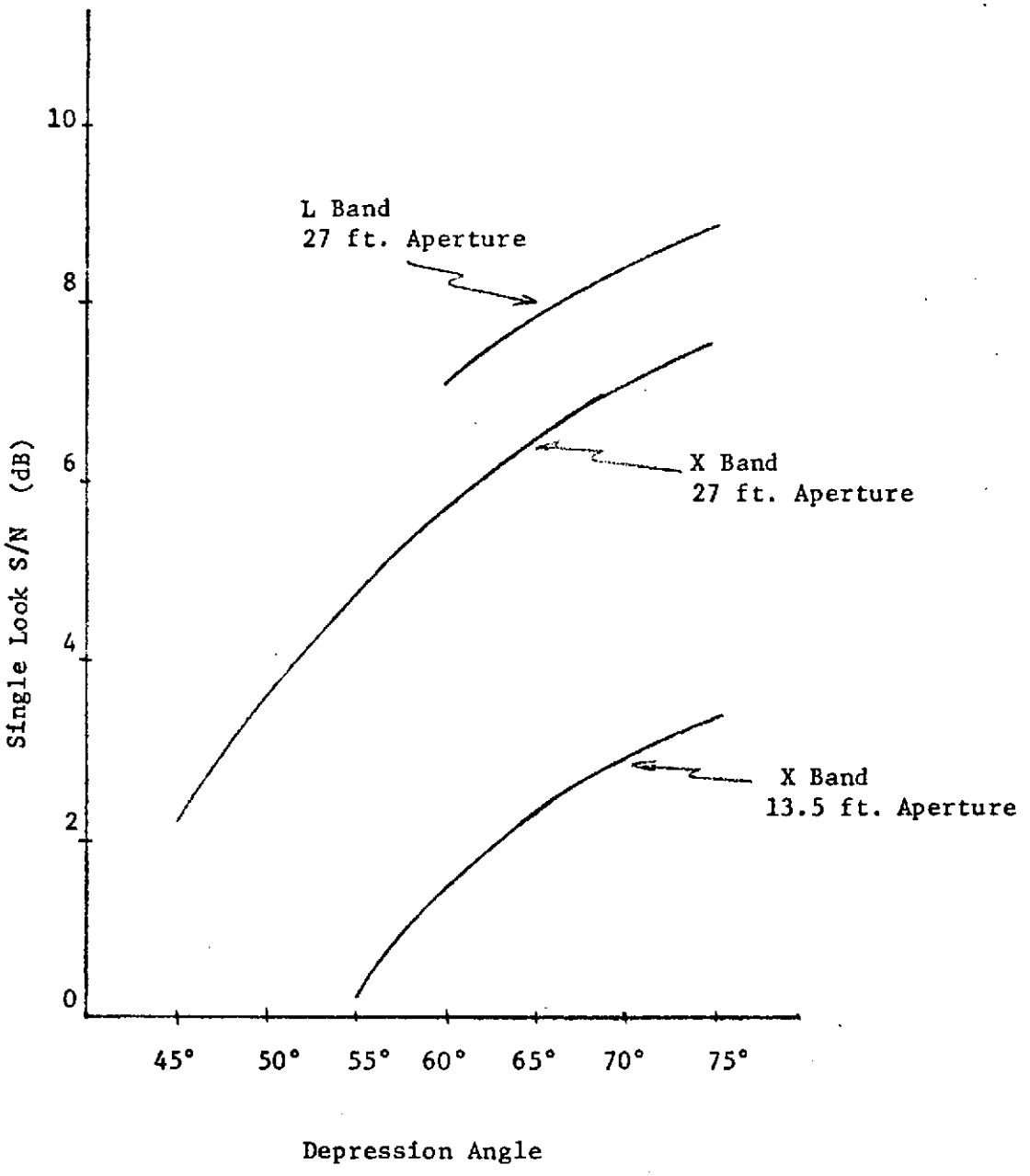

Figure 3.2.3.4-4. Single Look S/N vs. Depression Angle (S/N taken at swath center)

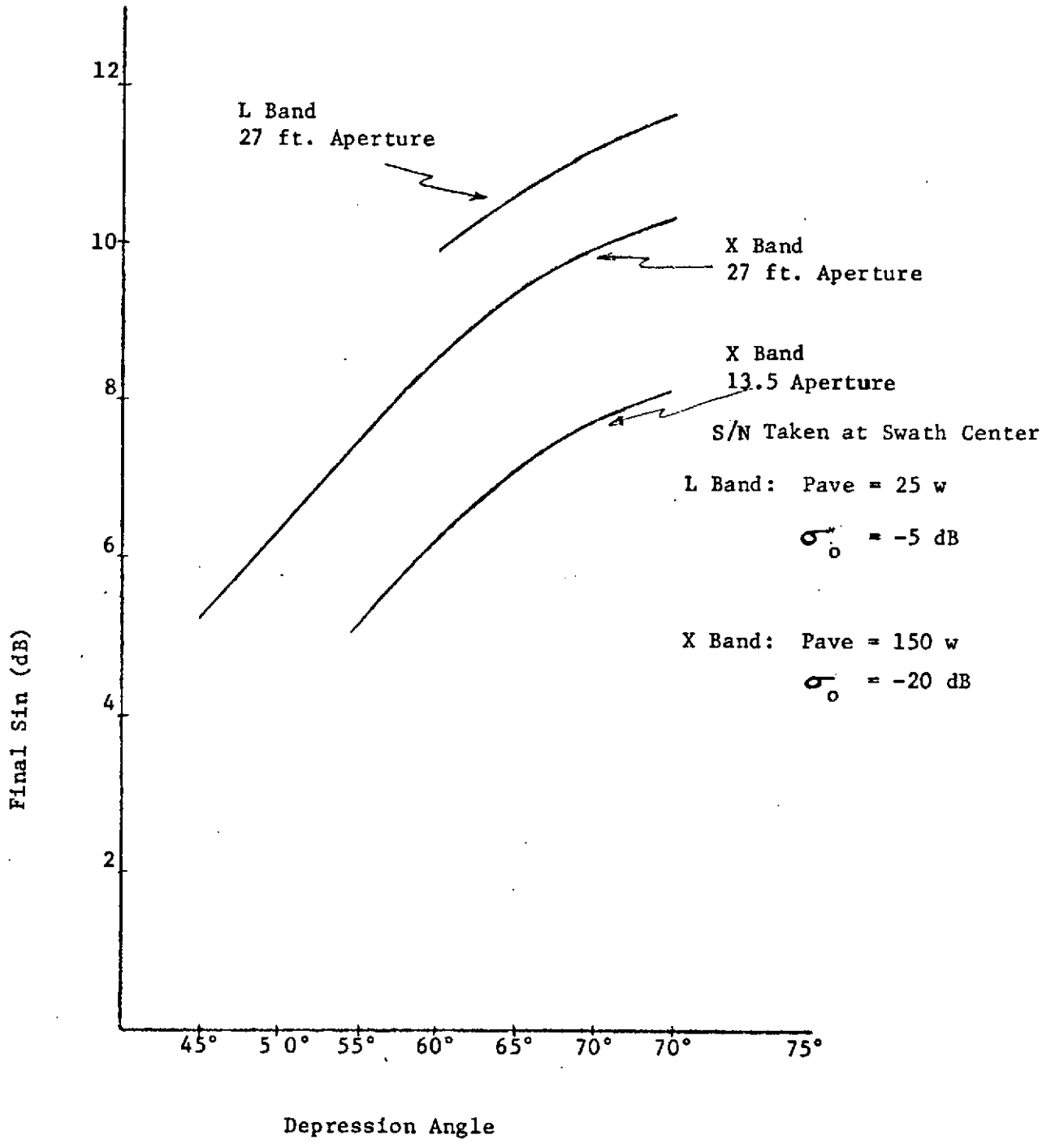

Figure 3.2.3.4-5. S/N vs. Depression Angle

The effects of multilook must now be added to the S/N calculation.

3.2.3.4.11 Final S/N Ratios

For 30m resolution in range and azimuth the system has azimuth multilook but no range multilook. The specific number of azimuth multilooks for the three systems considered here and the resultant S/N gains are given in Table 3.2.3.5-1. The subject of multilook and its associated gain is discussed in section 3.2.3.5. The specific multilook gains for 30m resolution are:

G = 4.8 dB X Band, 13.5 ft. Aperture

G = 2.6 dB X Band, 27 ft. Aperture

G = 2.8 dB L Band, 27 ft. Aperture

Figure 3.2.3.4-5 plots the final S/N ratios as a function of depression angle. These curves were calculated by adding the above multilook gain to the curves of figure 3.2.3-4. Again, these curves correspond to S/N at swath center. The S/N ratios vary from 5.0 dB to 11.5 dB; the goal of 3-10 dB S/N ratio against a weak backscatter target (3" grass) has then been met. These large S/N ratios are indicative of high quality imagery that is required for earth resources applications.

As a further illustration of these systems' detection capabilities, S/N as a function σ_o is plotted in figure 3.2.3.4-6. This was done for the X band system with a 27 ft. azimuth antenna aperture and a 60° depression angle. S/N is shown for three (square) resolution cell sizes: 30m, 60m, and 90m. The processor is extremely flexible; it can be adjusted to provide these or any other resolutions less than 30m. These curves include the multilook gains of Table 3.2.5-1. Several

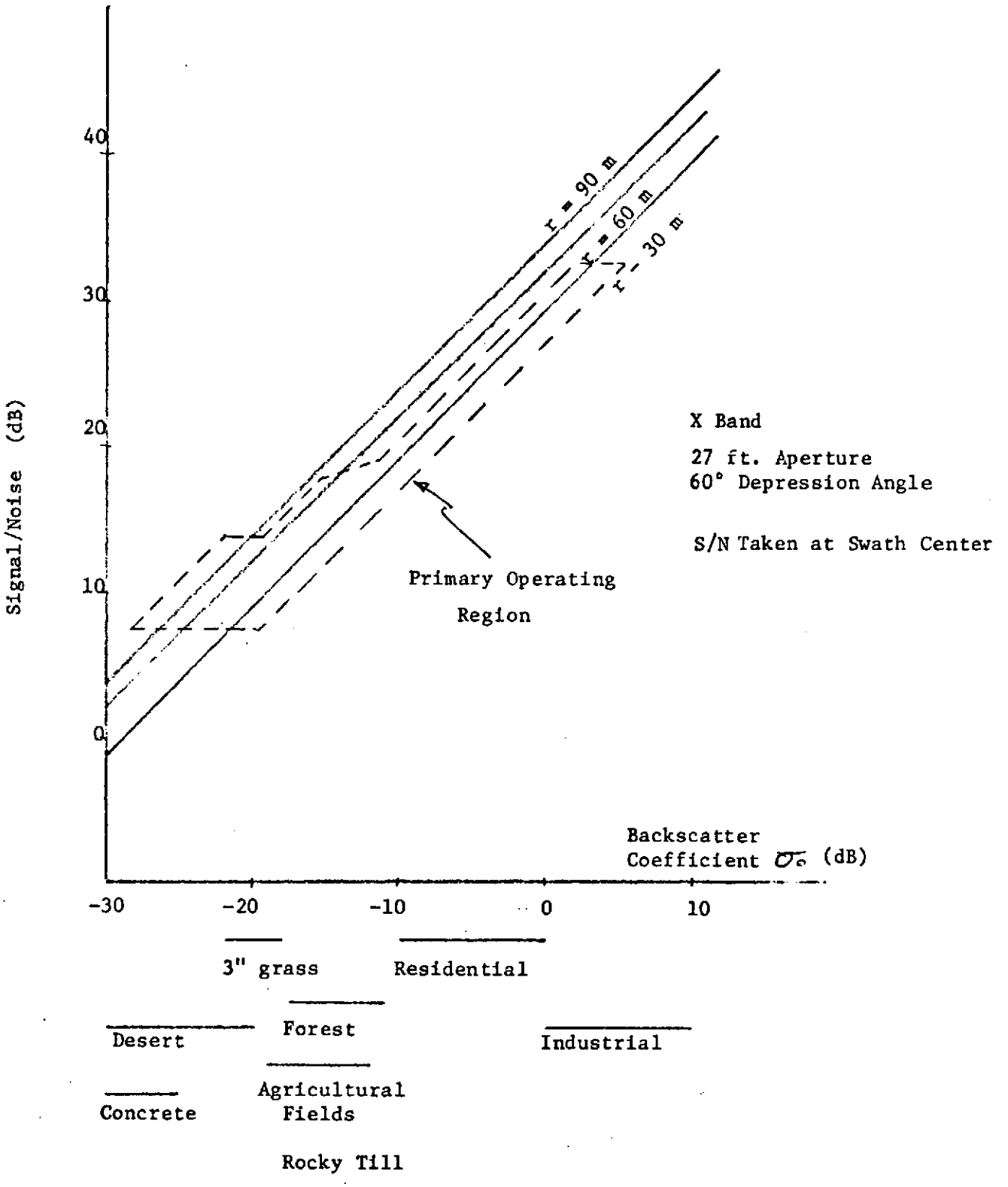

Figure 3.2.3.4-6. S/N vs. Backscatter Coefficient σ_o

terrain types, such as desert, agricultural fields, and industrial sites are located on the σ_o axis for convenience. The variations in σ_o for a given terrain type allow for individual variations, such as different types of agricultural fields and forests of varying density.

A primary operating region is sketched in figure 3.2.3.4-6. For cultural terrain, such as residential or industrial areas, the 30m cell would be processed. This cell size would also be used for agricultural fields, forests, and rocky hill type terrain. Grasslands and broken desert mapping requires less resolution; the 60m cell could be processed here. For smoother deserts, even less resolution is required, and a 90m resolution cell may be processed. For all of these terrain types, with the exception of very smooth deserts, this processing will result in S/N ratios of at least 9 dB. For many terrain types, the S/N is 15-20 dB or greater.

In conclusion, this section has derived the appropriate radar parameters required to provide the S/N ratios of figures 3.2.3.4-5 and 3.2.3.4-6. The pertinent parameters were summarized in Tables 3.2.3.4-1 and 3.2.3.4-2. The resultant S/N ratios are greater than 5 dB against a weak backscatter target (3" grass) for all systems and depression angles considered here. For stronger backscattering target, S/N can easily be 10-20 dB. These high S/N ratios will readily provide the high quality imagery required for earth resources applications.

3.2.3.5 Multilook

Extended targets are best modeled as being composed of many individual scattering centers. The net return signal is the sum of returns from each of these individual centers. The net signal level

seen at the radar depends upon the relative phases of each of the component signals, which determine how well the components add. These relative phases are random variables for rough (with respect to wavelength) surfaces; the amplitude of the return from a uniform clutter patch can then vary from one resolution cell to the next. The S/N equation of section 3.2.3.4.1 calculates a mean value of S/N; this effect results in a variance about this mean that can be several dB. If left uncompensated, this results in grainy maps with poor contrast between areas of similar backscatter properties. This effect is sometimes referred to as radar image speckling, or the "salt and pepper" image effect.

This graininess is very undesirable from the viewpoint of earth resources applications. Its presence makes the identification and classification of smaller area targets very difficult, if not impossible. To preserve high-quality imagery, as in the Westinghouse design, a method of smoothing the signal variance before displaying the map must be implemented. Two very effective methods of achieving this are azimuth and range multilook.

3.2.3.5.1 Azimuth Multilook

In azimuth multilook different portions of a target's doppler spectrum are processed independently and noncoherently added. Section 3.2.3.3.2 noted that more doppler spectrum was available than was required to process the desired azimuth resolution. The rest of this doppler spectrum may now be processed to form several azimuth looks. This is illustrated in figure 3.2.3.5-1 which shows a doppler spectrum divided into three bandwidths, or azimuth looks. Each individual

bandwidth is sufficient to process the desired azimuth resolution, and each corresponds to the same resolution cell position on the ground (when properly processed). Each look corresponds to a different observation angle to the cell; the scattering component phases are then random from look to look. Due to the nonoverlapping bandwidths of the azimuth looks, the looks are uncorrelated. Averaging these looks then results in a smoothing of the variance with a resulting improvement in contrast accuracy.

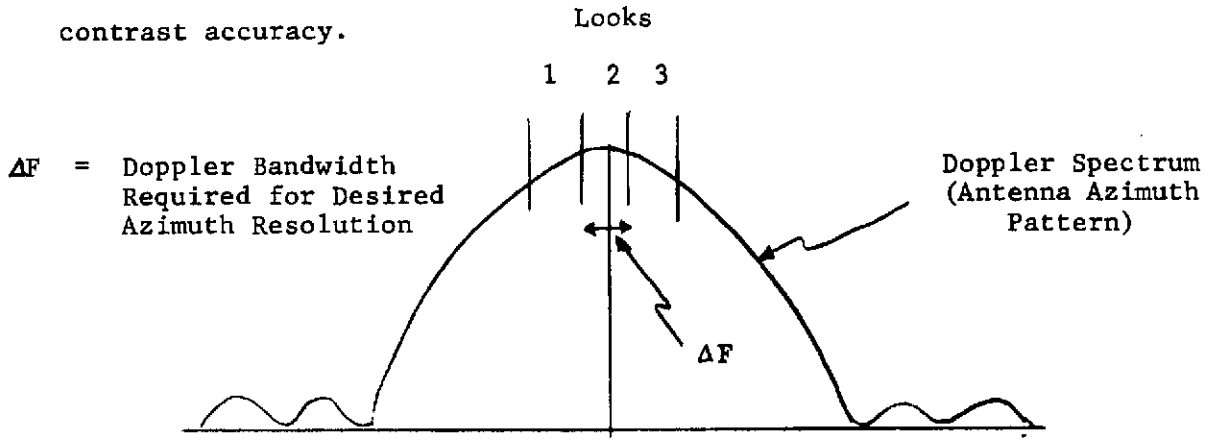

Figure 3.2.3.5-1

Azimuth Multilook

The three azimuth looks of figure 3.2.3.5-1 did not overlap in bandwidth. In these systems, however, each look has spectral amplitude weighting applied to reduce compressed response sidelobes. The 4 dB bandwidth of the weighted spectrum is approximately half of the total look bandwidth. To use the bandwidth most efficiently then, one additional look may be spaced between each pair, as in figure 3.2.3.5-2. Due to the spectral amplitude weighting, the adjacent looks are derived from essentially nonoverlapping bandwidths and as such remain uncorrelated. This type of multilook is used in these sytems.

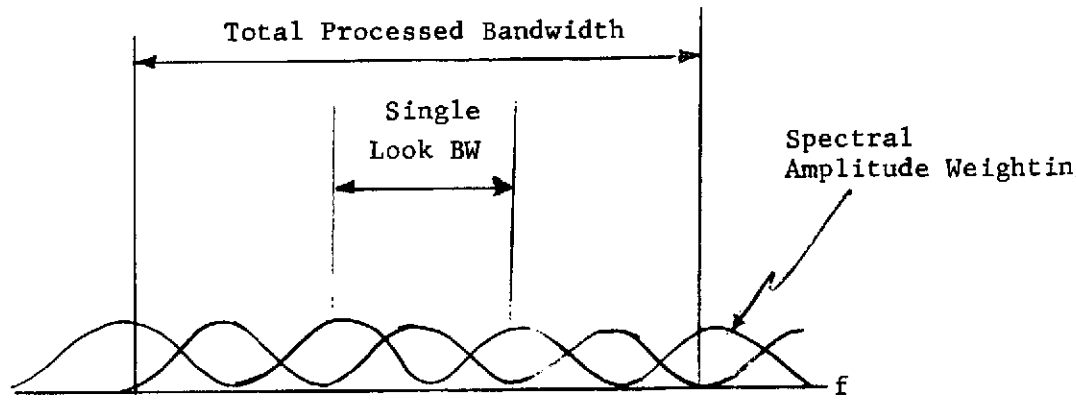

Figure 3.2.3.5-2

Overlapping Multilook

Multilook smoothing can be visualized with the aid of probability density functions. The map film density will be assumed to be Rayleigh (Gaussian pre-detection amplitude distribution). Figure 3.2.3.5-5a shows map film density distributions with no multilook for three signals: system noise, an area target with backscatter coefficient σ_o, and an area target with backscatter coefficient $2\,\sigma_o$. Due to the large variances, discrimination between the two targets and noise is difficult. In figure 3.2.3.5-5b, which shows the effects of multilook, the variances have been reduced, and target discrimination is much more accurate. This property is of extreme importance to earth resources applications.

3.2.3.5.2 Range Multilook

In range multilook the same sort of bandwidth manipulation may be done as in azimuth multilook. That is, three times as much chirp bandwidth (ΔF of section 3.2.3.3.1) may be mechanized as required. The return signal is then divided into three independent (nonoverlapping bandwidth) signals, each with one-third the original bandwidth. These are then independently processed and noncoherently added, as were the azimuth looks. Alternately, range multilook can be achieved by simply sloughing together contiguous range cells, figure 3.2.3.5-3. This does, of course, degrade range resolution, but it does provide the signal smoothing properties of multilook in that independent samples from a random field are summed together. Since some users desire resolutions degraded from 30m, the processor will be designed to slough range cells together. This sloughing will then provide range multilook. The design of mechanizing more chirp bandwidth than is required will not be implemented here.

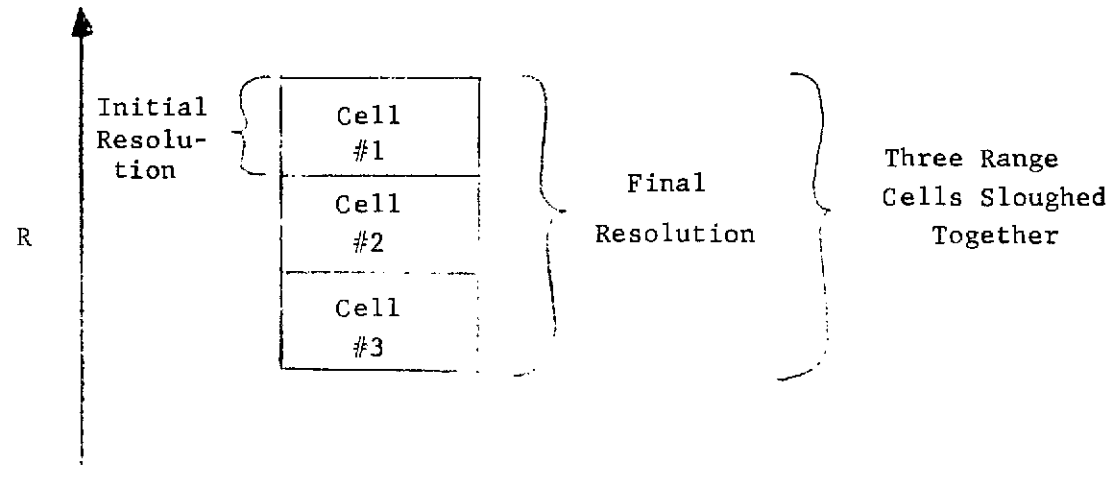

Figure 3.2.3.5-3
Range Multilook

3.2.3.5.3 Multilook Smoothing

The averaging of three individual looks together thus results in a smoothing of signal variance with a resultant increase in contrast accuracy. This effect is illustrated in figure 3.2.3.5-4 which shows a net signal level as a function of time as the satellite flies past two adjacent but different terrain types for both with and without multilook. The smoothing of the signal and resulting improvement in contrast accuracy make distinction of the two terrain types much easier. Westinghouse experience has shown that the untrained eye discerns

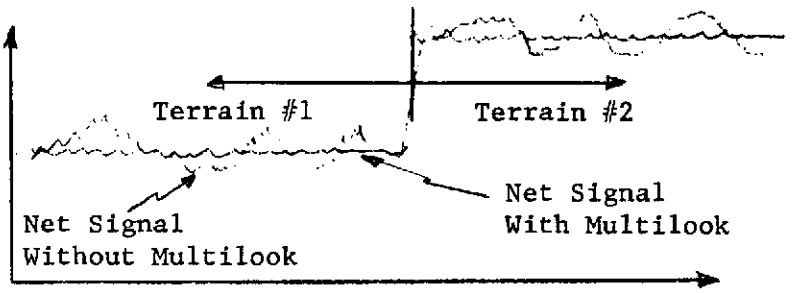

Figure 3.2.3.5-4. Contract Accuracy Improvement with Multilook

little contract accuracy improvement when more than four looks are averaged. For earth resource purposes, where investigators will be searching for small effects, as many looks as possible will be provided, with five being the absolute minimum provided. The effects of range and azimuth multilook are identical. The use of azimuth and range multilook has been discussed in the literature.[1]

[1] R. K. Moore and G. C. Thomann, "Imaging Radars for Geoscience Use,: IEEE Transactions on Geoscience Electronics, Vol. GE-9, No. 3, July 1971, pp. 155-164.

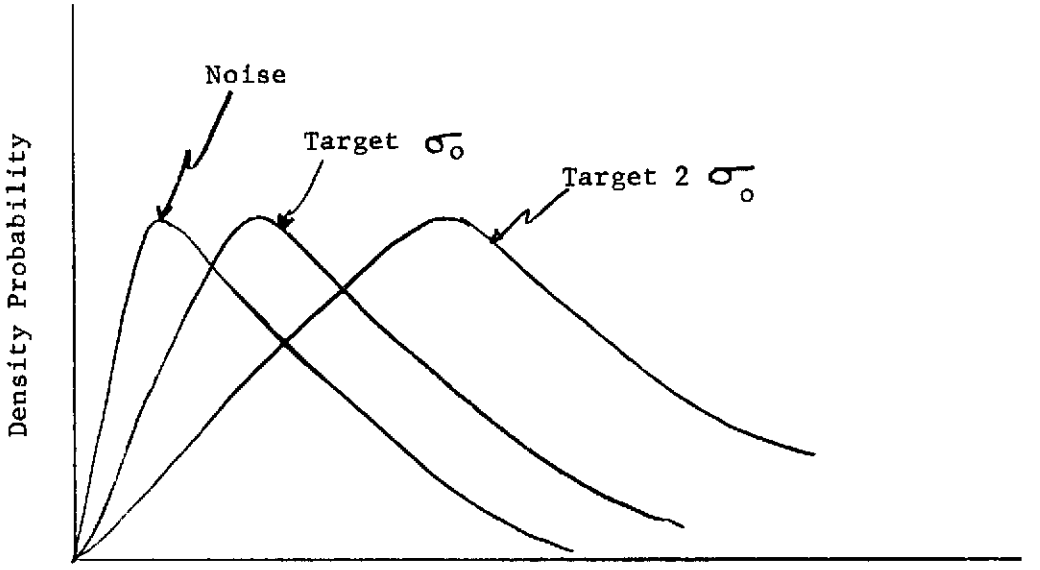

Figure 3.2.3.5-5a. Map Film Density with No Multilook

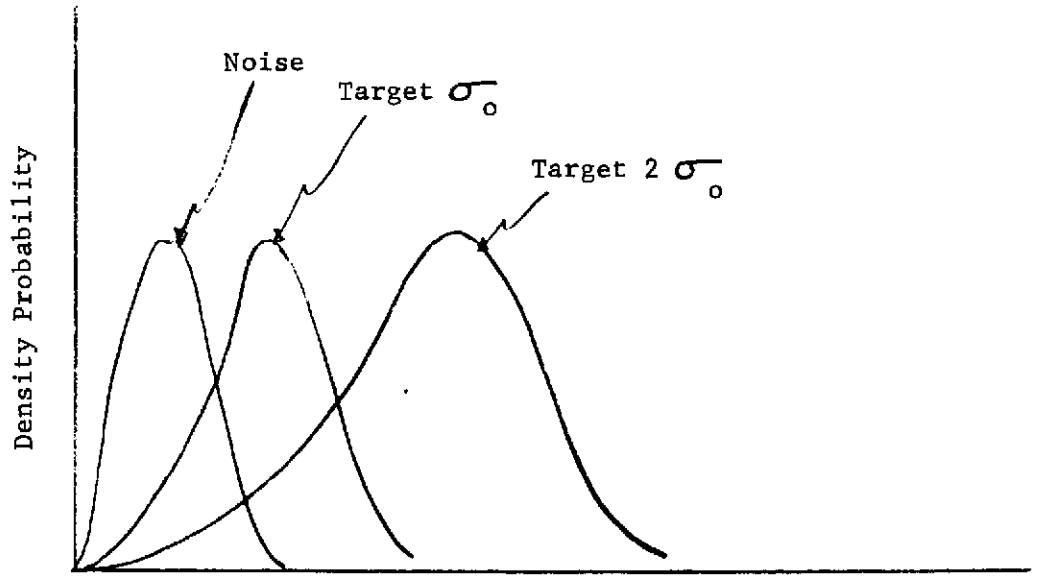

Figure 3.2.3.5-5b. Map Film Density with Multilook

3.2.3.5.4 Multilook S/N Improvement

As it reduces signal and noise variance, multilook improves the S/N ratio. This improvement cannot be determined exactly since the precise area target correlation properties are unknown. Since the individual looks are essentially uncorrelated, a very realistic measure of multilook S/N improvement G is

$$G = \sqrt{N}$$

where N = total number of looks

In addition, a beamshape loss may now be incurred. If the total 4 dB doppler bandwidth is processed, the beamshape loss is 1.6 dB.

3.2.3.5.5 Specific System Multilook Design

The doppler spectra for radars with 13.5 ft. and 27 ft. antenna azimuth apertures are shown in figure 3.2.3.5-6. These were derived from the antenna azimuth patterns (section 3.3.5.2.2) and the satellite velocity of 7.6 km/sec. The spectra are independent of transmitter frequency.

For 30m azimuth resolution, each azimuth look must contain (section 3.2.3.3.2) a bandwidth

$$\Delta F = 1.4 \frac{V}{r}$$

$$= 355 \text{ Hz} \qquad 30\text{m}$$

If only 60m azimuth resolution were desired, the required bandwidth is

$$\Delta F = 178 \text{ Hz} \qquad 60\text{m}$$

If 90m were desired, the required bandwidth further drops to

$$\Delta F = 118 \text{ Hz}$$

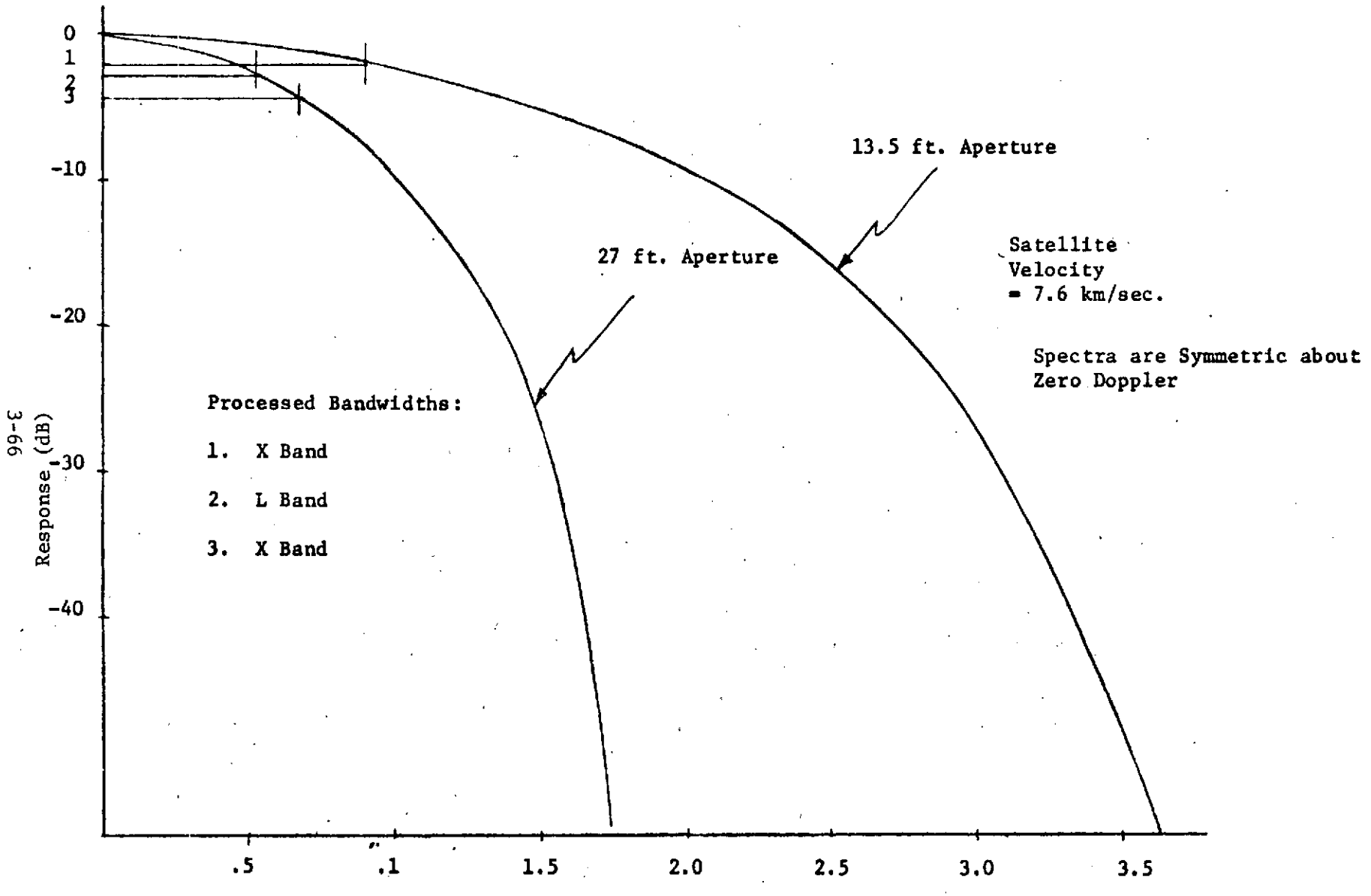

Figure 3.2.3.5-6: Doppler Spectra

Table 3.2.3.5-1 shows the total number of multilooks that are available for 30m, 60m, and 90m resolution. For the X band system with a 13.5 ft. azimuth antenna aperture, 1.8 KHz doppler bandwidth was processed to provide 9 looks. This resulted in negligible beamshape loss. For the X band system with a 27 ft. aperture, the entire 1.4 KHz 4 dB doppler bandwidth was processed to get 7 looks, with a resultant 1.6 dB beamshape loss. In the L band, 27 ft. aperture system, only 1.05 KHz is processed instead of the entire 1.4 KHz 4 dB bandwidth, to get 5 looks. Restricting the L band system bandwidth aids in range ambiguity suppression (section 3.2.3.6).

3.2.3.6 Swath Width and Ambiguity Suppression

A target can under certain circumstances, appear on a map at its true position and at positions displaced in range and azimuth from the true position. These displaced images are ambiguous or false targets (excluding moving targets, of course). In the case of area targets, these displaced images can smear an extended target over an area larger than its true area. If proper attention is not given to suppression of these ambiguities, they can result in poor imagery that will definitely not be of earth resource application quality. The ambiguous return from forested area may, for example, mask surrounding meadows. Achievement of high quality imagery, as is the Westinghouse design, requires that ambiguity suppression be 25 dB or greater.

The prime swath width motivation is, of course, to maximize it. With a wider segment of terrain imaged on a given orbit, the problem of achieving overlapped swaths from orbit to orbit is then eased somewhat. (The offset from orbit to orbit is discussed in section

TABLE 3.2.3.5-1

SYSTEM MULTILOOK CAPABILITY

	X BAND 13.5 ft APERTURE			X BAND 27 ft APERTURE			L BAND 27 ft APERTURE		
Resolution (m)	30	60	90	30	60	90	30	60	90
Azimuth Looks (Doppler Filters)	9	18	27	7	14	21	5	10	15
Range Looks (Sloughing)	1	2	3	1	2	3	1	2	3
Total Multilook	9	36	81	7	28	63	5	20	45
Beamshape Loss		0dB			1.6dB			0.7dB	
Multilook S/N Gain	4.8dB	7.8dB	9.5dB	2.6dB	5.6dB	7.4dB	2.8dB	4.8dB	7.6 dB

3.2.3.9). The approach taken was to maximize swath width under a given (25 dB, nominally) ambiguity suppression requirement.

Swath width and range and ambiguity suppression cannot be determined and adjusted separately; a parameter that effects one invariably effects the other. One is optimized at the expense of the other. Large swath widths are favored by wide antenna elevation patterns, low PRF's, and shallow depression angles. Range ambiguity suppression, on the other hand, is enhanced by narrow elevation patterns and steep depression angles. Normally, a low PRF aids ambiguity suppression, but with the phase shifting ambiguity suppressor used on the L band radar, a high PRF may be required.

The antenna elevation pattern is determined by the antenna elevation aperture and the transmitter frequency. Figure 3.2.3.6-1 shows the two-way patterns for a 2.5 ft. aperture at X (9.5 GHz) and L (1.7 GHz) bands. The elevation aperture is illuminated by a feed horn beam which may be adjusted to weight the aperture as much or as little as is desired. As the weighting becomes uniform over the aperture, spillover loss increases. In the X band system spillover loss must be minimized to maintain adequate S/N ratio. The feed horn beam is then adjusted to weight the elevation aperture slightly to yield a small spillover loss. This weighting spreads the elevation pattern mainlobe slightly and suppressed the two-way peak sidelobe level from -25 dB to -32 dB. In the L band radar mainlobe spreading cannot be tolerated if range ambiguity suppression requirements were to be met. Since spillover loss could be readily tolerated, the feed horn beam was adjusted to uniformly illuminate the aperture. These

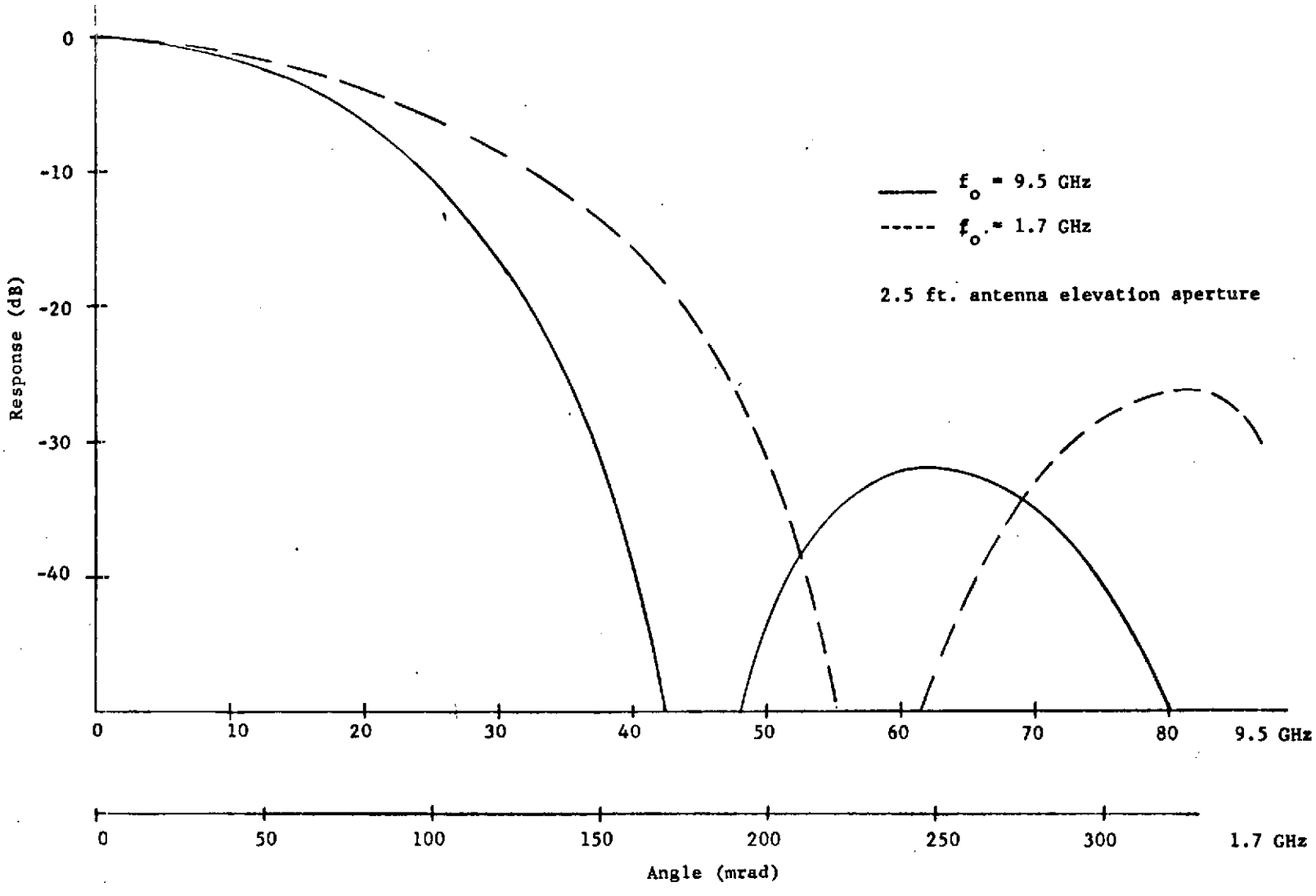

Figure 3.2.3.6-1. Two-Way Antenna Elevation Patterns

losses were discussed in section 3.2.3.4.4.

3.2.3.6.1 Swath Width Determination

Ground swath width must be calculated using spherical earth geometry, as in figure 3.2.3.6-2. For a given depression angle and satellite altitude H, a given antenna elevation beamwidth $\Delta\phi$ will intercept a ground swath width ΔS:

$$\Delta S = \alpha R_E$$

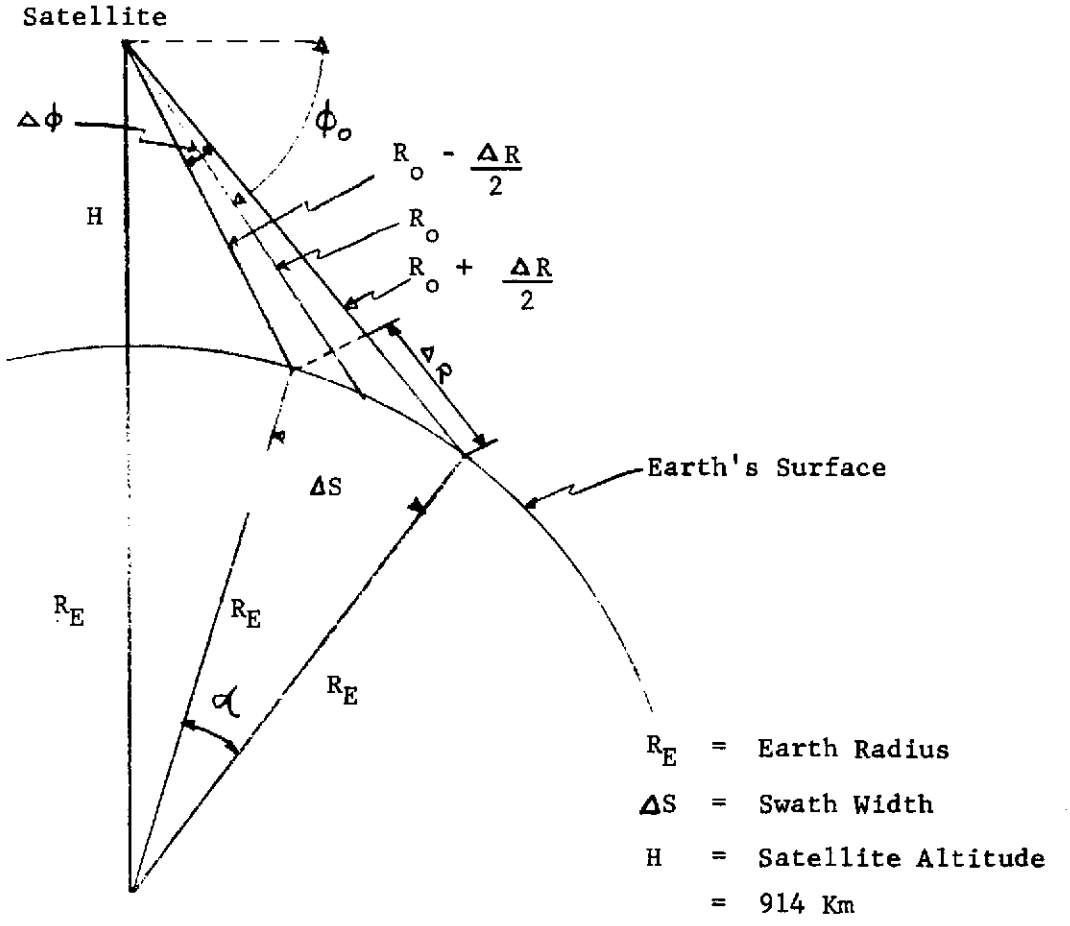

Figure 3.2.3.6-2

Swath Width Calculation

All ranges and angles are calculated using the equations of section 3.2.3.4.8. Satellite altitude was taken to be

$$H = 914 \text{ km}$$

for all the analysis. Swath width can be limited by two factors: PRF and gain loss. The PRF limits swath wdith by limiting unambiguous range. The swath ΔS is bounded by slant ranges $\sim R_o - \Delta R/2$ and $\sim R_o + \Delta R/2$ (angular separation $\Delta \phi$), where

$$\Delta R \leq \frac{c}{2f_R} \equiv R_v$$

R_u = unambiguous range

In practice, ΔR will always be less than the unambiguous range to allow adequate range ambiguity suppression. Large PRF's limit the unambiguous range and hence ground swath width, regardless of how broad the antenna elevation pattern is. The allowable beamwidth $\Delta \phi$ can thus be much less than the available elevation beamwidth.

The gain loss limits swath width due to S/N requirements. The S/N values of section 3.2.3.4 were all calculated at swath center with peak antenna gain. At any other point in the swath, the antenna gain decreases with resultant S/N loss. The maximum swath width is then determined by how much S/N loss can be tolerated, regardless of how much unambiguous range may be provided by a low PRF. The available antenna elevation beamwidth was determined by allowed aperture size and desired transmitter frequency, and is not an adjustable parameter for this analysis.

A given elevation beamwidth determined by allowable S/N loss will subtend larger ground swath widths at shallower depression angles. The required unambiguous range is then greater at these shallower depression

angles, so a smaller PRF may be required here than at steep depression angles to realize this larger swath width.

3.2.3.6.2 Range Ambiguities

For a satellite altitude of 914 km the slant range to the target is roughly 1000 km. Matching a PRF to this unambiguous range would require a PRF so low as to cause tremendous doppler ambiguities. The PRF must then be matched to the swath width being mapped, as it was in figure 3.2.3.6-2. The return from a given transmitted pulse does not arrive at the receiver until many IPP's after it was transmitted. Returns from ground points whose slant range is

$$R = R_o \pm n\, R_u \qquad N = \pm 1, \pm 2$$

R_u = unambiguous range

$$= \frac{c}{2 f_R}$$

R_o = slant range to point in desired swath, will arrive at the receiver simultaneously with the return from a point at range R_o which lies in the desired swath. Thus, targets at ranges R_o and $R_o \pm N\, R_u$ will appear on the map film at exactly the same range R_o. The returns from points at $R_o \pm N\, R_u$ are range ambiguities. These ambiguous swath widths are shown in figure 3.2.3.6-3

Range ambiguity suppression is provided almost exclusively by the antenna elevation pattern. As shown in figure 3.2.3.6-3, when peak gain is directed to a point at range R_o, the gain at points at ranges $R_o \pm N\, R_u$ is much less. The slant range to the ambiguous ranges is greater or less than the range to the desired swath, but this suppression or enhancement is negligible (0.5 dB at most). Range

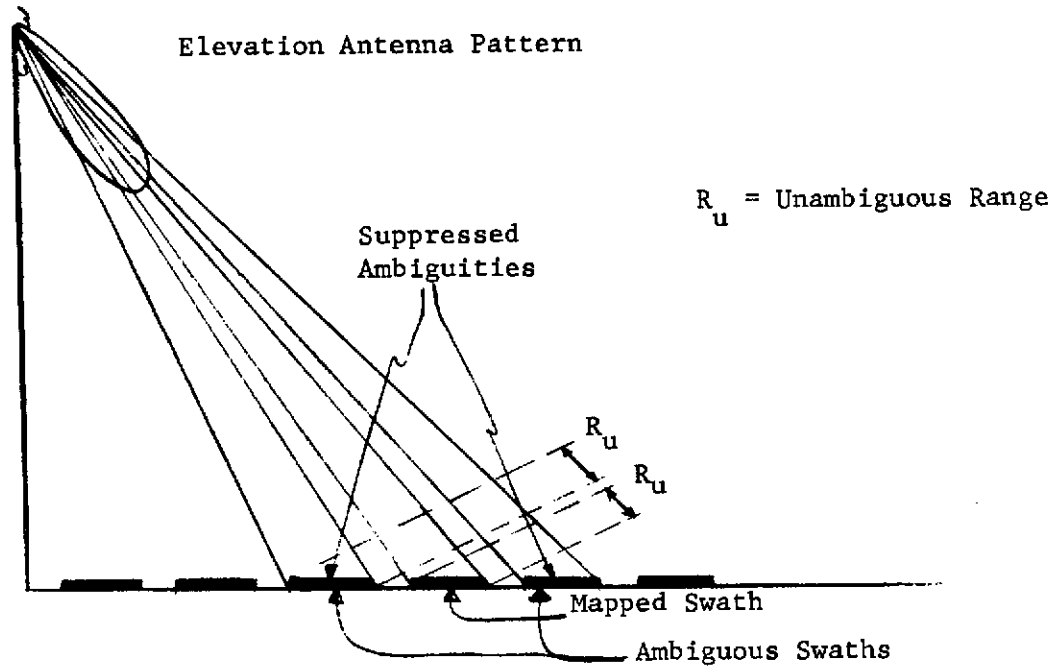

Figure 3.2.3.6-3
Location of Range Ambiguities

ambiguity suppression is enhanced, then by narrow antenna elevation patterns and by low PRF's. The low PRF requirement is in accordance with the swath width maximizing requirement. For a given PRF, range ambiguity suppression is greater at steep depression angles. Figure 3.2.3.6-4 shows range ambiguity suppression as a function of depression angle for several PRF's. This was evaluated using the 6 dB (4.0 mrad) beamwidth of the X band elevation pattern of figure 3.2.3.6-1.

3.2.3.6.2.1 Range Ambiguity Suppressor

Since ambiguous swaths are separated from the desired swath by very small angles, the antenna pattern along will sometimes not provide sufficient range ambiguity suppression. An ambiguity suppressor that adjusts the phase of transmitted and received signals must then be added.

This device shifts the phase of alternate transmitted pulses by 0° or 180°. Thus, every other pulse has 0° shift, and the pulses in between have 180° shift. During reception, the transmitted phase, either 0° or 180°, is removed (this must be modified to account for the many IPP delays between transmission and reception of a given pulse). Returns from the desired swath width receive no net phase shift, but returns from the ambiguous swaths on either side of the desired swath are transmitted on 0° and received on 180° on every other pulse and vice versa on the pulses in between. The effect of this is to shift the azimuth spectra of these ambiguous swaths by PRF/2 and hence out of the processor's azimuth passband. The suppression produced by this phase shifting increases with increasing PRF. The umbiguous swaths outside of the two adjacent to the desired swath are unaffected by this, since they receive the proper phase shift, but they will be adequately suppressed by the elevation pattern. This suppressor will be used in the L band radar.

3.2.3.6.3 Azimuth Ambiguities

Azimuth ambiguities arise due to sampling by the radar PRF. The doppler spectrum appears not only at its true frequency, but at multiples of the PRF as well. Since the antenna azimuth pattern is continuous and cannot be constrained, these doppler components overlap, as in figure 3.2.3.6-5. A target that lies in the azimuth sidelobes can thus appear in the processor passband; this target produces azimuth ambiguities since it can appear at an azimuth other than its true azimuth.

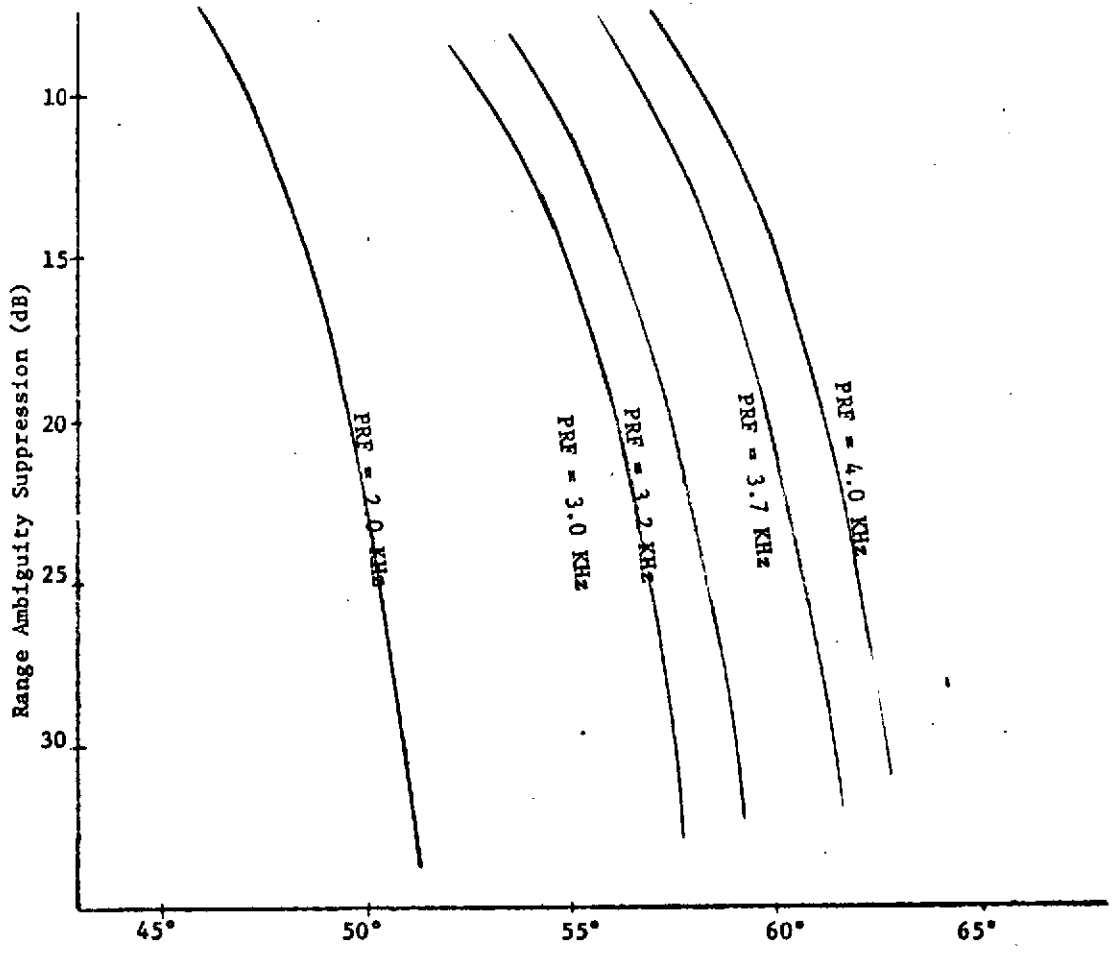

Figure 3.2.3.6-4. Range Ambiguity Suppression vs. Depression Angle

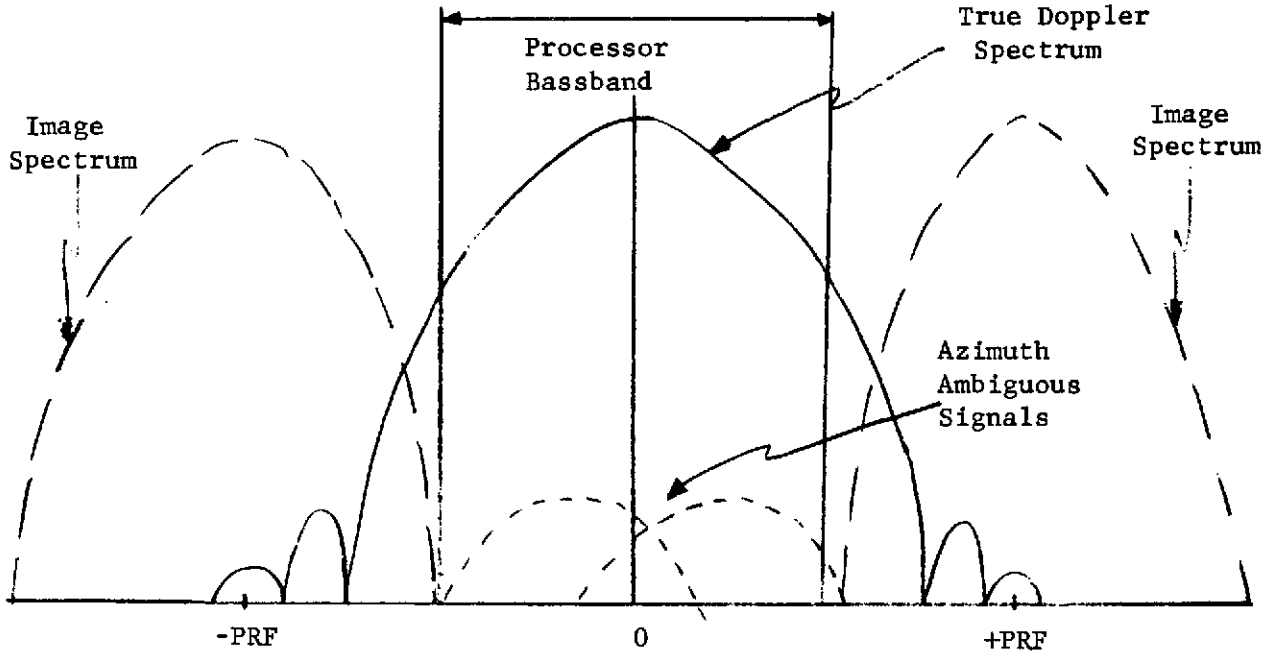

Figure 3.2.3.6-5

Azimuth Ambiguities

Azimuth ambiguities are supressed by choosing a PRF large enough so that only sidelobes of the image doppler spectrum appear in the processor passband and not part of the mainlobe. Figure 3.2.3.6-6 shows doppler spectra for the systems with 13.5 ft. and 27 ft. antenna azimuth apertures; these were calcualted using the antenna azimuth patterns and the 7.6 km/sec. satellite velocity. The processed bandwidths are indicated in the figure (section 3.2.3.5.5). From this figure azimuth ambiguity suppression was calculated as a function of PRF; the results are shown in figure 3.2.3.6-7. (For suppression greater than 25 dB the curve is accurate to within a few dB due to unability to control sidelobes exactly). A specific azimuth ambiguity

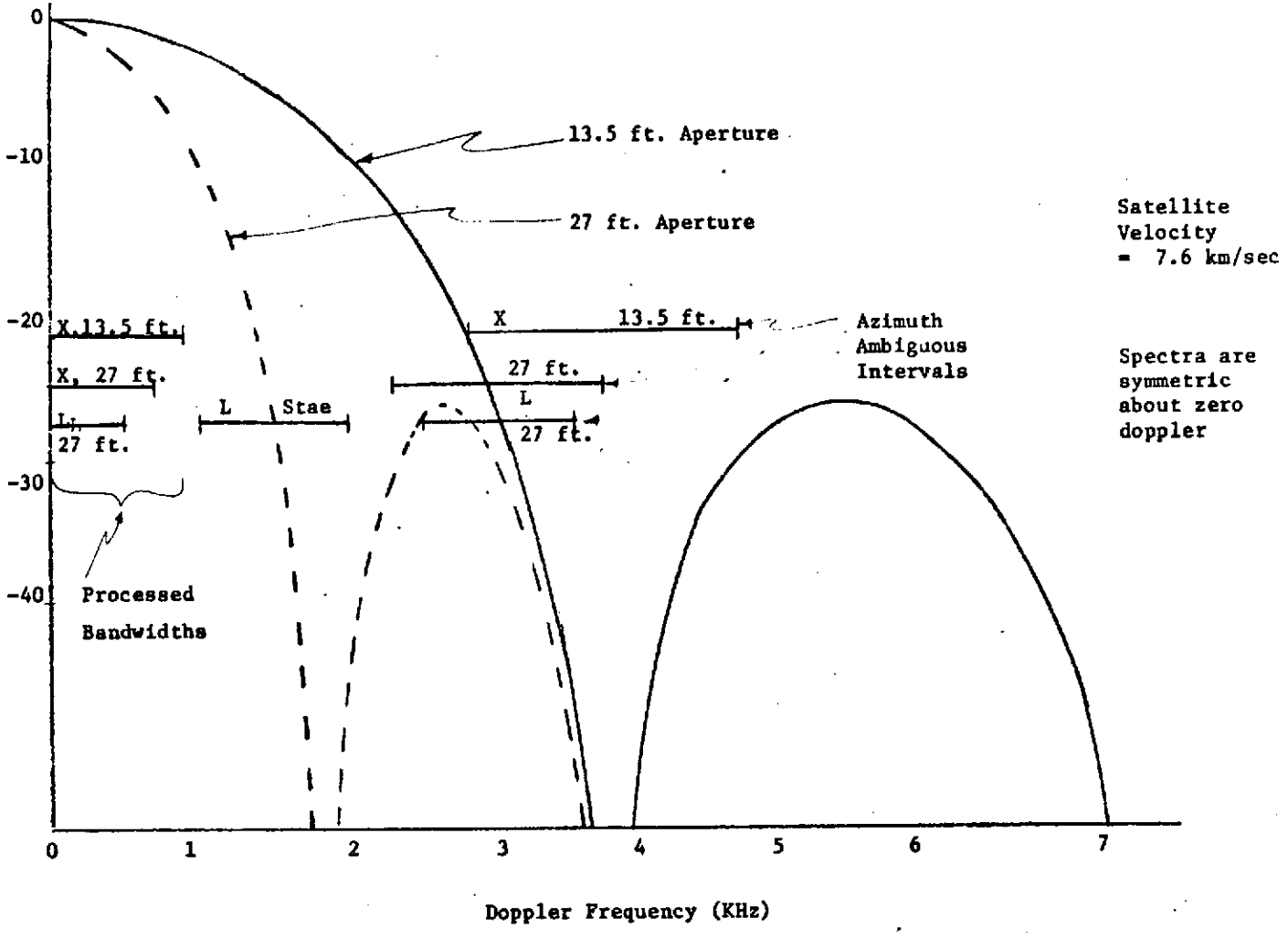

Figure 3.2.3.6-6. Doppler Spectra

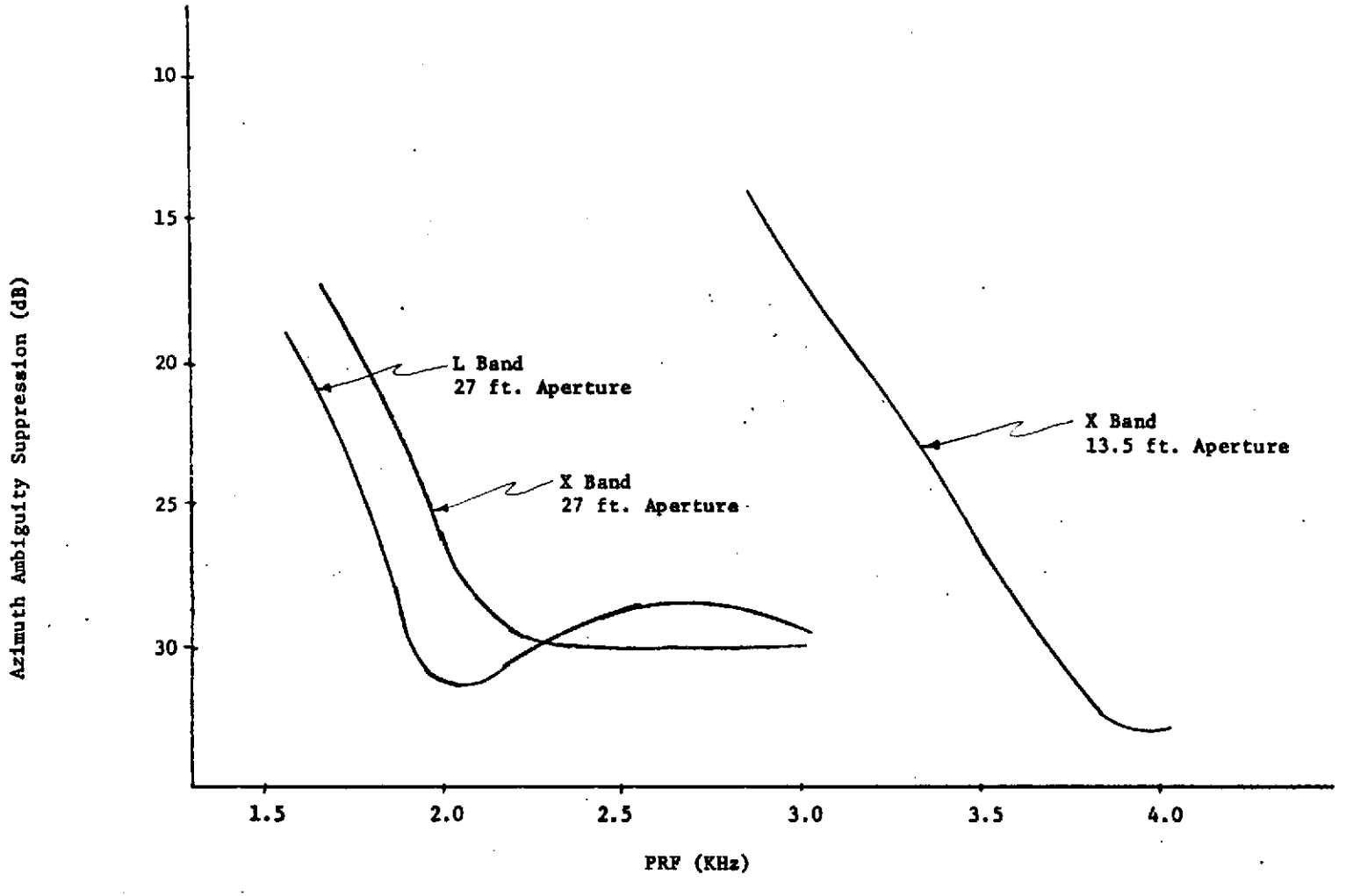

Figure 3.2.3.6-7. Azimuth Ambiguity Suppression vs. PRF

calculation is done in Appendix E. Figure 3.2.3.6-6 shows azimuth ambiguous intervals for three of the major system PRF's: 3.7 KHz with the X band, 13.5 ft. aperture radar, and 3.0 KHz for the X and L band radars with 27 ft. antenna azimuth aperture.

3.2.3.6.4 Results

Using all of the above techniques and information, swath width as a function of depression angle was calculated with the requirement that a given ambiguity suppression be achieved. Specifically, calculations were done for 25 dB and 20 dB ambiguity suppression. For a given ambiguity suppression, a minimum PRF could be found from figure 3.2.3.6-7. This insured that azimuth ambiguities were adequately supressed. With this minimum PRF, range ambiguity suppression could be calculated as a function of depression angle and allowed antenna elevation beamwidth using curves like figure 3.2.3.6-4. For a given depression angle, then, a PRF and a maximum allowed portion of the elevation beamwidth to be used were found that maintained a given ambiguity suppression. In many cases, particularly at steep depression angles, this ambiguity constrained elevation beamwidth was broader than the physical beamwidth. The portion of the beamwidth to be used was then narrowed to one that yielded an acceptable S/N loss; in these instances allowable S/N loss (physical elevation beamwidth) and not ambiguity suppression was the swath width limiting factor. At shallower depression angles, and with the entire L band radar, the ambiguity constrained beamwidth was narrower than the physical beamwidth; ambiguity suppression was then the swath width constraining factor. In either case, a ground swath width could be calculated from the resultant portion of the elevation beamwidth

allocated.

Figure 3.2.3.6-8 shows the results of these calculations for the X band radar with a 13.5 ft. antenna azimuth aperture. Three bounds on swath width are shown: S/N at swath edge of 5 dB, 3 dB, and 0 dB. (S/N ratios of section 3.2.3.4 were used for this calculation). This radar may operate between 55° and 75° depression with a nominal 40-50 km swath width, with a 50 km swath width at 60° depression angle. The PRF's calculated for this system are given in Table 3.2.3.6-1. No range ambiguity suppressor (section 3.2.3.6.2.1) is required.

Figure 3.2.3.6-9 shows the swath width for the X band radar with a 27 ft. antenna elevation aperture. With a 27 ft. aperture, this radar may operate over a wider range of depression angles, 45° - 75°, than the radar with a 13.5 ft. aperture. This is due to the lower PRF's (2.3.KHz) that may be used with a 27 ft. aperture. The PRF's for the radar with a 13.5 ft. aperture were 3.2 - 3.7 KHz. The PRF's are lower since the doppler spectra are narrower (figure 3.2.3.6-6); using PRF's of 2-3 KHz with the 13.5 ft. aperture radar would result in unacceptably high azimuth ambiguities (figure 3.2.3.6-7). The nominal swath width for the 27 ft. aperture radar remains 50 km. The specific PRF's used for this radar are given in Table 3.2.3.6-1. No range ambiguity suppressor (section 3.2.3.6.2.1) is required.

If a frequency higher than X band, namely Ku - Ka, had been chosen as the operating frequency, swath widths would have been less than those indicated in figures 3.2.3.6-8 and 3.2.3.6-9. If the operating frequency were 35 GHz, nominal swath width would have been only 15 Km, not 45 km. The operating range would, however, be extended over an additional 5° or

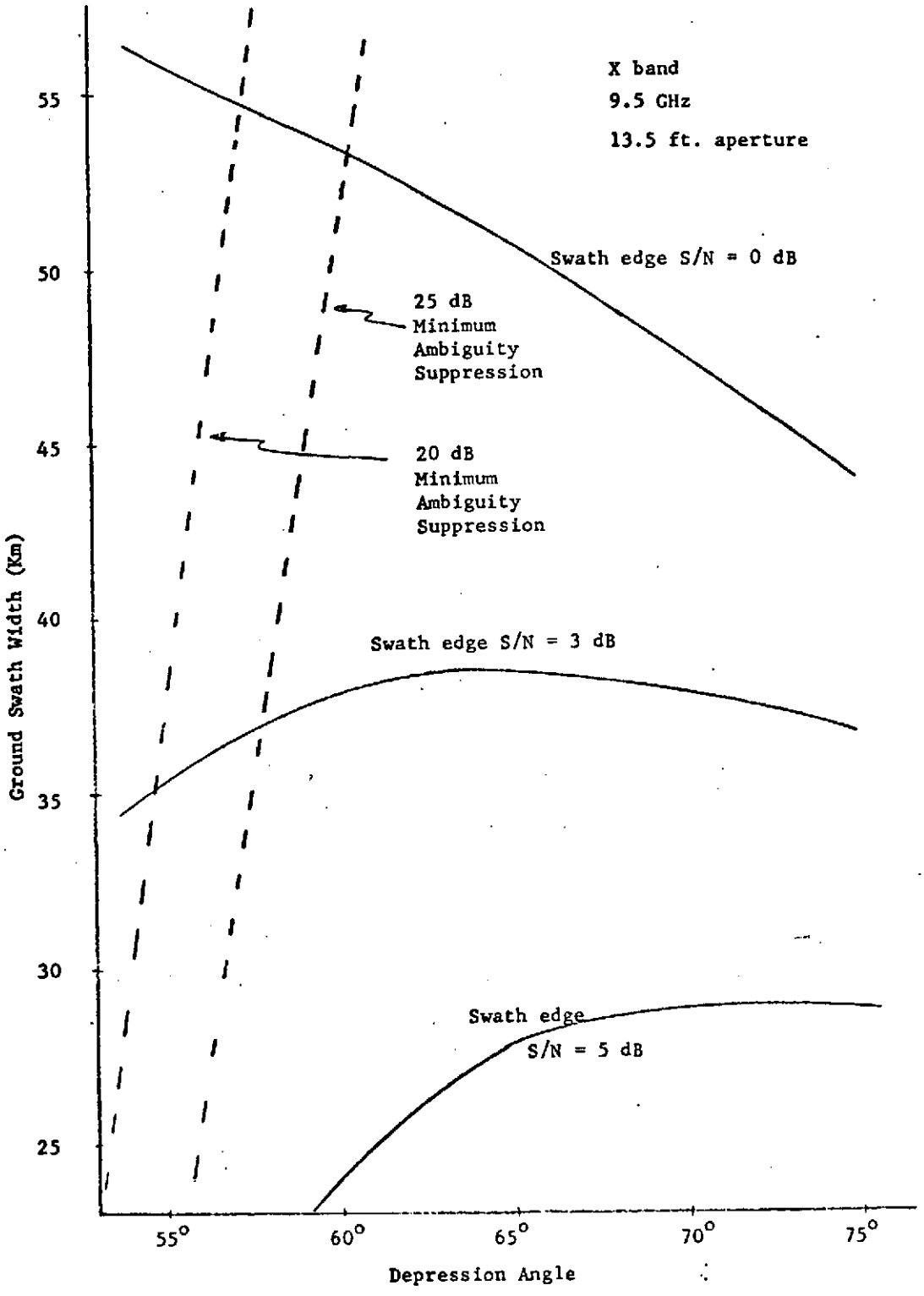

Figure 3.2.3.6-8. Swath Width vs. Depression Angle

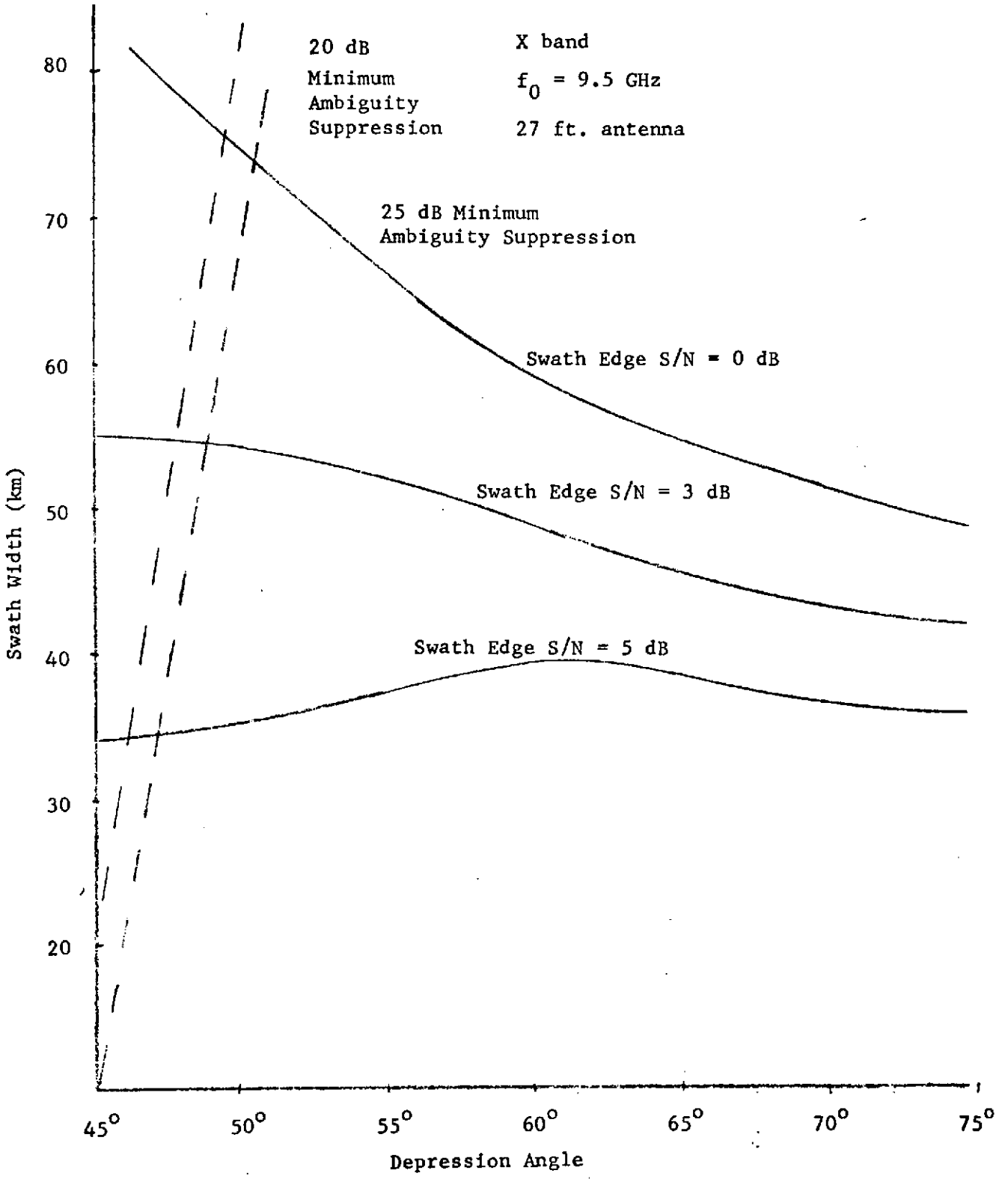

Figure 3.2.3.6-9. Swath Width vs. Depression Angle

TABLE 3.2.3.6-1

SWATH WIDTH PARAMETERS

PARAMETER	SYSTEM		
	X Band 13.5 ft. Aperture	X Band 27 ft. Aperture	L Band 27 ft. Aperture
Nominal Swath Width	50 km	50 km	40 km
Depression Angle	55° - 75°	45° - 75°	75°
PRF (Variation with Depression Angle)	3.2 - 3.7 KHz	2.0 - 3.0 KHz	3.0 KHz

so of depression angle at the shallow angle extreme. The shallowest depression angle achievable under any circumstance is about 40°, since at a 914 km altitude the horizon is at 35° depression angle.

Due to its very wide elevation pattern, maintaining an acceptable range ambiguity suppression with the L band radar was very difficult. Specifically the wide elevation pattern requires that the PRF be reasonably low; this in turn requires a narrow doppler spectrum to avoid excessive azimuth ambiguities. No acceptable PRF could be found for a radar with a 13.5 ft. azimuth aperture (wide doppler spectrum) that provided 25 dB suppression of back range and azimuth ambiguities. With a 27 ft. azimuth aperture, a 3.0 KHz PRF, and a 75° depression angle, 25 dB ambiguity suppression could be maintained over a 40 km swath width. This is indicated as one point in figure 3.2.3.6-10, which shows swath width as a function of depression angle for an L band radar with a 27 ft. azimuth aperture. A range ambiguity suppression (section 3.2.3.6.2.1) was required; its effective use required the 3.0 KHz PRF instead of a smaller one. If the depression angle is decreased from 75°, range ambiguity suppression is less than 25 dB. If only 20 dB range ambiguity suppression is required, depression angle may vary between 71° and 75°. S/N loss over the swath width is negligible ($\sim$ 0.5 dB).

Maintaining acceptable range ambiguity suppression is thus very critical to the L band radar design. If proper attention is not given to this, the resultant ambiguities can produce poor quality imagery. Raising the transmitter frequency above 1.7 GHz alleviates the problem somewhat, but with lower frequencies 25 dB range ambiguity suppression could not be achieved.

If the antenna elevation aperture is increased from 2.5 ft., the elevation beam narrows, and adequate range ambiguity suppression is more readily achieved. Figure 3.2.3.6-10 shows swath width as a function of depression angle for several elevation apertures. An increase from 2.5 ft. to 3.5 ft. allows depression angle variation from 65° - 75°. The S/N loss at swath edge is negligible.

The swath widths, depression angles, and PRF's are summarized in Table 3.2.3.6-1.

3.2.3.7 Antenna Pointing Requirements

3.2.3.7.1 Lateral Antenna Motion Requirement

The SAR collects phase history over an integration period. It is the correlation of these phase histories which allows the focusing of the return wavefront and resolution improvement. Arbitrary perturbation of the return signal phase will result in a reduction of resolution, production of false targets and, in some cases, loss of signal strength.

Phase perturbation can be introduced by slight translational movements of the antenna phase center, Δr, along the Line of Sight (LOS) to the target. Such variations could be introduced by rotation of the S/C as well as translation if the antenna phase center were not exactly located at the center of rotation. Generally speaking, low frequency movements result in resolution degradation, high frequency results in sidelobes (with the sidelobe position directly related to the frequency of movement) and signal loss.

It can be shown that regular periodic movement of peak deviation Δr over an integration time will cause sidelobes. The relationship is:

$$\Delta r = \frac{\lambda}{2\pi} \left(\frac{SL}{ML}\right)$$

where λ = wavelength

and SL/ML = sidelobe/mainlobe voltage ratio

Sidelobes are in effect false target and contribute to poor imagery background. A criterion of imagery background is Integrated Sidelobe to Mainlobe ratio $\left(\frac{ISL}{IML}\right)$. Instrumentation quality imagery is achieved with:

$$\frac{SL}{ML} = -30 \text{ db}$$

and $$\frac{ISL}{IML} = -15 \text{ db}$$

ISL/IML is achieved if the SL/ML ratio is achieved. any effects can contribute to SL/ML degradation, the spec for ant phase center movement is set to -33 db, so

$$\Delta r = \frac{1.4 \text{ in}}{2\pi} \quad (.0223) = .0049 \text{ in} \simeq 5 \text{ mils}$$

where $$\lambda = \frac{c}{f} = \frac{3.10^8 \text{m/sec}}{8500 \text{ MHz}} \left(\frac{3.28 \text{ ft}}{1\text{m}}\right) \left(\frac{12 \text{ in}}{1 \text{ ft}}\right) = 1.38 \text{ in}$$

as the X-band wavelength is the regulating constraint.

The low frequency motion may be analyzed as introducing a quadratic phase of 45° at the end of the aperture. The resulting equation is

$$\Delta r = \frac{\lambda}{2T_i^2 W_m^2}$$

where T_i = integration time $\simeq$ .1 sec

W_m = radian frequency of motion

for $W_m = 2\pi$ rad.

$$\Delta r = \frac{1.4 \text{ in}}{(2)(.1)^2(2\pi)^2}$$

$$\Delta r = 1.75 \text{ in} = 1750 \text{ mils @ f = 1 Hz}$$

The above movement tolerances were developed on the basis of sinusoidal motion and are shown in Figure 3.2.3.7-1; however, random motion described in terms of motion Power Spectral Density (PSD) will essentially be treated by the system as discrete sinusoids having the equivalent power of the noise within the system bandwidth. So, high

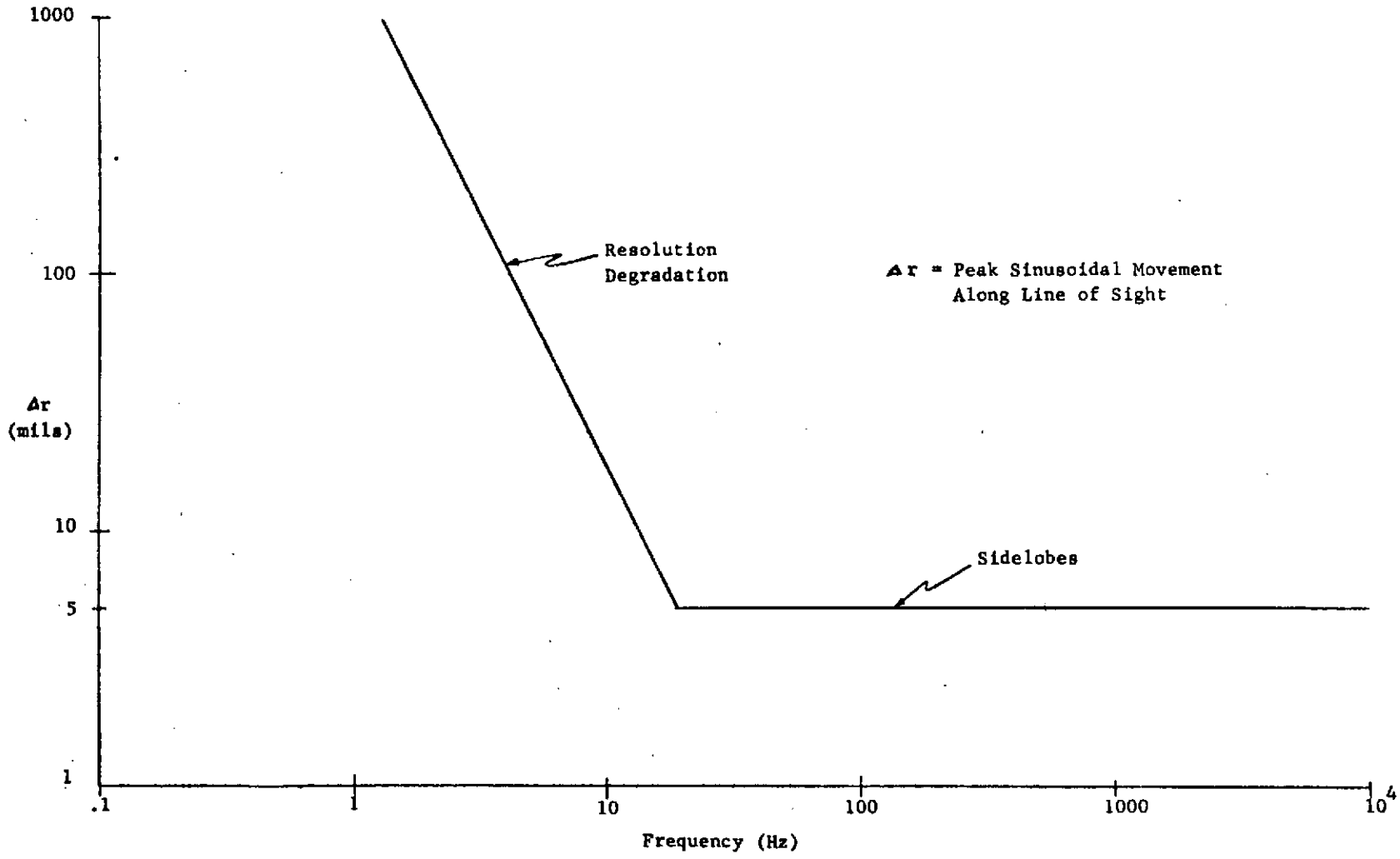

Figure 3.2.3.7-1. Deterministic Antenna Motion Requirement

frequency movement of 5 mils peak sinusoidal movement is equivalent to

$$\Delta r_{rms/\Delta f_i} \; (5 \text{ mils}/\sqrt{2})^2 \; / \; 10 \text{ Hz} = 1.24 \text{ mil}^2/\text{Hz}$$

where 10 Hz is the system integration bandwidth. For frequencies below 1/2 the integration bandwidth, the specification should roughly match the discrete requirements as the integration bandwidth is significantly more than the movement frequency. The PSD motion requirement is shown in Figure 3.2.3.7-2.

High frequency movement can result in signal loss as discussed in Section 3.2.3.7-2. An allowance of .1 db signal loss was used. The direct sideband requirements previously discussed as a result of deterministic sinusoidal motion is the pacing requirement; however, random noise components from 100 to 4000 Hz may require a 1/f slope shown in Figure 3.2.3.7-2. The slope and shape of this portion of the specification curve results from an assumed PSD shape and, consequently, the specification curve could have a different shape from that shown. Any PSD curve above 10 Hz or so having an integrated movement of less than 30 mils would be adequate.

3.2.3.7.2 Signal Loss

Angle modulation removes power from the Central Spectral Line (CSL) or carrier and transfers it to sidebands which may be outside the integration filter or into another compressed element filter. For small modulation indicies, only the first order sidebands are of interest as in Figure 3.2.3.7-3.

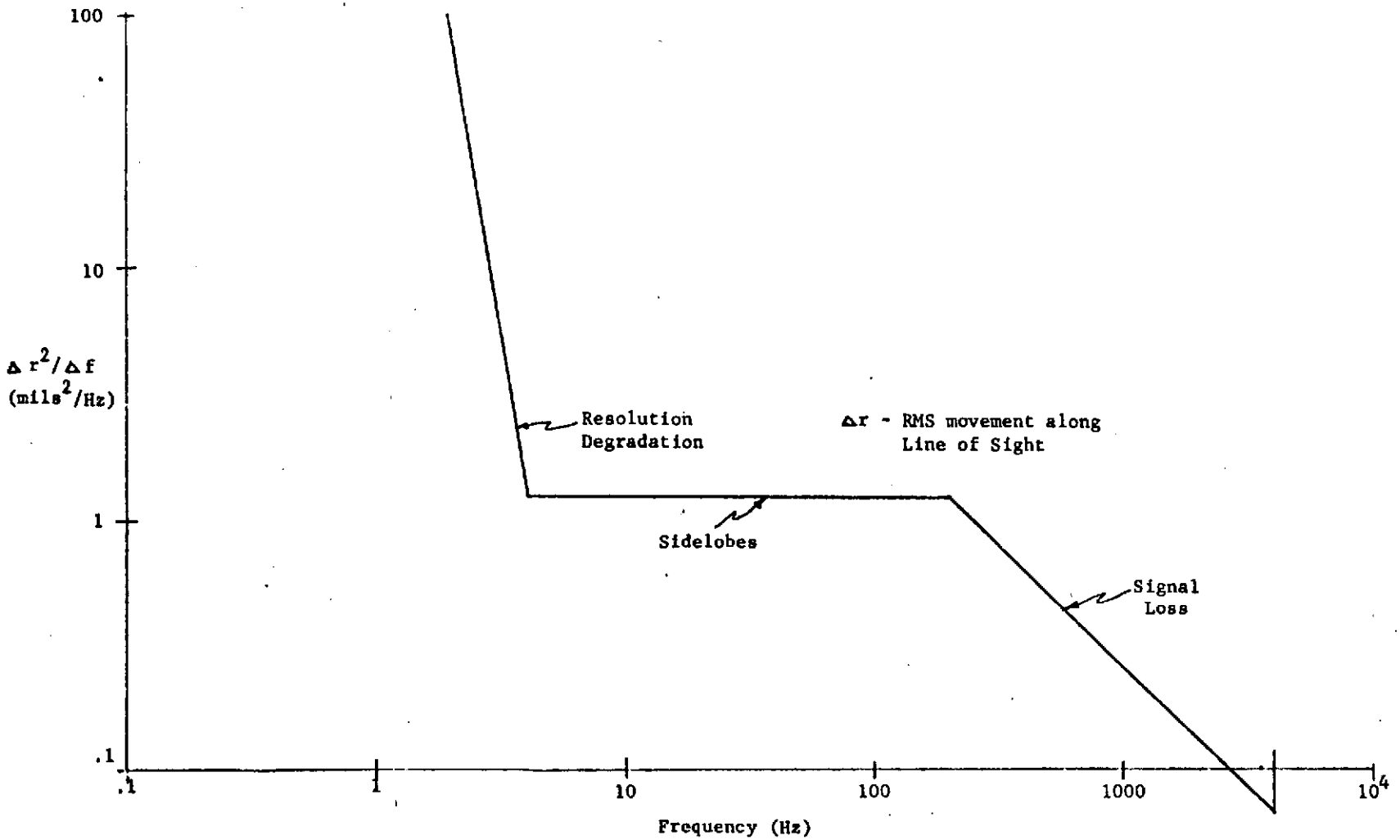

Figure 3.2.3.7-2. Nondeterministic Antenna Motion Requirement
(Power Spectral Density)

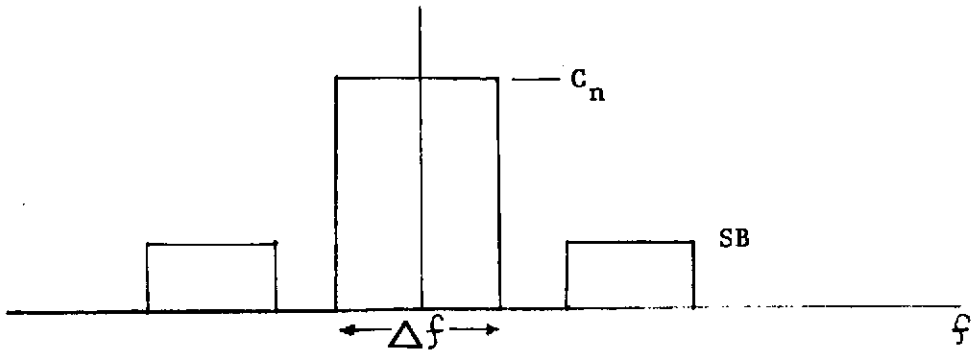

Figure 3.2.3.7-3 Angle Modulation Spectra

Assuming the net power to be unity

no modulation $C_1 \Delta f = 1$

with modulation $C_2 \Delta f + 2\ (SB)\Delta f = 1$

Combining the above equations, the carrier loss for a given sideband/carrier ratio may be determined as

$$\frac{C_1}{C_2} = 1 + 2\ (\frac{SB}{C_2})$$

For a sideband/carrier power ratio of -33 db

$$\frac{C_1}{C_2} = 1 + 2\ (\frac{1}{2000}) = 1 + \frac{1}{1000}$$

and the signal power loss is about .004 db and a .1 db signal loss is equivalent fo -17.4 db sidebands. This is equivalent to 30 mil rms movement, or 900 mil^2.

Random movement over some bandwidth can contribute to signal loss. Allowing a roll-off of the PSD from 200 Hz to 4 KHz of 1/f allows this specification to be met.

$$P_T = P_o\ f_o \int_{f_o}^{f_1} df/f = P_o\ f_o\ \ln \frac{f_1}{f_o}$$

where $P_o = 1.25 \text{ mil}^2/\text{Hz}$

$f_o = 200 \text{ Hz}$

$f_1 = 4000 \text{ Hz}$

$P_T = (1.25 \text{ mil}^2/\text{Hz})\ (200 \text{ Hz})\ \text{In}\ \frac{4000}{200}$

$P_T = 250 \text{ mil}^2\ (3) = 750 \text{ mil}^2$

The upper limit was taken as 4 KHz, the assumption being no significant components above 4 KHz are present.

3.2.3.7.3 Antenna Pointing Accuracy

Ideally, the antenna azimuth (along track) dimension is aligned parallel to the satellite velocity vector with elevation tilted to a desired depression angle. Error in both antenna pointing accuracy and stability can degrade SAR performance.

When the antenna azimuth dimension is aligned with the satellite velocity vector, the return signal doppler spectrum is centered about zero doppler. Also, the frequency time slope of the linear FM doppler signal is then a constant $\frac{2v^2}{\lambda R}$. Pointing errors in pitch and yaw shift the doppler spectrum off of zero doppler; this shifts the signal out of the processor passband and increases L-band range ambiguity level. Allowing only a 150 Hz shift at X-band (L-band shift will be only 30 Hz) will result in negligible signal loss. This corresponds to a combined pitch and yaw error of

$$\sin \theta = \frac{\lambda \Delta f}{2v}$$

$$= \frac{.103 \text{ ft} \cdot 150 \text{ Hz}}{2 \cdot 2 \cdot 5 \cdot 10^4 \text{ ft/sec}}$$

$$\theta = 0.02^\circ$$

where satellite velocity in a 914 Km altitude, 100 min. orbit is

$2.5 \cdot 10^4$ ft/sec. This is the total angular error, pitch plus yaw, that is allowed. The corresponding 30 Hz L-band shift results in negligible increase in range ambiguity level. If the 0.02° error were entirely in yaw, the resulting change in linear FM doppler slope is negligible, since

$$\frac{\cos 0^\circ - \cos .02^\circ}{\cos 0^\circ} < 10^{-5}$$

When the antenna is pointed at the proper depression angle, the swath width defined by the receiver on/off gating is illuminated with peak antenna gain. Pointing errors in roll, shift peak gain out of the received swath width. Since uncontrollable altitude changes may produce the same effect, the roll pointing accuracy specifications must allow negligible gain loss over the swath width. Examination of the X-band elevation antenna pattern shows that a roll pointing error of 0.06° will result in negligible gain loss. The L-band loss will be even less.

If the antenna jitters in roll, pitch, or yaw, the return signal will be phase and amplitude modulated. These errors can degrade resolution and produce sidelobes. In pitch and yaw, stability requirements of

$$10^{-2^\circ}/\text{sec}$$

will insure that the signal is not unacceptably degraded. Specifically, this means that the antenna moves no more than 10^{-3° during the 0.1 sec integration period; the corresponding amplitude modulation is less than 0.1 db. Instabilities in roll are equivalent to antenna lateral motions; these requirements were discussed in Section 3.2.3.7.1. Definitive roll stability requirements are a dependent upon antenna

position on the spacecraft.

Table 3.2.3.7-1 summarizes these requirements.

Table 3.2.3.7-1

Antenna Pointing and Stability Requirements

Function	Pointing Error	Stability Error
Pitch plus Yaw	0.02°	10^{-2}°/sec
Roll	0.06°	See Section 3.2.3.7.1

3.2.3.7.4 Potential Depression Angle Variation with Latitude

Satellite altitude variations due to orbit eccentricity, earth oblateness or local relief variations can result in loss in S/N or map displacement unless properly accounted for. Corrective measures could include constant altitude orbits over mapped area, slant range gate positioning and/or depression angle adjustment.

Mapping of a specific ground area within the depression angle limits can be achieved by appropriate antenna and range gate positioning. Coping with altitude variations over a complete pass requires a more discerning examination of system capabilities as discussed below.

It is very desirable to have peak antenna gain directed at the center of the received ground swath throughout an orbit over the U.S. or any other area being mapped. The average gain over the entire swath is then maximized. At a satellite altitude H, and an antenna depression angle $\emptyset$, the antenna beamwidth θ will illuminate a ground swath defined by slant ranges R_1 and R_2, as in Figure 3.2.3.7-4a. The receiver on/off gate is adjusted to accept returns from ranges between R_1 and R_2; the received swath is then illuminated by maximum

antenna gain. If the earth were spherical and the satellite orbit circular and concentric, the satellite altitude and earth radius would remain constant as a function of earth latitude. Then, for a constant antenna depression angle and receiver on/off gate interval, the received swath would always be illuminated by maximum antenna gain. Further, the swath ground offset range Rg, Figure 3.2.3.7-4a, would remain constant.

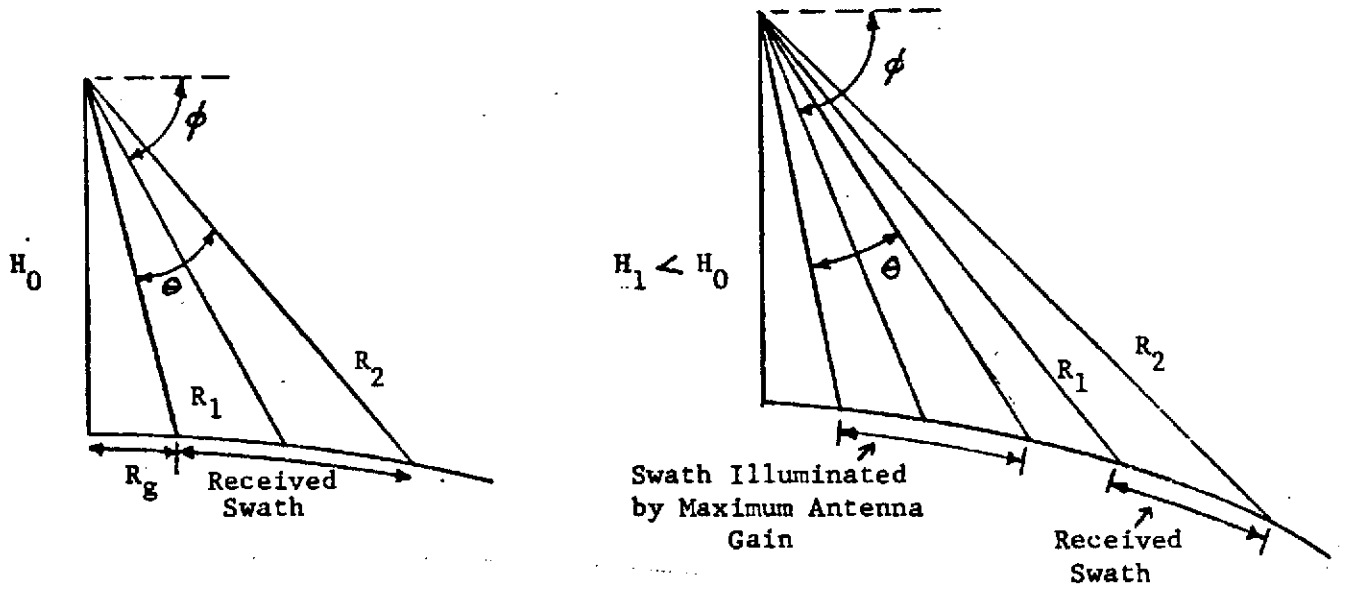

(a)

Received Swath Illuminated by Peak Antenna Gain

(b)

Received Swath Not Illuminated by Peak Antenna Gain

Figure 3.2.3.7-4. Received Swath Illumination

The earth and satellite orbit are, of course, really elliptical, and the satellite altitude then varies during the orbit. If the antenna depression angle ϕ remains constant and the receiver on/off gate remains "tuned" to the ranges R_1 and R_2, may no longer coincide with the swath illuminated by antenna maximum gain, as defined by

depression angle $\emptyset$ and the antenna elevation beamwidth θ. This is illustrated in Figure 3.2.3.7-4b. This results in S/N loss and calibration errors since antenna gain over the swath is inexactly known. Second, the swath ground offset range now varies with altitude, or time. If the variation is too rapid, a given range gate may traverse several range resolution cell widths on the ground during an integration time, as in Figure 3.2.3.7-5. This results in smeared range resolution cells.

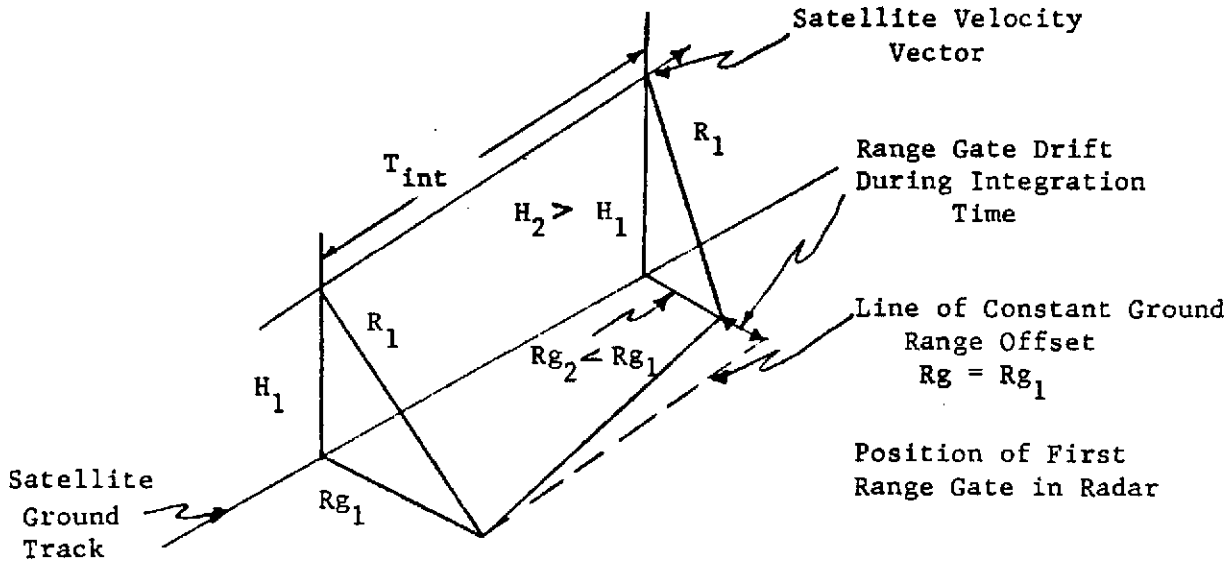

Figure 3.2.3.7-5

Range Gate Drift

Correcting these problems, if they are serious, may require changing antenna depression angle with latitude.

These problems will first be discussed for constant depression angle and gate interval for the initially assumed near-circular orbit of eccentricity 0.005. This is the lowest eccentricity normally achievable. The earth's radii are :

$R_{equatorial} = 6382$ Km

$R_{polar} = 6361$ Km

For a nominal satellite altitude of 914 Km, the altitude over the continental U.S. (25° - 50° latitude) varies by approximately 9 Km. This 9 Km variation arises since the satellite orbit is more circular than the earth is spherical ($\epsilon = 0.08$). This is, of course, an assumed orbit, but the 9 Km altitude variation over the continental U.S. is indicative of the variation for orbits of $\epsilon = 0.005$.

In this situation, optimum results would occur if, for a given constant depression angle, the receiver gate is adjusted so that the center of the received swath is illuminated by peak gain over mid-U.S. (911 Km altitude, 6374 Km earth radius). At 60° and 75° depression angles, the peak gain remains directed toward some point in the received swath during the orbit over the continental U.S., but swath edge gain loss is increased by 6 dB for 60° depression, and by over 20 dB for 75° depression over the northern and southern latitudes of the U.S. The usable swath width, i.e., that has adequate S/N ratio, is decreased somewhat at 60° depression angle but is virtually eliminated at 75° over much of the U.S. Further, the swath ground range offset varies by as much as 10m, or one-third of a range resolution cell, during an integration time at 75° depression. This will smear range resolution somewhat. To insure adequate performance at 75° depression angle, compensation must be introduced in some form.

If the orbit eccentricity matched that of the earth, namely, $\epsilon = 0.08$, the errors are virtually eliminated. Satellite altitude

variation over the continental U.S. would be only 1.5 Km, and, for constant depression angle and receiver gate interval, the additional antenna gain loss at swath edge as a function of latitude is almost negligible, never being more than 1 dB at 75° depression angle. The received ground swath is then always essentially illuminated by maximum antenna gain. Further, swath ground range offset from 25° - 50° latitude varies by only 5 Km, or 0.5 m maximum over an integration period, at 75° depression angle. These errors will not degrade system performance. Table 3.2.3.7-2 shows specific swath edge maximum gain loss, and ground range offset to near swath edge, for 60° and 75° depression angles. Matching the satellite orbit eccentricity to that of the earth, then achieves undegraded performance with constant depression angles and receiver gate intervals.

If the orbit eccentricity must be maintained near $\epsilon = 0.005$, then the receiver gate interval must be varied during an orbit over the U.S. The depression angle during an orbit is held constant and the receiver gate interval is continually varied so that it accepts the ground swath illuminated by maximum antenna gain. This updating may be accomplished via an uplink command to the satellite, or by an onboard computer. The range gate interval will vary in position by an amount equal to its width at 75°, but adequate time within an interpulse interval exists for this. Variations in swath ground range offset are similar to those encountered when orbit eccentricity was 0.08. Table 3.2.3.7-3 presents specific ground range offset data. By varying receiver gate interval then, the errors may be eliminated without varying antenna depression angle.

Table 3.2.3.7-2

System Performance when Satellite Orbit Eccentricity Equals Earth Eccentricity for 60° and 75° Antenna Depression Angles

Latitude	Antenna Gain Loss at Swath Edge (dB)		Ground Range Offset to Near Swath Edge (Km)	
	60°	75°	60°	75°
26°	5.5	6.0	514.0	224.0
28°	5.5	5.9	514.1	224.3
30°	5.4	5.8	514.3	224.6
32°	5.3	5.6	514.4	225.0
34°	5.2	5.4	514.6	225.3
36°	5.1	5.2	514.7	225.7
38°	5.0	5.0	514.9	226.0
40°	5.1	5.2	515.1	226.4
42°	5.2	5.4	515.2	226.8
44°	5.3	5.6	515.4	227.2
46°	5.4	5.8	515.6	227.5
48°	5.5	5.9	515.7	227.9
50°	5.5	6.0	515.9	228.3

Swath Edge Gain Loss in Spherical Case = 5.0 dB

Table 3.2.3.7-3

Ground Range Offset of Near Swath Edge

Receiver Gate Varied with Fixed Antenna Depression Angle of 60° or 75°

Latitude	Ground Range Offset to Near Swath Edge (Km)	
	60°	75°
24°	511.3	224.6
26°	511.7	224.7
28°	512.0	224.9
30°	512.4	225.1
32°	512.8	225.2
34°	513.2	225.4
36°	513.6	225.6
38°	514.0	225.7
40°	514.4	225.9
42°	514.8	226.1
44°	515.3	226.3
46°	515.7	226.5
48°	516.1	226.7
50°	516.6	226.9

The two methods described here each eliminate the errors of variable satellite altitude without resorting to varying the antenna depression angle as a function of altitude. The antenna pointing accuracies of Section 3.2.3.7.3 are thus taken with respect to a fixed depression angle during any given orbit.

The earth, of course, is not even elliptical, but has numerous local terrain elevation variations. In mapping terrain where the local elevation variations (ground extend $\geq$ 40 Km) from the elliptical model used above do not exceed 1 Km, negligible additional swath positioning errors occur. This includes virtually all of the earth except for mountain ranges. When local variations approach 2 Km or more, as they would if portions of the Rocky Mountains were being mapped, swath positioning errors become noticeable. Additional gain loss at swath edges may be 2-4 dB from 25°-50° latitude. While this is not serious, it may eventually be desirable to correct it. This can be readily done by adjusting receiver gate interval since terrain elevation is well known. This method would be required even if orbit eccentricity were 0.08. Under either circumstance, then, receiver gate adjustment may be necessary. The effect of slopes is discussed in Appendix D.

3.2.3.8 Earth Rotation Effects

Rotation of the earth causes doppler spectrum offset and range slippage. These phenomena are, of course, related since if there were no doppler, there would be no radial velocity (in a plane orthogonal to the flight path) and, of course, if there is no radial velocity, there can be no range slippage.

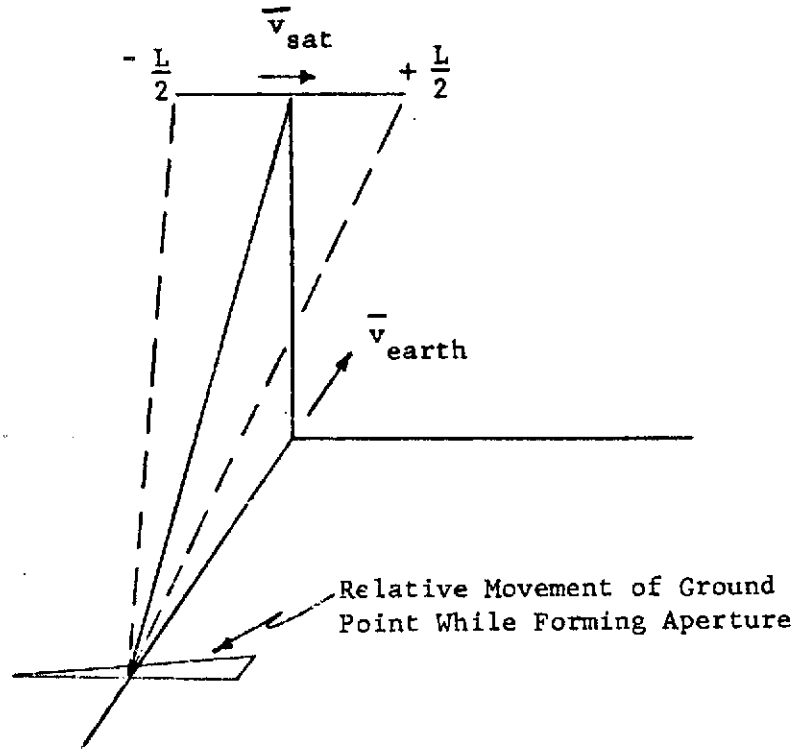

Figure 3.2.3.8-1 Earth Rotation Effect

Considering the satellite and earth relative motion vectors as in Figure 3.2.3.8-1, there is one vector direction along which there is zero radial velocity.

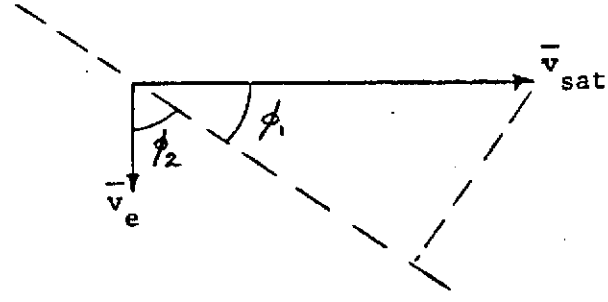

Figure 3.2.3.8-2 Vector Velocities

This is where

$$\bar{v}_e \cdot \bar{\mu} = \bar{v}_s \cdot \bar{\mu}$$

Where

$\bar{v}_e \triangleq$ earth's vector velocity

$\bar{v}_s \triangleq$ satellite vector velocity

$\bar{\mu} \triangleq$ unit zero radial velocity vector

Since

$$\phi_1 + \phi_2 = \frac{\pi}{2}$$

Since

$$\frac{v_e}{v_s} \ll 1, \quad \phi_2 \sim \frac{v_e}{v_s}$$

Consider a perfect circular polar orbit, there the earth's circumferential velocity becomes less as the satellite moves from the equator to the pole. Specifically, at some latitude n

$$v_n = \frac{C_n}{T} = \frac{2\pi R_n}{T} = \frac{2\pi}{T} R_o \cos \theta_n$$

Where

$v_n \triangleq$ earth's velocity at latitude angle n

$C_n \triangleq$ earth circumference at latitude angle n

$R_n \triangleq$ earth radius at latitude angle n

$R_o \triangleq$ equatorial radius

$T \triangleq$ 24 hours

$\theta_n \triangleq$ latitude angle

Taking into account the depression angle ϕ, the actual relative velocity is

$$v'_n = v_n \cos \phi$$

$$v'_n = \frac{2\pi}{T} R_o \cos \phi \cos \theta_n$$

$$= \frac{(2\pi)(6371) \cos 55^\circ}{(24)(3600)} \cos \theta_n \text{ m/sec}$$

Over the U.S., the latitude varies from 25° to 50°.

$$v'_{25} = 265 \cos 25 = 240 \text{ m/s}$$

$$v'_{50} = 265 \cos 50 = 170 \text{ m/s}$$

Then $$\phi_{25} = \frac{240}{6371} = 2.17^\circ$$

$$\phi_{50} = \frac{170}{6371} = 1.53^\circ$$

So, if the antenna were pointed at the angle ϕ from broadside, there would be no doppler offset and no range slippage. Antenna pointing accuracies would have to be about $\pm$ .05° to maintain ground map accuracy. This means continuous repositioning over U.S. with time constant relatively slow with respect to .125 sec.

If clutter positioning is done, preferably by open loop VCO slewing to match the incoming spectrum, the VCXO must slew about 5 KHz while traversing U.S.

The range slippage problem still has to be resolved, but can be done via ground signal processing.

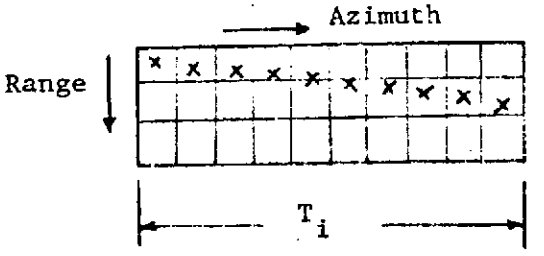

Figure 3.2.3.8-3 Range Drift

Range slippage or drift is about .8 to .6 of a 30 m range cell since

$$d_{25} = r'_{e_{25}} T_i \approx 24.0 \text{ m}$$

$$d_{50} = v'_{e_{50}} T_i \approx 17.0 \text{ m}$$

This could be corrected via ground processing interpolation. An alternate technique is to drift the range interval samples in the radar A/D converter without resetting in order to minimize pre-filter range registration problems. This could amount to 12 Km variation in absolute ground range offset, but this is not considered unreasonable.

In all of these techniques, orbit profile data is required by the radar to control gate drift rate and direction, depending on whether ascending or descending node or both is used. If the antenna is not steered to zero velocity and ground clutter tracking is done, then profile data should be available to ground correlator.

3.2.3.9 Orbit Relations

Figure 3.2.3.9-1 illustrates the orbit geometry of interest here. Polar circular sun-synchronous orbits are to be considered having nominal altitude of 900 km.

The sun-synchronous condition requires that the rate of rotation of the line of nodes match the angular rate of rotation of the sun direction. The line-of-nodes rotation is essentially due to earth oblateness, and is given by

$$\dot{\Omega}_s = \frac{2\pi}{\tau}\left(-\frac{3}{2} J_2 \left(\frac{Re}{p}\right)^2 \cos i\right)$$

where

τ is the orbital period: $= \frac{2\pi a^{3/2}}{\sqrt{\mu}}$

a is the orbit semi-major axis

u is the earth's gravitational constant: $\mu = 1.407639 \times 10^{16}$ ft^3/sec^2

J_2 is the second zonal gravitational parameter:

$$J_2 = 1.08228 \times 10^{-6}$$

R_e is the earth's equatorial radius:

$$R_e = 2.092564 \times 10^7 \text{ft.}$$

p is the semi-parameter $a(1-e^2)$, where e = orbit eccentricity

i is the orbit inclination.

In the case of circular orbits with equatorial altitude h,

$$a = R_e + h$$

$$p = a$$

The condition for a sun-synchronous orbit is then that the sunline rate (= $2\pi/(365.24 \times 24 \times 3600)$ radians per second) be equal to $\dot{\Omega}_s$:

$$\cos i = \frac{\tau}{(365.24 \times 24 \times 3600)} \left(\frac{3}{2} J_2 \left(\frac{R_e}{p}\right)^2\right)^{-1}$$

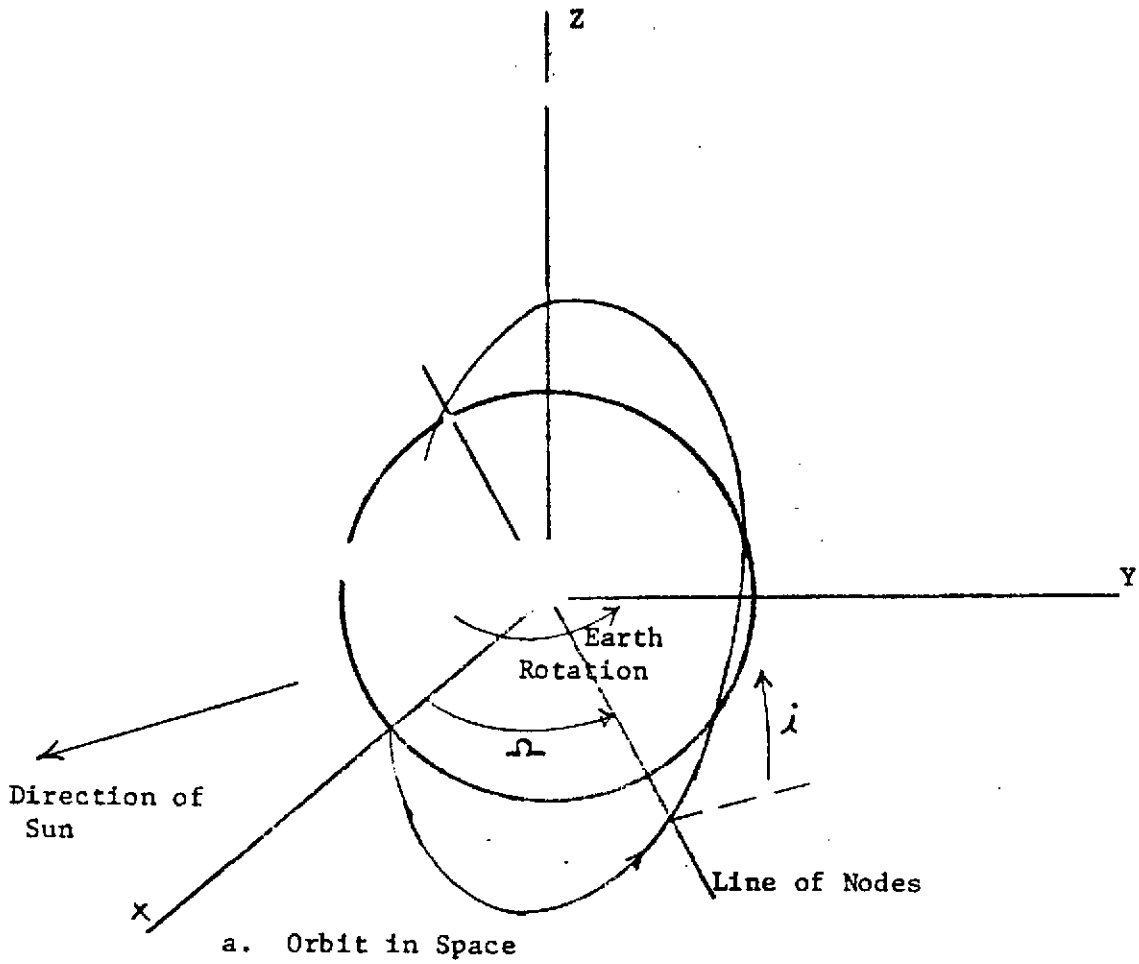

a. Orbit in Space

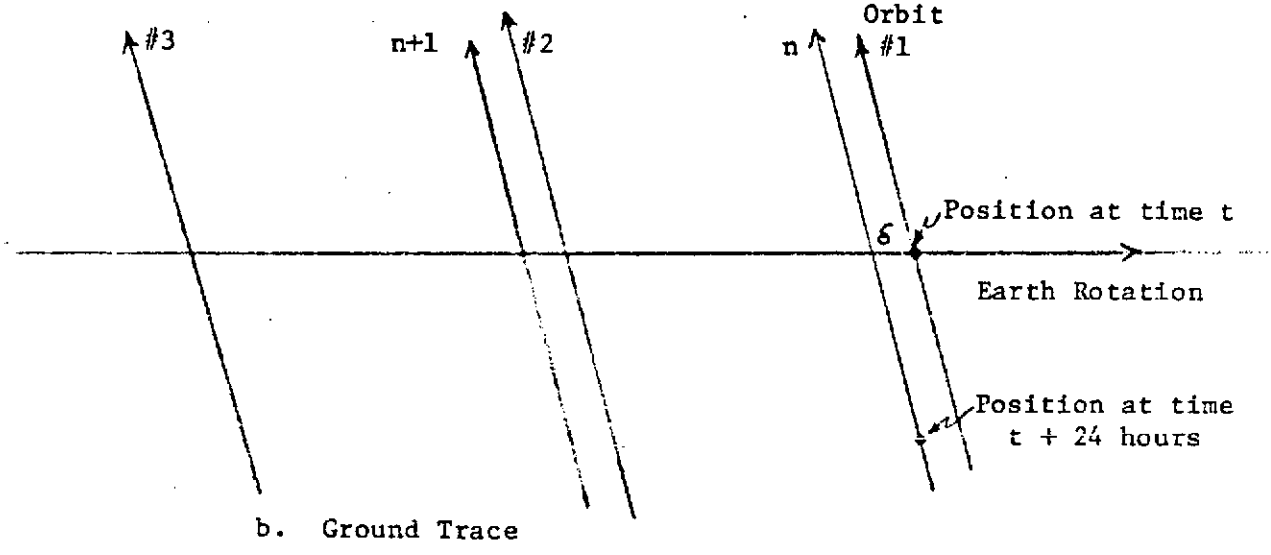

b. Ground Trace

Figure 3.2.3.9-1. Orbit Geometry

For a given period, the orbit produces a series of ground traces over an area as the earth rotates beneath the orbit, as shown in figure 3.2.3.9-1b. At the end of one day, the nth orbit will be incomplete, resulting in a displacement of orbit n relative to orbit #1. The displacement (assuming positive to the right) is given by

$$\delta_1 = (x_n - N_0)\tau\omega_s R_e \cos\lambda$$

$$\delta_2 = (x_n - (N_0+1))\tau\omega_s R_e \cos\lambda$$

where

N_0 is the greatest integer less than $\frac{Tday}{\tau}$

Tday = 24 x 3600 sec.

xn = Tday/τ

ω_s = earth's rotation rate, relative to the orbit plane (i.e., relative to the sunline from sun-synchronous orbits):

$$\omega_s = 2\pi/(24 \times 3600) \text{ rad/sec.}$$

λ is the longtitude of interest.

These relations are plotted in figures 3.2.3.9-2 and 3.2.3.9-3. For the nominal radar conditions of interest (50 km swath width and 60° depression angle), the swath position uncertainty due to $\pm$0.1° pointing error is small (about 0.5 km). Some overlap in swath is probably still desirable. Given a desired swath overlap, the required orbital altitude may be found from figure 3.2.3.9-2, and the corresponding period and inclination from figure 3.2.3.9-3. For example, for a 10% overlap, a δ of 50 km is required, yielding an altitude of 902 km, a period of 103.0 minutes, and an inclination of 99.04 degrees. Since the earth rotation between orbits is about 2200 km, the time required for a complete map of a large area is 2200/50 = 44 days.

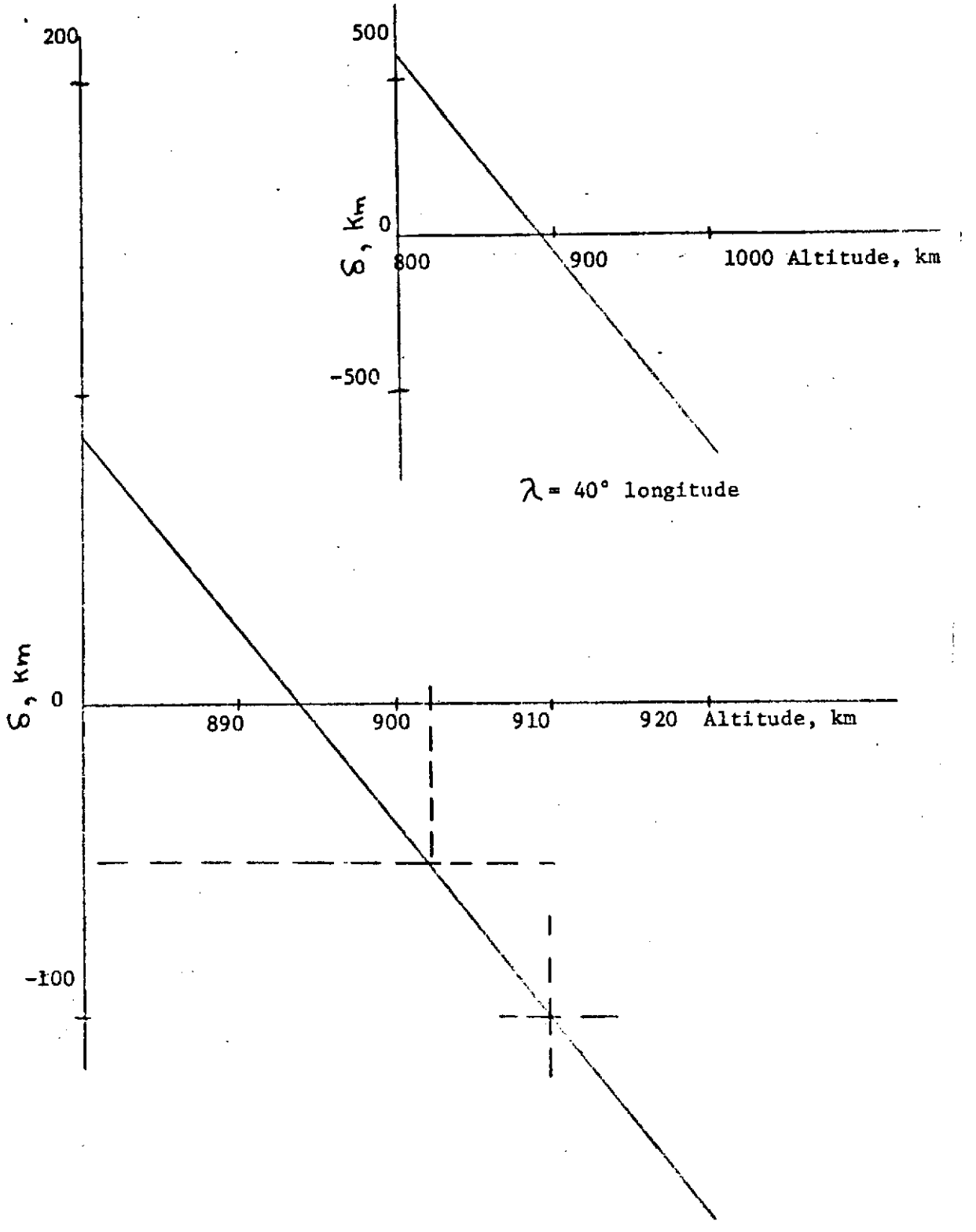

Figure 3.2.3.9-2. Path Increment δ vs. Orbit Altitude

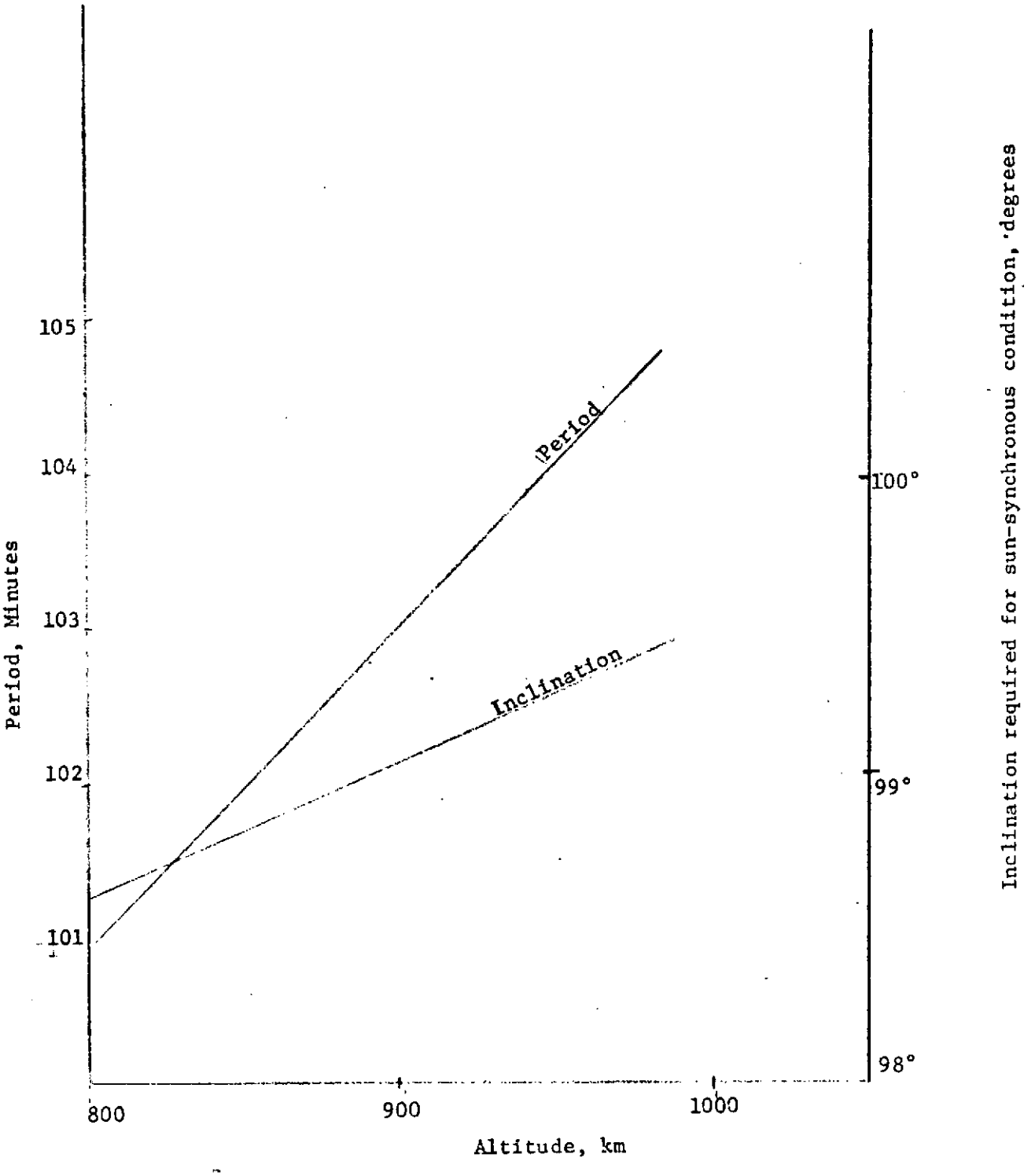

Figure 3.2.3.9-3. Period and Inclination vs. Altitude

3.3 Proposed Configurations

3.3.1 Configuration Summary

Two alternate configurations for the SSAR system are proposed. The configuration 1 radar (section 3.3.2.1) operates at X band only while the configuration 2 system (section 3.3.2.2) is a dual frequency radar operating at L and X bands. Both systems employ synthetic aperture and linear FM processing to achieve the desired resolutions. These radar configurations should be considered as baseline designs. Variations in these designs are indeed possible; however, in general, the parameters shown reflect presently known performance goals and result from a reasonably conservative design approach in order to achieve high instrumentation quality imagery commensurate with reasonable size, weight, etc. constraints.

These baseline parameters result from studies (section 3.2.3) indicating a tight interdependence of some of the parameters so extreme extrapolations from the baseline designs should be carefully considered.

For example, Tables 3.3.2-1 and 3.3.2-2 reflect 30m ground range resolution. There is no reason why 20m could not be achieved. Different dispersive delay lines and increased A/D and data link rates (still within 140 megabits/sec capacity) would be necessary. This sort of change from parameters shown in the table would not result in increased cost or reduced reliability. It should be pointed out that reductions to 12m range resolution would be possible; however, a reduction in image quality would be introduced since in order not to exceed data link capacity, 25% A/D oversampling factor would not be possible.

The hardware study objective is to identify and study critical design areas and to provide a description and verification of the proposed mechanization for each configuration.

The two radar configurations are coherent radars due to the synthetic aperture requirement. That is, a high degree of frequency stability is required such that successive ground return pulses may be added together. Two dimensional processing is utilized; that is, range and azimuth resolution are obtained through use of linear chirp FM techniques. Range compression utilizes surface wave dispersive delay lines and azimuth compression is achieved in the ground processor.

Dual polarization is achieved utilizing a unique Westinghouse antenna feed assembly. The dual frequency antenna uses a dual frequency feed and common reflector. X band horizontal and vertical transmission and reception are possible. The desirable S/N is achieved in part due to X band parametric and L band microstrip transistor front end receiver amplifiers. The receivers are dual conversion, one channel for each polarization or frequency. Complex digital video signal processing is utilized. The signal quantization and encoding takes place in the radar. Range slowdown is used in order to efficiently utilize universal time after analog/digital conversion. The map data is appropriately formatted for data link transmission.

The transmitter discussed in section 3.3.5.1 is a critical subsystem because of its impact on reliability, weight, power. The study considers:

1. Operation in a pressure controlled envelope.
2. Encapsulation of high voltage components.

3. Outgassing problem - how to control

4. Multipaction Breakdown

5. Heat dissipation

6. Reliability

Encapsulation of critical high voltage components rather than pressurization is a preferred approach because of the weight and difficulty of maintaining the pressure within a control envelope. The final power amplifier (FPA) utilizes a TWT to allow coherent operation with the required phase and amplitude linearity.

The antenna, discussed in section 3.3.5.2 is a critical subsystem primarily because the physical envelope may be too large to fit within a feasible launch vehicle for a given swath width, gain, ambiguity level, etc. The Westinghouse approach utilizes a unique dual polarization feed to obtain the multi-polarization flexibility required. The half-parabolic reflector was largely dictated by the coverage required and envelope storage space. Gain variations over the swath along with maximum gain impacts upon the maximum swath width.

3.3.2 Radar Parameters

The parameters for both configurations are given in Tables 3.3.2-1 and 3.3.2-2. Both baseline designs reflect similar nominal requirements such as: maximum azimuth and range resolution of 30m, swath width of 50 km, -25 dB ambiguity level and +3 to +10 dB S/N for a green grass reflector. As previously discussed, these requirements are nominal and can be readily increased or decreased subject to the tradeoffs discussed in section 3.2.3.

Basic differences in the two configurations: number one is X band dual polarization, 55° - 75° depression angle, number two is X and L band single polarization, 75° depression angle.

3.3.2.1 Radar Parameters - Configuration #1

Table 3.3.2-1 presents the preliminary radar parameters for configuration 1. This is a single frequency X band (9.3-9.5 GHz) system.

Detectability requirements led to a 150w average power specification for the transmitter. For spacecraft application peak power should be minimized to the extent possible to reduce voltage breakdown problems. Ambiguity constraints and swath width considerations require a nominal 3.5 KHz PRF. Varying the depression angle from 55° to 75° will require changes in the PRF from 3 to 4 KHz in order to maintain operation in a region not interrupted by "main bang" as well as sufficient suppression of range ambiguities.

Achieving a net 30m ground range resolution requires a 77 ns compressed pulse width (13 MHz linear FM bandwidth): with a 143:1 range compression ratio. The transmitted (expanded) pulse width is then 11.1 us. The duty cycle is 0.039, resulting in a peak transmitter power of about 4.0 kW.

The antenna size is 13.5 ft. in azimuth by 2.5 ft. in elevation by 1 ft. deep. No aperture weighting is provided in azimuth; the resulting two-way 4 dB azimuth beamwidth is 5.1 mrad. The elevation aperture is weighted just enough to yield a two-way peak sidelobe level of -30 dB for range ambiguity suppression purposes. The two-way 4 dB elevation beamwidth is then 30 mrad. The resulting one-way peak antenna gain, including shaping losses, is 44.9 dB.

Table 3.3.2-1 Preliminary Radar Parameters - Configuration #1

Frequency	9.3-9.5 GHz
Peak Power	4.0 kW
Average Power	150 w
PRF	3.5 $\pm$ .5 KHz
Transmitted Pulse Width	11.1 us
Compressed Pulse Width	77 ns (Δ f = 13.0 MHz)
Range Compression Ratio	143/1
Antenna	
Azimuth Beamwidth (two-way 4 dB)	.29^{o} (5.1 mrad)
Elevation Beamwidth (two-way 4 dB)	1.71^{o} (30 mrad)
Gain (one-way)	44.9 dB
Dimensions	4.5 x .76 x .3m (13.5 x 2.5 x 1 ft.)
Losses	
RF	2.5 dB
Weighting	2 dB
Field Degradation	0 dB
Atmospheric	1 dB
Nominal Depression Angle	60^{o} - 5^{o}, +15^{o}
Polarization	(HH, HV) (VV, VH)
IF	120 MHz
RF Noise Figure/Channel	1.7 dB
IF Bandwidth	$>$13 MHz
A/D Amplitude	4 + s bits
A/D Sample Rate	10.9 - 24.2 MHz
Output Data Rate	Two 78 megabit/sec channels[1]
Weight	119 Kg (262 lbs.)
Prime Power	1143 watts

[1]This figure commensurate with 30m and 50 Km ground range and swath width.

System losses included in detectability calculations are: a) 2.5 dB RF losses (such as waveguide, antenna feed line, circulator and receiver protector, b) 2 dB weighting loss due to weighting range and azimuth processed bandwidth to reduce peak sidelobes to 30 dB below mainlobe, and c) 1 dB atmospheric loss to account for atmospheric gases, heavy cloud cover, and very light rainfall. No field degradation loss was allowed. The antenna depression angle can vary between 55° and 75°. This can be accomplished by varying the antenna tilt angle with respect to the S/C or by rolling the S/C.

Four separate polarizations are available using a Westinghouse developed dual feed antenna. The four polarizations are transmit horizontal, receive horizontal (HH); HV, VV, VH; HH and HV or VH and VV are available simultaneously.

A dual conversion receiver is used with 120 MHz IF chosen primarily to facilitate fabrication of the surface wave dispersive expansion and compression line. An IF bandwidth of more than 13 MHz is desirable to process the spectrum resulting from the 30m ground range resolution.

The antenna depression angle will be 55° - 75°.

This radar will separately process and display images of like (HH) and cross polarization (HV) of the same ground area.

The system noise figure per channel is 1.7 dB, a very low value that eases detectability problems. The A/D converters sample s + 4 bits at a rate from 12.5 - 24.2 MHz depending upon depression angle. This 25% oversampling rate ensures that objects 30m apart on the ground may be discriminated. The output data rate to the spacecraft data link is equivalent to two 78 megabits/sec channels; this is consistent with

complex sampling at the above rates for both polarization channels.

3.3.2.2 Radar Parameters - Configuration #2

Table 3.3.2-2 lists the preliminary radar parameters for config. 2. This is the dual frequency X 99.3 - 9.5 GHz) and L (1.7 GHz) band system.

Detectability requirements led to average transmitter power specifications of 150w (X) and 25w (L). For spacecraft applications, peak power should be minimized to the extent possible. Ambiguity constraints require a 3 KHz PRF at 75° for both radars. The PRF is a function of the depression angle (section 3.2.3). Depression angle changes from 50°-75° require a 2-3 KHz PRF variance and result in acceptable (-25 dB) X band ambiguity levels. Operation over these angles and PRFs, which have been optimized for minimum ambiguities, will result in considerably worse ambiguity degradation in the L band system (see section 3.2.3 for performance levels under these conditions).

Achieving a net 30m ground range resolution requires a 37 ns compressed pulsewidth (27 MHz linear FM bandwidth); with a 300:1 range compression ratio, the transmitted (expanded) pulsewidth is then 11.1 us. The resulting duty cycle for both radars is then 0.0333, resulting in peak transmitter powers of 4.5 kW (X) and 0.75 kW (L).

One antenna, 27 ft. in azimuth by 2.5 ft. in elevation by 1 ft. deep, will utilize a dual feed at both X and L as opposed to using two separate antennas. No aperture weighting is provided in azimuth; the resulting two-way 4 dB azimuth beamwidths are 2.55 mrad (X) and 15.5 mrad (L). The elevation aperture is unweighted and yields a two-way peak sidelobe level of -25 dB for range ambiguity suppression purposes.

Table 3.3.2-2 Preliminary Radar Parameters - Configuration #2

Frequency X and L Band	9.3-9.5, 1.7 GHz	
Peak Power	4.5	.75 kW
Average Power	150	25w
PRF	3	3 KHz
Transmitted Pulse Width	11.1	11.1 us
Compressed Pulse Width	37	37 ns
Range Compression Ratio	300	300
Antenna		
Azimuth Beamwidth (two-way 4 dB)	2.55	15.5 mrad
Elevation Beamwidth (two-way 4 dB)	30	170 mrad
Gain (one-way)	47.9	32.0 dB
Dimensions	(8.85 x .76 x .3m) (27 x 2.5 x 1 ft.)	
Losses		
RF	3.4	3.4 dB
Weighting	2	2
Field Degradation	0	0
Atmospheric	1	.2
Nominal Depression Angle	75^{o}	75^{o}[1]
Polarization	HH	HH[2]
Range Ambiguity Suppressor	no	yes
RF Noise Figure/Channel	1.7	1.7 dB

[1] Depression angles from 50^{o} to 75^{o} can be used with an attendant decrease in image quality in the form of increased ambiguity level. Such variations require an A/D sample frequency variation of 9.7-24.2 megabits/sec. See section 3.2.3.

[2] Dual polarization X band along with single polarization L band option is available.

Table 3.3.2-2 (Cont'd)

IF	120	120 MHz
IF Bandwidth	27	27 MHz
A/D Amplitude	4 + s	4 + s
A/D Sample Rate	24.2 megabit/sec	
Output Data Rate	Two 62.4 megabits/sec channels[1]	
Weight	276 Kg (387 lbs.)	
Power	1262 watts	

The two-way 4 dB elevation beamwidths are then 30 mrad (X) and 170 mrad (L). The resulting one-way peak antenna gains, including shaping and blockage losses, are 47.9 dB (X) and 32.7 dB (L).

System losses included in the detectability calculations are a) 3.4 dB RF losses (such as waveguide, antenna feed lines, circulator and receiver protector), b) 2 dB weighting loss due to weighting range and azimuth processed bandwidths to reduce peak sidelobes to 30 dB below mainlobe, and c) 1 dB (X) or 0.2 dB (L) atmospheric loss to account for atmospheric gases, heavy cloud cover, and very light rainfall. No field degradation was allowed.

The antenna depression angle will be 75°. Since a single antenna with both beams aimed at the same depression angle is used, simultaneous coverage of the same ground swath at X and L bands is achieved. As previously mentioned, depression angles between 50° and 75° can be achieved with some degradation in L band performance due to increased ambiguity levels.

[1] This figure commensurate with 30m and 50 Km ground resolution and swath width.

Only one polarization, HH, will be processed and displayed.[1]

A range ambiguity suppressor that shifts the doppler spectra of returns from certain ambiguous range swaths out of the azimuth passband must be used in the L band system to achieve acceptable range ambiguity suppression. It is not required in the X band radar.

Each radar has a 1.7 dB per channel noise figure. The 27 MHz IF bandwidth accommodates the linear FM bandwidth; it is centered about 120 MHz. The A/D converters sample s + 4 bits at a 24.2 MHz rate. A 25% oversampling rate ensures that objects 30m apart on the ground may be discriminated. The output data rate to the spacecraft data link requires two 62.4 megabit/sec channels. This is consistent with complex sampling at the above rates for both the X and L band radars.

[1] An option is considered and illustrated in the antenna figures of a dual polarization X and single polarization L band system. An additional 53 lbs. is required for the dual polarization option.

3.3.3 Functional Block Diagrams

3.3.3.1 Introduction

The spacecraft (S/C) radar system has the function of developing electromagnetic returns from the ground in a suitable digital format for earth transmission such that imagery of sufficient quality can be obtained.

Each radar system has five major subsystems: antenna, transmitter, stabilized local oscillator (STALO)/synchronizer, system controller; low voltage power supply (LVPS), and receiver. These major system components are shown in the functional block diagrams, Figures 3.3.3-1 and 3.3.3-2.

Configuration #1 and #2 have many common functions so in the introductory discussion they will be jointly considered.

SAR radar with two-dimensional operation requires precise subsystem specifications, especially in the area of frequency and timing stability as well as time and frequency domain fidelity. These specifications have been developed and are given in section 3.3.5. Attaining high quality imagery requires a complete system approach to specification formulation and, in fact, even preliminary estimates require noise specifications as prepared for the STALO and transmitter.

The antenna has a dual polarization capability by incorporating a Westinghouse proprietary horizontal/vertical polarization feed. The antenna beam is precisely controlled in azimuth and elevation to maintain adequate signal/noise (S/N) ratio over the mapped ground swath while excluding undesirable responses.

The transmitter incorporates a high powered TWT, and high voltage power supply and modulator. The suggested TWT has been optimized for

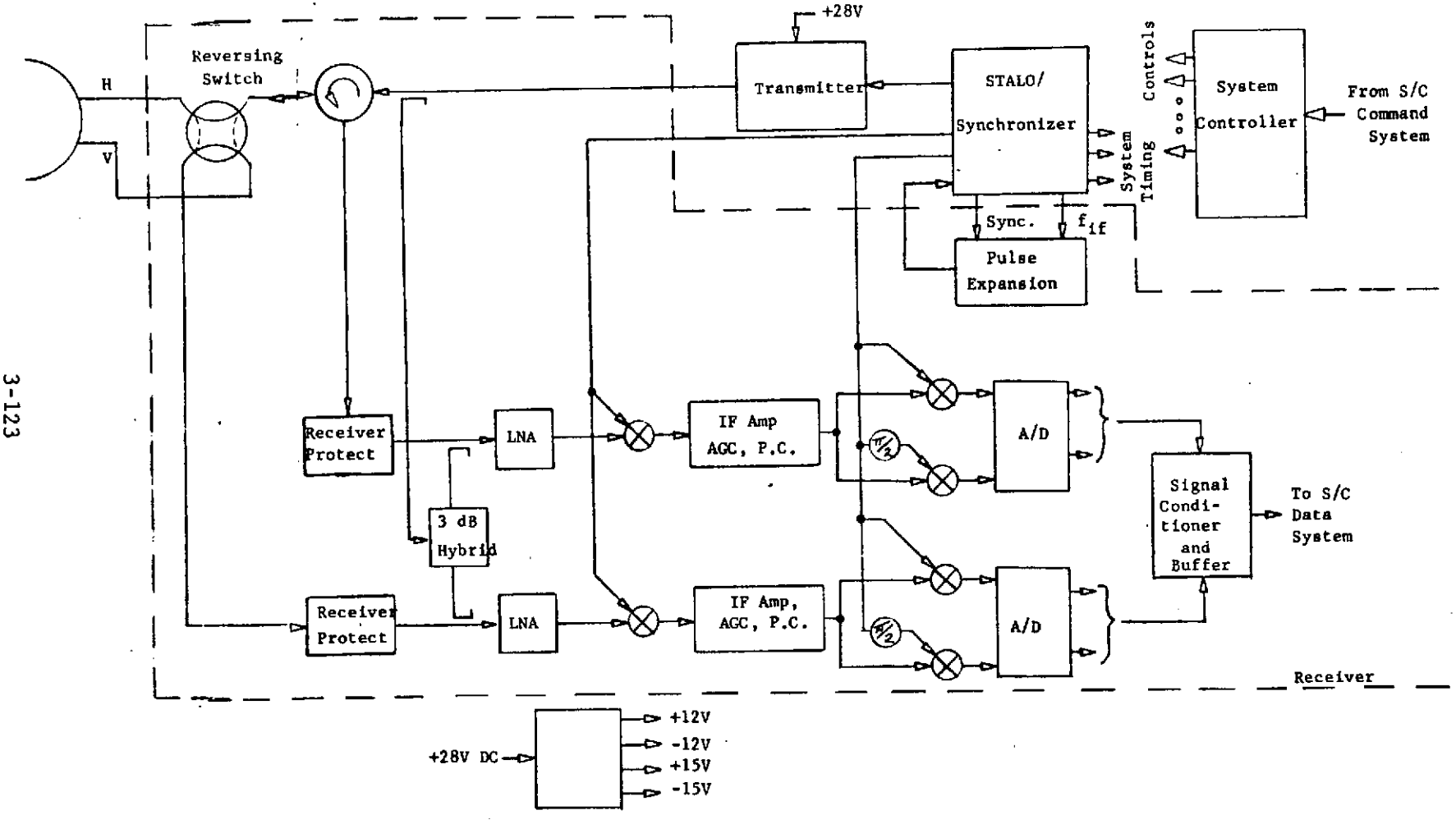

Figure 3.3.3-1. Spaceborne Synthetic Aperture Radar (SSAR) Configuration #1

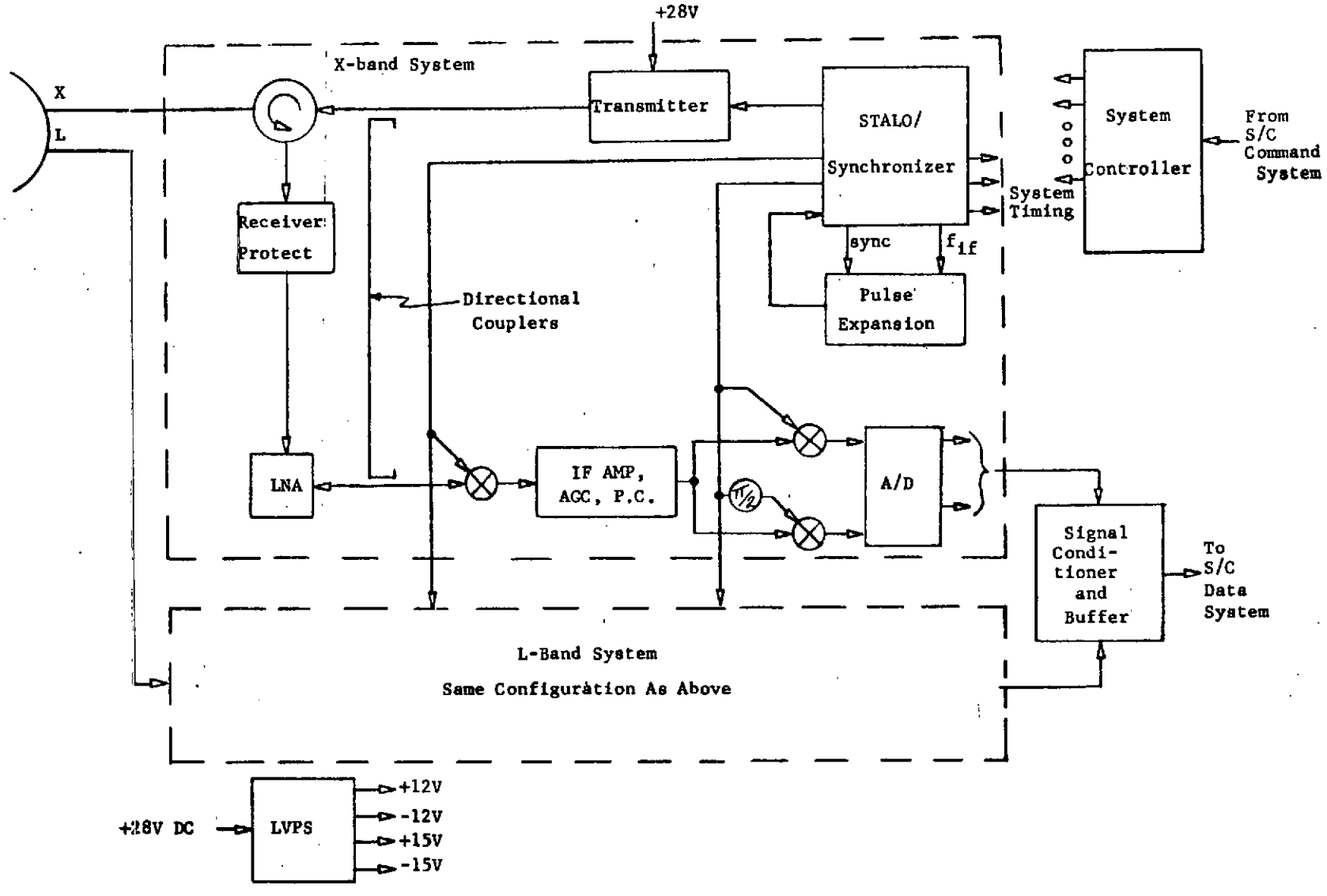

Figure 3.3.3-2. Spaceborne Synthetic Aperture Radar (SSAR) Configuration #2

maximum reliability. A relatively low peak power along with a coupled cavity structure results in a high reliability tube. To achieve this, tapering the design of a present "off the shelf" tube is necessary, which results in some relatively low risk development. The STALO/synchronizer provides basic system timing and the stable coherent transmitted and conversion signals. These signals have a high degree of short term stability commensurate with system requirements so as to negligibly degrade performance. The system controller receives and decodes radar command from the satellite up data link.

The receiver provides the low system noise, gain adjustment, frequency conversion, range pulse compression, analog to digital conversion and data prefiltering, so as to generate a standard data rate for delivery to the High Data Rate Processor. The calibration pulse generator is included in the IF. RF directional couplers are used to tap the transmitter output and inject the receiver with this calibration pulse. The low voltage power supply generates the required system voltages from prime power, +28v dc.

3.3.3.2 Configuration One

The signal to be transmitted actually originates in the STALO/synchronizer. Since repetitive pulses are added coherently to form the azimuth channel, a high degree of frequency stability is desired as compared to a non-coherent system. The STALO/synchronizer supplies highly stable timing pulses, various conversion reference signals, as well as the basic signals to be transmitted. These are generated by shocking a dispersive delay line with a quarter cycle of a phase stable reference of the IF. The dispersed output pulse is then converted to

the RF frequency and sent to the transmitter. The timing signals are generally derived from a stable oscillator in the STALO.

The transmitter is a critical subsystem in several respects. It contains the only vacuum tube (TWT) with its attendant reliability problems. Also contained are a high voltage power supply, which is of concern due to potential voltage breakdown problems. The transmitter assembly also dissipates some 600w or 60% of the system thermal power to be dissipated. The factors are analyzed further in section 3.3.5.

The transmitter amplifies in a phase distortion-free fashion, the STALO pulse. The transmitter must do this over the variable PRF range indicated.

The antenna function is to illuminate the ground swath with energy from the circulator and transmitter. The antenna must have a well-controlled antenna pattern with an elevation mainlobe of sufficient width to cover the ground swath and yet not introduce undue range ambiguities. The azimuth mainlobe must have sufficient width to allow multilook processing commensurate with the desired resolution. The sidelobes of the pattern must be sufficiently suppressed so as not to result in ambiguous responses.

Two polarizations are to be provided such that in conjunction with dual receiver channels, vertical and horizontal polarized backscatter components from the s: : ground terrain will be available. The use of a four-port waveguide switch will allow transmission and reception on all polarization combinations.

The received signal of each polarization is processed in each receiver channel. The major functional requirements of the receiver

include: low noise amplification, main bang gating, automatic gain control (AGC), dual conversion from RF to complex video, calibration pulse generation, expanded pulse generation, and compression A/D conversion, and digital data buffering. As mentioned too, receive channels must be provided for simultaneous dual polarization reception.

X-band parametric amplifiers are provided to achieve the desired low noise figure. The receiver protectors provide main bang gating such that the parametric amplifiers are not harmed by the transmitter main bang. AGC is necessary to provide compensation for variations in signal strength due to changes in backscatter coefficient, slant range variations, etc. The signal strength is adjusted to lie within the A/D dynamic range.

The receiver provides the calibration pulse generation as discussed in section 5.3. The pulse expansion and compression utilizes dispersive surface wave delay lines. The inclusion of the compression lines within the radar allows a significant decrease in processor complexity. Conversion to complex video is necessary to utilize the entire PRF interval. Compensation of earth rotation effects may result in drifting of the A/D samples as suggested in section 3.2.3.7. The digital data buffer provides the variable range slowdown to maintain constant output radar data rate such that data link channel capacity is used most effectively.

3.3.3.3 Configuration Two

Configuration two basically consists of two separate radar systems, X and L band, with the system controller, low voltage power supply, and some parts of the STALO/synchronizer being shared between the two radars. Many of the features discussed in section 3.3.3.2 for configuration one

are equally applicable to configuration two, so emphasis in this section will be on the differences.

The X-band radar is very similar to the radar of configuration one, except only one polarization is available and, consequently, there is no polarization switching and only one receiver channel. The antenna has twice the real azimuth aperture (27 ft. vs. 13.5 ft.) as the antenna of configuration one. The proposed configuration has only a single polarization for each radar; however, by adding an additional receiver channel and more complicated antenna feed assembly (total weight increase about 50 lbs.), dual X-band polarization may be achieved. The data rate requirements would be three 62.4 megabits/sec. channels.

The L-band radar has the same functional configuration as the X-band radar; however, the average power is only 25w instead of 150w. This and the lower frequency allows the use of a solid state transmitter. This transmitter has the same signal fidelity requirements as the X-band system and, as such, the requirements are given in section 3.3.5.1.2. The receiver noise figure of 1.7 dB is achieved using a microstrip transistor amplifier as opposed to a parametric amplifier. The power supply requirements are essentially the same as configuration #1.

The amplitude calibration system requires a precise directional coupler pick-off from each transmitter and injection into each RF amplifier.

3.3.4 Parametric Verification

3.3.4.1 Ground Range Resolution

The proposed radar configurations utilize surface wave dispersive delay lines to expand and compress the range pulses. The delay lines

are designed for a specific compressed pulse width. As the lines and associated electronics are relatively small (6 cu. in.), several pulse widths could be provided in a given radar configuration.

It has been assumed a single line/radar exists with the parameters indicated in Tables 3.3.2-1 and 3.3.2-2 of ground range resolution of 30m at a depression angle of 60° and 75° for configurations #1 and #2 respectively. As the radar effectively operates in slant range coordinates, 30m resolution is achieved only at the nominal design depression angles. Greater and less resolution is achieved for depression angles less and more than the nominal design depression angles assuming a constant A/D sampling rate. This relationship is shown in Figure 3.3.4-1.

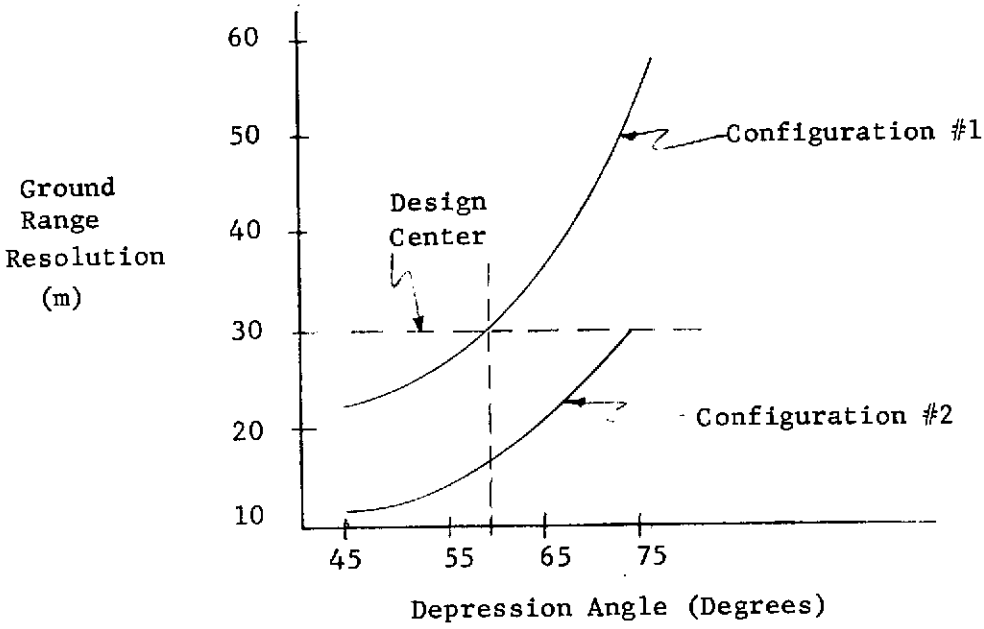

Figure 3.3.4-1. Pre-A/D Ground Range Resolution

As indicated in section 3.3.4.2, the A/D sample rate will vary with depression angle, so as to maintain constant ground range sampling

interval. For a constant ground range swath width, the number of samples taken will remain constant, thus, the sample interval decreases with increasing depression angle, but range slowdown increases to maintain constant output data rate.

The fact that the A/D sampling rate is changing as described to maintain 30m resolution will result in the resolution as shown in Figure 3.3.4-2 where the sampling degrades pre-A/D resolution to 30m. Operation with configuration #1 is between 60^{o} and 75^{o}. As mentioned, inclusion of a second dispersive delay line to be used between 65^{o} and 75^{o} will maintain 30m resolution throughout the depression angle range while maintaining adequate S/N.

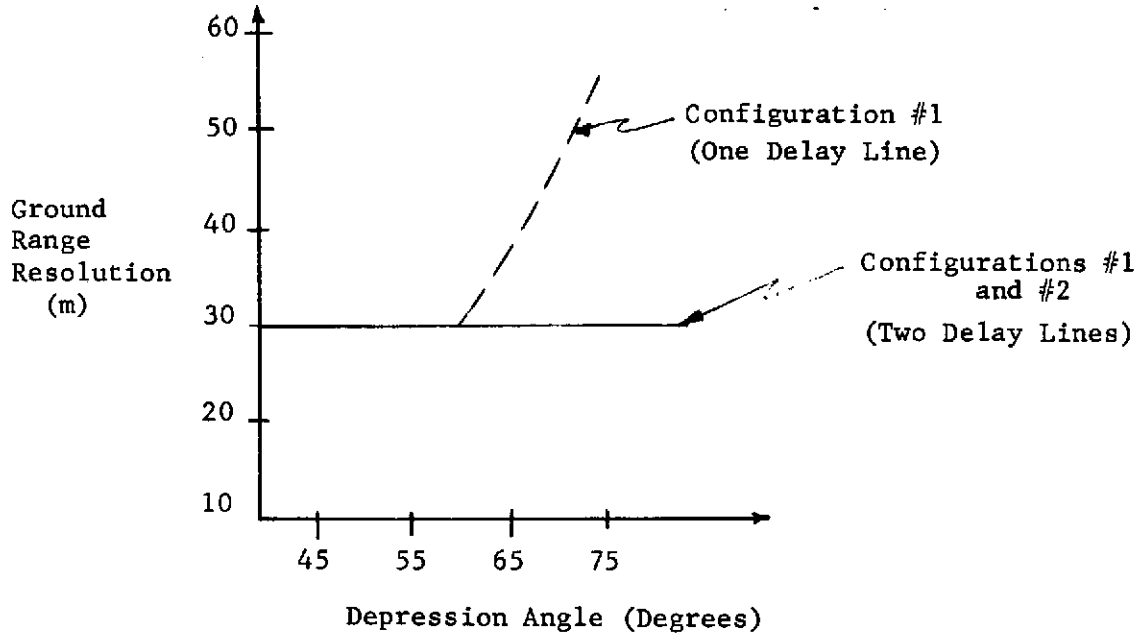

Figure 3.3.4-2. Ground Range Resolution

3.3.4.2 Spacecraft and Data Link Data Rates

Reference to the system block diagram will show two channels, I and Q, each of which require an A/D and two polarization channels, HH and HV. The data rate per A/D can be determined as:

$$r_1 = \frac{N_R N_b}{\Delta T} \left(\frac{1}{\text{A.S.D.}} \quad \frac{1}{\text{R.S.D.}}\right)$$

where $r_1 \triangleq$ precorrelation sampling rate per A/D

$N_b \triangleq$ amplitude and sign bits

$\Delta T \triangleq$ slant range time interval

$N_R \triangleq$ number of range cells/IPP = $\frac{\Delta T}{\tau}$

$f_s \triangleq$ sampling rate

A.S.D. $\triangleq$ azimuth slow down factor

R.S.D. $\triangleq$ range slow down factor

The sampling rate is related to the depression angle and image quality. Figure 3.3.4-3 indicates the greater the depression angle the shorter the slant range pulse width to be generated and, consequently, the greater the range (A/D) sampling rate.

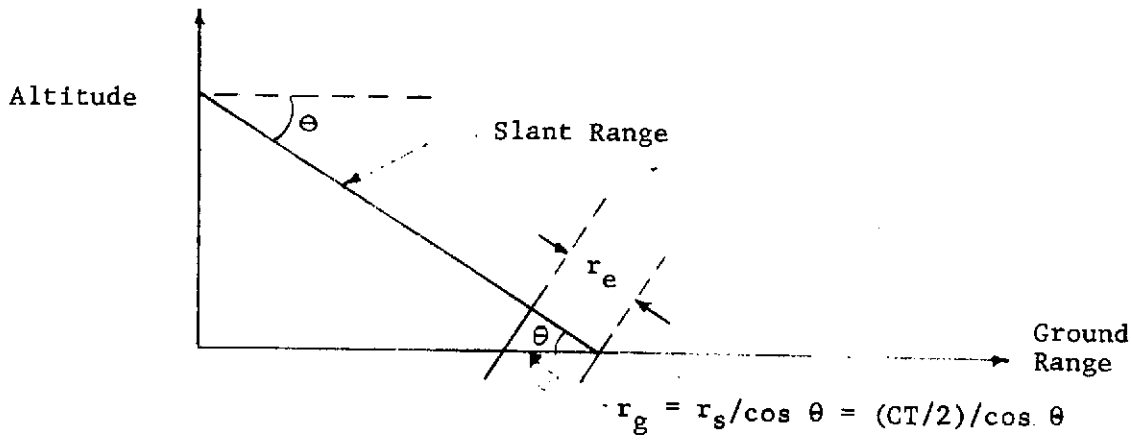

Figure 3.3.4-3. Slant Range/Ground Range

Image quality is related to oversampling rate and sidelobes. A factor of 25% per A/D oversampling is used to maintain actual resolution. A typical A/D input for two targets, separated in slant range by r_s, is

shown in Figure 3.3.4-4. If the sampling interval is equal to the slant range resolution, r_s, then the two samples are not resolved. Decreasing the sample period by 25% will tend to maintain resolution compatible with the pulse width. The required sampling rate becomes

$$f_s = \frac{1}{(r_g \cos \theta)} \quad \frac{1}{(1/1.25)} \left(\frac{m}{6.66 \text{ ns}}\right)$$

For a desired ground range resolution of 30m and depression angle of 60^o

$$f_s = \frac{(1.25)}{(30)(\cos 60^o)} \quad \frac{1}{6.66} \times 10^9 = 12.5 \text{ MHz}$$

The range swath time interval is some fraction of the IPP. Then

$$N_R = \frac{\Delta R_g}{r_g} = \frac{(\Delta R_g \ 6.66 \text{ us/km}) \cos \theta}{\tau}$$

$$= (40 \text{ km})(6.66 \text{ us/km})(\cos 60^o)(12.5 \text{ MHz}) = 1670$$

where ΔR_g = ground range swath

Note that the number of range cells/IPP and, consequently, the data rate r_1 is independent of the depression angle except that ΔR may be a function of the depression angle due to antenna pattern limitations.

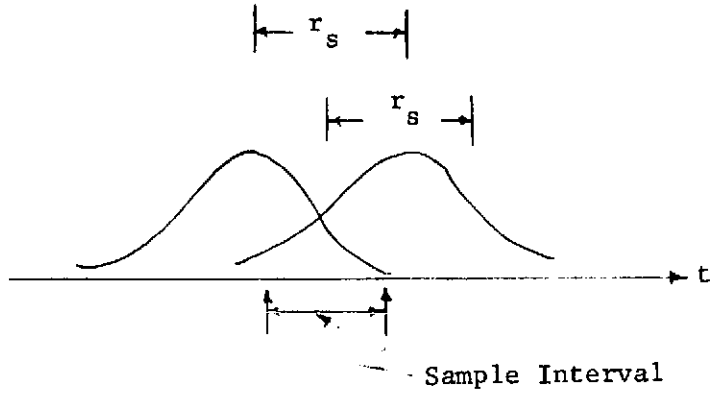

Figure 3.3.4-4 Target Separation

That is,

$$r_1 = \frac{N_R N_b}{\Delta T} \quad \frac{1}{(R.S.D.)} \quad \frac{1}{(A.S.D.)}$$

For

$$A.S.D. = 1$$

$$N_R = \frac{\Delta T}{\tau} = \Delta T \, f_s$$

$$R.S.D. \cong \frac{T_r}{\Delta T}$$

$$\Delta T = \Delta R_g \cos \theta \ (6.66 \ \mu s/km)$$

so $$r_1 = \frac{\Delta T \, f_s}{\Delta T \, \frac{T_r}{\Delta T}} \, N_b = \Delta T \, \frac{1}{r_g \cos \theta} \quad \frac{k_1}{6.66 \text{ us/km}} \quad \frac{N_b}{T_r}$$

$$= \frac{\Delta R_g \cos \theta \ (6.66 \text{ us/km})}{r_g \cos \theta \ (6.66 \text{ us/km}) \, T_r} \, k_1 \, N_b$$

$$r_1 = \frac{\Delta R_g}{r_g} \, k_1 \, N_b \, \frac{1}{T_r}$$

where $k_1 = 1.25$

Note that for R.S.D. = 1 and A.S.D. = 2

$$r_1 = \frac{N_R N_b}{2T_r}$$

The A/D's encode the analog signal into a sign bit and four amplitude bits. The 2 in the denominator of the equation for r_1 accounts for a 2/1 azimuth slowdown allowed by the prefilter. That is, the data has some amount of redundancy which can be reduced by filtering and selecting every other sample. This reduces the azimuth data rate by a factor of 2. For a range slowdown of 2, no azimuth slowdown

$$r_1 = \frac{(1670)(5)}{(2)(133 \times 10^{-6})} = 31.2 \text{ megabits/sec}$$

where $\Delta T = 133 \ \mu s$

Precompressed data requires In-phase and Quadrature (I & Q) samples per receiver, and for two polarizations and receivers, the total number is two 62.4 megabits/sec channels.

There is some difference between this and the post compression/ detection data.

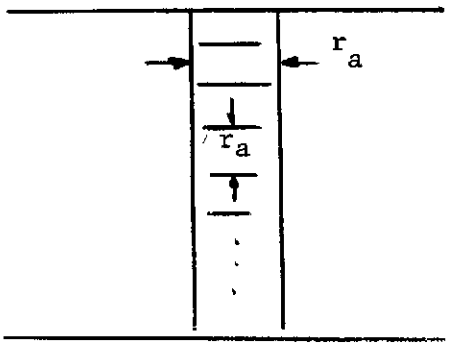

Figure 3.3.4-5. Number of Cells and Data Bits For Real Time Readout

The post correlation/post detection data rate becomes

$$r_2 = \frac{N_R N_A N_b}{T_a}$$

where N_A = azimuth channels passed in time T_a

$$T_a = \frac{r_a}{v} = \frac{30m}{7600m/sec} = 3.95 \text{ ms}$$

$$N_R = \frac{\Delta R}{R_a} 1.25 \frac{40000m}{30m} 1.25 = 1670$$

Assume $N_b \tilde{=} 5$ (it may be slightly more due to detection). Then

$$r_2 = \frac{(1670)(5)}{3.95 \text{ ms}} = 2.11 \text{ megabits/sec.}$$

The discrepancy between precorrelation data rate of 62.4 megabits and post correlation data rate is accounted for by two factors. The detected data of r_2 has eliminated phase information which accounts for

a factor of 2 and the precorrelated data bandwidth of Δf is contained in a periodic spectrum of period with f_r. Now,

$$\Delta f = \frac{v}{r_a}$$

Then

$$\Delta f = \frac{7600 \text{ ms}}{(30\text{m})} = 252 \text{ Hz}$$

$\Delta f/fr$ is a wasted spectrum factor and, therefore, is

$$\frac{\Delta f}{fr} = \frac{252}{3750} = \frac{1}{13.8}$$

So

$$\frac{2r_1}{r_2} = \frac{62.4 \text{ megabits/sec}}{2.11 \text{ megabits/sec}} = 29.7$$

and $$2\frac{f_r}{r_2} = 27.6$$

The reduction between pre and post correlation data rates is then closely accounted for.

The $\Delta f/fr$ factor cannot be further reduced because of practical filter skirt and phase limitations.

3.3.4.2.1 Summary

The post correlation data rate, after range slowdown, is less by a factor of about 29.7, than the precorrelation data rate. This is because phase information has been eliminated. Now if an azimuth slowdown of 2 were used, the data rate ratio could be reduced to about 15; however, further reductions would be difficult because of prefilter skirt limitations. Prefiltering would require onboard clutter tracking.

The A/D sample rate will vary with depression angle so as to maintain constant ground range sampling interval. For a constant ground

range swath width, the number of samples taken will remain constant; thus, the sample interval decreases with increasing depression angle, but range slowdown increases to maintain constant output data rates.

The preceding discussion assumed no azimuth multilooks.

The data rate per A/D for 30m resolution, 50 km swath, 60^{o} depression angle and sign plus 4 bits quantization is 31.2 megabits/sec. A range slowdown factor about 2 and no azimuth slowdown is used. A complete receiver requires I and Q channels or a 78 megabits/sec rate and a dual polarization receiver or dual RF frequency (X and L) single polarization radar would require two 78 megabit/sec channels.

3.3.4.3 Reliability

3.3.4.3.1 General

The following reliability analysis is based on both X and X/L band configurations proposed for the SSAR. Failure rates used in these models reflect the stringent component and system screening and burn-in program mandatory in achieving the high level of operational reliability needed in the space environment. In arriving at the final system reliability, mathematical model, various trade-offs directed at the usage of certain critical components were made such that the optimum balance between reliability, weight, performance, and power consumption could be made. These trade-offs along with the system reliability mathematical models and analyses are discussed in detail in the following sections.

3.3.4.3.2 Mathematical Model

The reliability mathematical models illustrated in Figure 3.3.4-6 show in block diagram form the reliability relationships of both the SSAR-X band and combination X/L band radar configurations. From this

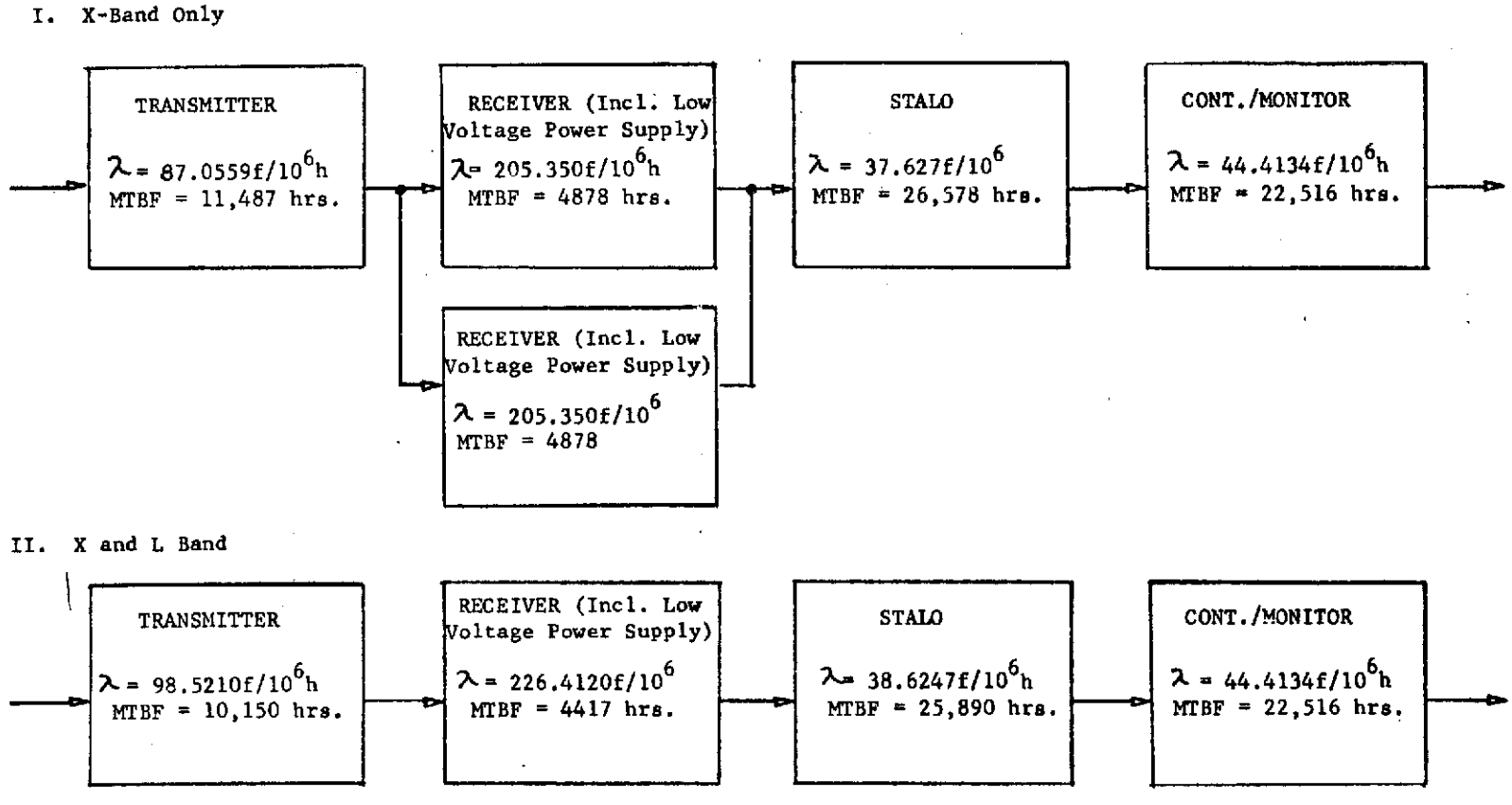

Figure 3.3.4-6. SSAR Reliability Block Diagram

illustration, the basic X-band radar has been divided into four major units: transmitter, receiver, stalo and controller. With the addition of the L-band capability, additional components and, thus, an increase in overall system failure rate, is reflected in the model. From this model, a failure in any of these major units with the exception of the receiver, would be catastrophic to system operation. In the receivers, where redundancy exists between horizontal and vertical polarization channels, a failure in either the horizontal or vertical polarization processing channel would not be catastrophic to system operation but would only limit the system performance to the processing of one channel's input data. Because of the mechanization of the X/L band configuration, redundancy in the receiver could not be implemented. Mathematically, the system Mean Time Between Failure (MTBF) for both these configurations is calculated as follows:

$$(MTBF)_{SYS} = \sum_{i=1}^{4} \frac{1}{(MTBF)_i}$$

where $(MTBF)_{SYS}$ = system MTBF

$(MTBF)_i$ = individual unit MTBF

4 = number of several reliability units in system

The individual component generic failure rates utilized in this model have been derived from NASA Technical Report 32-1544. These failure rates are indicative of the level of screening, qualification and system testing to be employed on the SSAR to remove early life and process-defect-type failures and ultimately achieve the high degree of operational reliability needed in the space environment. From Figure 3.3.4-6 and the mathematical model exhibited above, the system MTBF for X-band

configuration is 3289 hours and 2450 hours for the combination L/X band configuration.

3.3.4.3.3 System Reliability Trade-Offs

In the SSAR study program, four significant trade-offs were made as a result of the reliability study. Two of these trade-offs had direct impact on the STALO/System Controller configuration while the third affected the transmitter. These trade-offs were made as a result of a failure mode and effect analysis in which the SSAR critical signal processing path was studied and the design techniques employed in this path evaluated for criticality and probability of failure. In general, the object of this study was to (1) minimize adjustments, (2) minimize mechanical interactions, and (3) maximize standardization.

The first trade-off made was directed at the STALO/System Controller timing mechanism. Initially, three crystals were used in configuration #1 and four in configuration #2 to generate specific timing required for system operation. Reliability data has proven that instability in crystal timing generation is a major failure mode caused primarily by temperature variations and mechanical interactions generally resulting in a wear phenomenon within the crystal structure itself. Also, when more than one crystal is used in a system, the synchronizing of overall system timing mechanisms becomes extremely difficult to achieve. Resulting from this, two of the three crystals initially used in configuration #1 and three of the four in configuration #2 were replaced by a series of frequency multiplying and dividing networks. This reduces the overall probability of system failure by minimizing the number of crystals used in the SSAR and providing one standard timing

device for the overall radar. This design change resulted in an overall system failure rate reduction of $49.6098f/10^6$ hours for configuration #1 and $74.4147f/10^6$ hours for configuration #2.

The second reliability trade-off made in the STALO was the substitution of a resistive network for three potentiometers in configuration #1 and five potentiometers in configuration #2. Since the variable resistors were used for obtaining a resistance value peculiar to standard resistance values, a resistive network which would eliminate the inherent reliability problems associated with variable resistors was utilized. This eliminated the major failure mode of the variable resistors, i.e., an increase in resistance caused by a hotspot or imperfection in the resistance wire and resulted in an overall system failure rate reduction of $43.7485f/10^6$ hours for configuration #1 and $73.0315f/10^6$ hours for configuration 2.

The third reliability trade-off was made in the control and monitoring circuitry of the transmitter. Originally, five relays were used for controlling certain functions, however, due to the mechanical failure mechanisms inherent to relays, these components were eliminated from the design, and 20 transistors and 15 resistors were substituted. The redesign eliminated the possibility of system failure resulting from relay contact wear and effectively reduced the system failure rate by $9.3015f/10^6$ hours. These three trade-offs effectively reduced the system failure rate by $91.6598f/10^6$ hours for configuration 1 and $156.7477f/10^6$ hours for configuration 2.

The fourth reliability trade-off was made in the area of integrated circuits. Repackaging the 350 integrated circuits into 25 multi-chip

Packages (MHPs) and 20 integrated circuits reduced the thermal gradients and improved the overall reliability. This reliability trade-off resulted in an overall reduction in system failure rate of $60f/10^6$ hours.

3.3.4.3.4 TWT Reliability

To achieve the high degree of reliability required in the transmitter, the traveling wave tube used must be extremely reliable. In the SSAR, the TWT is not maintainable in the space environment and, therefore, must be designed for a tube life consistent with storage and mission duration requirement and a mean-time-to-failure compatible with mission performance requirements. A constraint placed upon maximum reliability attainment is incurred with the space tube requirement of optimum performance (power output, bandwidth, efficiency and gain) coupled to minimum weight, cost, and rugged construction. At first, these parameters may appear incompatible, however, the Hughes family of space qualified TWTs has achieved these basic design objectives and accumulated more than 800,000 hours of failure free life test and space operation.

The paragraphs which follow will highlight the design reliability characteristics of the Hughes traveling-wave tubes which are essential to reliable performance. These include the use of a mechanical configuration which couples reliability to excellent performance, the selection of proven materials, processes and manufacturing techniques established for high reliability space tube programs, and the incorporation of a long lifetime cathode design.

The mechanical design employs metal-ceramic construction which enhances reliability through an inherently rugged design. The electron

gun for the tube consists of a stacked self-aligning metal-ceramic assembly which allows close tolerances to insure excellent beam optics and performance repeatability from tube to tube. This is important since the success of any high-performance space tube is extremely dependent on the quality of the electron beam. A well-formed beam is essential to proper focusing with a minimum value of magnetic field, high beam transmission, low noise and good efficiency which adds to the overall reliability of the tube.

The electron gun construction also avoids a cantilever cathode-heater assembly prevalent in glass tubes and in many metal-ceramic tubes. In the cantilever design, gun elements are suspended from pins which extend through the end of the gun envelope yielding an increased susceptibility to shock and vibration. Perhaps the most prevalent failure mode of an electron gun is the heater open or short. The Hughes heater design consists of an alumina coated tungsten wire housed within an insulating ceramic assembly which essentially eliminates any possibility of shorts between heater and cathode. Sufficient area is allowed in the design of the electron gun to allow conservative electrical and thermal stresses on the heater element to eliminate embrittlement or mechanical failure. Experiments have shown this type of heater assembly to be highly reliable.

Focusing is accomplished by employing high-quality Samarium-Cobalt PPM magnets which fit closely over the barrel. Magnets are selected to provide the required performance and thermal stability.

One final item of importance to reliability which is often overlooked concerns the encapsulation of the TWT. The potting material must

perform two important functions: 1) insulation of high voltage areas to prevent arcing and corona at all expected pressures, and 2) provide a low resistance thermal path from the tube to the mounting surface of the package. Since the electronic package of the space vehicle is generally not pressurized, a potting compound must be used which is sufficiently stable for vacuum operation. This rules out the common silicon base materials previously used in airborne applications. A new material--flexible polyurethane, loaded with alumina powder to provide a good thermal conductivity has been developed for space tubes. In addition to providing the required electrical and thermal characteristics, this material provides shock damping and, most important, allows bending and twisting of the mounting frame without transmitting this to the tube.

3.3.4.3.5 SSAR Reliability

The reliability specification of SSAR is 500 hours operation with 95% probability of success. Using the exponential model for calculating the probability of success, this results in a system MTBF of approximately 10,000 hours. In general, the mission requirements for SSAR is a ten-minute operation per orbit with the orbit time being 100 minutes. If the radar was in orbit for four months, this results in a total radar operating time of 292 hours. Using this in the exponential equation for calculating reliability, the reliability for X-band configuration for this operating period is 92% and 89% for the combination X/L band configuration.

3.3.5 Subsystem Specifications

3.3.5.1 Transmitter

3.3.5.1.1 Introduction

Configuration one requires an X-band transmitter (9.3-9.5 GHz) while configuration two requires an X and L band (1.7 GHz) transmitter. The salient transmitter parameters are developed and presented in sections 3.2.3 and 3.3.5.1.2. Section 3.2.3 develops such requirements as PRF, power, etc. which are summarized in table 3.3.5-1 while those requirements bearing on signal fidelity and distortion are discussed in section 3.3.5.1.2. Attaining instrumentation quality SAR imagery requires the development of subsystem specifications to the point that reasonably accurate design estimates can be made. It is important the design take into account noise and power supply ripple, for example, in order that these phenomena do not introduce ambiguities or sidelobes. Thus, specifications for allowed signal degradation due to such phenomena must be generated as these requirements impact upon the transmitter power supply filtering and weight.

The design study shown in section 3.3.5.1.3 reports on (1) parametric verification, (2) description and (3) reviews available components for applicability to orbital operation. The possibility of using existing designs in a temperature and pressure controlled envelope is considered and traded off with the alternative of designing new equipment. The study considers, and comments on, such facets as:

1. Encapsulation of high voltage components
2. Outgassing problem - how to control
3. Multipaction breakdown
4. Heat dissipation and temperature control
5. Reliability

Necessary pressurization as well as what components should be pressurized are indicated along with weight and size of ancillary pressurization equipment such as the pump and envelope. Pressurization and multipaction breakdown considerations which include all waveguide, coax, receiver protection are considered as well as duplexer, although these are not part of the transmitter proper. Maximum DC voltages required for each configuration are indicated.

A specific tube requiring no development except heat pipe inclusion is selected. Reliability considerations are discussed. The FPA* which forms the principal operating lifetime constraint is carefully considered and means established to obtain long lifetime in orbit with high reliability. Thermal considerations are indicated.

A graph of weight versus average transmitter power for the two configurations is included.

The system has to operate at the orbit altitude and on the ground at normal atmospheric pressure.

The study indicates a non-pressurized, encapsulated (where necessary) environment with heat pipe from FPA TWT cold plate and heat pipes from there to the S/C skin.

*FPA - Final Power Amplifier

Table 3.3.5-1 Transmitter Requirements

	System 1	System 2	
	X	X	L
Frequency	9.3-9.5 GHz	9.3-9.5 GHz	1.7
Pavg (watt)	150	150	25
P_{pk} (kW)	4.0	4.5	.75
f_r (Hz)	3-4 KHz	2-3 KHz	2-3 KHz
(us)	11.1	11.1	11.1
Efficiency (%)			
FPA	---	---	---
Xmtr/Mod/HVPS	20	20	20
Operating Period (min)	10	10	10
Warm Up Period (min)	≤ 5	≤ 5	≤ 5
Orbit Period (min)	~ 100	~ 100	~ 100
No. of Failures/10^6 hours	≤ 50	≤ 54	
Lifetime (months)	4-6	4-6	

3.3.5.1.2 Transmitter Specifications

Included herein are a transmitter "off" noise, more complete time domain specifications, bandwidth justification, and random AM & PM requirements. These specifications are shown in Table 3.3.5-2.

Transmitter "Off" Noise

The transmitter "off" noise leaks into the receiver either through

Table 3.3.5-2. Transmitter Fidelity Specifications

Frequency Domain	
Bandwidth	50 MHz $\pm$1 dB
High order amplitude ripple across passband (30 MHz segment)	.4 dB peak
High order phase ripple across passband[1] (30 MHz segment)	3^{o} peak
Low order phase error across passband[1,2,3]	
Uncompensated quadratic	14^{o}
Cubic	4^{o}
Time Domain (Deterministic)	
Droop across pulse width	$\prec$4%
Amplitude ripple (10 Hz $\prec f_m \prec$ 30 MHz)[4]	.4 dB peak
Phase ripple (.10 Hz $\prec f_m \prec$ 30 MHz)[4]	3^{o} peak
Phase error over any .1 sec interval[1]	
Uncompensated Quadratic	30^{o}
Cubic	8^{o}
Phase error over pulse width	
Uncompensated Quadratic	8^{o}
Cubic	4^{o}
Pulse to Pulse Phase	3^{o}
AM to PM conversion factor at nominal drive level ($\pm$1 dB)	$\prec 8^{o}$/dB
Gain	56.5 dB
Jitter[3]	$\prec$ 5 ns
"Off" Noise	-162.2 dBm/Hz
Efficiency (Total dc power/RF power out)	$\geq$ 20%
Source Supply	+28v dc
Power Monitoring Accuracy	$\pm$.1 dB

[1]Deviation from phase linearity.

[2]Stationary phase errors can be compensated for.

[3]Subject to further analysis.

[4]These are equivalent to -30 dB sidebands over frequency.

the duplexer or as return loss from a non-perfect antenna VSWR. As seen in Figure 3.3.5-1, a 1.2 VSWR results in a nominal return loss of 20 dB which is also a good estimate for duplexer isolation.

In order to negligibly degrade 1.5 dB receiver noise figure, it is desirable to set "off" noise at 1/10 system noise or FKTB -1.5 dB = -172.5-10 = -182.5 dBm/Hz.

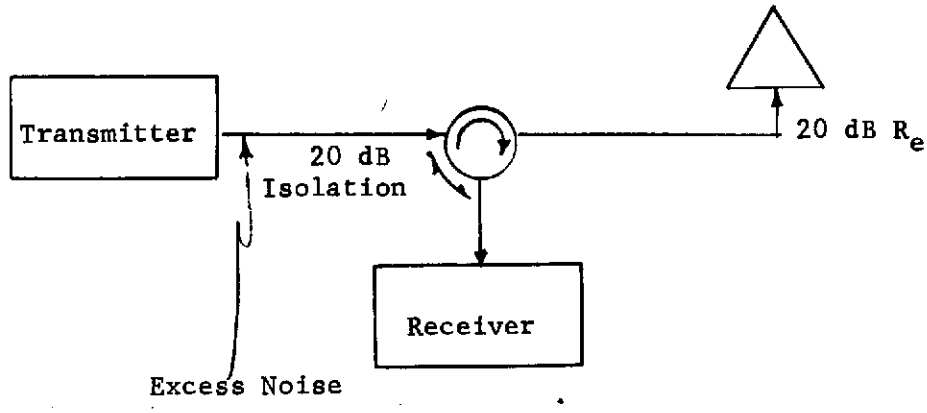

= -182.5 dBm/Hz + 20 dB

= -162.5 dBm/Hz

Total noise from transmitter in off condition

= KTB	174 dBm/Hz	= $.4 \times 10^{-17}$
+ excess	-172.5 dBm/Hz	= $\underline{5.6 \times 10^{-17}}$
	-162.2 dBm/Hz	= $.6 \times 10^{-17}$

Figure 3.3.5-1. Transmitter Leakage or "OFF" Noise

Shown in Figure 3.3.5-1 is the derivation of the allocated -162.2 dBm/Hz "off" noise requirements.

Time Domain Specifications

The STALO-transmitter combination can degrade system performance by creating sidelobes less than 30 dbc (below the carrier). Cyclic

phase or amplitude variations over the pulse width (synchronous from pulse to pulse) can cause range sidelobes while variation having a frequency higher than 10 Hz can cause azimuth sidelobes. The integration time is roughly .1 sec, and due to the sampling rate, perturbing frequencies higher than one-half the PRF appear substantially the same as lower modulation frequencies. Sidebands created by phase or amplitude perturbations must be down -30 dB from 10 Hz to 15 MHz.

High order time domain degrading modulation effects are specified in terms of frequency as small variations are easier to measure. However, some variations introduced in the STALO and transmitter, especially the transmitter, tend to be synchronous from pulse to pulse (for example, modulation pulse variations). These exhibit sidebands lying on top of the PRF lines, but still "chirp up" as range sidelobes. These must be measured in time.

Droop Over Pulse Width

To hold signal loss to .1 dB, 4% droop can be allowed.

Droop also introduces some quadratic phase error. To the extent it is stationary the correlator can compensate. Assuming an exponential droop of 4%,

$$f(t) = e^{-t/T_C}$$

A quadratic component exists as

$$f(t) \sim \frac{t}{T_C} + 1/2 \left(\frac{t}{T_C}\right)^2 - \frac{1}{6} \left(\frac{t}{T_C}\right)^3$$

If $f(T) = .96$

$$T_C = t/.045$$

Therefore, the quadratic component is

$$1/2 \left(\frac{t}{T_C}\right)^2 = (.045)^2 \sim .001 = .1\%$$

A typical grid voltage sensitivity is $7^{o}/1\%$, so a resultant quadratic phase error is 1.4^{o}, however, a body sensitivity factor of $40^{o}/1\%$ results in 4^{o}.

Droop also introduces some linear phase error. If it is consistent from pulse to pulse or at least has a rate change less than 10 Hz, $40^{o}/1\%$ body sensitivity with 4% droop results in one range cell shift.

$$4\% \times 40^{o}/1\% = 160^{o}$$

$$w = \frac{\Delta \phi}{\Delta t} = \frac{160^{o}}{57^{o}} \text{ rad} \quad \frac{1}{11.1 \text{ us}} = .25 \text{ MHz}$$

Flat time displacement

$$\Delta \tau = \frac{\Delta f}{k} = \frac{.25 \times 10^{6}}{13.5 \times 10^{6}} \quad 11.1 \times 10^{-6} = .206 \text{ us} = 206 \text{ ns}$$

$$\Delta r = 31 \text{ m}$$

To the extent this is a stationary error, it can be compensated for. Pulse to pulse variations shoul e held to 10 ns to maintain azimuth sidelobes below 30 dB. Pulse c /D jitter should be tightly controlled since this range jitter can introduce azimuth sidelobes due to incidental amplitude modulation. Assuming a matched filter response and a 60^{o} downlook angle, a given point target range response is shown in Figure 3.3.5-2.

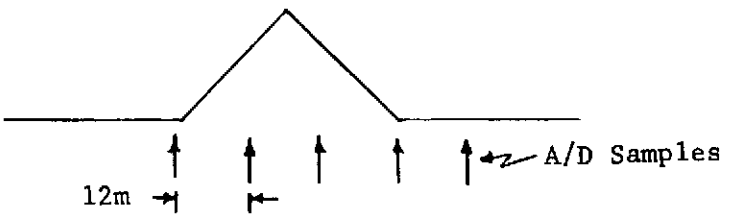

Figure 3.3.5-2. Matched Filter Discrete Target Response

The A/D samples should occur at the same place on the response. Jitter deviation will cause azimuth amplitude perturbations. If they were

periodic, a -30 dB sidelobe requirement results in .5 dB amplitude ripple. Since .5 dB = .944

$$\frac{1}{.7m} = \frac{.944}{x}$$

$$x = 11.3m$$

or the allowable jitter is

$$12 - 11.3 = .7m$$

which is equivalent to 4.65 ns.

If a 1/f slope is required from 100 to 1500 Hz, the net -20 dB requirement is met as

$$P_T = P_o \int_{f_1}^{f_2} f_o/f \, df = P_o \, f_o \, \ln \, (f_2/f_1)$$

where P_0 = noise power density at f_o

$f_1 = f_o = 100$ Hz and $f_2 = 1500$ Hz

$$P_T = P_o \, (100) \, \ln \frac{1500}{100} = P_o \, (270)$$

$$= -46 \text{ dB/Hz} + 24.3 \text{ dB/Hz}$$

$$P_T = -21.7 \text{ dB}$$

The resulting noise specification is shown in Figure 3.3.5-3.

Noise Power Density Spectrum

The three major factors which determine the noise power density spectrum are: 1) loss of resolution caused by quadratic phase shift due to phase modulation (PM) noise at modulation frequencies from 10 Hz to 20 Hz, 2) sidelobe generation due to PM and amplitude modulation (AM) noise sidebands from 20 to 1500 Hz, and 3) signal loss effects due to spectral smearing caused by AM and PM noise sidebands.

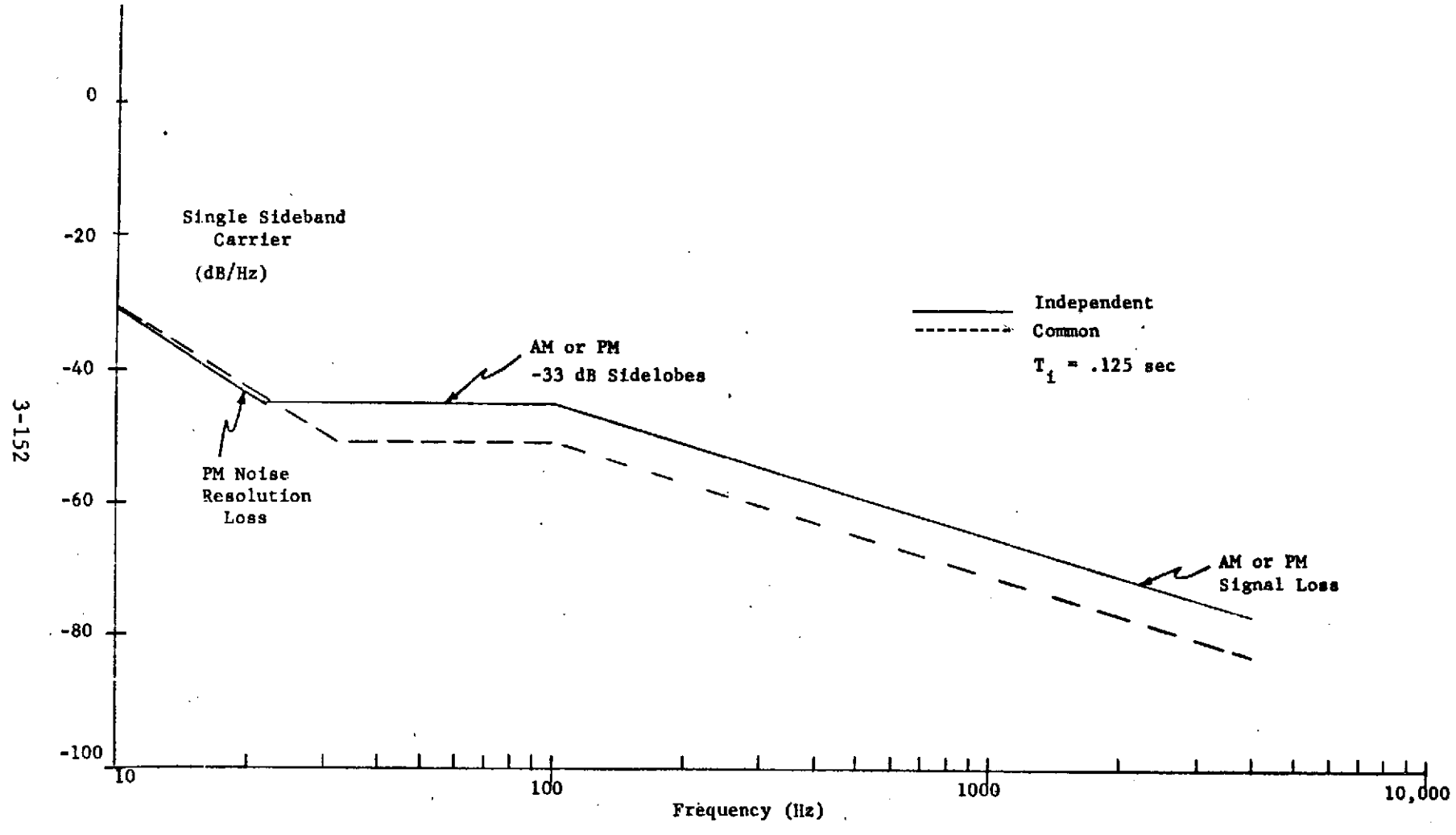

Figure 3.3.5-3. SSAR STALO/Transmitter Noise Specification

Quadratic Phase Shift

Phase perturbations over the aperture or at least over the integration time may have a quadratic component which reduce resolution. A 40° quadratic phase error allocation is made to the transmitter. A peak sinusoidal phase error having $\sim 40^{\circ}$ quadratic phase content as

$$\Delta\phi \simeq \frac{2\pi}{(T\omega_m)^2}\sqrt{2}$$

where T = integration time

ω_m = radian modulation frequency

For $\Delta\phi << 1$ only two significant PM sidebands exist where the sideband/carrier ratio is

$$\frac{SB}{C} = J_1(\Delta\phi) \cong 1/2\,\Delta\phi = \frac{\pi}{(T\omega_m)^2}\sqrt{2}$$

and $J_1(\Delta\phi)$ is the first order Bessel function. The assumption $\Delta\phi << 1$ is approximately valid to .1 Hz. For $\omega_m = 2\pi$ radians,

$$\frac{SB}{C} = \frac{\pi\sqrt{2}}{(T)^2(2\pi\ 10)^2}$$

The integration bandwidth is about .125 sec $\sim$ 8 Hz. This constitutes the most severe SL/ML requirement for the transmitter as can be seen from the above equation.

$$\frac{SB}{C} = \frac{\sqrt{2}\,\pi}{(.1)^2\ (2\pi 10)^2} = .07 \Rightarrow -22.5\ \text{dB}$$

However, this is to be considered as the equivalent integrated noise in an 8 Hz bandwidth since this equivalent signal power sideband will manifest itself as an effective quadratic error. On a per Hertz basis,

$$\frac{SB}{C} - 22.5\ \text{dB/8 Hz} = 31.5\ \text{dB/Hz}$$

It should be pointed out that this is a true sideband-carrier ratio and is then a single sideband measurement.

Sidelobes

A -33 dB sidelobe-mainlobe ratio requires the same sideband-carrier ratio; however, the equivalent noise power in some integration bandwidth will result in sidelobes. The bandwidth ($\sim$ 8 Hz) imposes the most severe requirement as it contains the most noise power.

$$-33 \text{ dB}/8 \text{ Hz} = -42 \text{ dB/Hz}$$

For PM or AM noise, only -42 - 3 = -45 dB/Hz. Both AM and PM noise can create sidelobes.

Signal Loss

Both AM and PM noise sidebands can cause signal loss by smearing the correlated reflector signal. For .1 dB signal loss, -20 dB sidelobes are required. The net integrated noise power from 1/2 the filter (8 Hz) bandwidth to the PRF (1 KHz) can cause this loss. As this is an integrated requirement, a 1/f slope for 100 to 1500 Hz is adequate to yield the cumulative net power.

3.3.5.1.3 Transmitter Design

Summary

The transmitter design concept advanced for radar configuration #1 is a low peak power coupled cavity TWT employing a multi-stage collector. The associated electronics consisting of modulator and high voltage power supply are encapsulated in an open environment and conduction cooled.

Configuration #2 has the same X-band hardware package as #1, but includes a solid state L-band transmitter. The relatively high peak power at L-band is derived from combining several lower peak power modules in parallel - a passive element microstrip combiner - divider achieves the necessary phase and amplitude matching. The transmitter is conduction cooled and does not require precaution for high voltage breakdown.

Study Approach

The subjects outlined in para. 3.3.5.1.1 will be covered and a design to meet subsystem specifications will be met. Areas of concentration are the following:

1. X-band power amplifier
2. A viable transmitter electronics package
3. State of the art L-band transmitter

This study takes into account a number of priorities to be considered in hardware in a space environment, namely, reliability, efficiency, size, weight, and cost.

System Configuration #1

Reference is made to table 3.3.5.1 which delineates transmitter requirements and table 3.3.5.2 which lists transmitter fidelity. A division can be made in the transmitter into the power amplifier and auxiliary electronics and weight the one bearing the major influence on performance.

	Power Amplifier	Electronics
Peak Power	XX	
Average Power	XX	
Frequency	XX	
Bandwidth	XX	
Efficiency	XX	X
Reliability	XX	X
Off Noise	XX	X
Jitter	X	XX
Phase Ripple	X	XX
Amplitude Ripple	XX	X
Droop	X	XX

X - Minor

XX - Major

Power Amplifier

For a system of this narrow bandwidth, the feasibility of using a klystron instead of a TWT was considered. The klystron offers good or even better stability characteristics than the TWT. However, the availability of a klystron with this wide a bandwidth was not found. Nor was there the possibility of achieving the efficiencies found in TWT, because collector depression is not used in klystrons. Isolated collectors are used to separate power supplies and thereby

ease the filtering required but normal depression of the anode does not work because of secondary emission.

Therefore, in examining the klystron and TWT, the TWT took preference. It provides the best flexibility and efficiency.

The criterion for choosing a TWT was to take a proven tube design and examine the risks and cost involved in tapering the proven design to our specification. Two vendors were contacted, Hughes Aircraft Company, Electronic Dynamics Division, and Litton Industries, Electron Tube Division. Hughes was more informative and showed more knowledge of high power pulsed TWTs in space environment. Table 3.3.5-3 describes the modified tube they proposed. The baseline tube is a 790H, 1 kW peak, 20% duty ppm focused tube.

TWT Reliability

The two major points brought out concerning the reliability of the tube are:

1) cathode life

2) durability of RF interaction circuit

The cathode used in this TWT is an oxide impregnated cathode operating at 1050°C. It is well known that in oxide cathodes, barium as liberated from its oxide will begin to coat electrode surfaces such as the grid, the anode, and ceramic insulators between them. Excessive boiling off of barium will decrease cathode emission, increase grid surface area, and increase leakage between electrodes across insulating surfaces. It is, therefore, best to keep cathode temperature at a minimum concurrent with the cathode emission necessary. The gun of this tube runs at a low cathode emission ($1.5 A/cm^2$).

Table 3.3.5-3. TWT Characteristics

RF and Video Parameters	
Frequency	9.5 GHz
Bandwidth (±1 dB)	150 MHz
Peak Power	4 kW
Duty	5%
Cathode Voltage	-17kV
Cathode Current	1.6A
Collector (1) Depression Voltage	-7kV
Grid (Shadow Grid)	
B+	+425V
Bias	-300V
Grid Current	10mA
Grid Capacitance	< 30pF
Heater	
Voltage	8.5V
Current	2A
Focusing	ppm
Beam Transmission	90%
Efficiency	25%
Amplitude Sensitivity	
Cathode to Body	.004 dB/V
Grid	.03 dB/V
Phase Sensitivity	
Cathode	.2°/V
Grid	1.5°/V
Collector	.002°/V
Phase Linearity	±10°
Size	18 x 6 x 4 in.
Weight	15 lbs.
Cooling	Conduction via heat pipes to baseplate
RF Structure	Coupled Cavity

To maintain optimum cathode emission over the expected life of the system, the power amplifier will be shut off completely during the non-operating part of the orbit and the heater will be programmed on to lessen thermal shock.

There are two types of RF interaction circuits used in TWTs:

1) helix or helix-derived circuits (ring bar, ring loop)

2) coupled cavity

There are advantages to the helix structure in this application. Because of the continuous nature of the helix, a much smoother phase and amplitude response can be obtained. Also, the structure is not so susceptible to instabilities looking into a mismatch. As a disadvantage, the helix is a delicate mechanical structure and it is difficult to get the heat out. Helices are usually positioned in the tube envelope with BeO or BN rods which can fracture and cause local hot spots. According to the vendors contacted, a helix, ring bar or ring loop tube is not a wise choice for these average power levels. It would be a significant jump in the state of the art to achieve this average power level at X-band with a helix. Therefore, we are left with a coupled cavity structure, one that has been used successively in ppm focused tubes at higher power levels. Coupled cavity tubes at this power level are found to be more rugged and reliable in space applications. The disadvantage of cavity tubes is its discontinuous structure. Mismatches between cavities cause considerable fluctuation in phase and amplitude across the passband. However, system performance can still be met.

TWT Efficiency

The efficiency of a TWT is defined as total RF power out/ total DC power in. The efficiency of the tube described in Table 3.3.5-3 is 25% minimum. Of course, in the absence of RF drive, there is no conversion and all the power in the tube is dissipated as heat. A multi-stage collector increases the efficiency significantly with the largest jump occurring with the second collector. A table follows of the number of collector stages vs. efficiency.

No. of Stages	Efficiency (Approx.) %
1	25
2	30
3	33
4	37
.	.
10	greater than 50

This table takes into account variations in depression voltages occurring in a system with fairly large long term fluctuations in supply voltages and an unregulated (DC) collector power supply.

The multi-stage collector is a low risk, low cost item for up to three stages. Weight and size are not increased substantially. A transmitter allocation of 20% efficiency overall cannot be met with a one-stage depressed collector TWT. A three-stage collector is recommended and will not complicate power supply design. Video characteristics of the tube remain the same up to the collector where the only difference is that the electrons are retrieved at lower potentials, thus converting less energy into loss (heat).

TWT Weight

Minimum weight is accomplished by use of ppm focusing, and heat pipes as efficient thermal conductors to the baseplate.

Ancillary Electronics

The transmitter electronics package consists of the following

1) Modulator
2) High voltage power supply
3) Low voltage power supply
4) Control and monitoring
5) Ion pump power supply

These are shown in Figure 3.3.5-4.

Modulator

The modulator receives low level logic signals from the synchronizer and gates the grid of the TWT. It must develop a trapezoidal pulse of sufficient speed and magnitude to efficiently pulse the tube. Ripple and droop on the plateau of the pulse must be kept to a minimum. Reviewing the grid specifications:

Pulsewidth	11.1 microsec
Rise Time	100 nanosec
PRF	3 KHz $\pm$ .5 KHz
Bias	300V
B+	450V
Grid Capacitance	30 picofarads
Jitter	less than 5 ns

To accomplish these requirements, a modulator consisting of a two-channel low voltage pulse amplifier sends up, via transformer coupling, start and stop triggers to a floating deck. There, a two-

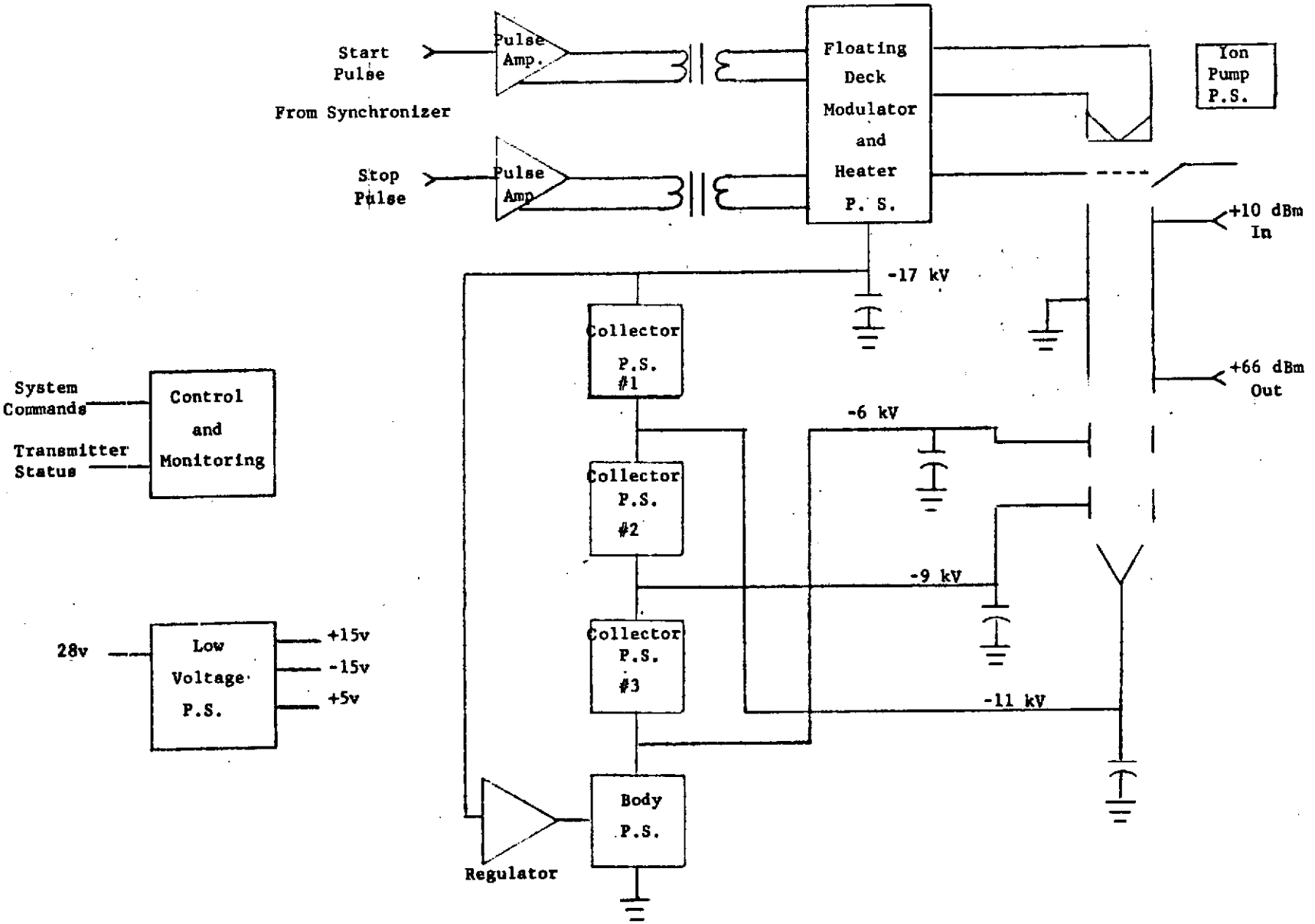

Figure 3.3.5-4. Block Diagram - TWT Electronics

transistor totem pole switch controls the grid. The floating deck is referenced to the cathode at -17 kV.

System specification places stringent requirements on the ripple and droop on the plateau of the pulse. An allocation must be made to perturbations introduced by the modulator and power supply. Because the grid is more sensitive than the cathode, the more lenient restraint is placed on it.

Amplitude droop across the pulse	3V (corresponds to .1 dB droop)
Ripple	1.5v peak (corresponds to -34 sidebands)

A power supply to provide floating DC voltages of +500V, -300V, and a filament voltage of 8.5V is required. The filament voltage must be regulated to within 2% to maintain optimum emission and cathode life. Flatness across the pulse is achieved with a clipper to truncate the pulse to the desired B+ level and maintain that level from pulse to pulse.

High Voltage Power Supply

Cathode voltage and collector voltages are derived using several dc-dc converters stacked in series with the bottom element as a regulator. The regulator controls the total voltage of the stack. Elements within the stack will have a varying output according to load and line changes. In a TWT, the cathode to body voltage regulation is critical. Output power and fidelity is dependent on a pure and stable supply. Collector voltages may be left unregulated. The regulator will use a constant frequency, variable pulsewidth switching regulator for efficiency. The overall efficiency will be 80% minimum.

Droop in cathode voltage	25V max.
Ripple	11V peak max.

Low Voltage Power Supply

Regulated power supplies provide ±15V and +5V to ground deck circuitry such as ground deck pulser, regulator preamp, and control and monitoring circuits.

Control and Monitoring

This section of the transmitter controls the turn-on sequence and monitors critical parameters to prevent damage to the TWT or catastrophic failure. It provides performance data and indicates deterioration so that corrective action can be taken.

Ion Pump Power Supply

A TWT will liberate free ions from the cathode and gaseous impurities absorbed on surfaces within the vacuum envelope. During manufacturing of the tube, the tube is pumped down at several hundred degrees C to clear as many impurities as possible. During this time, the cathode heater is also turned on. However, no baking procedure will guarantee vacuum integrity throughout the expected life of the tube. Such things as local heating of an RF cavity, internal tube arc due to build up of, or bridging of microscopic particles in a high E field, further evaporation from the cathode, and slow leaks in a metal seal, will gas up the tube. Standard procedure dictates that an ion pump be left on all the time. A 3 kV unregulated power supply energizes the pump. Ion current in the order of microamperes will be monitored and inhibit transmitter operation until the fault has corrected itself or has been overridden.

System Configuration #2

This configuration utilizes the same X-band transmitter as system #1 but includes a solid state L-band transmitter.

Peak powers of 750W are not possible using a single solid state device. Transistors of 150W peak at 1.2 GHz are available, such as the MSC 1100. At 1.7 GHz, 50 watts is possible with a single device. To achieve a combined peak power would require four modules of four transistors in parallel. This takes into account .5 dB loss in the module power combiner and phase and amplitude unbalances.

Peak powers of 1 kW have been achieved at Westinghouse using the technique described above. A typical amplifier module for our requirements is shown in Figure 3.3.5-5.

In designing the modules, it is necessary to achieve power and bandwidth repeatedly. To compensate for variations in transistor's characteristics, variable tuning will be incorporated in matching networks. Also, linearly-tapered lines will be employed to achieve appreciable bandwidth because of the low transistor impedance encountered.

Each amplifier module consists of ten transistors; two class A stages for gain, two 2-watt pre-drivers, two 10-watt drivers, and four 50W class C amplifiers. Special hybrid quadrature couplers split the power into each transistor and combine it after amplification. The amplifier transistors are matched for maximum power transfer using series transmission line sections.

The key to building up the peak power is the combiner-divider network. Of the various types of combiners possible, the most common

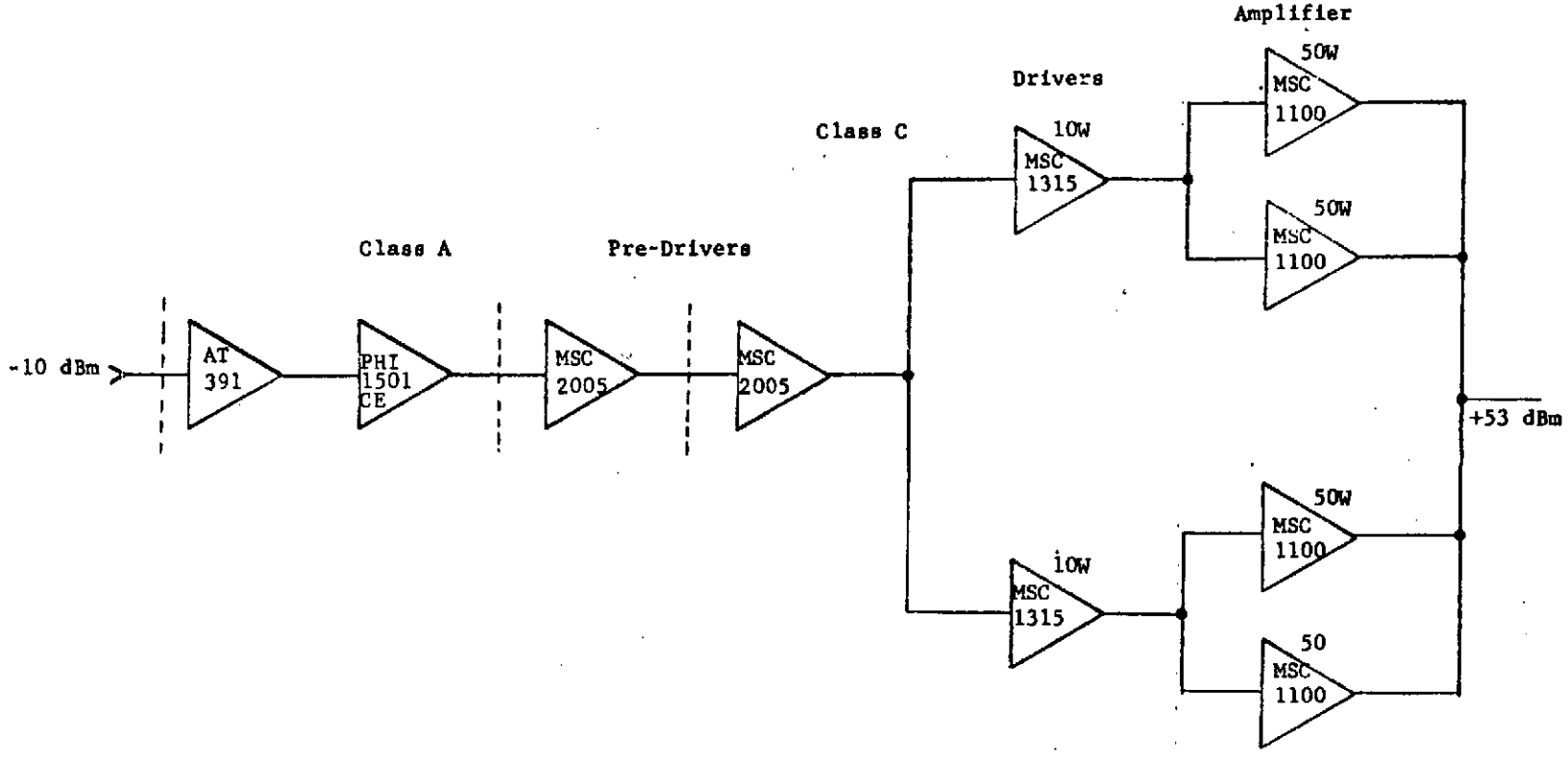

Figure 3.3.5-5. Amplifier Chain - Module

approach so far has been to use steps of 2:1 combiners to sum power. In microstrip, however, this means that each step represents about 0.3 dB loss. Combining this number of outputs would result in a high insertion loss for the combiner. A simpler technique is to use an N way combiner based on the type described by Wilkinson. This type uses quarter wavelength sections and a resistive star for isolation. It can be built to have less than .5 dB insertion loss. The design provides low dissipative losses, reciprocal operation, equal phase and amplitude splitting to all parts, high isolation between post, and high power handling capability.

Pulsed operation is achieved by gating in the class C stages. Supply voltage is 28V with an overall efficiency of 33%. Cooling is done by conduction to a cold plate.

Mechanical Package

The mechanical package ensures the viability of the electronics within the launch and space environment. A detailed description of the mechanical layout and thermal analysis is in section 4.

Confident that the package can be put into orbit and withstand the shock and vibration during orbital insertion, the main concern is the vacuum environment of space.

The following sections will go into length discussing the problems of high voltage breakdown and corona. It will be concluded that all electronic circuitry should be packaged in high density encapsulation.

More briefly, the problem of multipactor in waveguide and microwave components will be covered.

High Voltage Breakdown and Corona

It was the objective of this part of the study to determine which of several techniques or combination of techniques should be used to prevent high voltage breakdown or deleterious corona.

The basic problems are presented associated with the design of high voltage electronic equipment for use in a space environment. It is concluded that the equipment should be designed for operation at all pressure levels from 760 to less than 10^{-5} Torr.

It is concluded that the basic insulation medium should be high density encapsulation of all electronic circuitry. Proper design and encapsulation techniques should result in equipment capable of meeting all of the system design requirements including the required high reliability requirement.

Operation of equipment at voltage levels of from 20 to 30,000 volts in a space environment where the dielectric strength in a uniform electric field drops from a sea level value of 75,000 volts per inch to a few hundred volts per inch, is a basic and serious problem.

At first impression, this would not seem to be of concern for an equipment which is required only to operate at orbital altitudes where the hard vacuum of space has a very high dielectric strength.

Although the equipment is not required to function during the launch and orbit insertion period, past experience has shown that it should be designed to tolerate such an environment, that it should operate without arc-over or excessive corona at all pressures from sea level to space ($< 10^{-5}$ Torr). It has been found that one cannot rely on the near vacuum conditions encountered in orbiting vehicles

to hold off the high voltages required for high power transmitters. Components continue to outgas for long periods even without the application of input power. On each application of input power, temperature rises in the components will release additional gas molecules which can raise the local pressure level to the critical region of Paschen's curve and cause breakdown even at very low voltages ($\sim$ 300 volts).

Reliability

The choice of an insulating system must first be one which meets the high reliability requirements of the system. All other considerations must be secondary to this.

Weight

Because of the high cost per pound to launch the system, weight is, next to reliability, the most important constraint. It will be pointless to choose a system which has the highest reliability if the excessive weight prohibits its launching.

Volume

To a lesser extent, the constraints on weight also apply to volume. In any case, the value of widely spaced high voltage components to reduce the risk of voltage breakdown as would be desirable for ground based systems, is doubtful, when applied to systems which must operate through the critical P x D range of Paschen's curve. No matter how large a spacing "D" is used, there will exist a "P" such that P x D $\simeq$ 5 Torr x mm, at which point breakdown will occur at the minimum voltage ($\sim$300V).

General Discussion

Paschen's curve relating breakdown voltage to a produce of pressure times electrode spacing is shown in Figure 3.3.5-6. This curve has a similar shape for air, other gases and most fluids. For any given product P x D there is a breakdown potential where an arc occurs. Air at room pressure breaks down at 75,000 volts across a one-inch gap in a uniform electric field corresponding to a P x D product of 19,000 (p in mm of Hg. x D in mm). As the separation is decreased or as the pressure is decreased, the breakdown voltage follows an approximate linear curve until the break point, which is called Paschen's minimum, is reached. This occurs at a P x D product of approximately 330 volts. For smaller P x D products ($\lesssim$5 Torr-mm), the breakdown voltage again rises to a value exceeding 200,000 volts per inch for very small values of P x D product. From this, it is seen that a design based on voltage hold off for a small P x D product will break down at a lower voltage if either the pressure is raised or the electrode spacing is increased.

It has also been shown that even after considerable time in the hard vacuum of outer space, there is a pressure lag in inadequately vented enclosures, and that localized outgassing of components for a prolonged period of time after turn-on occurs. This serves to adjust the environment pressure level into the critical pressure region where catastrophic failure results at turn-on. So far, only breakdown, which is loosely defined as a complete breakdown between electrodes, with

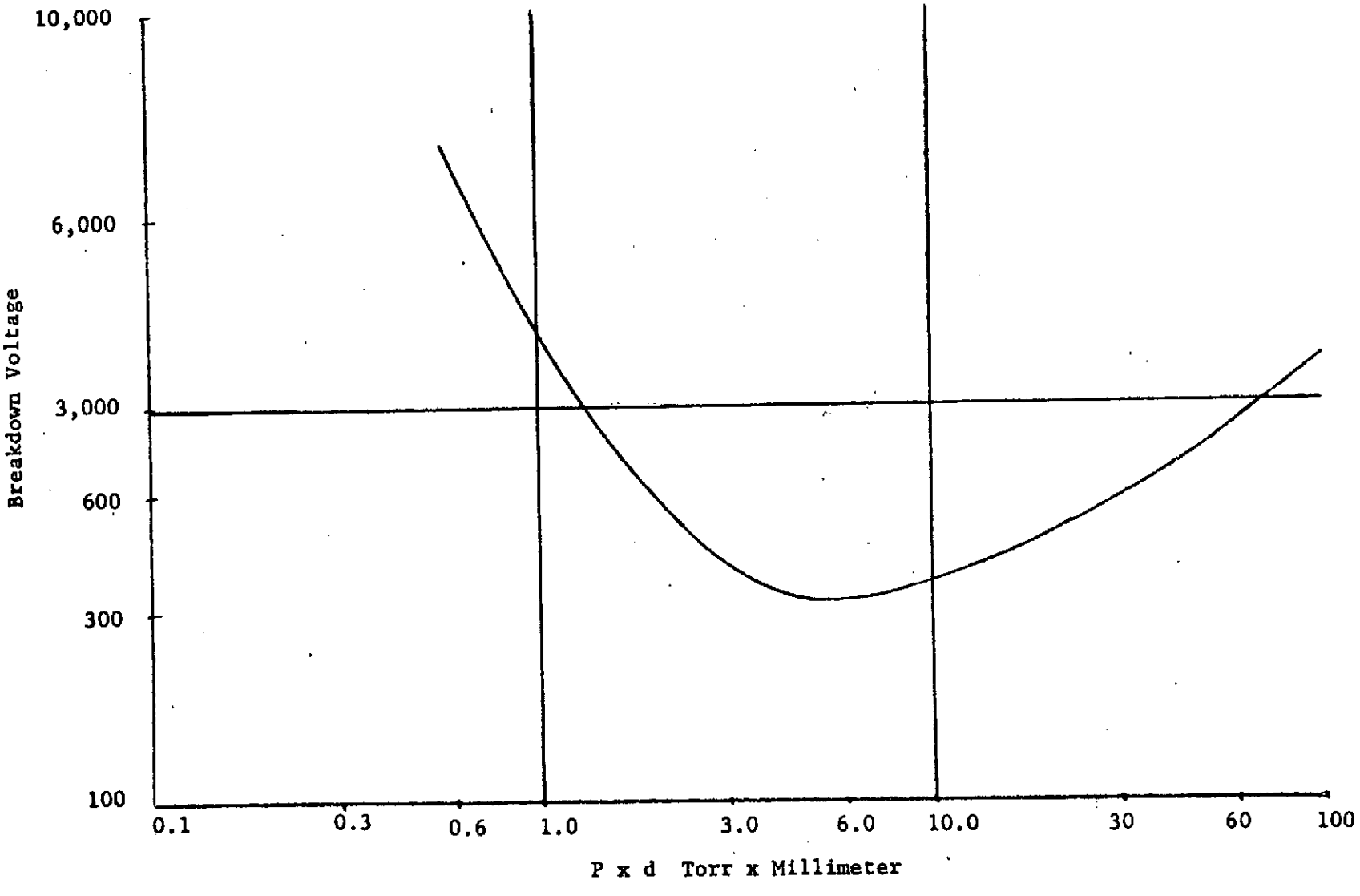

Figure 3.3.5-6. Paschen's Curve

current limited only by the internal impedance of the power supply, has been considered. Of equal concern is corona (loosely defined as a partial breakdown) since corona, once it starts, is a degenerative effect eventually leading to a complete breakdown.

Corona typically begins at much lower voltages than does a complete breakdown. Classically, for corona to occur, a number of conditions must exist. For instance, a high electric field strength and not just a high electrical potential must be present. Secondly, a gas must be present since the phenomenon is developed by electrons leaving an electrode and then creating a secondary ionization with the particles of gas in the region. The particles of gas ionize and, if enough energy is present, corona will exist. Some people have reported corona as existing in solids, which looks electrically like corona which exists in a gas. Whatever the phenomenon, the deleterious effects are the same, i.e., current flows, radiation is emitted and the life of the insulation is degraded.

Paschen's discovery is further modified by the following important facts:

- The type of insulation on electrodes is important.
- Floating particles in the potential gap can precipitate breakdown.
- Outgassing is important.
- Creepage paths are important.
- Electrode shapes and voltage gradients are important.
- Electrode cleanliness is extremely important.
- Source of free electrons is important (i.e., before breakdown or even corona can occur, there must be at least one free electron.)

- Corona is important; even if you can live with it from a breakdown standpoint, it can jam or block nearby sensitive receivers.
- Once corona has started, it can be avalanched into a complete breakdown by illumination of the gap, by any of several sources of ultraviolet or radioactive emissions or even cosmic rays.
- The frequency of the applied voltage is important; as the frequency increases, breakdown occurs at a lower voltage.
- The type of waveform is important.

Possible Insulation Systems

Several insulation system approaches are possible. They may be generally classified as liquid, pressurized gas, vacuum, or solid.

Liquids

Hydrocarbons such as oil and some fluorocarbons such as FC-75 have excellent dielectric properties as well as good thermal conductivity. They have been used extensively for power systems by industry and the military for ground based or airborne applications.

There are several disadvantages to the use of a liquid, particularly when considered for use in space. There is a tendency when high voltages are employed,for oils, if they break down, to carbonize. Low levels of corona can produce this effect which can, over a long period of time, result in complete voltage breakdown. For ground based systems, catastrophic failure can be prevented by periodic processing or replacement of the oil. Replacement in space would be impractical and reprocessing is difficult even on earth.

It is difficult to design and manufacture an oil-tight container even for ground based equipment where there is no pressure differential between the inside of the container and the environment. The problem becomes even more severe when the external pressure drops to less than 10^{-5} Torr. If leaks (even very slow ones) develop, eventually enough oil could be lost to expose high voltage components to critical pressures where breakdown can occur.

In large enclosures, it is virtually impossible to prevent local outgassing which, in weightless space, results in voids in the insulating medium which will break down at greatly reduced voltages.

The weight of the liquid required to completely immerse the high voltage circuitry can be high. For ground-based equipment, it is not uncommon to find that the system weight nearly doubles when the liquid insulator is added. Additional temperature expansion facilities such as bellows are required so that the vessel is always filled. Otherwise, high voltage components may become exposed as the volume of oil contracts on cooling. These expansion volumes add weight to the system.

Each liquid considered has certain compatibility restrictions. That is, only a limited number of materials can be immersed in the liquid for long periods without deleterious effects either on the liquid or the other materials.

Pressurized Gases

A number of gases, notably nitrogen, SF_6 and several fluorocarbons such as C_2F_8 have been used for years in high voltage systems. These gases, particularly SF_6 and the fluorocarbons, are considerably better

than air, both in terms of dielectric strength and heat transfer when pressurized to two or more atmospheres. Since the high voltage system must be sealed in order to contain the gas under pressure, a "controlled" atmosphere is realized. In a ground-based or airborne system, the effect of humidity, dust, etc., can be ignored. These are important advantages for ground-based and airborne equipment which often offset the disadvantage of pressure vessels.

It has been found in several cases that pressurization also permits the design to be smaller and lighter than when air or oil are used as the insulator. This is because the spacing between high voltage components can be reduced and components such as transformers can be smaller because of the superior heat transfer characteristics of the gas.

The pressurized gas approach could certainly be used for space applications. Some of the problems which are fairly easily solved for earth-bound equipment become considerably more difficult if the surrounding environment is the hard vacuum of space. For ground-based or airborne equipment, a make-up tank of gas at a pressure higher than that of the vessel is carried along. Manual or automatic means of maintaining adequate vessel pressure can be used. The automatic means could be employed in space. However, additional weight must be carried and the make-up tank itself could be difficult to design so that it would be adequately leakproof for long periods of time.

An electro-negative gas such as SF_6 has an additional important property. If there are free electrons in the gas, the gas molecules

molecules capture it and do not allow it to be in the potential gap to cause a breakdown. Thus, this type of gas has a feature which cannot be achieved with other gases or liquids.

Vacuum

The use of an evacuated container for high voltage systems would be desirable for several reasons. When a good vacuum ($<10^{-5}$ Torr) can be maintained, voltage clearances can be considerably reduced without the fear of corona or arc-over. The system could operate all the way from launch to orbit with the attendant wide range of external pressures without difficulty. Once in orbit, the integrity of the evacuated enclosure would be unimportant. In fact, it might even be opened to space vacuum intentionally to allow the escape of gases evolved within the enclosure.

Unfortunately, unlike vacuum tubes which can be designed using only materials which can be "baked-out" at high temperature during vacuum processing, many high voltage power supply components cannot tolerate such temperatures ($>500^{o}C$). It would be possible to design inductive components and possibly even filter capacitors using ceramic insulation able to tolerate the "bake-out" process. However, the solid state devices such as rectifiers, transistors used in regulator circuitry, etc., would be destroyed. Unless all such items are completely outgassed initially, they will continue to release gas into the evacuated enclosure for very long periods. Each time the equipment is energized and temperatures rise, more gas will evolve. It is probable that a very fast, continuous vacuum pumping system would have to be carried to overcome this problem.

A problem exists when using a liquid, pressurized gas, or vacuum insulating system in weightless space which is more severe than when using the same insulation system in a ground environment. This problem is associated with how clean and how free of particles the enclosed volume can be made and maintained. In spite of all precautions taken, minute particles of contamination will exist in the enclosure which, under weightless conditions, will float around and eventually align along electrostatic potential lines and serve as a path for a flash-over. This may happen repeatedly, each time liberating gas or constituents thereof which serve to further enhance the conditions for voltage breakdown. Equally as important, if particles are present, is the partial discharges caused by the particles carrying charges from one electrode to another which can precipitate a complete breakdown.

Solids

Solid insulating materials have been used for most high voltage systems designed for space applications. When properly employed, solids can result in lighter, smaller and more reliable systems. However, extreme care in the choice of materials in processing and in testing are essential to success.

High density solid dielectric encapsulants have been used most frequently in similar applications for several reasons.

- The number of conditions under which corona can exist are reduced.
- Heat dissipation problems are more readily solved.
- Local outgassing is a problem only if the encapsulation is not done properly.

- Their relative weight is low.
- Structural integrity is quite high.
- Repairability is difficult but can be solved with the proper techniques.

Considerable work has been done on the use of solid encapsulation in low pressure regions.

- High density encapsulants are preferred for reducing or completely preventing corona phenomenon.
- The encapsulant should not produce a mechanical strain on the component it it encapsulating.
- It is absolutely essential that all parts encapsulated be white-room clean.
- The encapsulating medium must adhere to the component without restriction during complete temperature cycling.
- Voids in potting compounds must not be present.
- The units must be repairable.
- External electrostatic shields must be used where there is a possibility of introducing even low voltages into adjacent components which may be in the critical pressure region.
- High voltage components should be free of internal voids and absorbed gas before encapsulating. Voltages applied to resistors with a hollow ceramic core should be kept below the minimum breakdown potential for the particular gas entrapped. Resistors with solid cores are preferred.
- High voltage leads from the high voltage power supply should be encapsulated in place with external shields.
- The cure cycle for encapsulants should receive detailed attention to preclude outgassing, moisture absorption, etc.

Conclusions and Recommendations

High voltage and corona phenomenon has been known and understood for years. Recent work has extended and amplified the knowledge available into the critical pressure region. Many techniques have been successfully used. No single technique or combination of techniques will satisfy all the conditions likely to be encountered in complex high voltage equipment in the critical pressure region.

The solution to high voltage problems begins with the selection of the proper basic components and ends with how they are put together and applied in the equipment. It is necessary to understand the basic principles which apply and to follow a discipline in their application. If this is done, there should be few problems in achieving reliable high voltage equipment.

The following basic considerations are recommended:

- Use clean-room technology.
- Keep the voltage levels and voltage gradients as low as possible.
- Limit or control the available amount of energy capable of feeding corona or an arc.
- Where possible, make power supplies short circuit proof.
- Keep the turn-to-turn voltage on transformers, chokes, etc., low.
- Don't use materials that cannot be perfectly bonded by the encapsulating materials.
- Eliminate or control electrodes or insulators which tend to produce high field concentrations.
- Shield or provide grounding planes so as to reduce fringing fields in adjacent low pressure regions.

- Eliminate or control transients caused by high voltage discharges. In particular, isolate them so that they are not coupled into low level circuitry which will not withstand them.
- Eliminate the necessity for high voltage connectors.
- Encapsulate and shield all high voltage wire.
- Adequately vent all connectors, screw threads, and other possible sources of entrapped gases.
- Vacuum degas all components and potting compounds.
- Use potting materials to mechanically anchor components.
- Do not use foam potting unless other techniques will not do.
- Separate all high voltage and low voltage circuits.
- Use RFI filters where necessary to prevent transfer of energy between circuits.
- If connectors must be used, continue the shielding through the connectors.

Multipactor Breakdown

Multipactor is the RF breakdown mechanism in transmission lines at high power where:

1) Surfaces have a secondary emission factor greater than 1
2) Gas pressure is typically below 10^{-4} Torr
3) Electric field strength is within a correct range to produce resonant electron impacting with surfaces; the range of field strength is dependent upon frequency and surface spacing.
4) Electron impact energies lie within a range where more than one secondary electron is produced on the average for each impacting electron.

The external microwave subject to the maximum RF output power are:

1) Waveguide
2) Duplexer
3) Waveguide switch
4) Receiver protectors

No coax will be used in the high power microwave.

The use of pressurization is to be avoided because of the extra weight and volume of a regulated gas fill system. A microwave output chain capable of operating below 10^{-4} Torr does not present a serious problem for 4 kW peak.

Full height or even half height waveguide will not multipactor at powers an order of magnitude higher than the proposed transmitter peak power.

The duplexer, as a complex device involving narrowing of waveguide, ferrite elements, slots and dielectrics cannot be easily analyzed. However, a design capable of 10 kW peak power will operate in the environment without deterioration.

The waveguide switch matches the waveguide interfaces. Small discontinuities in the rotor switch will not give rise to deleterious glow discharge and breakover.

Power input to the receiver protectors is nominally 20 dB down. The receiver protectors employ multipactor to short the waveguide and prevent damaging RF energy from entering the receiver. The protector can sustain peak powers of 1 kW. The protector will normally see powers of 40 watts peak during the "big bang".

Existing Transmitter Designs

The possibility of using existing design presents several difficulties that preclude their use in this application.

Present configurations are not designed for the high reliability of space equipment. Approaches in the past for airborne transmitters have been to make them as light and compact as possible to increase single mission capability (flight time and range). Periodic maintenance of the electronics could be done during grounding of the aircraft. Thus, such reliability enhancements as redundancy, extremely high reliability components (which, in transmitters, can mean extremely conservative high voltage designs in passive components) could be excluded or relaxed. The latest in-house developed airborne radar (WX-200) is guaranteeing 100 hour overall system MTBF. This number drops well below the SSAR system requirement.

Existing designs do not fall into the RF output power levels required for the system.

An airborne transmitter is not built for the efficiency required in space where prime power is a premium. All transmitters are designed for three phase, 400 Hz, 115v AC input power. No system has been built for a low voltage DC source.

Transmitters for SAR applications require particular frequency stability requirements. In general, noise and discrete sideband levels at relatively low frequencies (10 Hz) must be sufficiently suppressed not to degrade imagery. Other transmitters designed for coherent airborne radars such as pulse doppler for search or fire control have higher frequency requirements such as -80 dB at 1 KHz.

Contemporary available SAR transmitters such as the Westinghouse-developed UPD-5 (circa 1972) do not have the reliability requirements. The transmitter High Voltage Power Supply and internal filtering design is based on 400 Hz AC, not 28v DC prime power, and stability requirements would not be met either.

All existing hardware depends on a liquid or pressurized environment. The problems associated with this approach are discussed later in the study.

In summary, the specialized requirements of SAR, S/C do not make the incorporation of existing designs feasible.

A graph of average power versus weight for system configuration #1 is included in Figure 3.3.5-7.

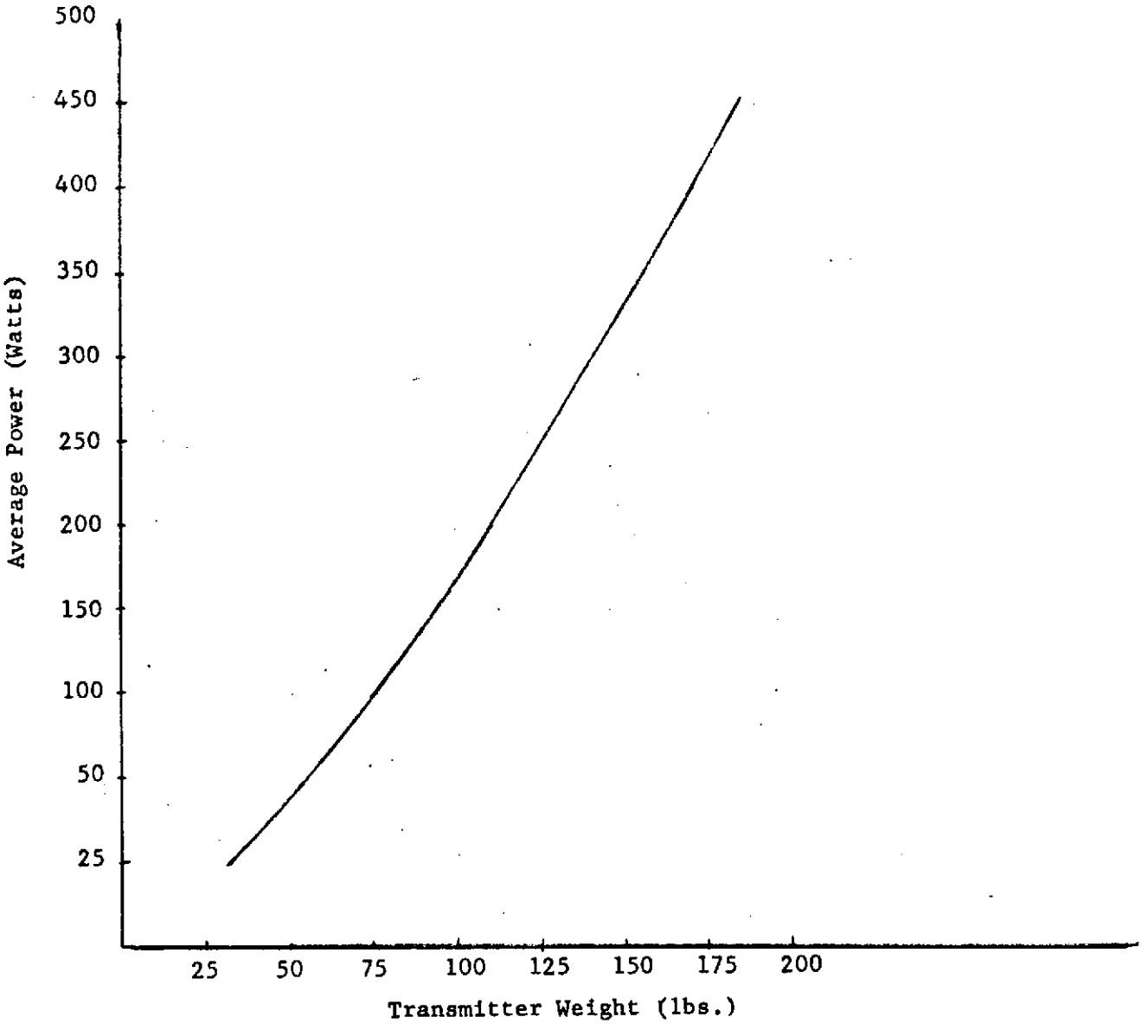

Figure 3.3.5-7. Transmitter Weight Power Trade-Off

3.3.5.2 Antenna

3.3.5.2.1 Introduction

The study reflects the two baseline radar systems presently being considered: #1 X-band (8.5 or 9.5 GHz) and #2, X and L band (8.5 to 9.5 GHz and 1.7 GHz). The salient antenna parameters are given in Tables 3.3.5-4 and 3.3.5-5 and section 3.3.5.2.2 and 3.3.5.2.3. The study discusses: (1) the practicality of building and deploying the large antenna required for satellite operation as well as mechanical and thermal characteristics, (2) parameter verification, and (3) provides additional descriptive data.

This descriptive data includes a discussion of advanced graphite/epoxy material and fabrication technique, as well as where and how conductive layer exists, itemized weight breakdown, stowed tolerance to launch forces, tolerable and actual deformation due to temperature, etc.

The option for two X-band polarization for configuration #2 is discussed. The system will operate at the orbit altitude and on the ground at normal atmospheric pressure. Consideration is given to a variable tilt angle from 55^{o} to 75^{o} depression angle.

3.3.5.2.2 Antenna Specifications

Configuration One

The antenna specifications are given in Table 3.3.5-4. These specifications reflect the major system constraints of maximizing gain and minimizing range and azimuth ambiguities. Specifically, the azimuth pattern (Figure 3.3.5-8) represents trade-offs between bandwidth pro-

Table 3.3.5-4 Antenna Specifications

Configuration #1

Frequency	8.5, 9.5 GHz $\pm$ 10 MHz
Approx. Antenna Dimension	13.5 x 2.5 x 1 ft. (length x height x depth)
Peak Gain (one way)	45.9 dB
Azimuth Pattern	See Figure 3.3.5-4
Elevation Pattern	See Figure 3.3.5-5
Sidelobes	$\leq$ -30 dB (except the first) Horizontal, Vertical
Allocated RF Losses	.25 dB
Bandwidth	30 MHz $\pm$ .5 dB
Polarization Isolation	-25 dB
Frequency Domain Linear Distortion (over average 15 MHz segment)	
Phase Ripple	$\leq 3^{\circ}$
Amp. Ripple	$\leq$ .4 dB
β_a (-4 dB) (two way)	5.1 mrad
β_e (-4 dB) (two way)	30 mrad
Peak Power	4.0 kW
Average Power	150w
No. of Failures/10^6 Hours	$\leq$ 1
Weight	92 lbs.

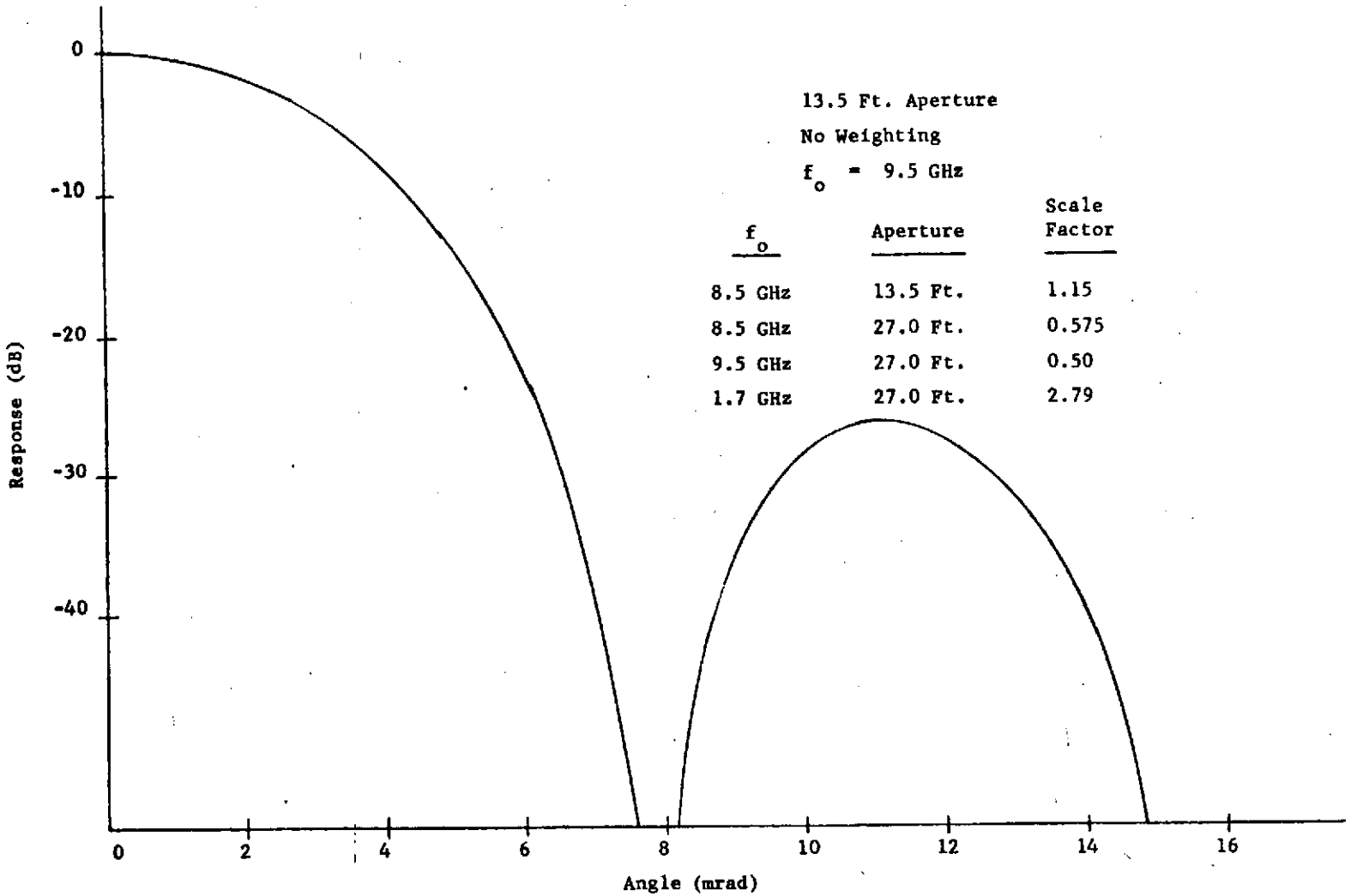

Figure 3.3.5-8. Two-Way Azimuth Antenna Pattern

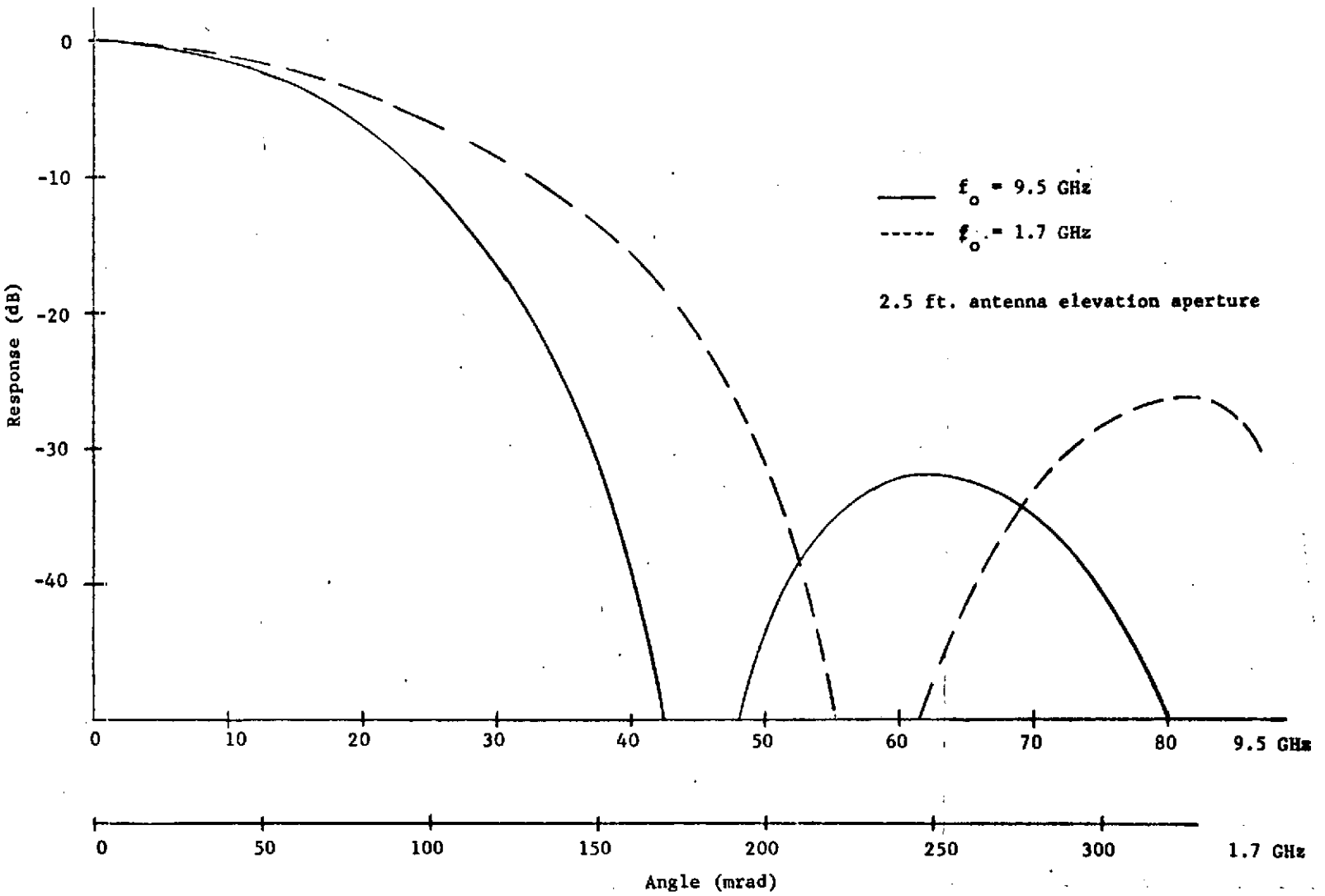

Figure 3.3.5-9. Two-Way Antenna Elevation Patterns

cessed, STAE, PRF, and sidelobe requirements. The elevation pattern reflects peak gain and evenness of gain over the range swath and elevation sidelobes. (See Figure 3.3.5-9).

Two polarizations are desired and achieved using a dual polarization feed discussed below.

The antenna is a unique concept developed at Westinghouse and used successfully on two separate surveillance radar programs. In one case, the antenna was a 13-foot wide K_a band reflector and in the other was a six-foot wide X-band reflector. The recommended antenna for SSAR follows the same design features and is 13.5 feet long and 2.5 feet high. The reflector is a section of a parabolic cylinder with the feed offset to reduce feed-blocking effects.

The feed is a line source with a capability of radiating both horizontal and vertical polarizations simultaneously.

Configuration #2

This antenna is similar to Configuration #1 in that the basis for the design is a line-fed cylindrical reflector. Specifications are given in Table 3.3.5-5. However, the antenna width has been increased to 27 feet to provide a narrow L-band beamwidth. The X-band feed is modified to allow an L-band (1.7 GHz) line feed to be included. The L-band feed is a center-fed resonant edge-slotted waveguide radiator producing a horizontally polarized beam. The X-band feed is a single polarization configuration but the option to changeover to a dual polarization design can also be made at the expense of 33 lbs. additional weight. The L-band feed is not flared out into a larger aperture in order to prevent a large blockage of the reflector. This results in a

Table 3.3.5-5 Antenna Specifications

Configuration #2

	X-Band	L-Band
Frequency	8.5, 9.5 GHz ± 10 MHz	1.7 GHz ± 10 MHz
Approx. Antenna Dimension	27.5 x 2.5 x 1 ft. Length x Height x Depth	
Peak Gain (one way)	47.9 dB	32.7 dB
Azimuth Pattern	Figure 3.3.5-4	Figure 3.3.5-4
Elevation Pattern	Figure 3.3.5-5	Figure 3.3.5-5
Sidelobes	≤ 30 dB (except the first)	≤ 30 dB (except the first)
Polarization	Horizontal Vertical (option)	Horizontal
Allocated RF Losses	.25 dB	
Bandwidth	30 MHz ± .5 dB	30 MHz ± .5 dB
Polarization Isolation	25 dB	----
Frequency Domain Linear Distortion (over any 15 MHz segment)		
Phase Ripple	≤ 3°	≤ 3°
Amp. Ripple	≤ .4 dB	≤ .4 dB
β_a (-4 dB) (two way)	2.55 mrad	15.5 mrad
β_e (-4 dB) (two way)	30 mrad	170 mrad
Peak Power	4.5 kW	.75 kW
Average Power	150w	25w
No. of Failures/10^6 Hours	1 hour	
Weight	174 pounds	

more uniformly illuminated reflector and higher edge illumination in the vertical plane. The result is a slightly reduced aperture efficiency for the L-band antenna. However, this appears to be the simplest and lightest weight approach to combining two frequencies having a 5:1 frequency separation ratio into one antenna system.

3.3.5.2.3 SSAR Antenna Design

Introduction

Conceptual designs of array-fed reflector antenna systems applicable to a synthetic aperture radar in an orbiting spacecraft are presented in the sections which follow. The practical considerations of construction and deployment of these comparatively large aperture antennas have received attention in the course of this investigation.

General Electrical Description of Antenna System

Two general antenna system baseline configurations have been investigated. These are basically "chin fed" parabolic cylinder reflector antennas utilizing a one-dimensional slotted waveguide array as a line source feed. This type of antenna is particularly appropriate to the SSAR application because of: 1) its comparatively light weight as compared to two dimensional phased arrays with approximately the same electrical characteristics and 2) its suitability for the desired unsymmetrical radiation pattern characteristics (with a beamwidth ratio of 5:1 or more between cardinal planes).

Antenna - Configuration #1

The first antenna configuration consists of a parabolic cylinder reflector which is illuminated by a one dimensional slotted waveguide array feed. The antenna aperture is 13.5 feet long and 2.5 feet high.

The feed is a unique design concept which is capable of simultaneous radiation of orthogonal linear polarizations. It was developed at Westinghouse and has been utilized in several surveillance radar antenna designs and both K_a band and X-band frequencies. It is shown in cross-section in Figure 4.5.1-1. The equivalent focal length to aperture ratio of the feed is approximately 0.3.

The properties of the feed which permit dual polarization include the use of a pair of slotted waveguides: one with broadwall slots for vertical polarization and the second with edge slots for horizontal polarization. The pair of waveguides are coupled to a common horn aperture through a set of polarization sensitive grids. Choke grooves parallel to the long aperture dimension of the feed are employed externally for shaping the primary radiation from the feed in the vertical plane for maximum efficiency and to minimize backlobe interference from the feed.

To further enhance the antenna system efficiency, the slotted waveguide feeds are designed as resonant structures so that no energy is lost in resistive feed terminations. Also, from considerations of maintaining high efficiency, the antenna is fed at its center through a pair of tee junctions, which reduces feed losses when compared to end-feeding. With the resonant feed design, an instantaneous bandwidth of 50 MHz at X-band is still realized at the levels of performance as shown in the accompanying table.

Table 3.3.5-6. Configuration #1 Antenna Characteristics

Frequency	9.5 GHz
Antenna Size (Stowed)	13.5 ft. x 37 in. x 9 in.
Aperture Dimensions	13.5 ft. x 2.5 ft.
Gain (one way)	44.5 dBi
Half Power Beamwidth (one way)	2.1^{o} elevation; 0.45^{o} azimuth
Peak Sidelobe Level (one way)	-16 dB elevation; -16 dB azimuth
Polarization	linear - H and V
Bandwidth	50 MHz
Weight	92 pounds

Antenna Configuration #2

This configuration is basically similar to configuration #1 in that it is also a parabolic cylinder reflector illuminated by a one dimensional slotted waveguide array feed. The antenna aperture, however, is increased to 27 feet long by 2.5 feet high to obtain a reduced half power beamwidth of the radiation pattern (at X-band) as compared with configuration #1. A dual frequency feed structure is utilized consisting of an L-band (1.7 GHz) edge-slotted waveguide array (horizontally polarized) mounted above a vertically polarized X-band feed as shown in Figure 4.5.1-3 . Optionally, a dual polarization X-band feed design of the identical variety proposed for configuration #1 may be utilized if desired. The L-band feed does not incorporate an integral horn flare aperture so that more significant blockage of the reflector aperture is avoided. This produces a broader primary illumination and, consequently, somewhat increased spill-over losses for the L-band frequencies. This, however, appears to be the simplest and most lightweight approach to combining two frequencies having a

5:1 separation ratio into a single antenna system.

Performance characteristics of antenna configuration #2 are summarized in Table 3.3.5-7.

Table 3.3.5-7. Configuration #2 Antenna Characteristics

Frequency	9.5 GHz	1.7 GHz
Antenna Size (stowed)	27 ft. x 37 in. x 1 ft.	
Aperture Dimensions	27 ft. x 2.5 ft.	
Gain (one way)	47.1 dBi	32.0 dBi
Half-Power Beamwidth (one way)	2.1° elev.; 0.23 az.	11.7° elev.; 1.2° az.
Peak Sidelobe Level (one way)	-16 dB elev.; -16 dB az.	-13 dB elev; -13 dB az.
Polarization	V (or H and V)	H
Bandwidth	30 MHz	50 MHz
Beam Coincidence	Within 0.1 HPBW at X-band	
Weight	174 lbs.	V polarization X-band H polarization L-band
	270 lbs.	V & H polarization X-band H polarization L-band

3.3.5.3 STALO/Synchronizer/System Controller

The STALO (Stable Local Oscillator) provides the transmitted and conversion reference signal with a high degree of spectral purity while the synchronizer provides basic system timing, gates and clocks in a near jitter-free fashion. The high degree of spectral purity is essential as phase perturbations over the integration period will result in lack of azimuth compression, sidelobes, etc. Jitter on basic timing can result in degraded imagery also.

The system controller receives the commands from satellite data link and/or on-board computer, converts them to the proper form, and assigns them to the appropriate radar subsystem.

System status which includes calibration information is received from the radar and sent to earth as auxiliary data.

Because of the commonality between configurations one and two, they are jointly discussed.

The preliminary specifications are given in Table 3.3.5-8 and the block diagrams in Figures 3.3.5-10 (a), (b), and (c).

The STALO functional block diagram illustrates the STALO key features. Crystal oscillators or possible variable crystal oscillators and frequency multipliers are used to generate the reference signals which have a high degree of short term stability as required by the specifications. The phase keyer shifts the first LO and the transmitted RF by $\overline{\pi}$ radians each IPP such that the undesired range ambiguities contiguous to the desired range swath are shifted by fr/2 and thus, lie outside the prefilter passband.

Table 3.3.5-8. Preliminary STALO/Synchronizer/System Controller Spec.

	Configuration 1	Configuration 2	
	X band	X Band	L Band
Stalo			
Transmit Center Frequency	9.3-9.5 GHz	9.3-9.5GHz	1.7 GHz
Transmit Input Power	+ 10 dbm	+ 10 dbm	+ 10 dbm
Amplitude Ripple	.4 db peak	.4 db peak	.4 db peak
Phase Ripple over any .1 sec interval			
Ripple	≤ 3°	≤ 3°	≤ 3°
Low Order Quadratic	≤ 40°	≤ 40°	≤ 40°
Cubic	≤ 7°	≤ 7°	≤ 7°
Random			
AM & PM Noise	See Fig. 3.3.5-3	See Fig. 3.3.5-3	See Fig. 3.3.5-3
Jitter	σ < 4 ns	σ < 4 ns	σ < 4 ns
1st LO Frequency	f_o + 120 MHz	f_o + 120MHz	f_o + 120MHz
1st LO Power	0 dbm	0 dbm	0 dbm
2nd LO Frequency	120 MHz[1.]	120 MHz	120 MHz
2nd LO Power	0 dbm	0 dbm	0 dbm
Pulse Expansion Reference Freq.	120 MHz	120 MHz	120 MHz
Pulse Expansion Reference Freq. Pwr	+ 10 dbm	+ 10 dbm	+ 10 dbm
PRF (Adjustable)	3-4 KHz	3 KHz	3 KHz
Range Ambiguity Supressor Accuracy	-	-	1°
Synchronizer			
Jitter	σ < 4 ns	σ < 4 ns	σ < 4 ns
Pulse Expansion Impulse Width	~ 2 ns	~ 2 ns	~ 2 ns
A/D Sample Rate	15 MHz	15 MHz	15 MHz
Swath Width Position Range	± 200 μs	± 200 μs	± 200 μs

1. If antenna positioning to account for earth rotation effects is not possible 2nd LO variation specifications are:

Deviation (max)	± 5 KHz
Accuracy (open loop)	± 20 Hz
$\Delta f/\Delta T$	~ 8 KHz/10 min. (no discontinuity)

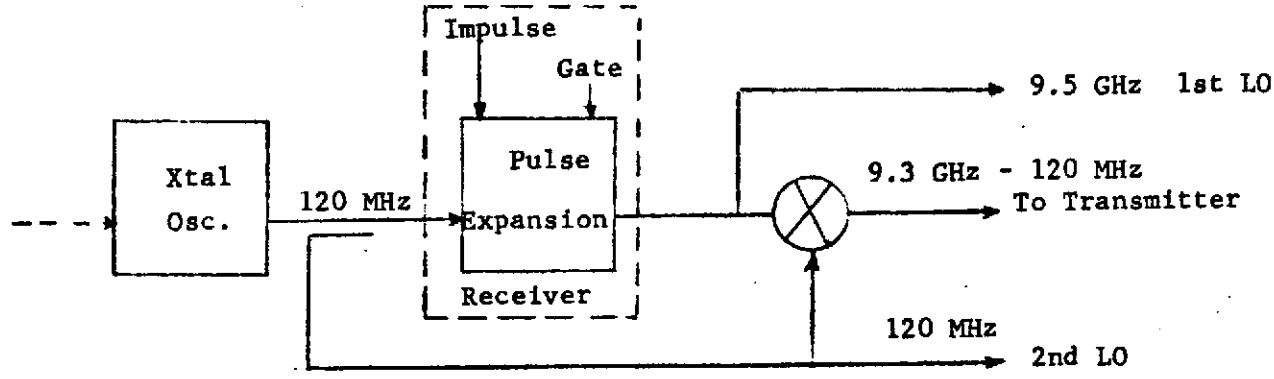

(a) STALO
Configuration #1

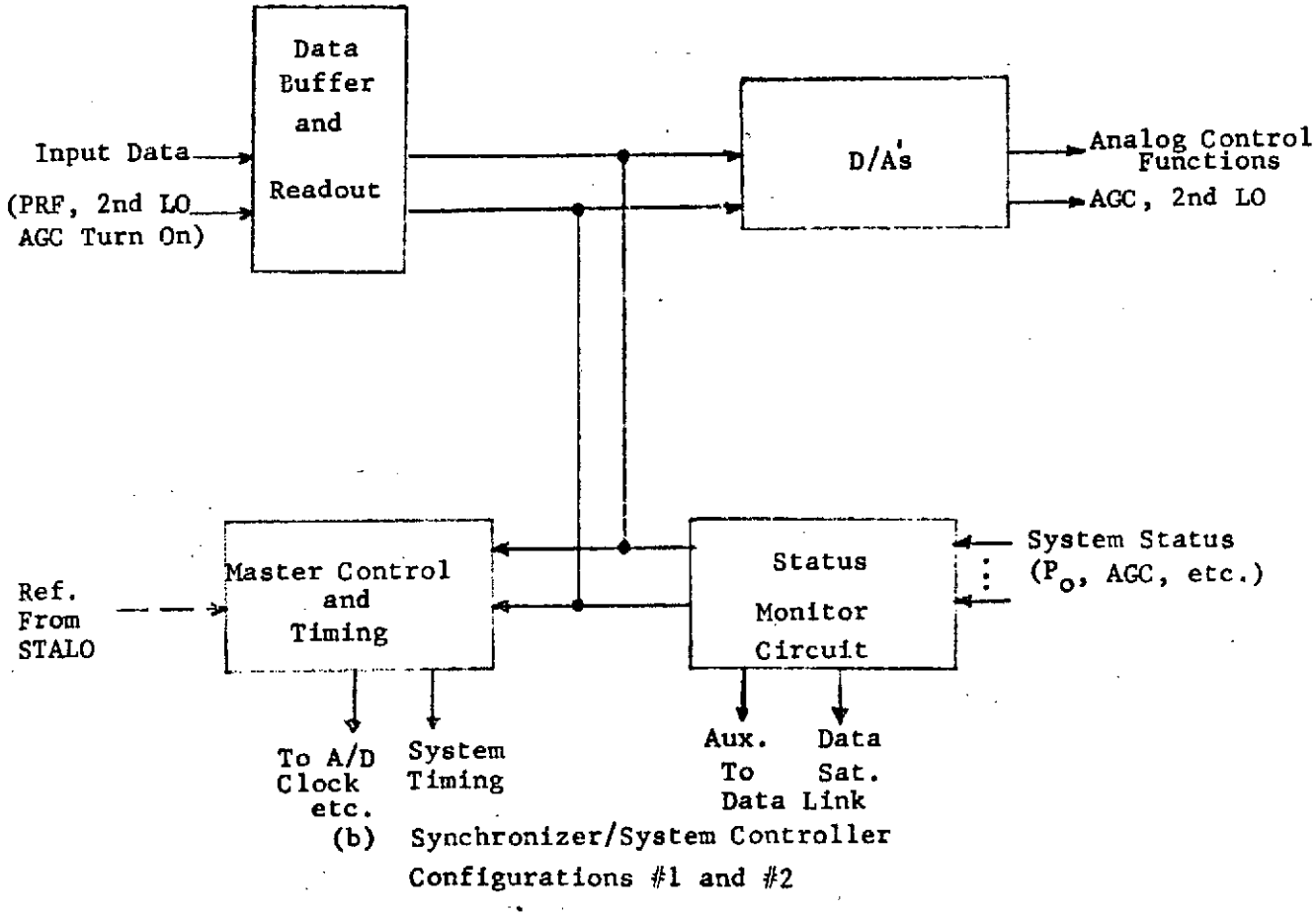

(b) Synchronizer/System Controller
Configurations #1 and #2

Figure 3.3.5-10. Functional Block Diagrams

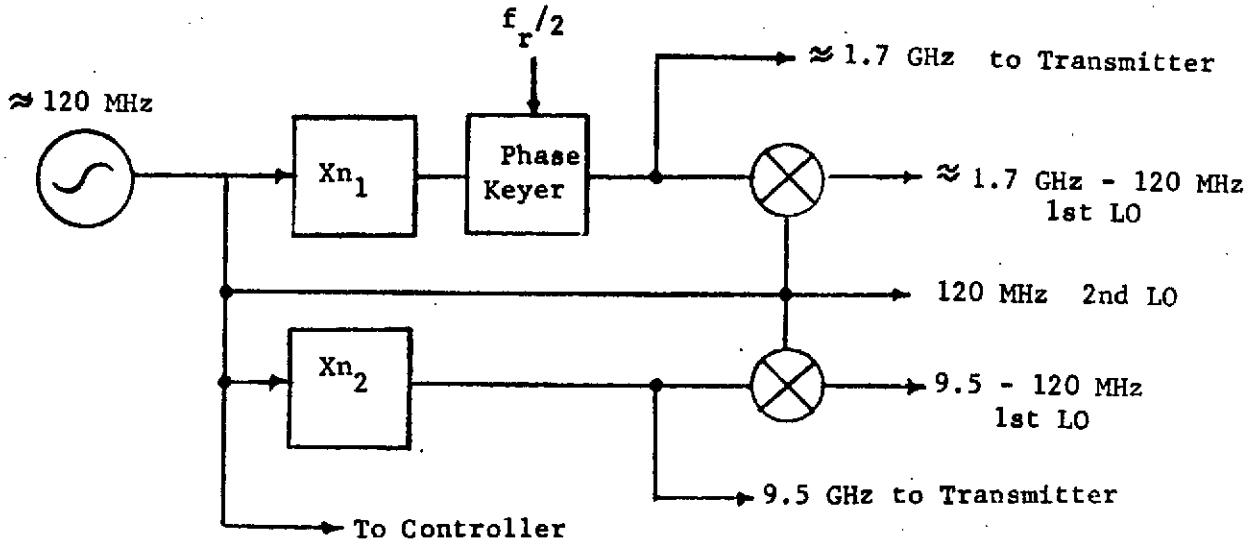

(c) STALO

Configuration #2

Figure 3.3.5-10. Continued

A 1/4 cycle or so sample of the 120 MHz signal is used to impulse a surface wave dispersive delay line creating the expanded pulse which is converted to X or L band and transmitted.

If the doppler due to earth rotation effect is not corrected by slewing the spacecraft, the main beam spectrum must be shifted (section 3.2.3.7) so as to fit within the prefilter passband. This can be done by offsetting the transmitted signal and second LO half of the incurred doppler due to earth's rotation. Then, one half of the incurred doppler is removed prior to transmission and the other half upon IF to video conversion. This correction technique is assumed not necessary and, therefore, not shown in Figure 3.3.5-10.

Variations in satellite altitude may require slight open loop variations in range interval position as well as PRF. Even though the AGC is closed loop, there could be special circumstances under which it is desirable to vary receiver gain in an open loop fashion. Provision is made for variation of these and other parameters via the satellite data link and system controller.

The noise specification mentions common and independent requirements. These refer to common phase component present to both transmit and receive paths and those independent perturbations present in either the transmit or receive paths.

The derivation of common PM instability (common to both transmit and receive path) requirements may be better understood by the following:

$$\text{If } f(t) = \text{Re}\ \ e^{j\,[\omega_o t + \phi(t)]}$$

where ω_o = transmitted frequency

$\phi(t)$ = common phase perturbation

$f(t)$ = transmitted signal

The complex received converted signal becomes

$$f_r(t) = e^{-j[\omega_o(t-\tau)+\phi(t-\tau)]} e^{j[\omega_o t + \phi(t)]}$$

$$= e^{j\omega_o t} e^{-j[\phi(t-\tau)-\phi(t)]}$$

where τ is a time delay equal to round trip radar transmit time. Then $e^{-j\omega\tau}$ is a constant; the perturbing effect $\phi(t)$ has been partially cancelled dependent upon τ. If $\tau = 0$, the perturbing effect is nullified. Now

$$f_r(t) \simeq e^{-j\omega\tau}\{1+[\phi(t)-\phi(t-\tau)]\}$$

for $\phi(t)-\phi(t-\tau) \ll 1$

This approximation is true over the region of interest. Then taking the Fourier Transform

$$F_r(\omega) = e^{-j\omega_o\tau}\{2\pi\delta(\omega)+j[\Phi(\omega)-e^{-j\omega\tau}\Phi(\omega)]\}$$

$$= e^{-j\omega_o\tau}\{2\pi\delta(\omega)+j[\Phi(\omega)(e^{-j\omega\tau/2}\, j2\sin\omega\tau/2)]\}$$

$$= e^{-j\omega_o\tau}\{2\pi\delta(\omega)-e^{-j\omega\tau/2}\Phi(\omega)2\sin\omega\tau/2\}$$

$$|F_r(\omega)|^2 = [2\pi\delta(\omega)]^2 - |\Phi(\omega)|^2 4\sin^2\omega\tau/2$$

The received converted power signal consists of a component at the origin corresponding to the desired unperturbed signal and a perturbation component $\Phi(\omega)^2$ modified by the factor $4\sin^2\omega\tau/2$. For

the longest range, 1550 Km,

$$\omega\tau/2 = 1 = \pi f\, 10^4\,\mu s$$
$$f = 31.8\ Hz$$

So up to the maximum range and for perturbing frequencies less than 31.8 Hz, the perturbation spectrum may be represented by

$$\simeq |\Phi(\omega)|^2 (\omega\tau)^2 \qquad \tau \leq 10^4\,\mu s,\ R < 1550\ Km,\ f \leq 31.8\ Hz$$

where $\omega\tau/2 < 1$

The modifying value becomes periodic in ω for $\omega\tau/2 < 1$; however, the peak value is 4 or 6 dB and this will be used. The partial cancellation of deterministic and nondeterministic phase perturbations allows common frequency deviation and sideband levels to be raised for $\omega\tau/2 < 1$ and lowered by a factor of 2 for $\omega\tau/2 > 1$. The deviation modifying factor is, of course, $2\left|\sin \omega\tau/2\right|$.

3.3.5.4 Receiver/LVPS Specifications

The receivers have the following capability: amplify in a relatively distortion-free fashion the ground return signals in separate channels for both horizontal transmit-horizontal receive (HH) and horizontal transmit-vertical receive (HV) as well as VV and VH polarizations, provide duplexing and receiver protection, vary gain in an adaptive manner, provide range pulse compression, IF to complex video conversion, complex A/D conversion, prefilter complex data and reduce physical data rate, multiplex and assemble digital video into appropriate format for ground transmission.

The LVPS provides the +28v dc to required supply voltage conversion and regulation.

Receiver specifications are shown in Table 3.3.5-9.

Table 3.3.5-9 Receiver Specifications

General	Configuration #1	Configuration #2
Transmitted Pulsewidth	11.1 μs	11.1 μs
Compressed Weighted Pulse (-4 dB pk)	75 ns	50 ns
Frequency Dispersion	13.3 MHz	27 MHz
Sidelobes	-30 dB	-30 dB
Noise Figure (total, no AGC)	1.7 dB	1.7 dB
PRF	3-4 KHz	3-4 KHz
Phase Ripple (total)	$\leq 3^{o}$	$\leq 3^{o}$
Amp. Ripple	$\leq$ .4 dB	$\leq$ .4 dB
Integration Time	.125 sec	.125 sec
Third Order Products from two equal signals at -64.3 dB at INA input	36 dB below fundamental signals	36 dB below fundamental signals
Assumed RF Losses (from ant. through rcvr. protect)	1.50 dB	1.3 dB
Low Order Phase		
Quadratic	45^{o}	45^{o}
Cubic	20^{o}	20^{o}
Operating Temperature Range	$+20^{o}$ - $+50^{o}$C	$+20^{o}$ - $+50^{o}$C
AGC Control Range	~ 45 dB	~ 45 dB
IF Limiting Characteristic ⇒	Lin Log commensurate with A/D saturation	Lin Log commensurate with A/D saturation
IF Frequency	120 MHz	120 MHz
Gain Calibration Accuracy each IPP using calibration pulse sequencer	$\pm$.5 dB	$\pm$.5 dB
A/D		
Amplitude	s + 4 bits	s + 4 bits
Rate	~ 13 MHz	27 MHz
Jitter	$\sigma \prec$ 5 ns	$\sigma \prec$ 5 ns
Clutter plus noise set by AGC to 2q		

Table 3.3.5-9 Receiver Specifications (Cont'd)

General	Configuration #1	Configuration #2
Multiplex		
Combine A/D outputs for 2 channels	78 Mbits/sec each	78 Mbits/sec each
Number of range cells/IPP	2080	2080
Auxiliary Data (radar housekeeping)	~30 channels @ 8 bits each	~30 channels @ 8 bits each

The compressed pulse width, not including any pulse widening due to quadratic phase errors is:

$$\tau = \frac{2r_g}{c} \cos \phi / 1.1$$

The 1.1 factor allows for these errors. Weighting further reduces the pulse width requirement or increases the required dispersion such that the net spreading factor is some 35%.

Then,

$$\Delta f = \frac{1}{\tau'}$$

$$\tau' = \frac{2}{c} r_g \cos \phi / 1.35$$

for a ground range resolution (r_g) of 30m and depression angle (ϕ) of 60°. $\tau' \cong 75$ ns

& $\Delta f = 13.3$ MHz

For $\phi = 75^\circ$ $\tau' = 37$ ns

$\Delta f \cong 27$ MHz

The low noise figure is achieved using a non-cryogenic parametric amplifier.

The RMS clutter level is controlled via an AGC whose time constant

is long compared to an integration time. The clutter is controlled to about 2 quanta at the A/D input. Thus, an 18 dB dynamic range above mean clutter level is provided to handle discrete (point targets) and statistical clutter variations. The AGC control range is required to be about 45 dB as seen from variations of section 3.2.3. This allows for 10 dB of reserve gain. Actually, the rms uncompressed clutter cell size for configuration #1 is about 132×10^6 m^2 such that even with a range compression gain of 133 ($132 \times 10^6/133 = 1.32 \times 10^6$ m^2) there are few discretes that exceed the RMS clutter level prior to A/D conversion. The statistical amplitude density function is then essentially Rayleigh where those components 10 dB more than the RMS level amount to less than .1%. These sort of requirements indicate a minimum of non-linear distortion, however, a third order product specification commensurate with the maximum input LNA signal level has been specified along with a "Lin-Log" limiter to exclude video limiting for those rare signals which are larger than the norm.

Linear distortion requirements are specified in the frequency domain as both high order phase and amplitude which result in range sidelobes and low order symmetric (quadratic) and asymmetric (cubic) which result in resolution loss and a sidelobe. Azimuth degradation requires variance of gain or phase over a significant part of the integration time. To this end, the AGC is slow with respect to integration time.

Some amount of open loop AGC control may be desirable to allow for better clutter positioning within the A/D window--conceivable an AGC profile for each orbit pass should be used. The A/D samples provide the swath definition. In order to provide a swath with a constant

ground range offset from the flight path the round trip time, ΔT, from transmitter pulse to A/D initiation must be a variable as a function of the local altitude. This will require slight variations in initiation time and PRF. Again, this requires orbit by orbit profile data. Range swath timing is shown in Figure 3.3.5-11 below.

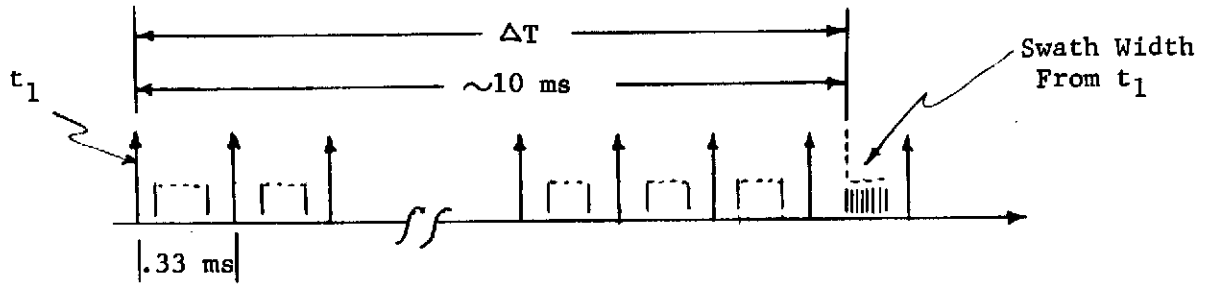

Figure 3.3.5-11. Range Swath Timing

The multiplexer or data buffer performs a slow down in data rate and combines the A/D output into a form compatible with High Speed Data Processor (HSDP). The A/D conversion takes place at the rate shown in Table 3.3.2-1 over the depression angle variation. The the Range Slow Down (RSD) factor changes from about 1.6 to 3.1 from 55^{o} to 75^{o} depression angle variation. This variation is necessary such that multiplexer output rate or (HSDP) input rate remain constant and to extend the limited swath width data over all time so as not to exceed the data link capacity.

4.0 MECHANICAL DESIGN

4.1 Requirements

For this study effort, the mechanical design requirements include, (1) packaging the electronics and antenna in a minimum of space and for a minimum weight with a goal of 500 lbs. maximum, (2) dissipating the thermal load in the simplest manner consistent with maintaining component temperatures below 100°C, (3) providing an antenna hinge design and latch design and (4) restricting antenna distortions to less than 0.1".

The spacecraft orbital parameters used in determining the thermal performance are (1) 914 km attitude (103 minute period), (2) 9:30 A.M. and 3:30 P.M. sun synchronous orbits.

While the launch vehicle has not been specified, an acceleration level of 20 g's has been selected for design purposes to be conservative and assure compatibility with the TITAN 3C or any other candidate vehicle.

4.2 Summary of System Mechanical/Thermal Characteristics

Two configurations of the SSAR have been studied. Configuration #1 weighs 262 lbs. including the 13.5' antenna and the electronics package measures 31" x 22" x 9-1/2". The primary structure is nominally a one-inch aluminum honeycomb plate with all components mounted thereon.

The thermal control system is entirely passive and component temperatures are maintained below 100°C with load of 1235 watts. Heat dissipation is by conduction and radiation internally and by radiation to space externally.

Thermal distortions of the 13.5' antenna have been computed to be less than 0.1" through the use of appropriate thermal coatings and graphite epoxy composite material in the construction of the antenna.

Configuration #2 weighs 388 lbs. including the 27' antenna and the electronics package is 38" x 24" x 9-1/2". Dynamic and thermal performance are similar to those of configuration #1.

4.3 Electronic Packaging

4.3.1 Radar Electronics

The factors considered in determing the optimum layout of electronic components include:

- Minimum volume
- Minimum coax and waveguide lengths
- Minimum high voltage lead lengths
- Access to connectors and mounting flanges
- Fixed shapes on certain off-the-shelf components such as LVPS, paramps, Waveguide, directional couplers, and waveguide switch tube.
- Heat Transfer
- Minimum structure weight

The individual packages for each configuration are listed under electronics in the Weight Summary Table 4.3.1-1. The final layouts are shown in Figures 4.3.1-1 and 4.3.1-2.

Thermally, the best location for the hottest element, the X-band tube, is in the corner opposite the output to the antenna. This provides the shortest conduction path to the two side

Table 4.3.1-1. Physical Properties Summary

WEIGHT SUMMARY				
	Configuration 1		Configuration 2	
Antenna		92.0		174.0
Electronics				
X-Band XMTR	75.0		75.0	
L-Band XMTR	-		20.0	
Stalo	5.0		8.0	
P.C. Bd. Support	3.0		4.0	
LVPS	20.0		30.0	
L-Band RF Amp	-		.5	
Circulator	3.0		3.0	
Receiver Protectors	6.0		6.0	
Couplers	1.0		1.0	
High Power Coupler	2.0		2.0	
Paramps	4.0		2.0	
Chassis	5.0		5.0	
Boards	4.0		4.0	
Hybrid	.5		-	
Waveguide Switch	2.5		-	
Misc. (Wiring, etc.)	10.0		15.0	
	141.0	141.0	175.5	175.5
Radiator		13.5		17.0
Structure		15.5		21.0
	TOTAL	262.0 lb	TOTAL	387.5 lb

VOLUME SUMMARY		
Overall Dimensions	31 x 22 x 9.5	38 x 24.5 x 9.5
Volume (in^3)	6479	8845
Volume (ft^3)	3.75	5.12

Table 4.3.1-1. Physical Properties Summary (Cont'd)

THERMAL POWER SUMMARY

	Configuration 1	Configuration 2	
	X	X	L
XMTR	600	600	100
P.C. Board Chassis	110	- 110 -	
Power Supplies	100	- 100 -	
Paramps	100	50	20
Shielded Chassis	50	- 50 -	
Stalo	33	- 57 -	
	TOTAL 993 Watts	TOTAL 1087 Watts	

ELECTRICAL POWER DRAIN SUMMARY

	Configuration 1	Configuration 2	
	X	X	L
XMTR	750	750	125
P.C. Board Chassis	110	- 110 -	
Power Supplies	100	- 100 -	
Paramps	100	50	20
Shielded Chassis	50	- 50 -	
Stalo	33	- 57 -	
	TOTAL 1143 Watts	TOTAL 1262 Watts	

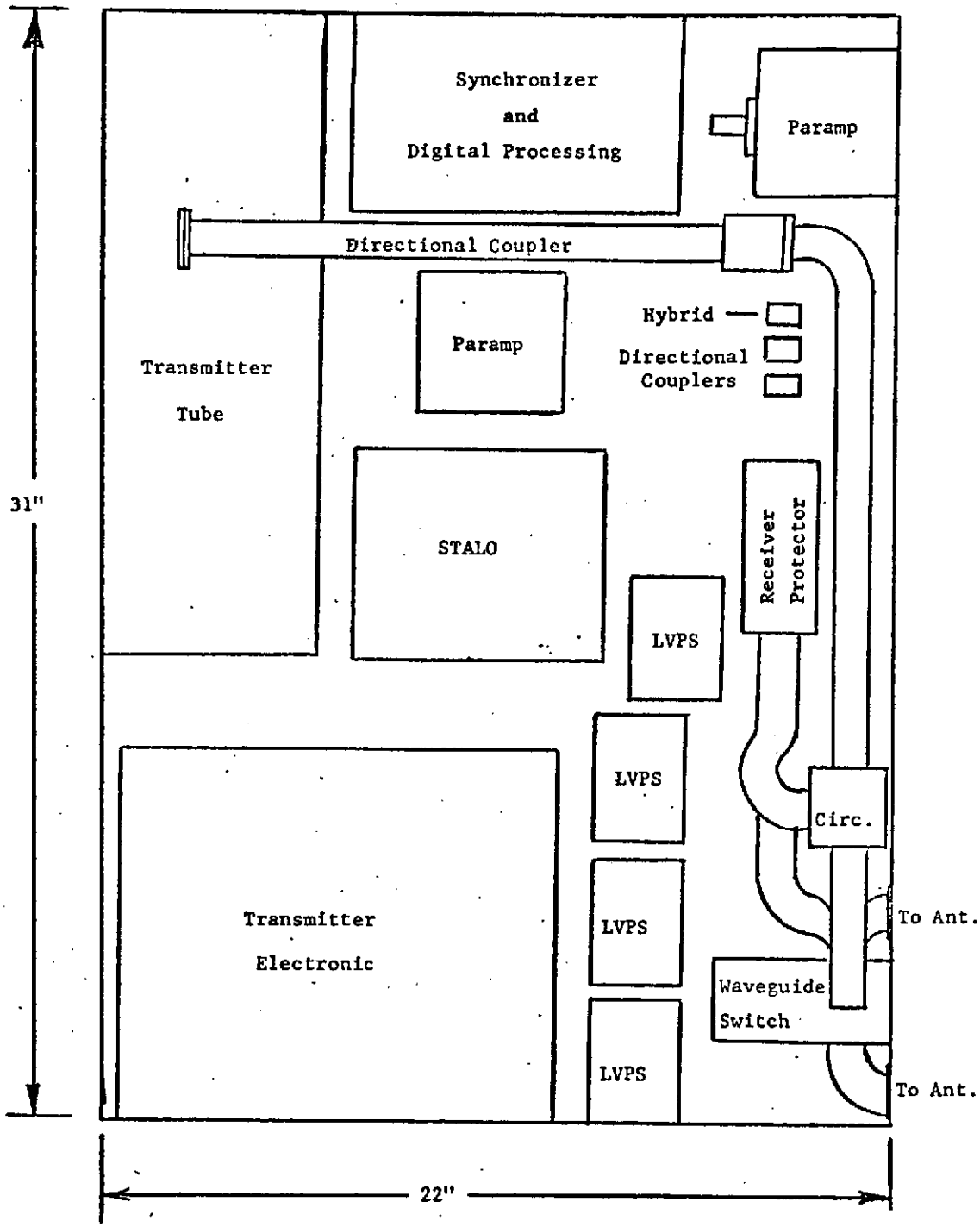

Figure 4.3.1-1. Configuration #1 Layout

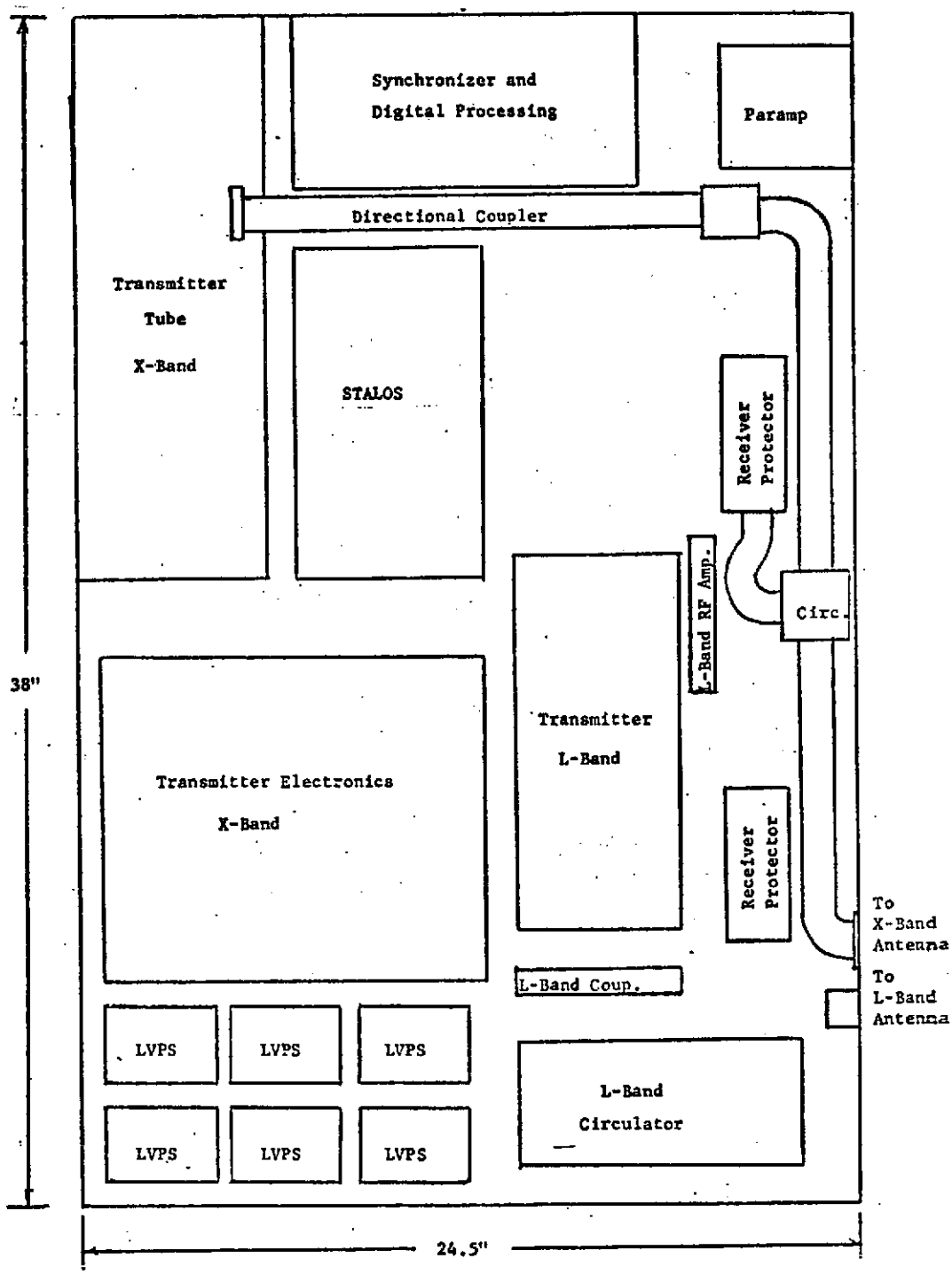

Figure 4.3.1-2. Configuration #2 Layout

radiators and provides some isolation from the other packages. The 17" directional coupler and need for physical proximity of shielded chassis, paramps, p.c. board, chassis, stalo receiver protectors and coax directional couplers determine to a large extent the rest of the layout. The X-band tube electronics were kept close to the tube to minimize high voltage lead lengths. In Configuration 2, the L-band transmitter was located as close to the output as possible to minimize coax lengths.

Except for the LVPS and tube in Configuration 1, and circulator and coupler of Configuration 2, the average package height, including boards, is 8 to 8-1/2". The waveguide and coax coupler were stacked over the cover to the five shielded chassis and because it is possible to remove each chassis individually from its drawer in the cover there would be little need to remove the cover itself.

There was no other stacking because it would markedly decrease the accessibility and require considerable additional structure. The size of the other packages and waveguide prevents the stacking of these small packages from being turned into a useful space reduction.

The packaging density for Configuration 1, including structure and radiators, is 45.3 lb./ft^3. The density for Configuration 2 is 41.7 lb/ft^3.

These values demonstrate that the system has been packaged efficiently.

4.3.2 Structure

For supporting the electronics, a rigid honeycomb deck, which provides the greatest strength with the least weight, is used. For uniform loading with the assumed 20G load and the honeycomb structure freely supported along all edges, the stresses and deflections were calculated. The results, shown in Figs. 4.3.2-1 and 2 show that adequate strength and stiffness are achieved. For any changes in the loading environment, the structural parameters can be modified at the time of the detailed design. It is anticipated that such changes would result in an even lighter structure.

4.3.3 Construction & Radiator Mounting

The sandwich is fabricated from a .188" thick 3003 AL top faceplate (for heat conduction) and a .020" thick 5052 Al bottom faceplate (for strength). The core is hexagonal honeycomb with 3/16" cells of 5052 foil, .015" thick. The core thickness for Configuration 1 is .9" and it is 1.0" for Configuration 2. Inserts will be used to mount electronics packages.

The sides and top of the unit are non-structural and act as thermal radiators. They are constructed of .08" 3003 Al coated with second surface vapor deposited Teflon for low absorbtivity and high emissivity radiation. The sides are fixed to the structural plate with screws and the gap is sealed with epoxy for better heat conduction.

4.3.4 Weight

The weight of Configuration 1 is 15.5 lbs structure and 13.5 lbs radiators. The weight of Configuration 2 is 21.0 lbs

structure and 17.0 lbs. radiators. It is possible that the structure weight of Configuration 1 could be reduced by 6.0 lbs., and Configuration 2 by 8.0 lbs. if it is decided to mount components with thermal grease or epoxy instead of dry mounting. This option would be exercised if it was decided that the weight reduction more than offset the loss in maintainability associated with the use of either grease or epoxy thermal joints. While analysis shows that the bottom face sheet need only be .012", it will be increased to .020" in detail design to provide additional surface rigidity to withstand the effects of handling during manufacture, assembly and test. This will increase the weight of the system by about 0.5 lbs.

TABLE 4.3.2-1

CONFIGURATION 1 STRUCTURE SUMMARY

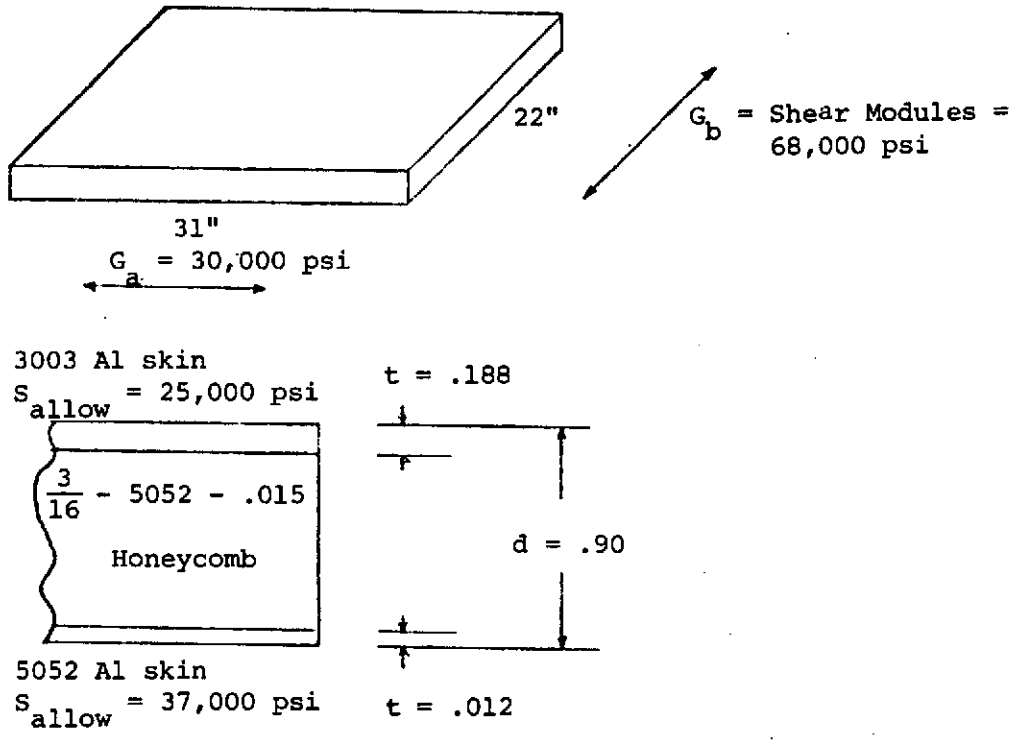

Maximum bending moment, 'a' direction = 102.99 in.-lb./in.

Maximum bending moment, 'b' direction = 162.10 in.-lb./in.

Stress upper plate, 'a' direction = 685 psi

Stress lower plate, 'a' direction = 10,728 psi

Stress upper plate, 'b' direction = 1,078 psi

Stress lower plate, 'b' direction = 16,885 psi

Maximum deflection = .0987" at center

TABLE 4.3.2-2

CONFIGURATION 2 STRUCTURE SUMMARY

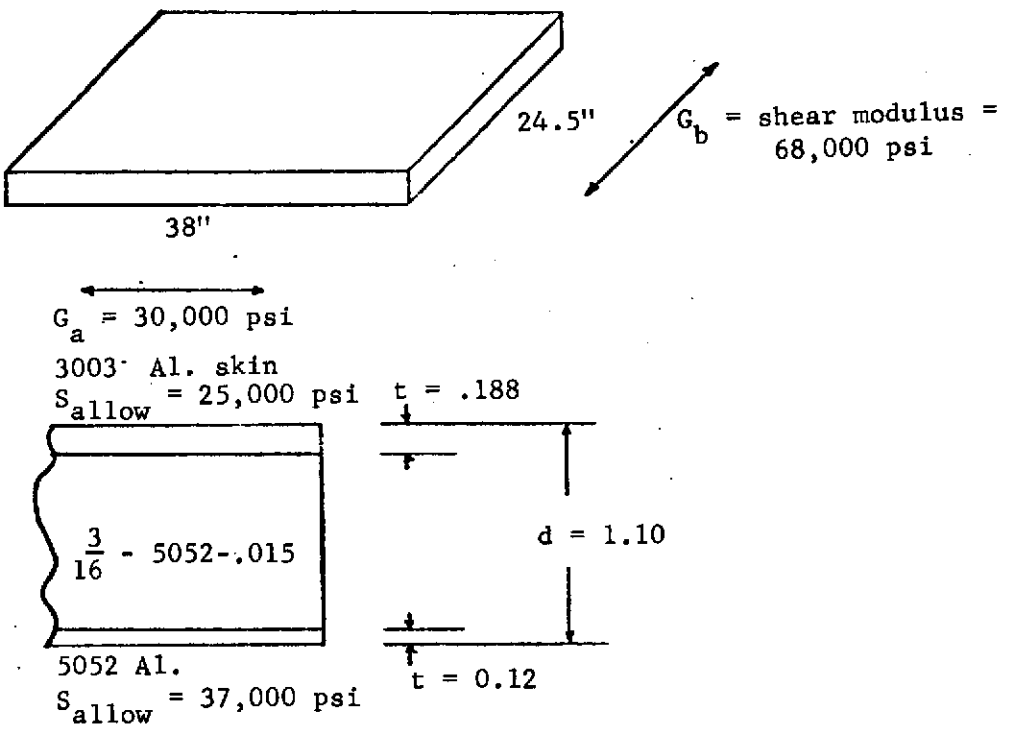

Maximum bending moment, 'a' direction = 116.8 in.-lb./in.

Maximum bending moment, 'b' direction = 203.7 in.-lb./in.

Stress upper plate, 'a' direction = 621

Stress lower plate, 'a' direction = 9732

Stress upper plate, 'b' direction = 1084

Stress lower plate, 'b' direction = 16,976

Maximum deflection (at center) = .089"

4.4 Thermal Analysis

4.4.1 Radar Electronics

The purpose of this study was to determine the temperatures to which the electronic equipment of the SSAR will be subjected. These temperatures must remain within specified limits to insure reliable operation. The temperature profile and gradients were calculated for the SSAR as it moves around the earth at an altitude of 914 kilometers (568 miles). The path defined for the spacecraft is a polar orbit which is sun synchronous at either 9:30 A.M. or 3:30 P.M. (See Figure 4.4.1-1).

The configuration analyzed placed the electronics at the top of the spacecraft payload. The analysis included the effects caused by the presence of the craft as well as the antenna. The existence of these (1) prevents the base plate of the structure from radiating to space, (2) reduces the view to space of the sides and top, and (3) partially shades the unit from incident radiation. The surface properties of the coating of the electronics package were assumed to be the following:

Electronics Package - Second surface vapor deposited silver teflon

$\alpha = .08$

$\epsilon = .77$

The actual analysis of the unit was divided into two portions. The first part included the development of the external geometry of the electronics, antenna, payload, and spacecraft for the Lockheed Orbital Heat Rate Package (LOHARP). With the seasons

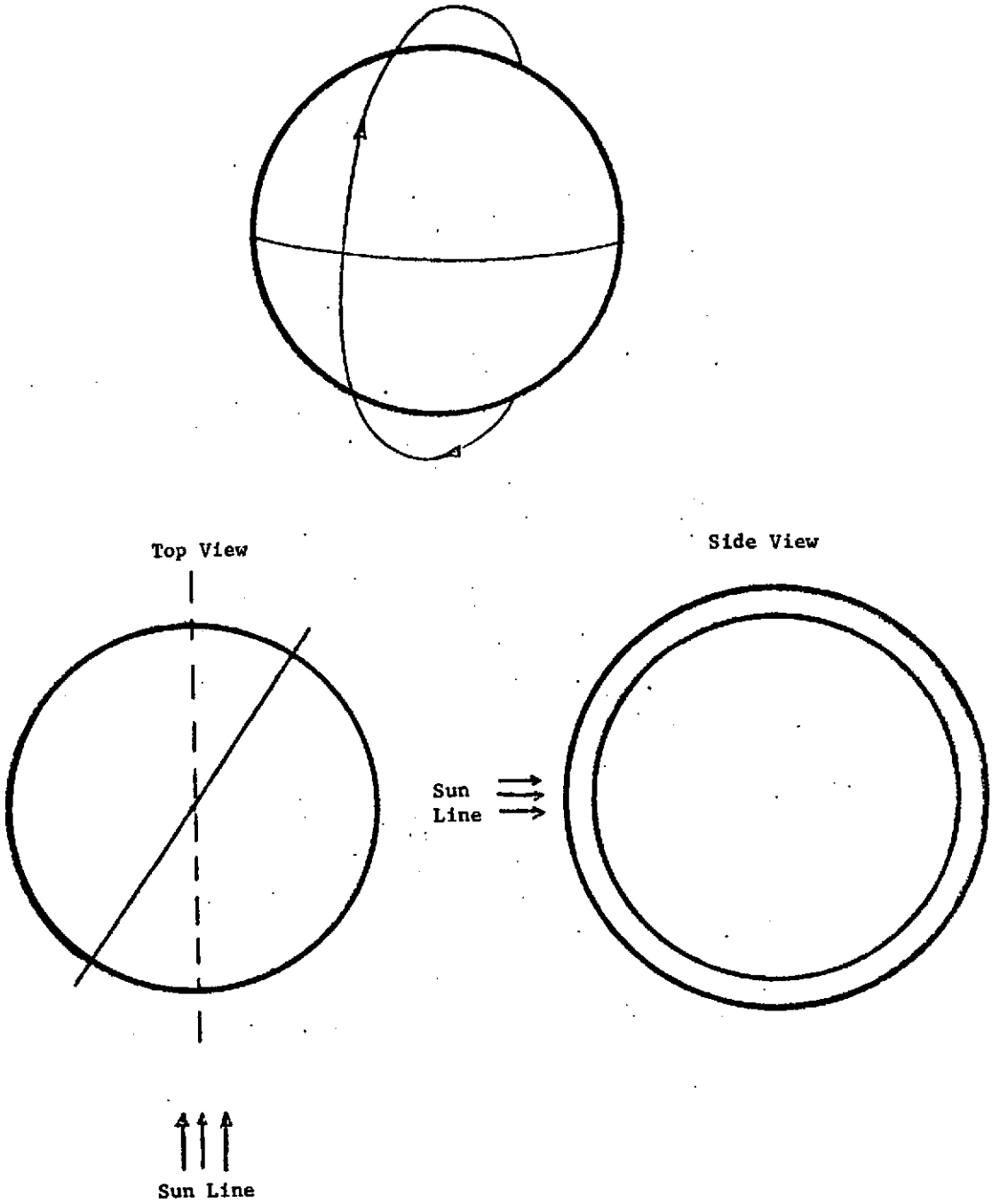

Figure 4.4.1-1. Polar Sun Synchronous Orbit

assumed to be either the vernal or autumnal equinox, the required orbital information was also input to the program. The results of this computation on the Univac 1108 Digital Computer were the radiation couplings of the package to space, the incident solar energy, the albedo input, and the planetary input due to the temperature of the earth.

The second part of the analysis was the calculation of the temperatures of the base plates of the components in the SSAR. A complete internal and external thermal model was developed as shown in Figure 4.4.1-2. This model was analyzed using the Nodal Network Thermal Balance Program (NETWK) developed at the Goddard Space Flight Center. The power input to the individual components and the corresponding node in the thermal model are shown in Table 4.4.1. It is important to remember that the power shown in this table is applied for a period of ten (10) minutes during each 103.2 minute orbit. The time of application of this power was during the period of maximum external inputs to simulate the worst case condition. In addition, it should be noted that if the temperature of the PARAMP is allowed to be maintained at a value greater than 25°C, the internal heater power of this unit is no longer necessary.

To establish realistic operating conditions for the SSAR, the following assumptions were made:

1. Since the internal configurations of the individual units such as the PARAMP, Stalo, etc., are not definite, the temperature of the base plates of these components

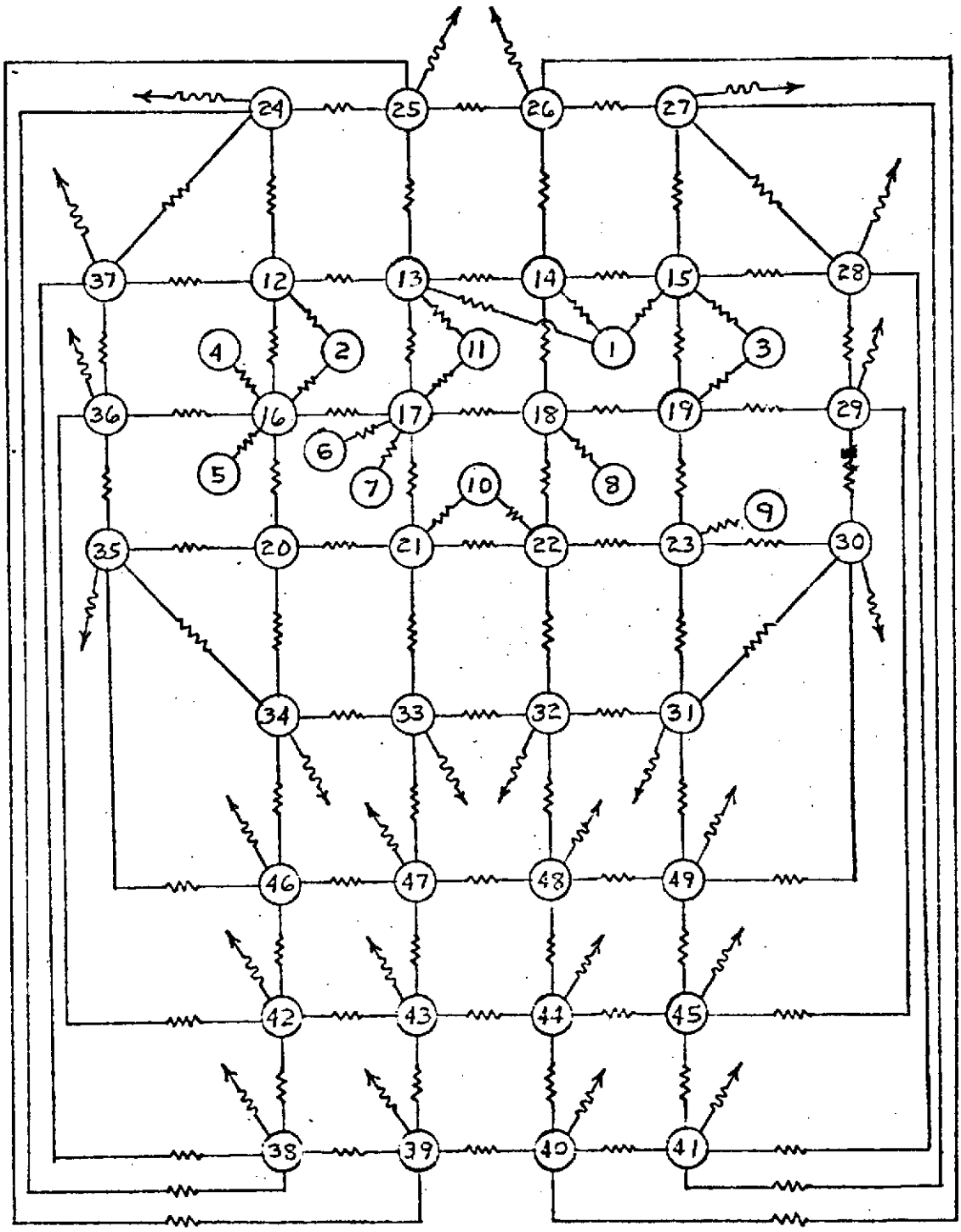

Conduction Coupling

Radiation Coupling

Node Designations

1-11	Component Bases
12-23	Structure Base
24-37	Structure Sides
38-49	Structure Top

Figure 4.4.1-2. SSAR Thermal Model

TABLE 4.4.1-1

SSAR POWER DISSIPATION

The following power is dissipated for 10 minutes during each 103 minute orbit:

LOCATION	POWER (WATTS)	THERMAL MODEL NODE NUMBER
TRANSMITTER		
Tube	702	1
Electronics	140	2
PC BOARDS & WIRE WRAP BOARD	110	3
POWER SUPPLIES		
#1	25	4
#2	25	5
#3	25	6
#4	25	7
*PARAMP		
#1	50	8
#2	50	9
SHIELDED CHASSIS	50	10
STALO	33	11
TOTAL	1235 Watts**	

* Approximately 70 watts can be subtracted from the total PARAMP power dissipation if it is regulated to remain at a temperature $\geq 25°C$.

**This power valve is based on an early concept and represents a conservative design since the actual dissipation has decreased.

were calculated. Limits were placed on the acceptable temperature of these base plates with the most critical being that of the transmitter tube. The goal of this study was to maintain this temperature below 100°C.

2. The temperature of any component inside a particular unit can be determined from the base plate temperature.

3. Two cases were established for conduction between the base plate of the component units and the base plate of the structure.

   CASE I: The coupling is a combination of conduction around the bolts tying the plates together and radiation between the plates.

   CASE II: The coupling is a combination of conduction around the bolts tying the plates together and conduction through a .003 inch interface of Ablefilm 504. This thermally conductive epoxy has a thermal conductivity of .45 Btu/hr ft °F.

4. The base plate of the structure is constructed of 3/16 inch aluminum with honeycomb reinforcement.

5. The sides and top of the structure are made of .080 inch aluminum.

6. The sides are connected to the base plate with epoxy.

7. The top is mechanically fastened to the sides with a contact conductance occurring at the intersection.

8. The sides and top surfaces radiate to space according

to the couplings calculated by the LOHARP program.

9. The nodes radiate to space at a temperature equal to the average nodal temperature. To increase the accuracy of the final analysis, the radiating areas will be adjusted slightly to reflect the efficiency of a radiation, conduction system.

The results of the analysis show that for Case I and Case II, the base plate of the transmitter tube can be maintained at a maximum temperature of 90°C and 40°C, respectively, as illustrated in Figure 4.4.1-3. The maximum and minimum base plate temperatures of the remainder of the units are presented in Table 4.4.1-2. From these values, it is apparent that the temperatures can be maintained at values sufficiently low to insure reliable operation. Should a unit be operating too cool, the external radiating surfaces or contact interfaces can be adjusted to control temperatures within desirable limits. An illustration of the maximum and minimum temperatures in the base plate of the structure are shown in Figure 4.4.1-4. For reference purposes, it can be noted that the transmitter tube is located in the upper right corner, and the antenna is outside the lower left corner.

In conclusion, it can be stated that the analysis has shown that heat pipes and phase change material are unnecessary to maintain the operating temperatures of the SSAR within desirable limits. Consequently, the cooling scheme is a simple conduction-radiation system in which the temperatures of component units can be controlled by passive means.

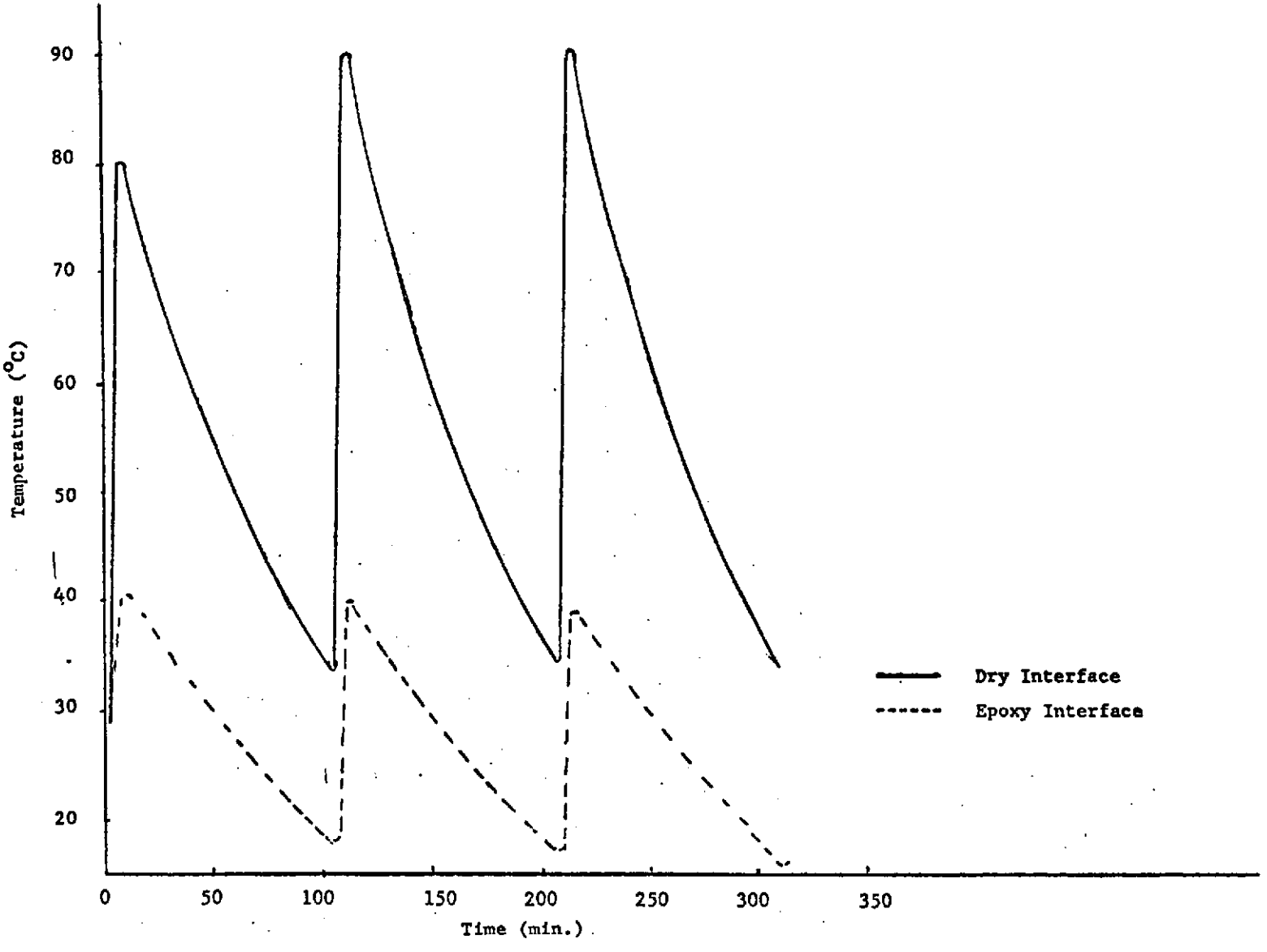

Figure 4.4.1-3. Transmitter Tube Interface Temperature

TABLE 4.4.1-2

MAXIMUM AND MINIMUM BASE PLATE TEMPERATURES OF THE COMPONENT UNITS OF THE SSAR

UNIT	CASE I (DRY INTERFACE) (°C)	CASE II (ABLEFILM 504 INTERFACE) (°C)
TRANSMITTER		
Tube	90/33	40/15
Electronics	23/13	15/4
PC BOARDS & WIRE WIRE BOARD	37/5	12/1
POWER SUPPLIES		
#1	22/15	20/10
#2	22/15	20/10
#3	15/8	10/4
#4	15/8	10/4
PARAMP		
#1	38/12	26/11
#2	33/8	17/5
SHIELDED CHASSIS	26/13	20/9
STALO	26/18	22/12

13.4 4.3	27.3 12.1	37.7 15.0	35.1 13.0
15.3 3.8	21.6 8.5	22.4 10.6	19.0 9.6
9.4 -1.5	12.9 2.9	13.0 4.8	9.8 3.7

This side faces the Earth

Figure 4.4.1-4. Maximum and Minimum Base Plate Temperatures (^{o}C)

4.5 Antenna

4.5.1 General Description

The mechanical design goals established in this study for the two configurations consist of meeting several requirements, namely:

a) lightweight design - to facilitate the launch and orbiting processes,

b) components that did not deform (and thereby degrade performance) under high thermal gradients,

c) and, obviously, a design that would be strong enough to resist the shock and vibration loads encountered in service.

The following description indicates in detail our selection (and reasons) of materials, methods and processes in order to meet the above design goals. In general, the design concept selected for the reflector consists of a honeycomb sandwich structure with graphite epoxy face skins and an aluminum honeycomb core.

The entire sandwich is contoured to form the desired reflective surface. The structural elements of the feed are likewise fabricated with graphite epoxy materials. The numerous advantages offered by this material make it a logical choice for the application under study. The waveguide runs required will be made of aluminum since this is readily available and easily fabricated in the slotting processes involved.

4.5.1.1 Properties of Graphite Composite Structures

Graphite fiber reinforced components and structures have

unique capabilities which can fill specific engineering needs. Data is available from existing hardware programs which demonstrates the high strength properties, fatigue resistance, exceptional vibration damping characteristics, and tailorable coefficient of thermal expansion that these compounds offer. In addition to these properties, the low density offers substantial weight savings compared to a commonly used material as aluminum. A brief summary of the properties of a typical graphite composite laminate is given below as compared to aluminum:

	Graphite Comp.	Aluminum
Tensile Strength	180,000 psi	50,000 psi
Tensile Modulus	20×10^6 psi	10×10^6 psi
Density	0.057 lbs/in.^{3}	0.10/lbs/in.^{3}
Fatigue Strength (Stress at 10^7 Cycles)	120,000 psi	20,000 psi

Additional Properties of Graphite Composites

Coefficient of Thermal

Expansion - (-350°F to 350°F)

Fiber Orientation	x 10^{-6} in./in/°F
0°	- 0.20
90°	12.68
0°, 90°	0.88
± 45°	1.04
± 60°	7.55

(Figure 4.5.1-1 indicates how this coefficient may be tailored by angular orientation of the fibers; such orientation is not required in this design, however.

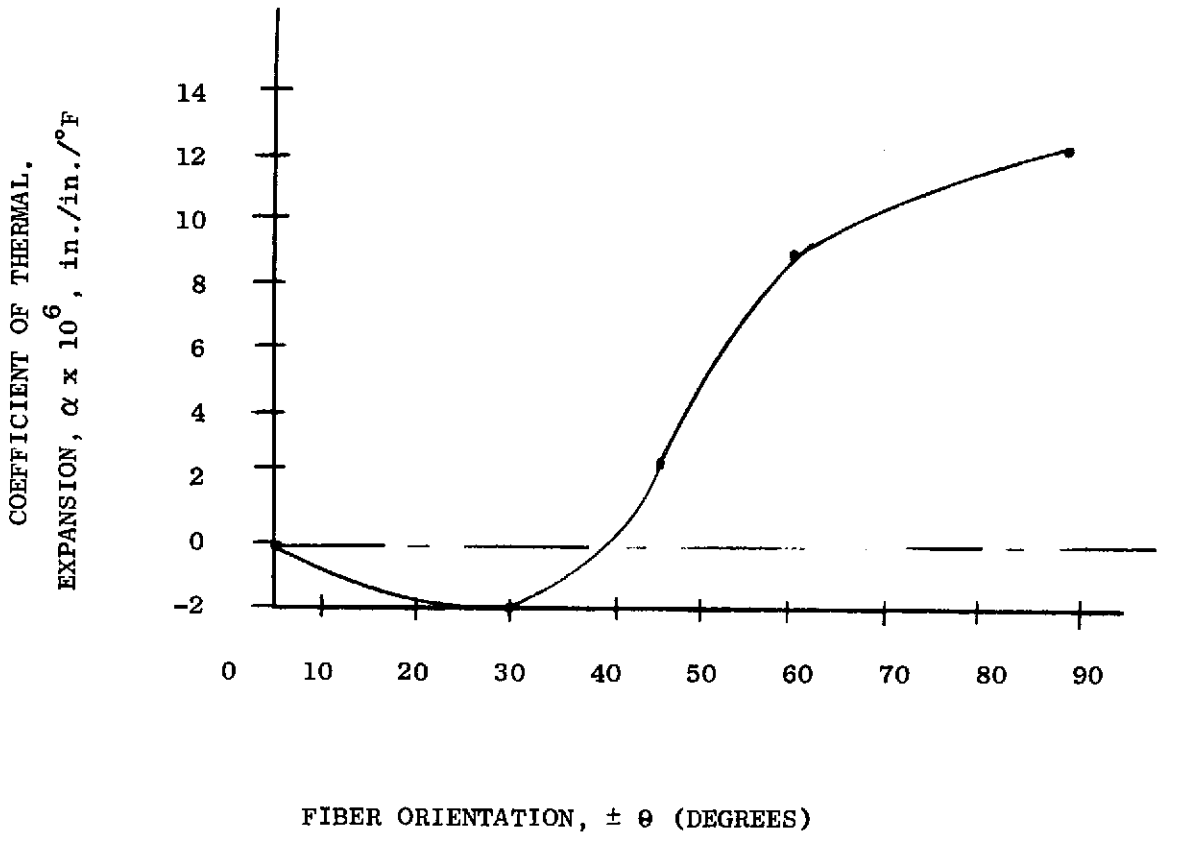

Figure 4.5.1-1. Thermal Expansion Graphite Composite Laminate

Damping Factor 0.016 - 0.032

Thermal Conductivity

One layer - across fiber = 0.40 - 0.50 Btu/hr. Ft. °F

along fiber = 18 - 27 Btu/hr. Ft. °F

Several layers laminate

± 60° orientation 60 Btu/hr. Ft. °F

± 45° orientation 12.0 Btu/hr. Ft. °F

± 30° orientation 17.0 But/hr. Ft. °F

4.5.1.2 Fabrication Methods

Depending on the shape, graphite composite layers are fabricated either by filament winding or hand lay-up processes (similar to fiber glass laminates techniques). The hand lay-up process is generally used since there are only a few geometrical shapes which lend themselves to automated filament winding methods. The hand process involves the use of forms and molds and the various layers of graphite cloth are positioned and impregnated with liquid resin, either epoxy or polyester, and then cured. To achieve a rigid and lightweight unit, as the reflector, this design will use an aluminum honeycomb core material (density of 3.5 lbs/cu. ft.), with facing skins of graphite epoxy .020-inch thick each - total thickness of the panel to be 1/2 inch. The core density is a function of the autoclave pressure required to obtain a good bond with the graphite skins (35 psi) and the limit of 10 to 1 ratio of pressure to core density - resulting in the above mentioned figure of 3.5 lbs/ ft^3. The reflective surface of the antenna is composed of a metal foil .003 thick bonded to one surface.

A detailed weight analysis of the reflector (minus the insulation, reflective foil, paint, etc.) used in Configuration 2 (324 in. long x 30 in. parabola x 1/2 in. thick) fabricated as outlined above is as shown:

Component	Weight
Exterior skins (2-total .04 thick) 38 in. x 324 in. x 0.04 in. x 0.57 $\frac{lbs}{in.^3}$	28.1 Lbs
Honeycomb Core (Alum.) 38 in. x 324 in. x 1/2 in. x 3.5 $\frac{lbs}{ft.^3}$	12.3 Lbs
TOTAL	40.4 LBS

This compares to a weight of 61.7 lbs if this structure were to be fabricated with aluminum skins rather than graphite composite.

4.5.1.3 Antenna Thermal Analysis

The primary thermal problem of a space application is the expansion and contraction resulting from exposure to large temperature extremes (+250°F on the sunlit side and -250°F on the shaded side). To reduce the deformations caused by these forces, it is proposed that the thermal gradient between the two temperature extremes be reduced to a minimum. This will be accomplished by selecting a material such as graphite epoxy which has a negligible coefficient of expansion and incorporating the following features in the design:

a. The side of the reflector opposite the reflecting surface will be covered with a multilayer insulating blanket (3/8 in. thick) having an effective emissivity of .015 to reduce the heat transfer at this surface.

b. The reflecting surface of the assembly will be covered with white paint having a high emmisivity (ϵ = .88) and a low solar absorptivity (α = .20) to reflect most of the energy impinging upon it.

With these conditions, the calculated temperature difference between the two surfaces will be less than 1°. The resulting thermal gradient is of such small magnitude that distortion in the reflector is also small (less than 0.1"). Similarly, the expansion (and/or contraction) in the major dimensions of the reflector (324 in. x 30 in.) resulting from orbital temperature variations yields negligible increments of 0.1 inch and 0.01 inch, respectively. The feed source and its structure will also be designed using the same techniques; and therefore, will not encounter any problems due to excessive thermal deformations.

4.5.1.4 Positioning - Variable Tilt Angle

In order to vary the angular attitude of the reflector with respect to the Earth, it is proposed that the spacecraft be rotated on its longitudinal axis in increments as required. In this manner the reflector and antenna feed, when deployed, are in a fixed angular position with respect to the spacecraft. If it is desirable, an option could be offered that would provide a means of positioning the antenna reflector by moving it in incremental steps through a 20° range of travel with respect to the spacecraft (and the Earth). This would necessarily increase the weight and complexity of the antenna reflector assembly. It is estimated that the extra weight would be 10 pounds in Configuration 1, and 12 pounds in Configuration 2. The design would consist of an electrical motor drive

coupled with mechanical ratchet detents at several positions on the hinge axis. These detents are considered necessary in order to closely control the alignment and positioning angle when increments as small as 0.2° are used.

4.5.1.5 Shock and Vibration Resistance

The basic design concept of the antenna reflector assembly (i.e., a lightweight structure with a high degree of stiffness) readily meets vibration requirements since the small mass and large spring constant yield a natural frequency high enough that any deflections due to random vibrations would involve insignificant amplitude. Similarly, the above mentioned structural properties (light and stiff) will enable the assembly to withstand the launch shock loads without creating excessive stresses.

4.5.1.6 RF Lines at Pivot

In both configurations, the RF lines between the spacecraft and the antenna reflector assembly will consist of a short length of flexible coaxial cable (to allow flexure for stowing and deploying) plus a transition to waveguide at the earliest suitable location toward the feed (in order to reduce the RF losses to a minimum consistent with the mechanical requirements). This arrangement will be used for each of the feeds (which are waveguide) involved.

4.5.1.7 Configuration 1 (Figures 4.5.1-1 and 4.5.1-2)

Weights

The weights of the antenna reflector assembly items are as shown below:

Component	Weight
Reflector	28.9 Lbs
Feed waveguide runs (2)	4.5 Lbs
Feed structure	34.6 Lbs
Hinge and posts	9.3 Lbs
Hardware, cables, etc.	3.7 Lbs
Stowing and deployment parts	11.0 Lbs
TOTAL	92.0 LBS

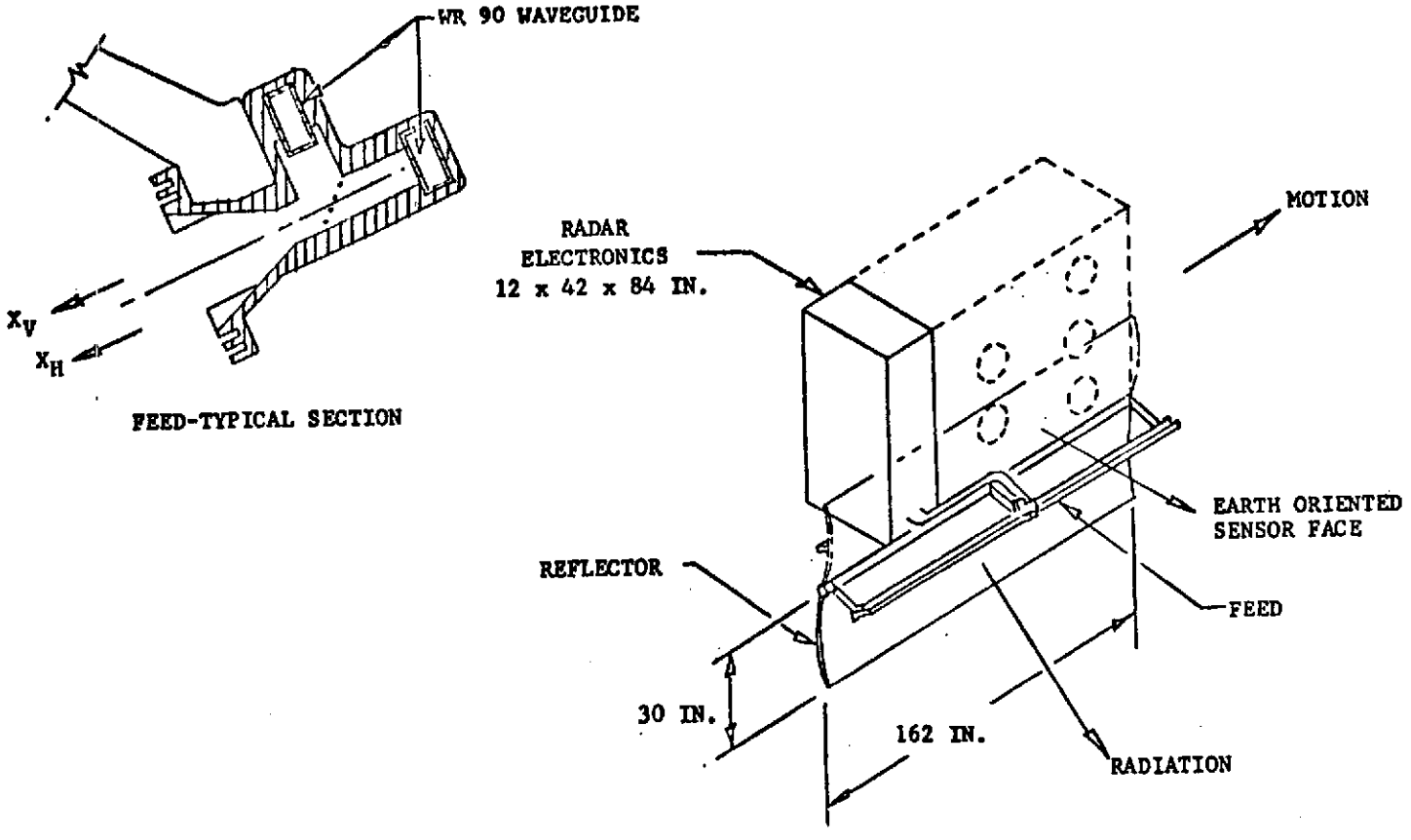

Figure 4.5.1-2a SSAR Antenna Configuration #1

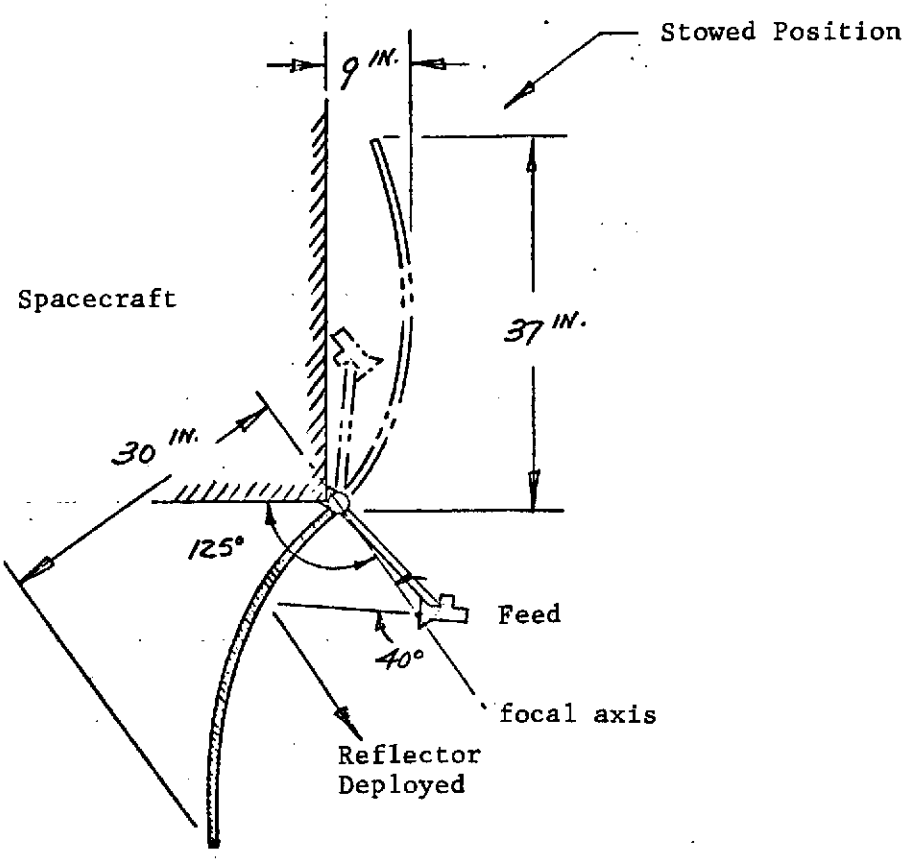

Figure 4.5.1-2b Stowed Dimensions Configuration #1

4.5.1.8 Configuration 2 (Figure 4.5.1-3 and 4.5.1-4)

Weights

The weights of the antenna reflector assembly items are as shown below:

Component	Weight
Reflector	57.8 Lbs
Feed waveguide runs (2)	37.0 Lbs
Feed structure	41.5 Lbs
Hinge and posts	18.5 Lbs
Hardware, cables, etc.	5.2 Lbs
Stowing and deployment parts	14.0 Lbs
TOTAL	174.0 LBS

Note: A second "X" band feed source providing horizontal polarization could be added as an option, and, in that case, would add 33.0 pounds to the above, resulting in a total of 207.0 LBS.

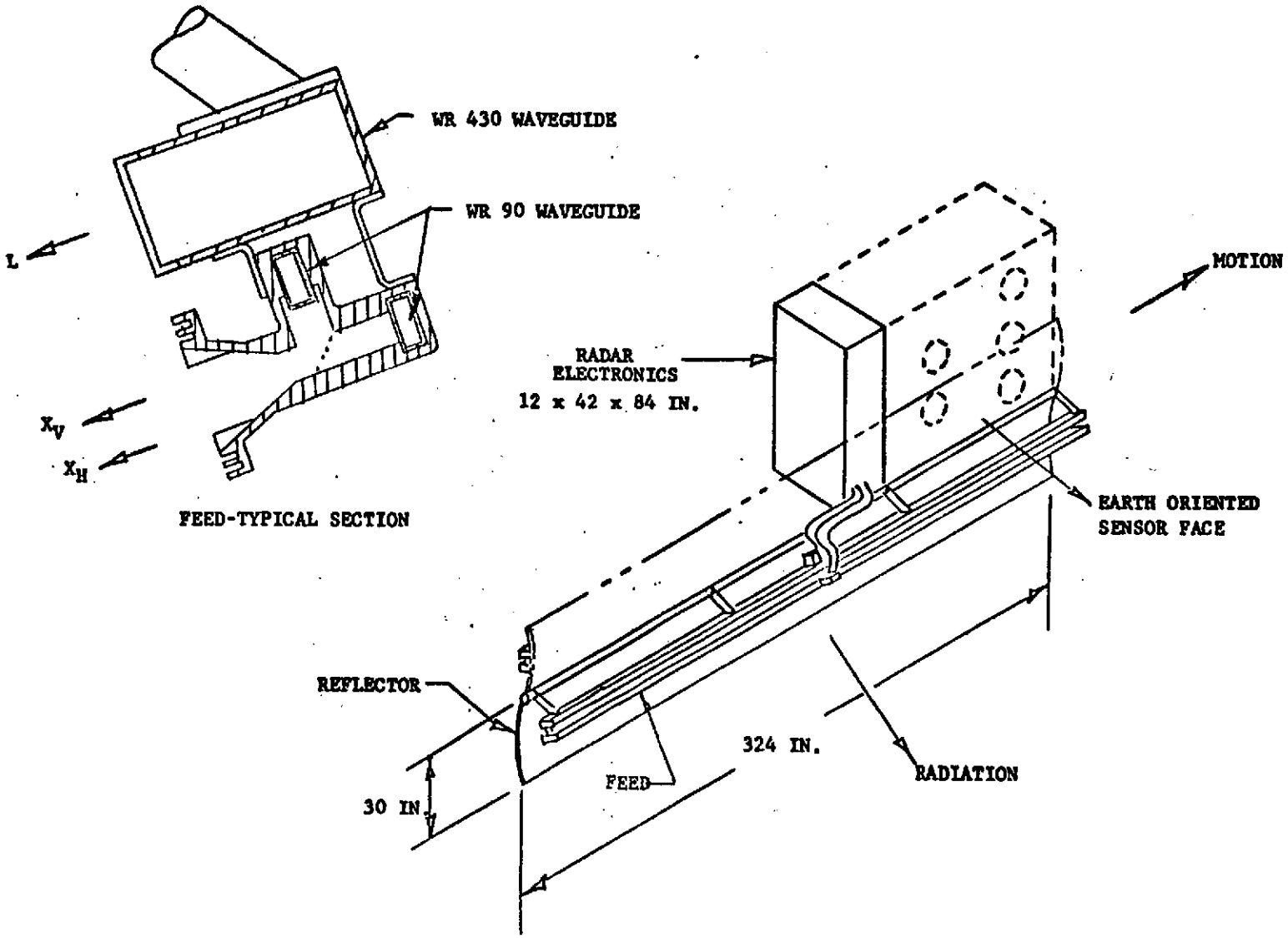

Figure 4.5.1-3a SSAR Antenna Configuration #2

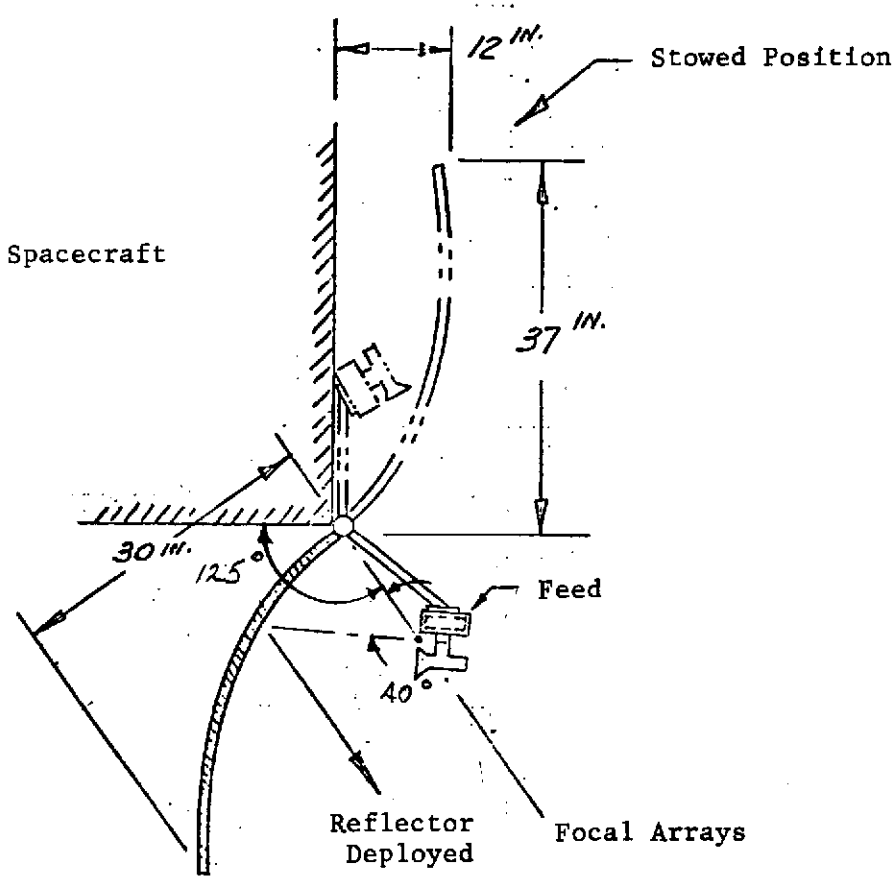

Figure 4.5.1-3b Stowed Dimensions Configuration #2

4.5.2 Spacecraft Connections

4.5.2.1 Hinge (Figure 4.5.2-1)

Based on the stress calculations for 20G loading, Configuration 1 will require at least two hinge posts having .25" thick stainless steel plates. Configuration 2, which requires a larger offset from the spacecraft so the reflector clears the feed in the stowed position, will require three hinges having .375" thick stainless steel. In vibration, more hinges are desirable - but weight, alignment, and equal distribution of the load become more critical.

The design is a simple pinned hinge arrangement with both reflector and feed pivoting about the same point on the same hinge position. A torsional spring is supported between the posts by an aluminum tube and is fixed on one end by the hinge post and by the reflector hinge on the other. The hinge for the reflector is imbedded in the honeycomb and attached with faceplates. The hinge can be covered with the reflector skin as well to give a smoother surface and better bond. Once the tips of the reflector and feed are released by the locking mechanism, the spring acts on the reflector turning it into position. Pins on the reflector and feed engage as the reflector moves around end position, the two relative to each other at the stop position.

4.5.2.2 Locking Device (Figure 4.5.2-2)

The feed array and antenna are secured with a cable looped over a pin in their tips. The cable is severed by one of two guillotine mechanisms. The small additional weight more than

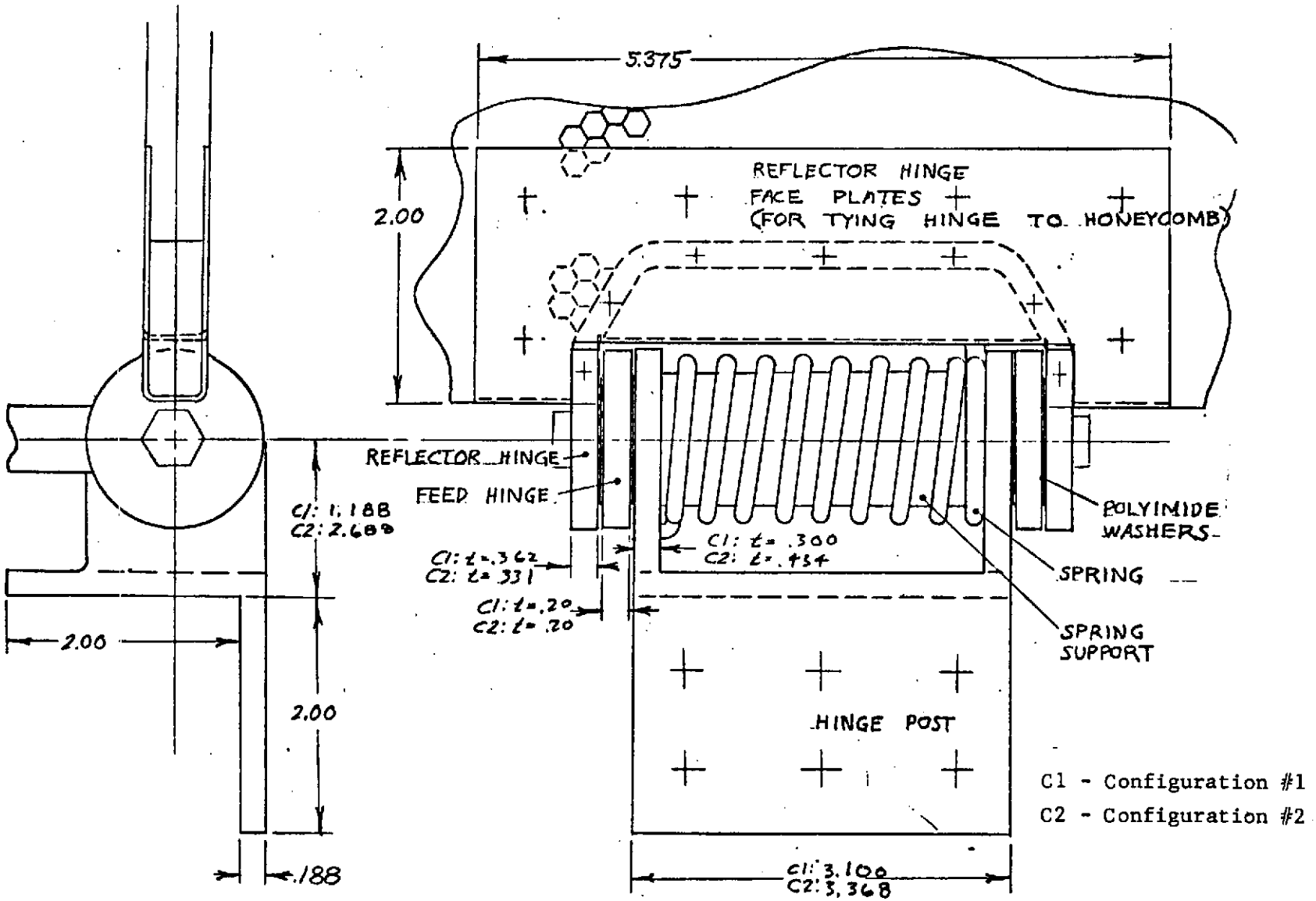

Figure 4.5.2-1. Antenna Hinge

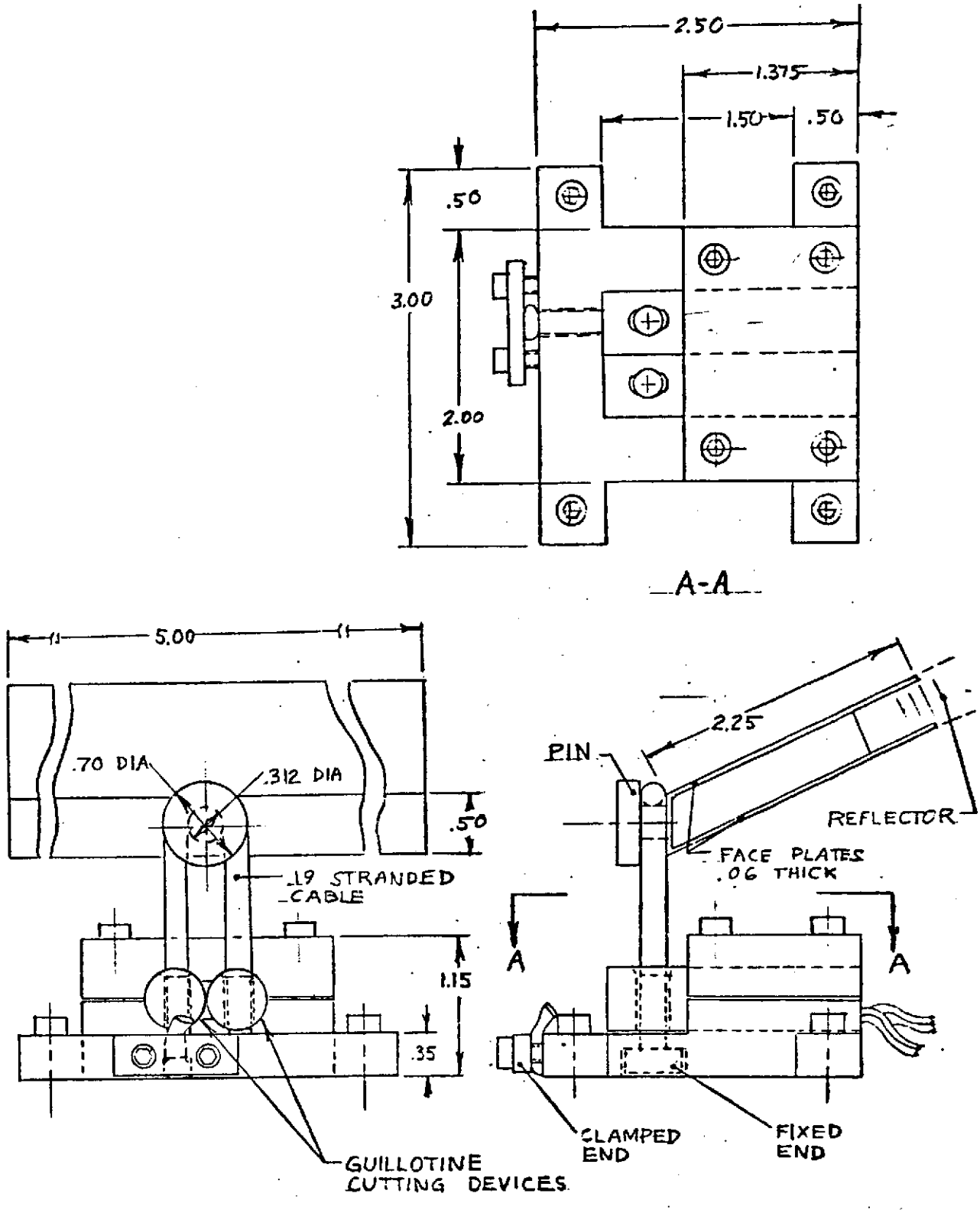

Figure 4.5.2-2. Locking Device

justifies the use of a second device which clearly improves the reliability of deploying the antenna.

4.6 Potential Mechanical Problem Areas

There are two potential problem areas that have been identified in the SSAR mechanical design. These are: (1) the thermal contacts between components and the structure, and (2) the antenna hinge and locking device.

The thermal contacts may be either dry or epoxy. If dry contacts are used, the temperature at the transmitter tube-structure interface reaches 90°C. By using epoxy at this interface, this temperature can be reduced to 40°C. However, use of epoxy reduces the ease with which the tube can be replaced. The approach to this problem will be to determine the minimum tube contact area required for thermal purposes and to design a contact interface which could be separated easily. This task would be accomplished in the detailed design phase. Since dry contact is thermally sufficient for all other components, only the transmitter tube will need the epoxy contact.

The antenna hinge and storage locking device depend on adequate margins in terms of stress, freedom of motion, and driving force. In order to assure reliable operation, it will be necessary to provide for suitable part tolerances. These will influence the fit of hinge parts and determine the resultant dynamic loads. Material and finish selections will determine the friction characteristics and therefore influence the driving force margin of deployment. The geometry of the latch details will also play a

significant role in determining the deployment performances. The approach to providing a satisfactory hinge and deployment system for the antenna will be to determine detailed design specifications for the parts and to perform a kinetic analysis to confirm proper operation.

5.0 GROUND SUPPORT EQUIPMENT RADAR CALIBRATION

5.1 Ground Support Equipment

5.1.1 Introduction

In order to record, store and process the large volume of data transmitted to earth from the sensor, a suitable ground support equipment must be combined into a working system. Data received from the sensor at a maximum rate of 200 Mbits/sec. must be tracked, split into its major components and processed into a final image. A system capable of meeting such requirements is shown in figure 5.1.1-1. Its major components are: a) recording equipment, b) processing equipment, and c) hard copy recorders. Since a short turn around is desired, a two hours per process was selected as reasonable. Tentative feasibility study generated the concepts outlined in the sections that follow.

5.1.2 Overall System Description

The system is divided into two major parts, spaceborne and ground stationed. The airborne equipment is made up of a sensor and a data link. The ground station equipment is made up of receive stations, recorders, library, processor, control computer, film recorder, display and a hard copy processor. The system configuration is outlined in the system block diagram (figure 5.1.1-1) while a working system flow chart is given in Figure 5.1.2-1, and Baseline Design Parameters are in Table 5.1.2-1.

With the aid of these figures the processing chain will be discussed together with its associated key members.

Data is transmitted from the spacecraft via a 200 Mbits/sec. capacity channel. The data contains complex components of two polarization channels as well as additional data such as PRF, I.D. parity check and sync pulses. Therefore for a 50 Km swath, 30m resolution, and 1.25 for

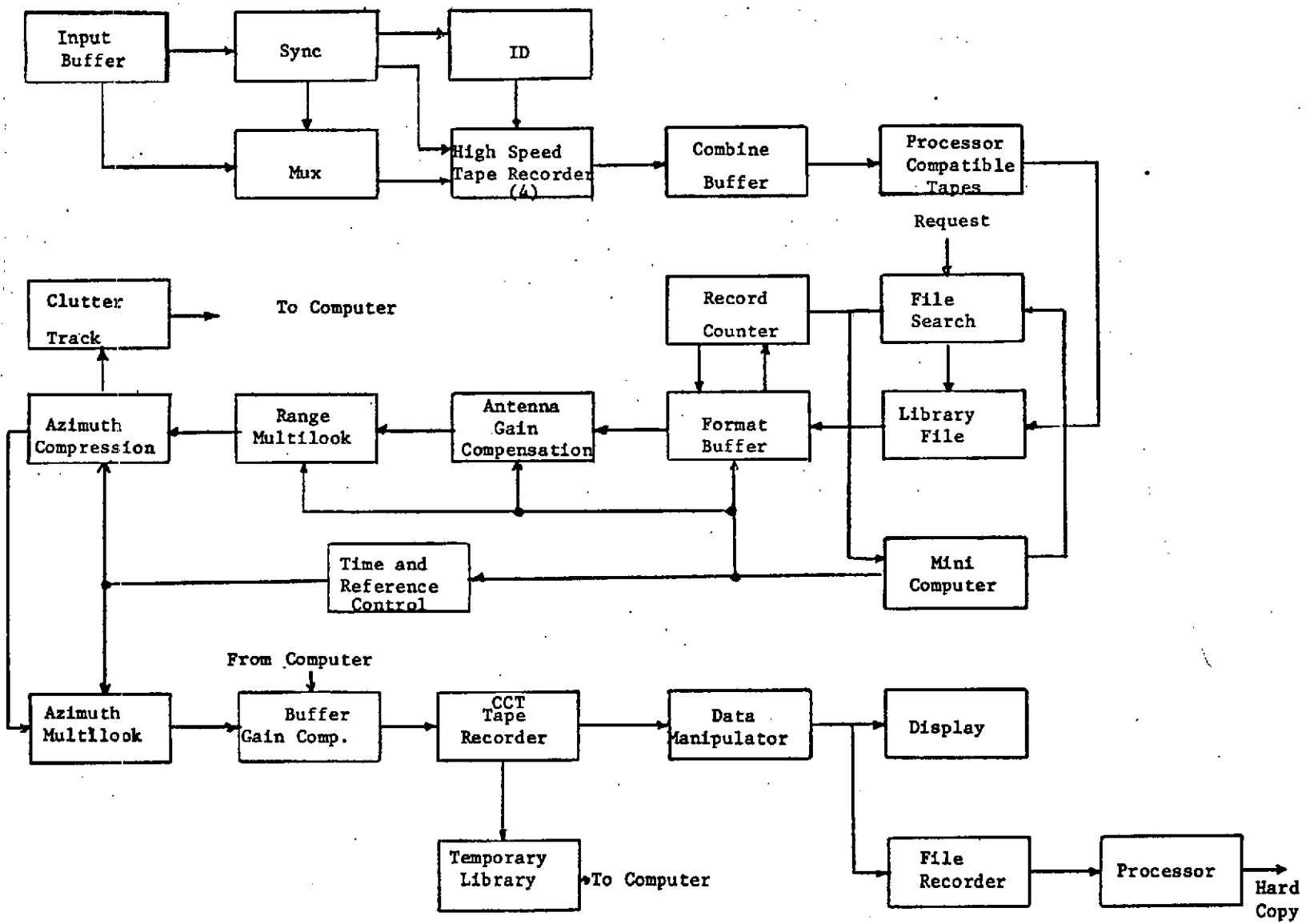

Figure 5.1.1-1. SSAR Processing Block Diagram

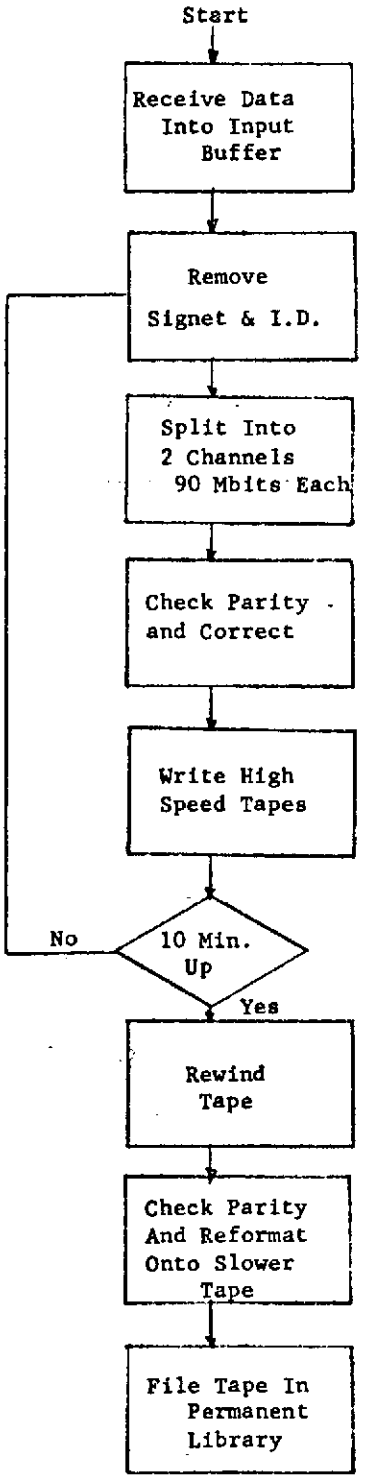

Figure 5.1.2-1(A). SSAR Operational Flow Diagram

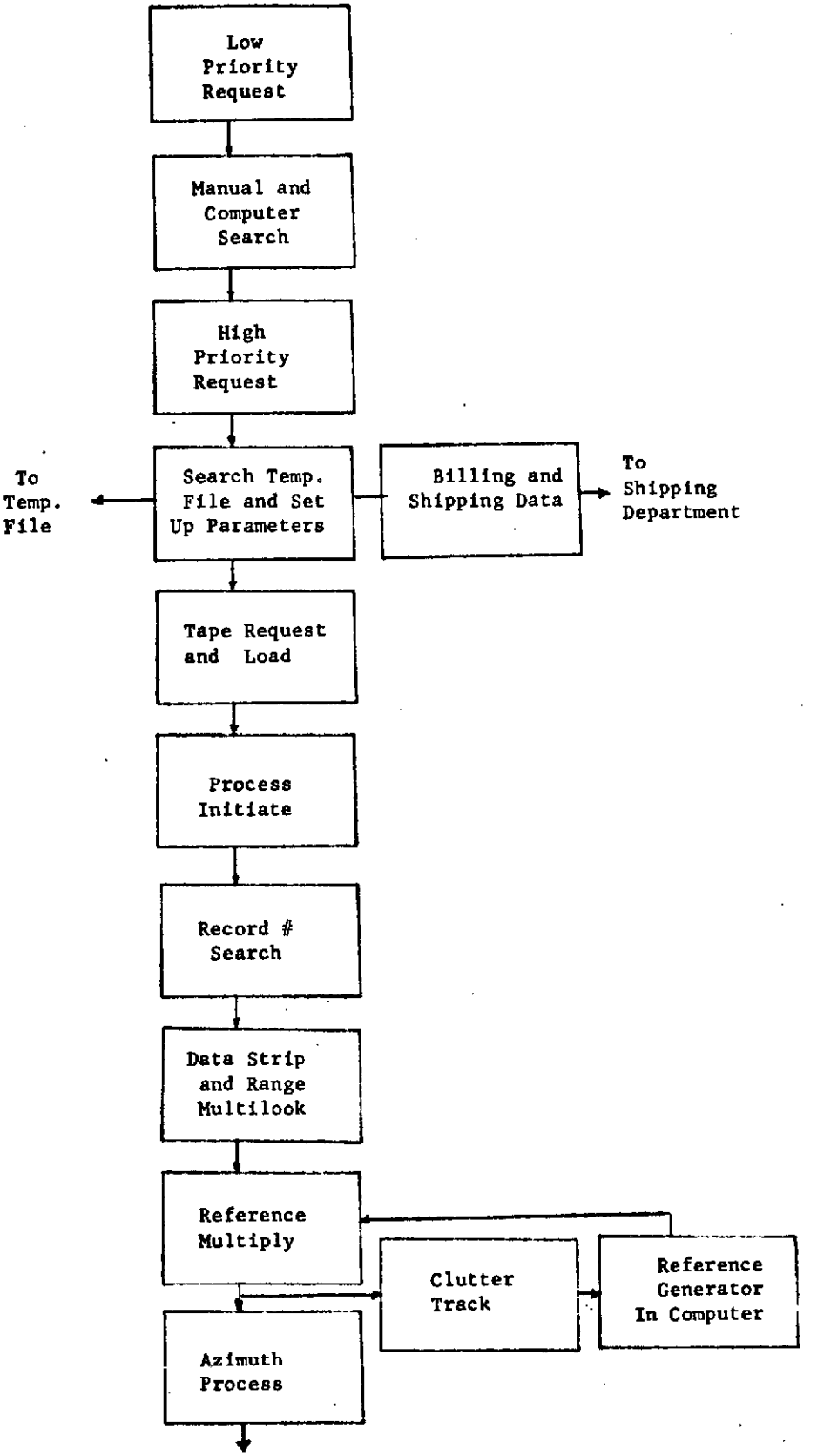

Figure 5.1.2-1(B). SSAR Operational Flow Diagram

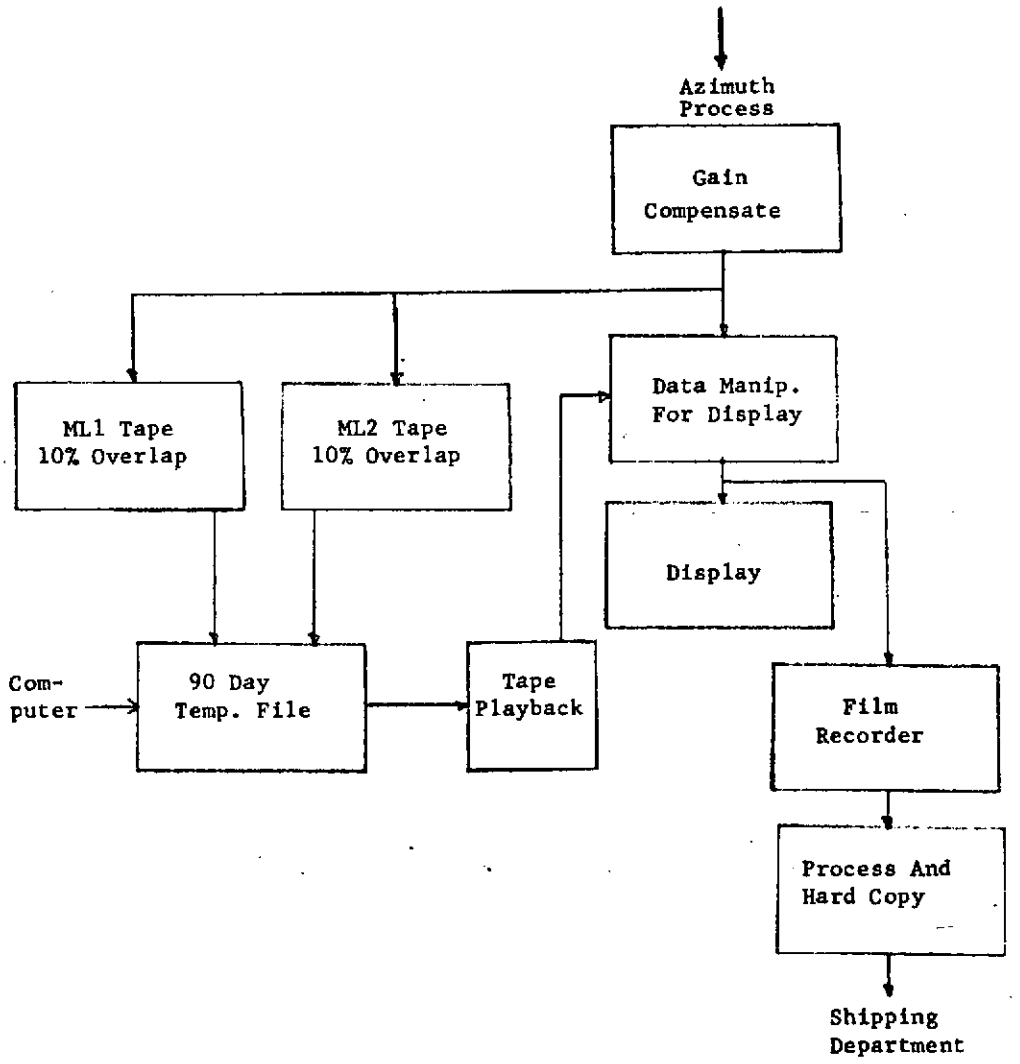

Figure 5.1.2-1(C). SSAR Operational Flow Diagram

Table 5.1.2-1 Baseline Design Parameters

Function	Value X-Band				Value L-Band				Comments
Resolution (m)									
Range	30	60	90	480	30	60	90	480	
Azimuth	30	60	90	480	30	60	90	480	
Coherent Time (ms)	100	47	31	5.8	514	235	157	29.4	
Bandwidth (Hz)	355	165	110	20.6	355	165	110	20.6	
Az Compression Ratio	35.5	16	11	2	182	78	52	10	
No. of Looks									
R	1	2	3	16	1	2	3	16	
Az	1-7	1-15	1-23	1-159	1-5	1-11	1-17	1-95	
Swath Width	50 Km				50 Km				
Depression Angle	60°				75°				
Range Nominal	1082				951 Km				
$\nearrow$	.1 ft.				.576 ft.				
Available Az BW	1420 Hz				1065 Hz				
PRF	4 kHz				3 kHz				
Data Rate	170 Mbits/sec.				130 Mbits/sec				2 channels, each complex
Effective Data Rate for process	1.418 mw/sec.				1.08 mw/sec.				
No. of Range Cells	2084				2084				
A/D Bits	S+4				S+4				
A/D Rate	12.5 MHz				12.5 MHz				
Range Slow down	1.5				2.0				
Process Slow down	12				12				Based on 2 hrs. processing per 10 min. of data

25% over-sample:

$$\frac{50 \times 10^3 \text{ m}}{30 \text{ m}} \times 1.25 = 2084 \text{ range cells}$$

Likewise for an 80 ns A/D rate and 4 kHz PRF one obtains a slow down factor which is utilized in the transmission of data.

$$\text{Slow down ratio} = \frac{1}{80 \text{ ns} \times 2084 \times 4 \times 10^3} = 1.5$$

Thus the data rate is

$$\frac{12.6 \text{ mHz (A/D rate)} \times 2 \text{ channels} \times 2 \text{ complex} \times 5 \text{ bits}}{\text{Slow down ratio} = 1.5} = 167 \text{ Mbits/sec.}$$

with a 3 Mbits safety factor (for ID, sync, etc)

Total data rate = 170 Mbits/sec. complex per two channels.

The reciever on the ground separates the sync and corrects any reasonable errors within each block. Since errors are assumed to be in the $1/10^5$ range, our block of data was made much smaller so as to guarantee the validity of error correction by parity. For convenience a block of data is equivalent to one record which in turn is 2084 data points plus a slight overhead for I.D., etc. The record counter relies on the record I.D. so that it can select record to record processing. Incoming data is then separated into two channels (one per each polarization) tagged properly and recorded on two high speed tape recorders (85 Mbits/sec. each). Since data is collected for 10 minutes every 100 minutes, a slow down factor of 8 can be utilized (allowing some dead time for tape loading). This means that for one polarization channel with a data rate of 85 Mbits/sec. we can slow down to $\frac{85 \text{ Mbits/sec.}}{8(5\text{bits})} = 2.125$ MW/sec. where words are serial complex with parallel bits (bit per track).

This enables the use of a slower tape recorder which can be slowed down further during play back (depending on the processing slow down factor). These processor compatible tapes are stored in a permanent library and upon request drive the processor.

Not shown in the block diagram is the implicit feature enabling the processing of previously recorded and translated data and viewing the result on the display. This makes it possible to correct any data-collecting-orbit within 2 orbits. That is, pending on displayed data quality, the spacecraft can be ordered to switch modes or parameters. Thus 4 high speed tape recorders and 4 PCT (Processor Compatible Tape) units are needed.

Incoming requests are divided into two groups: High priority (HP) and Low priority (LP). The HP request specifies precise data to be processed. Information on the raw data available for a HP request can be obtained from a reference atlas. A LP request specifies general parameters of data to be processed. To fill this request, it may take two steps before processing can occur. HP requests are converted into cards which in turn are entered into the control computer. The computer searches to see if identical request has been processed in the past 90 days and proceeds to execute the request accordingly. That is, if the request is new, it fetches the proper tape from the permanent library and begins to process the data in accordance with the requester's information. The processor tape is read at a speed acceptable to the processor and selected groups of records are passed on for processing. Since 10 minutes of data is processed in two hours, the slow down factor is 12 which means that the PCT must be read at a

speed of $\frac{85 \text{ Mbits}}{12 \times 5}$ = 1.418 MW/sec. complex.

The computer manages the various parameters needed for processing such as clutter cancelling, multilook requirements and gain compensation. Its computational load is light and it must be capable of timesharing.

The processor chain contains antenna gain conpensation over the swath, range multilook, azimuth correlation, clutter track, azimuth multilook, and gain compensation. The correlation and multilook in azimuth may be carried out by way of a two stage FFT or a line per line correlation. For low compression line per line correlation is the choice, yet for highCR the FFT route is preferred. The processed data is then written onto tape (CCT-computer compatible tape) as well as displayed and recorded on film. The data on the CCT can be processed further to compress its dynamic range as desired. If the processed data is to be manipulated in different ways, the CCT are used. If the data is acceptable, a hard copy is made. The CCT is stored in a temporary library for a 90 day period so that it can save reprocessing when and if identical requests are filled. A CCT can be made of simple or multilook azimuth data if line per line correlator is used (parallel recordings) while each channel utilizes multiple recorders with 10% overlap so that the processing is continuous and a mosaic can be made out of it. The display's function is to check data for meaningfulness and to abort processing in the event of some malfunction. Data manipulation as referred to above means the modification of the processed data in some fashion such as log compression, translation, biasing, saturation, etc. That is, the same processed data may be recorded

differently in order to enhance different aspects of the finished picture.

The film recorder, the only high quality means of seeing the processed data, is a key element of the overall system. It is composed of an accurately controlled and compensated CRT, an accurate film drive, optics and servo loops. The unique characteristics of the system can be clearly shown by way of an example (refer to table 5.1.2-2).

It is desirable to determine the writing rate of the CRT, its spot size, the speed of the film, the scale factor and max enlargement. Thus for a system with CR of 36 and Tcoh = .1 sec, we generate 360 lines per second.

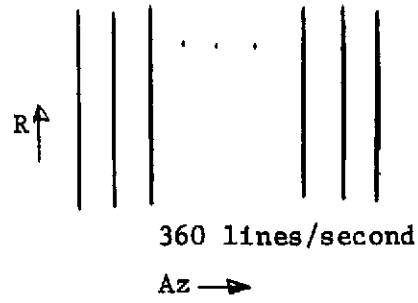

If we select to use 70 mm film, only 60 mm is usable. Therefore, reserve 50 mm for the picture and 10 mm for I.D. or timing marks. The scale factor is (for 50 Km swath)

$$\frac{50 \text{ Km}}{50 \text{ mm}} = 10^6$$

Thus the spot size = $\frac{30\text{m}}{10^6} = 30\,\mu$ (for 30 m resolution).

The film motion is $\frac{360 \text{ lines/sec.} \times 3 \times 10^{-5}}{1.3\ (12)}$ m = .69 mm/sec

Pack Factor; slow down factor

Table 5.1.2-2

Processing - Output Parameters

Description	Data X,L Band	Comments
Tape Recording Density	4800 bytes/inch	
Inter-record Gap	3/4 inch	
Tape Type	9 track	8 bits of data
Tape Read Speed	120 inch/sec,	
Start Stop per Record	2.5 millisec	
Recording Overlap	10%	
Packing Factor in Az	1.3	
Packing Factor in R	1.25	
Film Size	70 mm	
Picture Aperture Utilized in R	50 mm	
Scale Factor-Picture to Ground	10^6	
Spot Size	30 μ	
Film Motion	.69 mm/sec	
Writing Rate	1200 mm/sec	
Records per Reel of Tape	24324	
Tapes Per 10 mm of Data	10	
Film Used by One Tape	560 mm	

With the scan rate or CRT writing rate = $\frac{50 \text{ mm}}{\frac{1}{360} \text{ sec.}} = 1200 \frac{\text{mm}}{\text{sec}}$

(1.25) packing; 12 slow down

With the data generated, how many CCT tapes will be made and what size picture will each tape produce?

Each record (line) consists of 2084 words (range cells) each of 8 bits. Thus for a 9-track tape each record is 2084 bytes long. At 4800 bytes/inch

$$\frac{2084}{4800} \text{ inch/record} + 3/4 \text{ inch/gap} = 1.184 \text{ inch/rec. including inter-record gap.}$$

Therefore a full reel can store $\frac{2400 \text{ feet} \times 12 \text{ inch/ft.}}{1.184} = 24324$ records

In 10 minutes we generate 10 mm x 60 sec/mm x 360 line/sec = 216000 records. With 10% overlap total number of records = 237600.

Therefore $\frac{237600}{24324} = 9.77 \text{ tapes} \approx 10 \text{ tapes}$

Each tape can generate a picture which is

$$\frac{24324 \text{ sec/tape} \times .69 \text{ mm/sec}}{\frac{360}{12} \text{ rec/sec}} = 560 \text{ mm in length}$$

This corresponds to 560 mm x 10^6 x 10^{-3} m/mm = 560 Km on ground. Total distance on gorund is 10 tapes x 560 Km = 5600 Km. This latter figure contains 10% overlap, therefore the net gorund swath is 5040 Km.

Time allocated per tape = $\frac{2 \text{ hrs.} \times 60 \text{ min/hr.} \times 60 \text{ sec./min}}{10 \text{ tapes}} = 720 \frac{\text{sec}}{\text{tape}}$

At 120 inch/sec max tape speed and recalling that start/stop delay of .0025 sec/rec exist we get

$$\frac{[720 - (.0025 \times 24324)] \times 120}{12} = 6591 \text{ feet net}$$

which means that a safety factor of $\frac{6591}{2400} = 2.7$ exists. In other words, the tape speed can be reduced by a factor of 2.7 or multiplexing can be carried out with the aid of a buffer.

A summary of the above calculations is given in table 5.1.2-2.

It should be evident that the end product of the processing may be in the form of a tape, negative, or a print. A special filing system and search hardware will be utilized in order to minimize reprocessing of data. Net turn around time will be kept to a minimum of 2-3 hours per tape.

Combine Buffer and Processor Compatible Tape

Incoming data is recorded serially on the high speed tape recorders. In order to process the data per polarization channel the I and Q have to be separated and all bits must be in parallel, that is words are serial but their bits are in parallel. Each record must be tagged so that the record counter can select (enable) the records of interest. Two tapes are translated simultaneously and the data rate can be slowed by a factor of 8. Four tape recorders are needed to allow for flip-flop operation as well as spot monitoring. The buffer will also attempt to correct errors which resulted in the high speed recorders. This can be achieved by means of blocking and 2-D parity checks. A case in point is

b_1	b_1'	b_1''	p_1'
b_2	b_2'	b_2''	p_2'
b_3	b_3'	b_3''	p_3^1
p_1	p_2	p_3	p_4

where b's are data words and p's are parity bits. If one and only one bit error occurs within the block, the parity on the tape will not match the parity generated when reading the tape. The location "XY" can be found from the P's which are at disagreement (one per row or column), where a bit reversal is carried out. In the event of more than one error per block of data this scheme breaks down.

The processor compatible tape (PCT) is stored in a library file whose retrival relies on key words or run number and the specialized search computer whi h carries it out.

The buffer must have 2084 x 4 x 6 bits (include parity) = 50,016 bits/min. storage to enable the parity check and conversion of data to the PCT.

5.1.3 Data Management

For the given mission some 400 tapes/month will be collected for a period no less than 6 months. This yields a minimum volume of 2400 tapes. Considering all the possible processing combinations it becomes evident that the overall data management task is rather complex.

5.1.3.1 Library Files

Two major files and one minor (dependent) file will be needed in order to process the data in an efficient manner. The major files will be divided into a permanent and temporary. The permanent file will contain the translated data tapes (PCT) all of which will be ordered by run number. More specific information such as date, PRF, polarization, etc. will be part of the header of each tape. This will be known as the run abstract and will be tabulated as part of the run atlas. When request comes up, the tape will be fetched and loaded and the run initiated with the computer overlooking the processing and recording

phases. To expedite runs the mini computer will notify ahead of time the tape number to be processed next so that minimum lost time will occur. The temporary file contains processed data for a 90 day period. If any request is a duplicate of any previously processed data (within the 90 days limit), the hard copy can be fetched from the minor file containing hard copies or negatives of all data previously processed. If the new request is for display manipulation only, then the CCT from the temporary file can be manipulated and recorded.

Storage of the tapes does not seem to pose a real problem since for 2400 tapes each 1" x 14" (1 1/2" x 15" with space) utilizing 7 levels requires a circular room of 7 ft. diameter (minimal requirement). For the 90 day file some 10800 tapes can be stored, however, their size is significantly smaller than the PCT.

The general layout of the library and processing equipment can take the following form. (Figures 5.1.3-1 and 5.1.3-2)

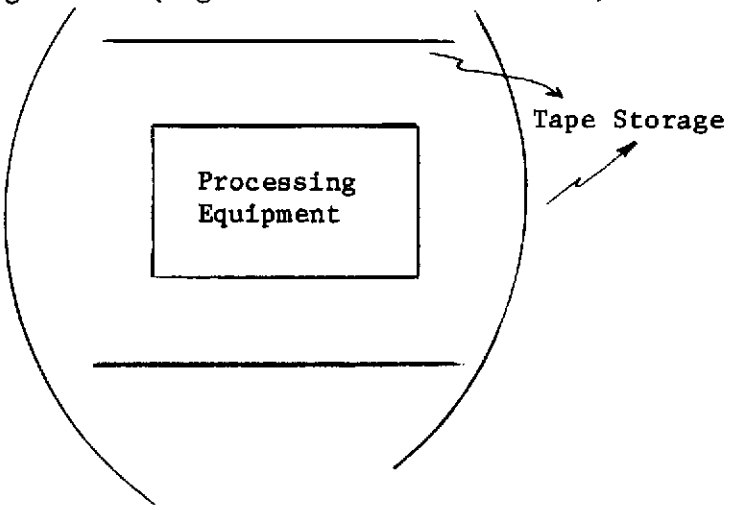

Figure 5.1.3-1. Library Layout

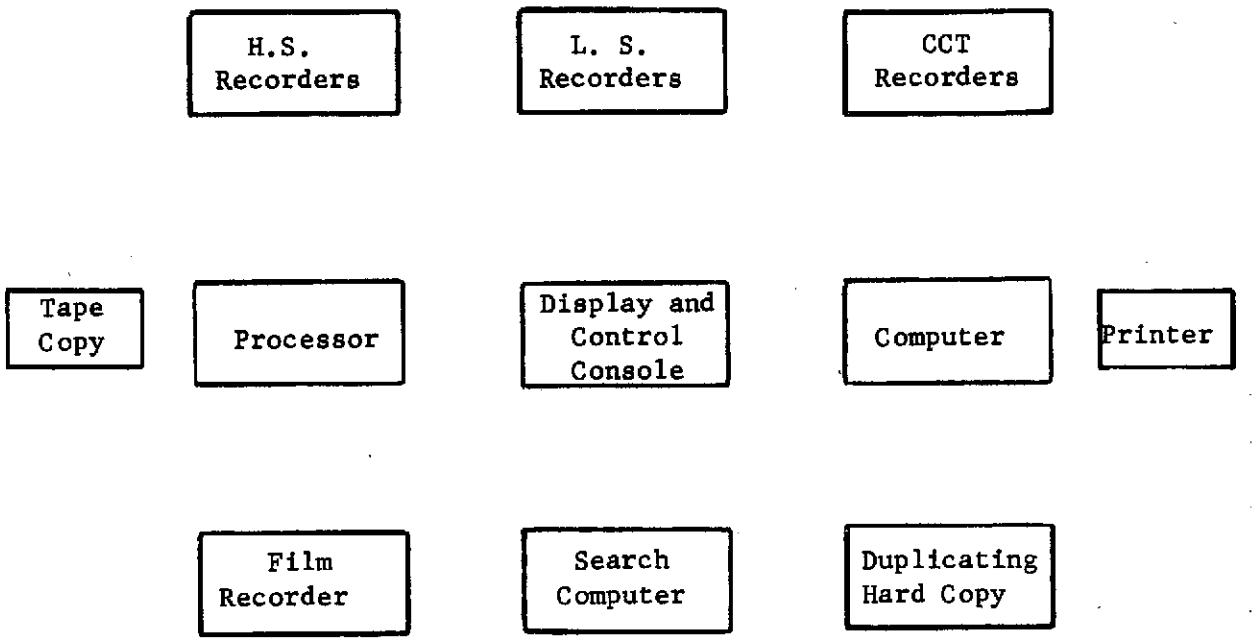

Figure 5.1.3-2. Processing Equipment Layout

5.1.3.2 Reference Atlas

Since requests are divided into two groups, Hi Priority (HP) and Lo Priority (LP), an efficient method for specifying requirements must exist. For HP request minimal paper processing is needed and the fastest turn around time is obtained. The LP request may take two iterations before it is converted into a HP request and its turnaround time is quite long. To enable a requester to generate a HP request a specialized Run Atlas will be put together. The atlas will contain maps showing the geographic locations of each pass as well as weather overlays enabling the requester to pinpoint his area of interest. Thus geographical location, weather conditions as well as more specific dependent data such as record number, PRF, altitude, etc.,

will be readily available. Abstracts by run numbers will specify some of the salient points of each run. In additional cross reference will enable the reader to locate runs by their areas of coverage and terrain type. Order forms (condensed check list) will be supplied with the atlas thus providing the requester with a HP request.

LP requests are based on key words and only general knowledge of the data available. With the aid of a search computer the key words can yield a list of runs. The list of runs and their associated abstracts are then returned to the requester for a final selection which automatically converts the original request into a HP request. An expressed indifference in a LP request will eliminate the need for a second selection by the requester thus shortening the turnaround time.

5.1.3.3 Search Computer

When LP request is processed, a need arises for an efficient technique to retrieve tapes. This can be done by means of key words and a special purpose search computer. Each tape will be classified with the aid of a large set of key words, thus for each keyword one can form an array of documents all of which share the same key words then each will be an array $a_1 \ldots a_n$, $b_1 \ldots b_n$, $d_1 \ldots d_k$, $e_1 \ldots e_j$ where Xi(i = ordering index, X_i = run number) is a particular document number. When a set of key words is used to determine a set of tapes, a level search can be carried out by a specialized search computer. It will scan its memory for all the arrays in question and generate a table of documents with their associated level match. An example may point out the scheme:

given: A = 108, 33, 17, 9, 4

B = 110, 80, 33, 20, 15, 9, 1

C = 109, 70, 33, 16, 3, 1

That is three key words are given and their associated ordered arrays. Select A as reference then 108 is checked against the B & C arrays which yields zero matches. Thus 108 is a level zero match. Next the same process is repeated for 33 and so on until all of the A group is exhausted. The results are tabulated as follows:

Key words = A, B, C

Reference = A

Document #	Level
108	0
33	3
17	0
9	2
4	0

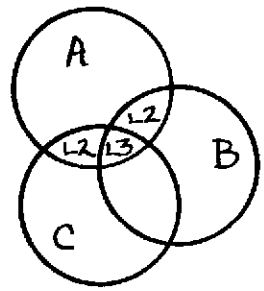

Next discard A and use B as a reference

Key words = B, C

Reference = B

Document #	Level
110	0
80	0
33	2
20	0
15	0
9	0
1	2

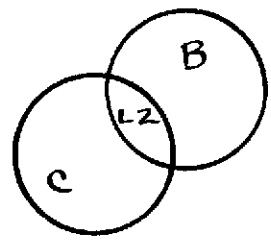

When a perfect match is desired (i.e., level 3 for this example), then only the first iteration is necessary. When lower levels are needed and key words have no priority, multiple iterations are needed (N-1 where N = number of key words). When key words have priority, they should be used as references in decreasing order of importance. Specialized hardware is utilized to compare, index and read the arrays from the memory. Since the sets are ordered, comparison for values smaller than the reference are superfluous, thus decreasing the search time. Also, since the next reference value is smaller than the previous one, all comparisons may start where the last value exited.

Somewhat slower and cheaper techniques may be used to achieve the same goal and that is with the aid of punched cards and visual correlation. Each card corresponds to a unique key word while each hole represents a document (or tape) whose location is the exact run number. Stacking of all the cards, which are in the requester's key word list, and placing it over light indicates immediately the run numbers which match. A lower level would just mean a repetition of the above with card(s) removed but permutated.

5.1.3.3.1 Control Computer

A central computer is an essential part of the overall system. Its functions are not complex but varied and, therefore, it acts as an executive overlooking the various aspects of the processing. Functions such as clutter track, reference generation, parameters and weights generation, accounting/billing, etc. must be handled which means time share-like capability. During the processing, the computer load is light

and therefore it can be shared with needed tasks. A mini computer with expanded memory whould be sufficient for the job, its capabilities will never be taxed.

Accounting/billing is carried out for all jobs entered so that the bill is attached to the end product as it comes out of the processor. Parameters are generated and stored in the computer which in turn loads the processor as it calls for it.

The computer will act as an interface between the operator and all other equipment Communication between operator and machine will be carried out by way of a keyboard/printer.

5.1.3.4 Format Buffer and Record Counter

Data from the PCT is loaded into the format buffer where the ID is stripped off, parity correction is carried out and clock pulses for each IPP are generated. These clock pulses control the record counter which enables the processing throughout the desired region of interest. In order to save time the PCT can be wound to approximately the correct record and then let the record counter do the rest. If only one interrecord region is to be processed, upon completion of the required swath, the record counter will rewind the tape and will terminate the run.

Storage allocation for the buffer is approximately 2084x4x6 = 50016 bits, but the actual number depends on the processing scheme as well as its options.

5.1.3.5 High Speed Tape Recorders

5.1.3.5.1 Requirements

The high speed tape recorders must be capable of recording the 170 Megabit/Second data link from the spacecraft. This data may be split into two independent channels of approximately 85 Mb/sec each. These channels contain radar returns taken at different antenna polarization combinations and will be processed separately. Also included in this recorder data rate are up to 1.5 Mb/sec for identification, parity, 1PP marking bits, and a safety factor.

The recorder bit error rate will be specified as one in 10^5 bits. This rate is reasonable to achieve at these recording rates and also easy to correct with a parity check scheme.

The tape recorder must be capable of recording continuous 85 Mb/sec data for 10 minutes every 103 minutes (each orbit), and playing back that data in about 90 minutes. This time includes approximately 10 minutes for rewinding and remounting tapes. A third, and possibly fourth, machine should be on line and ready to record in case of a breakdown or operator error should threaten the relatively tight time schedule. These extra machines would also serve as backup should one of the prime machines break down. This is an important consideration in light of the requirement to run the recorder almost continuously for 4 to 6 months. (See Table 5.1.3.5-1).

5.1.3.5.2 Proposed Approaches

Two approaches were considered for achieving the 85 Mb/sec record rate. The first, and most straightforward would be to find a machine which could handle this data rate directly. The second

Table 5.1.3.5-1

SSAR INPUT DATA TAPE RECORDER

SPECIFICATIONS

Specification	Value	Comment
Number of Recorders Required	4	2 record, 2 backup
Record Rate	85 Mb/Sec	Each recorder, serial data rate
Bit Error Rate	1 in. 10^5	One error per IPP
Record Time	10 min.	Every 103 minutes
Playback Time	80 min.	Slowdown by 8:1
Playback Rate	10.625 Mb/Sec	Slowdown by 8:1, serial rate

consideration was to synchronize two "lower" data rate machines (~43 Mb/sec each) during record and playback. The latter approach would be no simple task for the two data streams would have to be synchronized bit for bit during playback. Discussion with some major tape recorder manufacturers have confirmed that this approach would require considerable development effort, whereas machines have already been built to record at 85 Mb/sec.

High speed digital recorders may be classed as either transversal or longitudinal, according to how data is written on the tape. The transversal recorder employs a scanning tape head which moves at some angle (up to 90°) with respect to the direction of tape travel thus achieving a much higher effective tape speed and bandwidth. The longitudinal recorder generally employs many tracks across the tape, each parallel to the direction of tape travel. High data rates are accomplished by multiplexing the data onto the multiple tracks, and then recombining upon playback.

Although transverse recording eliminates the track skew problem inherent in the longitudinal approach, data rates in excess of 50 Mb/sec are difficult to achieve. At least one company, on the other hand, has built an 85 Mb/sec longitudinal machine.

The capability of a recorder to handle these data rates is dependent on design paramters such as tape speed, number of tracks, record code selection, required bit error rate, etc. In the next section, a design is proposed which will perform the required job.

5.1.3.5.3 Proposed Solution

A recorder typical of one that would satisfy the requirement

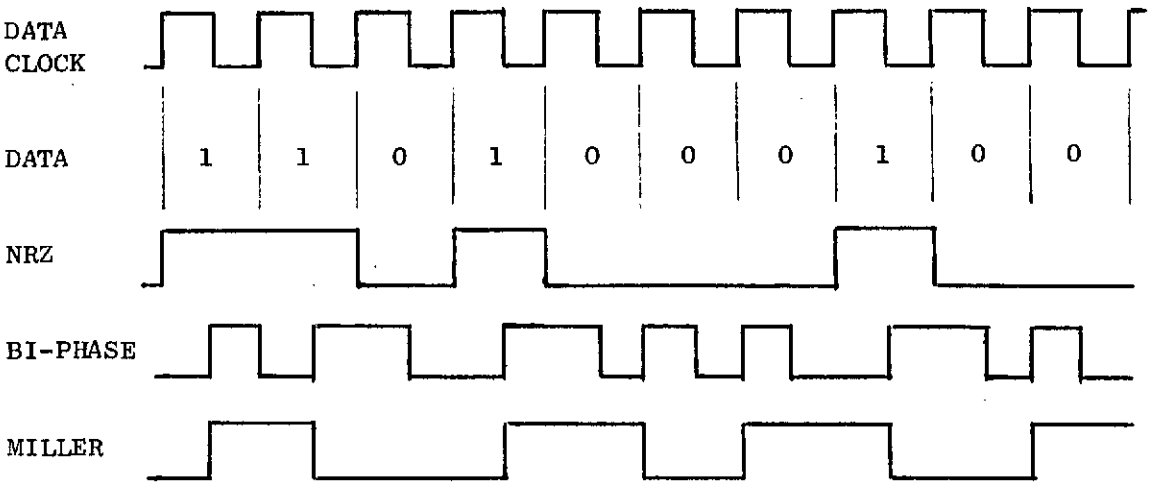

Figure 5.1.3.5-1. Codes for Digital Recording

is specified in Table 5.1.3.5-2. A recorder similar to this one, capable of an 85 Mb/sec data rate, has been built by Ampex and delivered to another customer.

Key to the recorder's performance is selection of the proper form, or code for the digital data. The familiar non-return-to-zero (NRZ) format has a low bandwidth for a given data rate. Generally, a data rate of 1.5 times the analog bandwidth may be accommodated. However, NRZ suffers from baseline shifting for a long string of one's or zero's, since the recorder is AC coupled. It also lacks sufficient transitions for adequate clock recovery unless packing densities are kept under 6000 bits/inch.

Bi-phase (Manchester) coding alleviates the clocking problem by providing transitions every data bit (see Figure 5.1.3.5-1), thus also eliminating the D.C. component from the power spectrum. This requires a wider bandwidth than NRZ, but the self clocking feature allows for higher packing densities on the tape: up to 12,000 bit/inch on each track (at a bit error rate of one in 10^6).

A code which combines the best features of both of the above has been developed by Ampex and designated the Miller, or Delay Modulation Code. A one produces a transition in the middle of a bit period whereas a zero produces a transition at the end of the period, but only if it is followed by another zero. This leads to an adequate number of transitions for reliable self clocking, low D.C. component, and relatively narrow bandwidth. It is claimed that packing densities of 30,000 to 40,000 bit/inch/track can be achieved with this code at an error rate of 5 in. 10^6.

Table 5.1.3.5-2

SSAR INPUT DATA TAPE RECORDER

PROPOSED DESIGN

Parameter	Value	Comment
Tape Speed	120 ips	
Number of Data Tracks	24	Out of 28 total
Bit Density	$\geq$ 30,000 bits/in/track	Using Miller (Ampex) Code
Bit Error Rate	5 in. 10^6	1 in. 10^5 required
Serial Data Rate	$\geq$ 86.5 Mb/sec	Each channel
Tape Width	1"	
Tape Length	8900 ft.	14" reel size
Tape Record Time	11.3 min.	
Tape Capacity	2.16 x 10^9 bits	Bits, entire reel, all 24 tracks

This design proposes to use the Miller code with a 28 track longitudinal recorder (see Table 5.1.3.5-2). Four of the 28 tracks are set aside for internal housekeeping and synchronizing, leaving 24 for recording data. In order to handle 85 Mb/sec, then we need $\frac{85}{24} = 3.54$ Mb/sec per data track. At 30,000 bits/inch, then, we need a tape speed of $\frac{3.54 \times 10^6}{3.00 \times 10^4} = 1.18 \times 10^2$ inches/sec, or 120 ips, as standard speed. In order to provide 10 minutes of minimum record time at that speed required $\frac{(10)(60)(120)}{(12)} = 6000$ feet of tape. We must allow for a leader at each end of the tape plus a safety factor, totaling 30%. Thus, we need (1.3)(6000) = 7800 feet of tape. The next largest standard size reel for this amount of tape is 14", which holds about 8900 feet for 11.3 minutes of effective record time. The total amount of data for a 10 minute run, stored on a tape, is then (24 tks)(6000 ft)(12 in/ft)(30,000 bits/in.) = 5.18×10^{10} bits. (See Figure 5.1.3.5-2).

A machine having the general characteristics of the proposed recorder has been built by Ampex for another customer. It operated at 85 Mb/sec with a bit error rate of better than one in 10^6. Although not an off-the-shelf equipment, such a recorder could be developed for this application within existing technology.

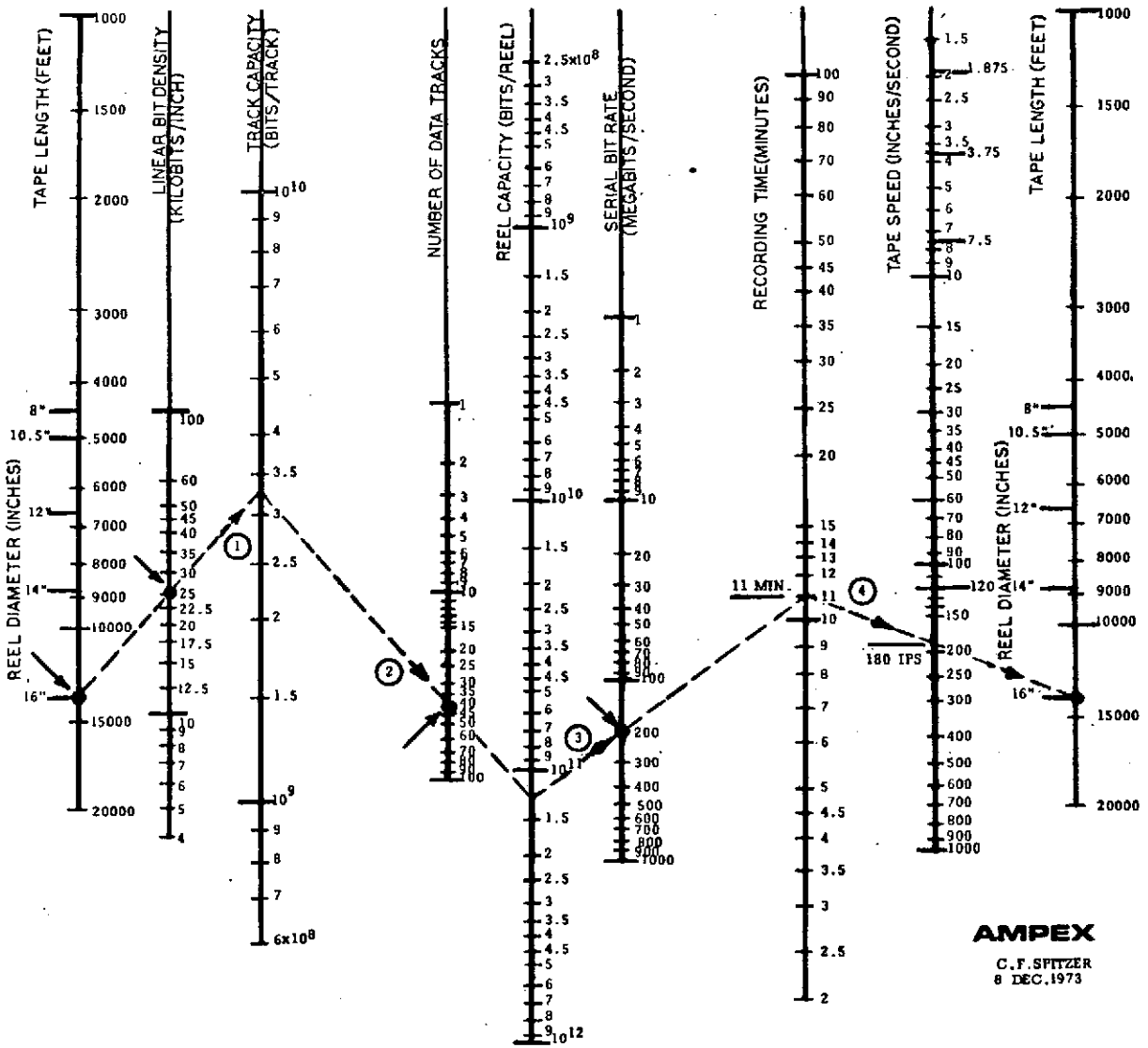

Figure 5.1.3.5-2. Design Chart for Space-Multiplexed PCM Recording

5.1.3.6 Film Recorder and Processing

The film recorder is designed to make a quick, permanent, hard copy of the processed imagery. Its design is well within the present state-of-the-art.

5.1.3.6.1 Requirements

Data from a 10 minute (real time) mapping run is slowed down by a factor of 12 (to 2 hours) during processing, with output data being recorded on tape. Each output tape is limited to 1/9th of the data run, and the film recorder will make a continuous strip of this run. It is desirable to be able to make a continuous strip contact print of this sub-run which will be of a viewable dimension. Also, the recorder must obviously be able to provide the required resolution (30 meters).

5.1.3.6.2 Implementation

Eight and a half-inch (8-1/2 in.) film will be selected for the film recorder. This will provide an 8" wide strip of imagery, which is large enough for easy viewing (of contact prints), and yet the scanning lines will not be visible from normal viewing distances.

The scale factor for imagery on the film is determined by the requirement for sweeping 50 kilometers of range data on 8 inches of the 8.5 inch film. This gives a scale factor of: $\frac{50 \times 10^3 \text{m}}{(8 \text{ in})(2.54 \times 10^{-2} \text{ m/in.})}$ $= 2.46 \times 10^5$. For 30 meter resolution, then the spot size on the film must be: $\frac{30 \text{ m}}{2.46 \times 10^5} = 12.2 \times 10^{-5}$ m = 122 μm. The line spacing in the azimuth direction, then, will be: $\frac{\text{overlap factor}}{\text{Spot size}} = \frac{1.3}{1.22 \times 10^{-4} \text{m}} =$ 1.066×10^4 lines/meter, or 10.7 lines/mm. The overlap factor occurs because processor outputs are oversampled by approximately 1.3 with

respect to a 30 meter resolution cell and should be overlapped accordingly.

The film speed is dictated by the processor output rate, which dumps 33 channels every $\frac{0.1}{12}$ seconds, where 0.1 seconds is the integration time, and 12 the processor slowdown factor. Each dump must be spaced on the film a distance representing $\frac{30}{1.3}$ meters. Thus, the film speed must be: $\left(\frac{\text{line spacing}}{\text{film scale factor}}\right)\left(\text{processor dump rate}\right)$

$$= \left(\frac{30/1.3 \text{ mm/in}}{2.46 \times 10^{5}}\right)\left(\frac{33 \text{ lines}}{(0.1)(12 \text{ sec})}\right)$$

$$= (9.38 \times 10^{-5})\ (2.75 \times 10^{1}) = 2.58 \times 10^{-3}\ \text{m/sec}$$

$$= 2.58\ \text{mm/sec}$$

A second approach to finding the film speed will serve as a check; it must be simply the spacecraft velocity scaled down by the film scale factor and the processor slowdown factor:

Film speed $= \frac{7.6 \times 10^{3}\ \text{m/sec}}{(12)(2.46 \times 10^{5})} = 2.58$ mm/sec, which checks with the first result.

The minimum required writing speed in the range dimension is:

$$\text{Writing speed} = \frac{\text{usable film width}}{\text{time between dumps}} = \frac{(8 \text{ in})(2.54 \text{ cm/in})}{(12/330) \text{ sec}}$$

$$= 5.57 \times 10^{2} = 557 \text{ cm/sec}$$

The recorder must run continuously for one complete output tape, which is 1/9th of a run, approximately 557 km. This requires a length of film of $\frac{557 \times 10^{3}\ \text{m}}{2.46 \times 10^{5}} = 226$ cm, or 89 inches. The time to expose this film is $\frac{(266 \text{ cm})}{0.258 \text{ cm/sec}} = 1030$ sec, or 17.2 minutes.

A recorder having the capabilities of one described above has been built by Westinghouse for use on another program.

Specifications for this recorder are shown in Table 5.1.3.6-1.

Table 5.1.3.6-1

RECORDER SPECIFICATIONS

Parameter	Value	Comment
Scale Factor	2.46×10^5	Range & Azimuth, on film
Spot Size	122 μ m	
Film Speed	2.58 mm/sec	or, 15.5 cm/min.
Writing Speed	557 cm/sec	Does not include reset time
Film Length	226 cm (89") = 557 km of map	For 1/9th of 10 min. pass, + 10% overlap
Line Spacing	10.7 lines/mm	
Run Time	17.2 minutes	For 1/9th of pass = 1 mag tape

5.2 Ground Data Reduction

5.2.1 Introduction

The ground data reduction will be performed by means of a digital signal processor (DSP).

Digital signal processing offers many advantages over optical processing methods; among these are flexibility, in accommodating multiple modes and wide parameter variations, ease of operation, reliability, precise control of processing parameters, adaptability to near real time operation, and built-in tests capabilities. Flexibility and ease of operation are of particular value in the present application since the processing parameters will be varied to satisfy the needs of different users. For example, parameters such as range resolution, azimuth resolution and number of multilooks can easily be varied by merely changing the input data card to the processing system.

The DSP will perform the correlation function to compress the received data in the azimuth dimension. Weighting will be applied to the data to reduce sidelobe levels and also clutter tracking will be provided to remove the doppler offset due to the earth's rotation.

The baseline processor will be capable of processing a 50 Km range swath to range and azimuth resolution elements 30m x 30 m, 60 m x 60 m, 90m x 90 m and 480m x 480m. Under these conditions, the system will provide 1, 2, 3, and 16 range multilooks, respectively. The maximum number of azimuth multilooks will be seven for 30m x 30m resolution cell, fifteen for 60m x 60m cells, twenty-three for the 90m x 90m cells and 159 for the 480m x 480m cells.

5.2.2 Processor Requirements

Both proposed configurations (the X-band system or the dual frequency system) for the SSAR system employ linear FM processing and synthetic aperture techniques to achieve the desired real time processing and azimuth resolution. In both configurations, the processing to form the synthetic aperture will be done on the ground by means of a digital signal processor (DSP). The requirements for both systems are listed in Table 5.2.2-1 below.

Table 5.2.2-1 Baseline System Requirements

Parameters	X-Band (System I)	L-Band (System II)
Swath Width	50 km	50 km
Depression Angle	60°	75° nominal
Range (nominal)	1082 km	951 km
Transmitted Wavelength	0.1 ft.	0.576 ft.
Resolution		
Range	30 60 90 480 meters	30 60 90 480 meters
Azimuth	30 60 90 480 meters	30 60 90 480 meters
Available Azimuth Bandwidth	1420 Hz	1065 Hz
PRF	~4 KHz	~3 KHz
Data Rate	170 megabits/sec	130 megabits/sec

These system requirements lead to the baseline processor parameter listed in Table 5.2.1-2.

The processor design described assumes a time slow down of 12. Therefore, 10 minutes of raw data collected during one pass over the continental United States will be processed in two hours, which is the approximate time for one satellite orbit.

Table 5.2.2-2 Baseline Processor Parameters

Parameter	X-Band System				L-Band System			
No. of Range Cells	2084				2084			
Coherent Integration Time	100	47	31	5.8 msec	514	235	157	29.4 msec
Bandwidth/Az. Look	355	165	110	20.6 Hz	355	165	110	20.6 Hz
Azimuth Compression Ratio	35.5	16	11	2	182	78	52	10
No. of Looks								
Range	1	2	3	16	1	2	3	16
Azimuth	1-7	1-15	1-23	1-159	1-5	1-11	1-17	1-95
Input Data Rate	1.42 mW/sec.				1.08 mW/sec.			

5.2.3 Basic SAR Principles

Synthetic aperture radar achieves its high resolution by coherently processing ground returns over a relatively long time. The amplitude and phase of each ground return and measured and stored as the radar platform moves through space. At any instant of time, returns from targets at different azimuth positions have different doppler frequencies. The return from each azimuth target has a distinct time-phase history. The matched phase history required to combine the returns for a target at any given azimuth position can be computed from known parameters.

Table 5.2.3-1 lists the basic equations required to determine processor parameters such as integration time, synthetic-aperture length, and time-bandwidth requirements to achieve a given resolution from the known parameters.

5.2.3.1 Doppler Frequency Spread

The doppler frequency relation results from the relative motion

between the radar antenna and the ground target. In general, the doppler frequency is given by

$$fd = \frac{v}{\lambda}$$

where v = relative velocity between radar antenna and target

and λ = the RF wavelength

The instantaneous doppler frequency is therefore a function of angle, α, between the velocity vector and the line of sight to the target and is given by

$$fd = \frac{2v}{\lambda} \cos \alpha$$

where v = spacecraft velocity

The variation of doppler frequencies across the synthetic array length, L, is of interest because it is a factor in the selection of PRF, and dictates the filter bandwidths required to achieve the desired azimuth resolution.

Consider figure 5.2.3-1, in which

v = spacecraft velocity

h = radar platform altitude

B_H = antenna beamwidth

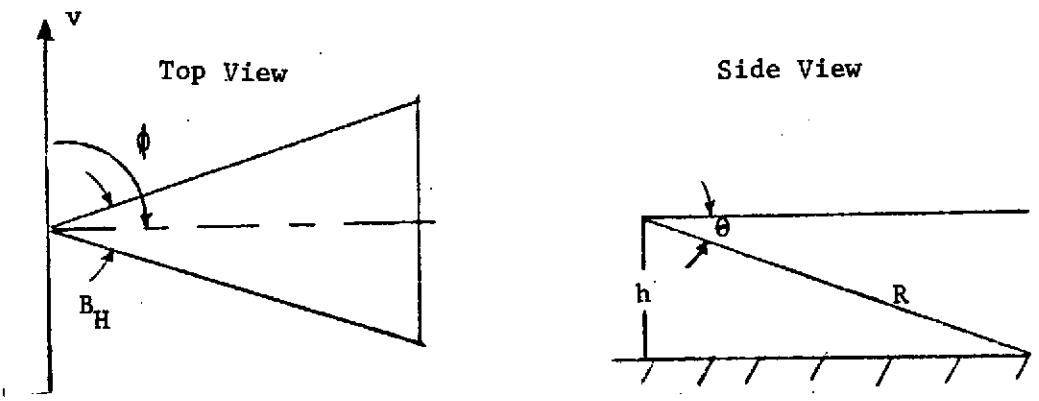

Figure 5.2.3-1. Doppler Frequency Spread Geometry

The doppler frequencies at 1 and 2 are:

$$f_{d_1} = \frac{2V}{\lambda}\cos\left(\phi - \frac{B_H}{2}\right)\cos\theta = \frac{2V}{\lambda}\cos\theta\left[\cos\phi\cos\frac{B_H}{2} + \sin\phi\sin\frac{B_H}{2}\right]$$

$$f_{d_2} = \frac{2V}{\lambda}\cos\left(\phi + \frac{B_H}{2}\right)\cos\theta = \frac{2V}{\lambda}\cos\theta\left[\cos\phi\cos\frac{B_H}{2} - \sin\phi\sin\frac{B_H}{2}\right]$$

The doppler spread across the beamwidth is the difference between these two values or

$$\Delta fd = fd_1 - fd_2 = \frac{2v}{\lambda}\cos\theta\left[2\sin\phi\sin\frac{\beta_H}{2}\right]$$

Since B_H is small,

$$\sin\frac{B_H}{2} \approx \frac{B_H}{2}$$

and

$$\Delta f_d \approx \frac{2V}{\lambda} B_H \sin\phi\cos\theta$$

Table 5.2.3-1 Basic SAR Equations for Sidelooking Radar

Parameter	Equation
Doppler Frequency	$fd = \frac{2v}{\lambda}$
Doppler Frequency Spread	$\Delta fd = \frac{2v}{\lambda}\beta_H$
Doppler FM Slope	$\dot{f}d = \frac{2V^2}{R\lambda}$
Coherent Integration Time	$Tc = \frac{Ks\ R\lambda}{2v\ ra}$
Synthetic Array Length	$L = \frac{K\ R\lambda}{2\ ra}$
Time-Bandwidth Product	$TBW = \frac{Ks^2\ R\lambda}{2\ ra^2}$

Also, since

$$\sin\theta = h/R \text{ and } \cos\theta = \sqrt{1-\left(\frac{h}{R}\right)^2} \approx 1 - 1/2\left(\frac{h}{R}\right)^2$$

Therefore,

$$\Delta fd \approx \frac{2v\beta_H}{\lambda}\left[1 - 1/2\left(\frac{h}{R}\right)^2\right]\sin\phi$$

Expressed in terms of α ,

$$\Delta fd \approx \frac{2v}{\lambda} \beta_\alpha \sin \alpha$$

where β_γ in the beamwidth in the plane formed by the velocity vector and the line of sight to the target. For a sidelooking system, Δfd can be written as

$$\Delta fd \approx \frac{2v}{\lambda} \beta_H$$

5.2.3.2 Doppler FM Slope

The parametric relationships involving resolution are developed in terms of doppler spread, Δfd, and doppler frequency with respect to time, $\dot{fd}$. The doppler spread provides the basis for target azimuth resolution and the doppler slope describes the phase shift that must be applied over the coherent integration time to focus the synthetic aperture.

Correlation, which is used for extracting the information from the input data, involves the implementation of phase shift to match the phase change of the data over the coherent integration time. The instantaneous doppler and FM are directly proportional to range rate (velocity) and range acceleration, respectively, i.e.,

$$fd = \frac{-2\dot{R}}{\lambda}$$

and

$$\dot{fd} = \frac{-2\ddot{R}}{\lambda}$$

These quantities can be related to inertial quantities or flight parameters as can be seen from Figure 5.2.3-2. In general, a plane is formed by the triangle YXR. X is the component of the distance from the antenna center to the target in the direction of the velocity

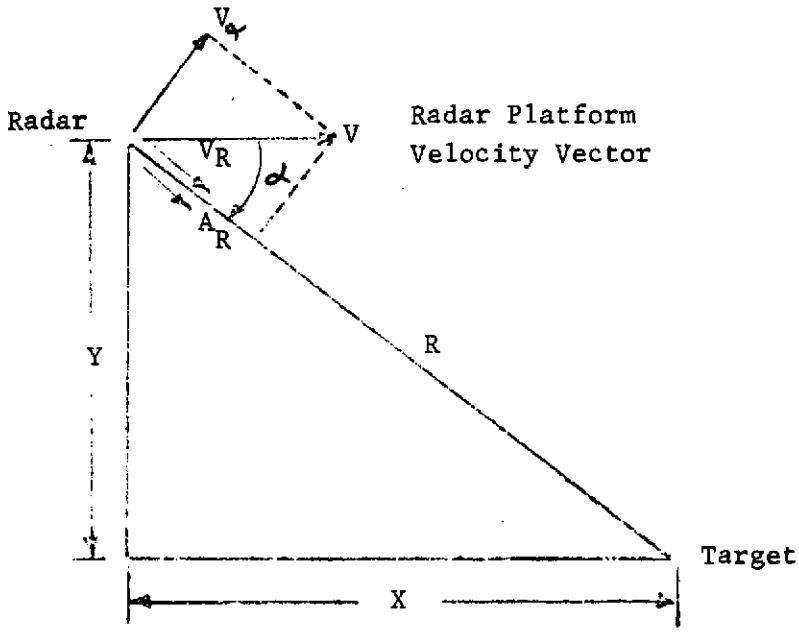

Figure 5.2.3-2. Geometry From Which Doppler Frequency and FM Slope are Calculated

vector. Y is the distance from antenna center to the X plane (on which the target is situated), i.e., orthogonal to X, while R is the distance from the antenna center to the target located anywhere along the X-axis. From geometry, the following relationship is derived:

$$R^2 = X^2 + Y^2$$

Taking the time derivative of both sides of the equation yields

$$R\dot{R} = X\dot{X} + Y\dot{Y}$$

Note, however, that $\dot{Y} = 0$, since V and X are parallel and the plane is assumed to be flying in a straight path. Therefore,

$$\dot{R} = \frac{X\dot{X}}{R} = -V \cos \alpha = -V_R$$

where V = spacecraft velocity

V_R = component of spacecraft velocity along the line of sight to the target

α = angle between the velocity vector and the line of sight to the target.

Then

$$f_d = \frac{2V}{\lambda} \cos \alpha = \frac{2V_R}{\lambda}$$

An additional differentiation with respect to time of the previous equation yields

$$\dot{R}^2 + R\ddot{R} = \dot{X}^2 + X\ddot{X} + \dot{Y}^2 + Y\ddot{Y}$$

$$\ddot{R} = \frac{\dot{X}^2 - \dot{R}^2}{R} + \frac{X\ddot{X}}{R} + \frac{Y\ddot{Y}}{R} \; ; \; \dot{Y} = 0$$

$$= \frac{V^2 (1 - \cos^2 \alpha)}{R} + \ddot{X} \cos \alpha + \ddot{Y} \sin \alpha$$

$$= \frac{V^2 \sin^2 \alpha}{R} + \ddot{X} \cos \alpha + \ddot{Y} \sin \alpha$$

or $$\ddot{R} = \frac{V_\alpha^2}{R} - a_r ,$$

where $V_\alpha = V \sin \alpha$ = spacecraft velocity component perpendicular to line of sight

a_r = component of acceleration along the line of sight

Thus, the doppler FM slope is

$$\dot{f}d = \frac{-2}{\lambda} \left[\frac{v_a^2}{R} - a_r \right]$$

For constant velocity and a side-looking radar,

$$\dot{f}d = \frac{-2v^2}{\lambda R}$$

5.2.3.3 Coherent Integration Time

Various methods exist for calculating resolution and coherent integration (processing) time for a synthetic-array radar. The correlation technique is used here to develop the desired relationship.

Correlation is achieved by proper comparison of the input signal with a reference signal over a narrow doppler frequency band. Let f_{do} be the doppler frequency from a target at a reference angle α_o. Targets removed in angle by $\Delta\alpha$ from this position are displaced in frequency by

$$\Delta f_d = f_d - f_{do} = \frac{2V}{\lambda}\left(\cos\alpha - \cos\alpha_o\right) \approx \frac{2V}{\lambda}\sin\alpha_o\,\Delta\alpha$$

and will not correlate if $\Delta\alpha$ is sufficiently large (i.e., if Δf_d is greater than the correlation filter bandwidth).

Referring to Figure 5.2.3-3, the resolution of the SAR will be calculated. From Figure 5.2.3-3

$$(R + s)^2 = R^2 + y^2$$

$$R^2 + 2sR + s^2 = R^2 + y^2$$

For $s << R$

$$s \approx \frac{y^2}{2R} = \frac{V^2t^2}{2R} \equiv R(y)$$

Let $S(y)$ = voltage output of synthetic array

and $W(y)$ = antenna array amplitude weighting function

Then

$$S(y) = W(y)\,e^{\frac{j4\pi R(y)}{\lambda}}$$

Let

$$r(y + y') = e^{-j\frac{4\pi}{2R\lambda}(y + y')^2}$$

be a correlation reference function that is matched to $S(y)$. Also let 2ℓ be the array length projection normal to the line of sight, or

$$\ell = \frac{L}{2}\sin\alpha$$

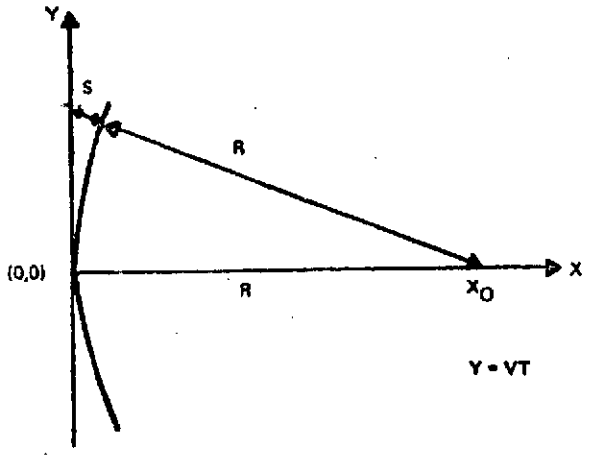

A. Phase Geometry

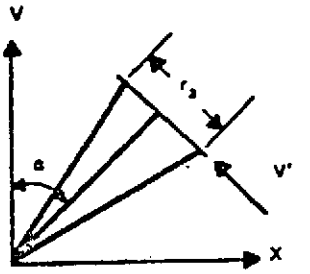

B. Top-View Geometry

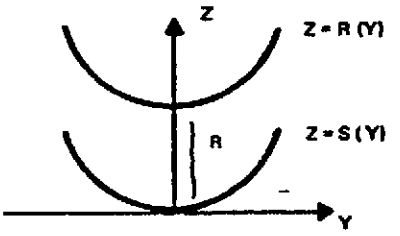

C. Phase Variation Along Flight Path

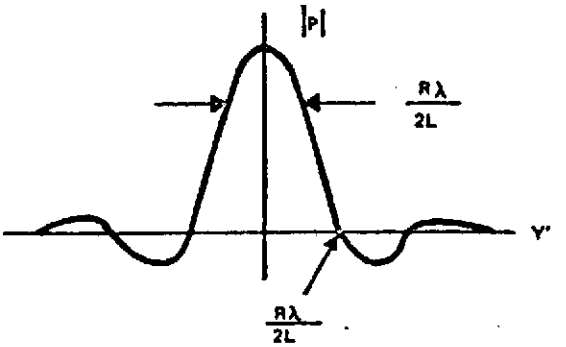

D. Correlator Output

Figure 5.2.3-3. SAR Geometrics

where L = integration distance or array length. Then the output of the correlator,

$$\rho(y') = \int_{-\ell}^{\ell} S(y)\, r(y + y')\, dy$$

$$\rho(y') = \int_{-\ell}^{\ell} W(y)\, e^{j\frac{4\pi y^2}{2R\lambda}}\, e^{-j\frac{4\pi}{2R\lambda}(y + y')^2}\, dy$$

$$\rho(y') = \int_{-\ell}^{\ell} W(y)\, e^{-j\frac{2\pi}{R\lambda}(2y\,y' + y'^2)}\, dy$$

Let $\xi = e^{-j\frac{2\pi}{R\lambda}y'^2}$

$$\rho(y') = \xi \int_{-\ell}^{\ell} W(y)\, e^{-j\frac{2\pi}{R\lambda}(2y\,y')}\, dy$$

Consider a uniformly weighted aperture where

$$W(y) = \begin{cases} W_1, & |y| < \ell \\ 0, & |y| > \ell \end{cases}$$

Then the correlation function can be written as

$$\rho(y') = W_1\, \xi \int_{-\ell}^{\ell} e^{-j\,2\pi\left(\frac{2y'}{R\lambda}\right)y}\, dy$$

But this is the Fourier transform of a pulse, or

$$\rho(y') = W_1\, \xi\, \frac{2\ell \sin 2\pi\left(\frac{2\ell y'}{R\lambda}\right)}{2\pi\left(\frac{2\ell y'}{R\lambda}\right)}$$

$$\left|\rho(y')\right| = W_1\, \frac{2\ell \sin 2\pi\left(\frac{2\ell}{R\lambda}\right)y'}{2\pi\left(\frac{2\ell}{R\lambda}\right)y'}$$

This correlation function has its first null at $y' = \frac{R\lambda}{4\ell}$ (see Figure 5.2.3-3). The resolution cell size is taken as

$$r_a = \Delta y' = \frac{R\lambda}{4\ell} = \frac{R\lambda}{2L \sin \alpha}$$

But, $L = VT_c$, where T_c = dwell or integration time

V = spacecraft velocity

Then, for a uniformly weighted aperture, the resolution normal to the line of sight

$$r_a = \frac{R\lambda}{2VT_c \sin \alpha}$$

For the more general case in which the aperture weighting is non-uniform to reduce sidelobe levels, the integration time must be increased by the factor K_s to compensate for spreading of the resolution function, which is caused by the aperture weighting. Therefore, the coherent integration time,

$$T_c = \frac{K_s R\lambda}{2 r_a V \sin \alpha}$$

For a sidelooking radar,

$$Tc = \frac{K_s R \lambda}{2 r_{\alpha} v}$$

where $K_s = 1.4$ in the present application.

5.2.3.4 Synthetic Array Length

The synthetic array length is given by

$$L = vTc = \frac{K_s R \lambda}{2 r_a \sin \alpha}$$

For a sidelooking radar, this becomes

$$L = \frac{K_s R \lambda}{2 r_{\alpha}}$$

5.2.3.5 Time-Bandwidth Product

Another fundamental quantity is the time-bandwidth product, which defines correlation storage requirements. Since the minimum complex sampling rate required to reconstruct a bandlimited signal with bandwidth β is β samples per second, the minimum number of complex samples over a coherent integration time is

$$
\begin{aligned}
Mp &= Tc \ \Delta fd \\
&= \frac{K_s R}{r_\alpha} \beta_H \\
&= \frac{K_s R}{r_\alpha} \cdot \frac{L}{R} \\
&= \frac{K_s^2 R \lambda}{2 r_\alpha^2}
\end{aligned}
$$

5.2.4 Processor Configuration

The basic SAR data processing function is the correlation of overlapping chirp waveforms generated by the varying doppler shift as the radar flies past target areas. This processing has heretofore been performed by optical means whose large numbers of signal histories stored on film can be correlated in parallel.

At this time, digital processing of SAR data has become competitive with optical techniques by virtue of the rapid improvements in speed, capacity, reliability, and cost of digital components. The advantages of digital processing are many, among these are its flexibility in accommodating multiple modes and wide parameter variations, its more precise control of processing, and its adaptability to near real time operation.

There are two major digital processing techniques available for correlation of synthetic aperture radar data: the discrete sequential correlator (DSC) or line-by-line correlator and the fast Fourier transform (FFT) or batch processor. In addition, there are techniques which are variations and/or combinations of the above.

5.2.4.1 Discrete Sequential Correlator

The DSC or line-by-line correlator approach is the easier of the two approaches to describe because of its simplicity. Basically, the processor performs a cross-correlation function between the received signal and the reference function which is matched to the phase history of the ground return. The simplified block diagram for this configuration is shown in Figure 5.2.4-1 below. In the sequential correlation,

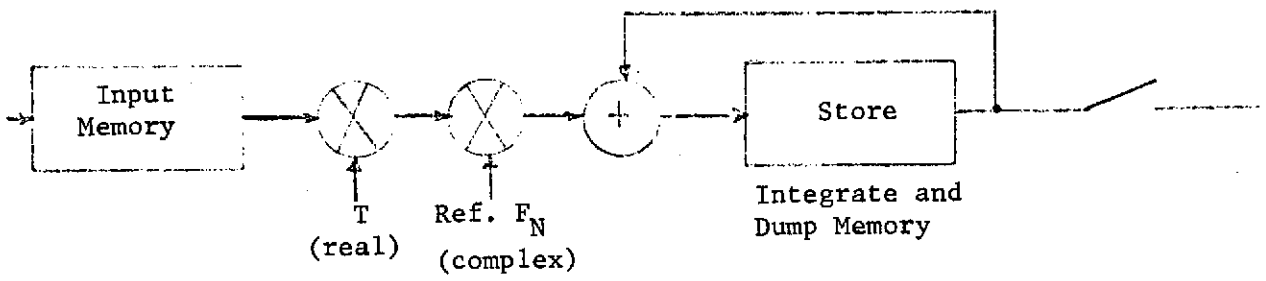

Figure 5.2.4-1. Simplified Sequential Correlator

each output is computed by multiplying the input waveform with a reference and integrating. The data is first multiplied by a weighting function to reduce sidelobe levels. The number of parallel channels required by this process can be determined by the time-bandwidth product (TBW) of the processed data. For small time bandwidths, less than 100, this simple approach is efficient to implement and is the preferred approach.

Due to the high speed of present-day digital circuits, it is possible to use one arithmetic element (complex multiplier and adder) to process several channels in parallel. However, if the TBW becomes too large, the arithmetic unit requirements become to prohibitive.

5.2.4.2 Batch Processing

In batch processing, a substantial batch of data are analyzed into multiple channels. In so doing, savings can be achieved by employing efficient analysis methods such as the FFT. For large time-bandwidth products, rather remarkable savings are possible with efficient block algorithms. Batch processing should be distinguished from parallel processing. It is quite feasible to process in parallel sequentially with multiple channels as described in the previous section. Of course, the batch processing efficiencies are not achieved.

Storage requirements are also important in SAR processing. Large amounts of storage are required because the data is received sequential in range but is processed sequential in azimuth as depicted by Figure 5.2.4-2.

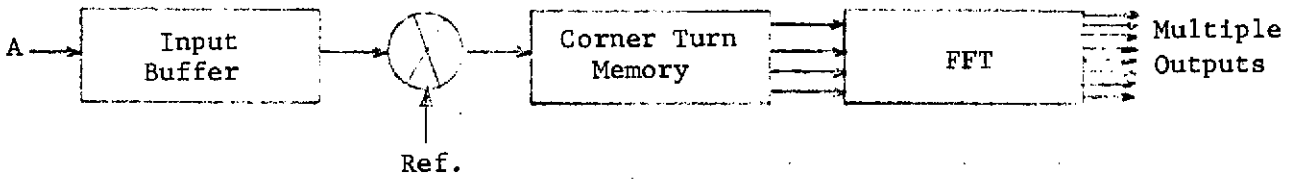

Figure 5.2.4-2. Batch Processing

A convenient visualization of the operation of the FFT correlation is provided in terms of the time-frequency histories of the waveforms involved. Figure 5.2.4-3 illustrates a series of histories representative of continuous ground return in a mapping radar. The histories

are those of azimuth elements as they pass through the beam normal to the flight path approaching and then receding in range.

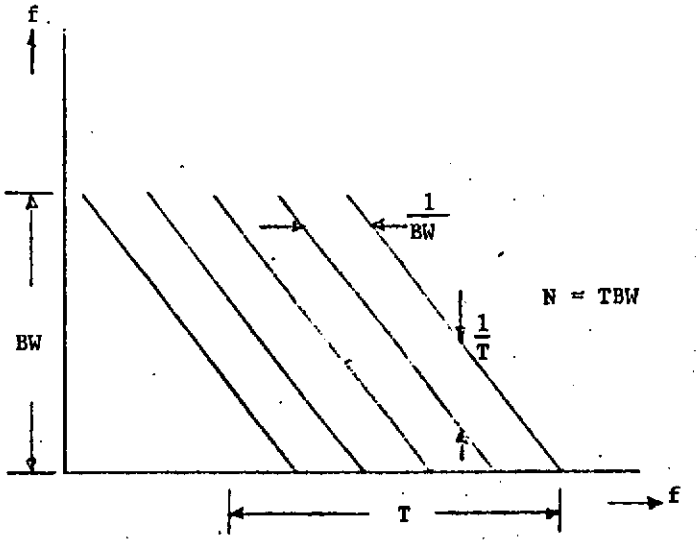

Figure 5.2.4-3. Time Vs. Frequency Histories of Ground Return

The bandwidth is BW, the dwell time or coherent integration time is T; the time resolution is 1/T, the chirp slope is BW/T, and the waveform degrees of freedom are N = T · BW.

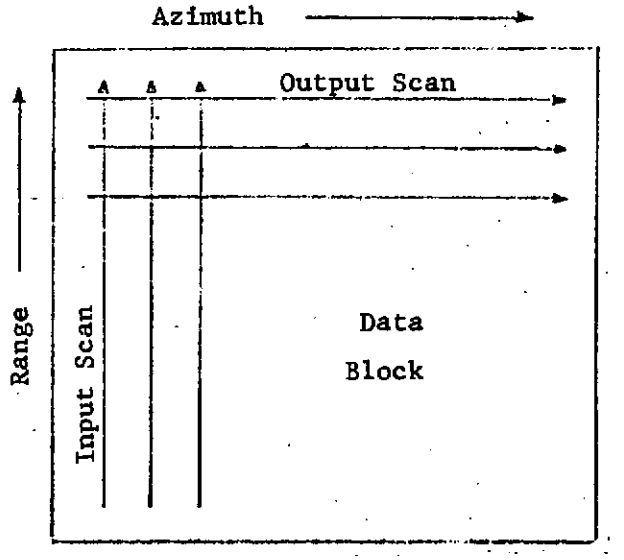

Figure 5.2.4-4. Corner Turning

Since synthetic aperture radar data is received sequential in range and the data must be sequential in azimuth at constant range for azimuth processing, the data must be transposed. This coordinate transposition will be referred to as a corner turn. To perform such a turn requires that the whole data block being processed be stored. This function is illustrated in Figure 5.2.4-4 shown on the previous page. In radar applications, where there are large numbers of range elements, the storage required can become large, and the input and internal buffering required by an algorithm is a critical factor.

In most cases, processing will be performed in sequential blocks, and the corner must be turned on a block before processing. Initial buffering in these cases corresponds to the data spanned by two successive blocks. That is, space provided for the block itself plus the incoming data accumulated during the processing of that block. This is illustrated in Figure 5.2.4-5 where blocks of length N are stepped M with an overlap of N-M.

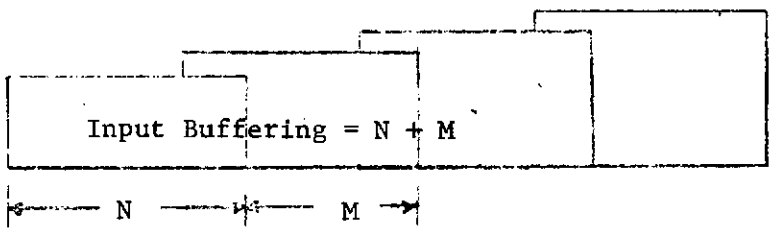

Figure 5.2.4-5. Input Storage for Continuous Block Processing

Storage required in such cases is N + M.

Similarly, time delay from initial data reception until the block is completely processed is N + M.

Batch correlation transforms a sequence of chirp waveforms into an

array of constant frequency components. This is illustrated in Figure 5.2.4-6 below.

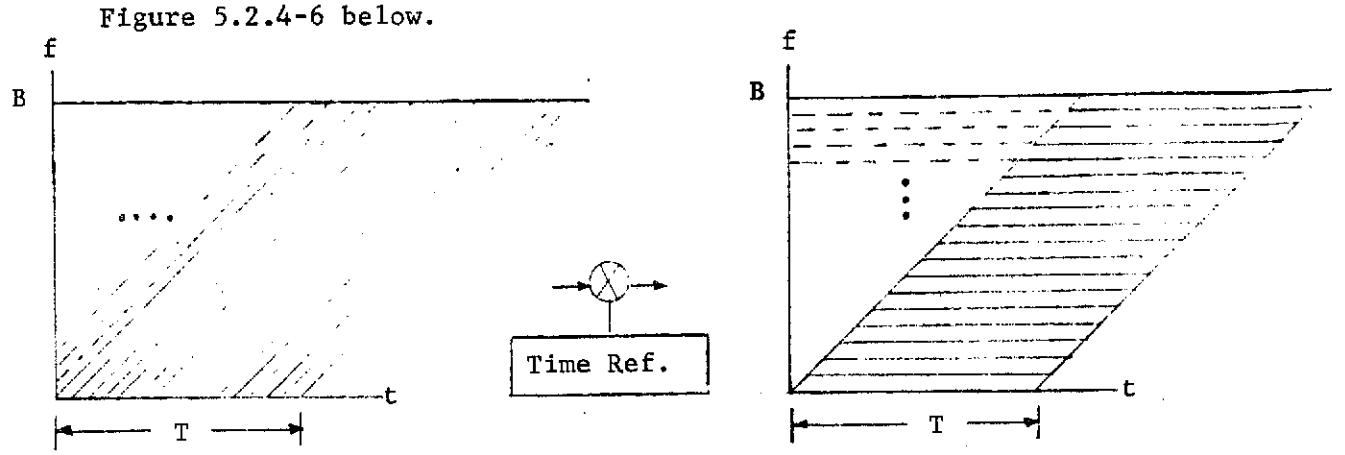

Figure 5.2.4-6. Batch Correlation of Chirp Waveforms

These components can be isolated by a Fourier analysis where multiple frequency components are generated and analyzed simultaneously. Provisions must be made to suppress the dashed components of Figure 5.2.4-6. To achieve this, some oversampling must be introduced or resolution must be sacrificed. The exact design is somewhat arbitrary. For present purposes, a reasonable design can be derived by assuming that waveforms with the same FM slope as previously sweep over a 33% larger bandwidth than B, but are processed to the same time resolution as previously, 1/B.

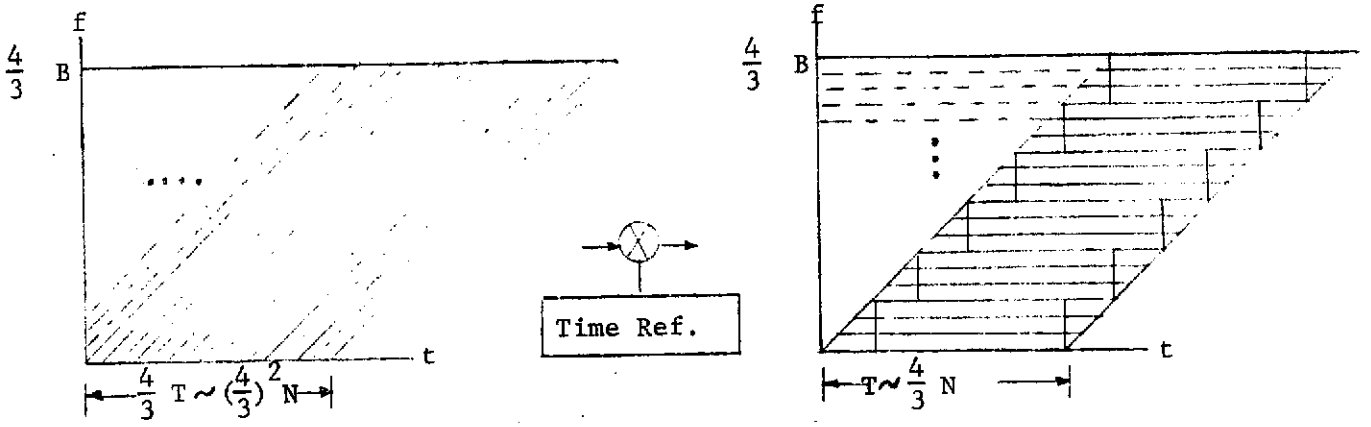

Figure 5.2.4-7. Single-Stage Time Correlator Example

Thus, there will be a 33% loss relative to the potential resolution which is incurred to avoid the folding problems noted above. The time-frequency histories involved are illustrated in Figure 5.2.4-7 shown on the previous page.

The 33% loss assumed allows the data to be processed in blocks of length T overlapped 3 to 1. Total samples in a chirp will be $(4/3)^2N$, and a block of length T will contain (4/3)N samples. One-quarter of the components from such a block will be uncontaminated by folded signals. The procedure is to process blocks of length T and retain only the N/3 uncontaminated components. The block structure is indicated on the right-hand side of Figure 5.2.4-7. With the structure indicated, N/3 samples are generated in T/3 or N in T which is identical to the original data rate of B.

5.2.4.3 Two-Stage Time Correlation

Two-stage time correlation is a Westinghouse proprietary technique for processing chirp waveforms with minimum storage and a very small computation rate. This technique has been demonstrated very successfully to obtain high resolution imagery under contract to the USAF. The basic concept is first to process small blocks and then to process a sequence of the first stage outputs. This concept is illustrated in Figure 5.2.4-8. In this configuration, data is read into the first stage from a small input buffer memory. The first stage, FFT_1, analyzes the data into coarse frequency bands. The components of FFT_1 are stored in an intermediate "triangular" memory until needed for the second stage processing, FFT_2. FFT_2 analyzes first stage outputs into the final resolution elements.

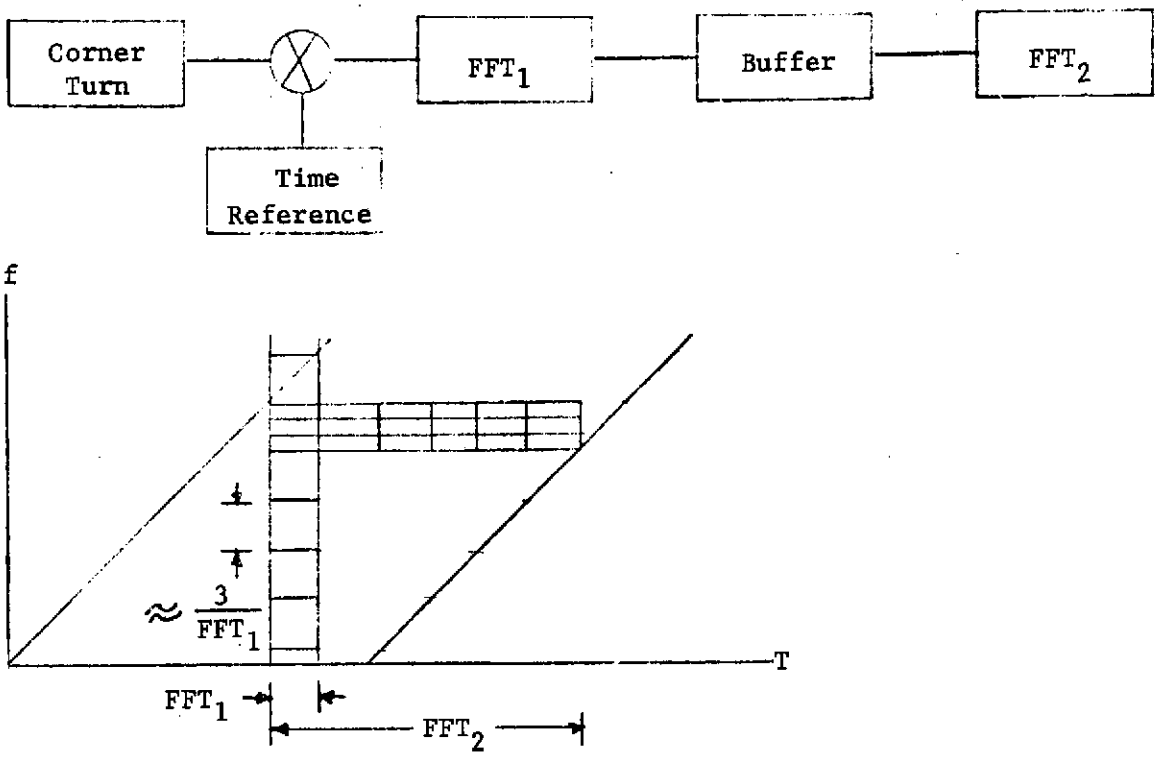

Figure 5.2.4-8. Two-Stage Time Correlation Concept

A more detailed understanding requires a few basic ideas from Fourier analysis. These are reviewed with an example in Figure 5.2.4-9. The first diagram in Figure 5.2.4-9 shows the spectrum of an 8-point FFT such as might be generated by the first stage. Components have a sin x/x shape and zeroes of a component are separated by $2/FFT_1$. The second diagram shows the spectra with weighting similar to Hamming. Separation of component zeroes is approximately $4/FFT_1$ and energy outside the first zeroes is down at least 40 dB. The third diagram shows how the frequency band can be spanned by retaining only every third component. It is assumed that first-stage blocks are overlapped in time 3 to 1 and so provide block samples at a rate of $4/FFT_1$.

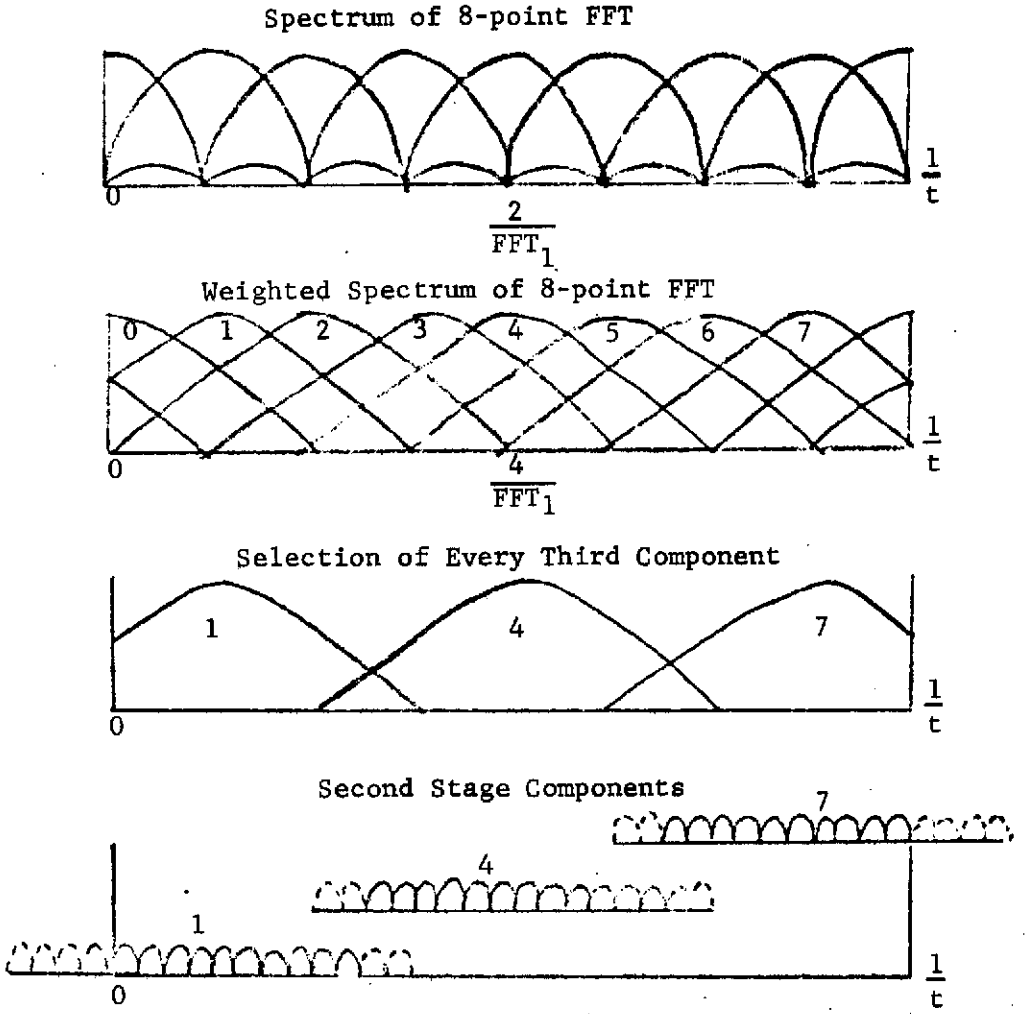

Figure 5.2.4-9. Related Fourier Analysis Concepts

Analysis of a series of first-stage component samples will thus resolve the frequency band spanned by that component, $4/FFT_1$, unambiguously. The fourth diagram in Figure 5.2.4-9 shows the second-stage output components of sequences of 16 samples of the three first-stage components retained. Output components from only one of the first-stage components are retained in the overlap region. Dashed output components are discarded. Those indicated with a solid line are retained to provide an unambiguous sequence across the whole band. Residual ripple from the first stage response curves can be compensated by individually

correcting each output component.

Large savings in storage result with this technique because the corner turn memory size is only N_1 elements (where N_1 is the size of FFT_1) long instead of N = TBW. The bulk memory between FFT_1 and FFT_2 is when a significant savings is realized because it assumes a triangular shape instead of being rectangular, as shown in Figure 5.2.4-10. The N_1 outputs from FFT_1 represent N_1 frequencies from the coarse filters.

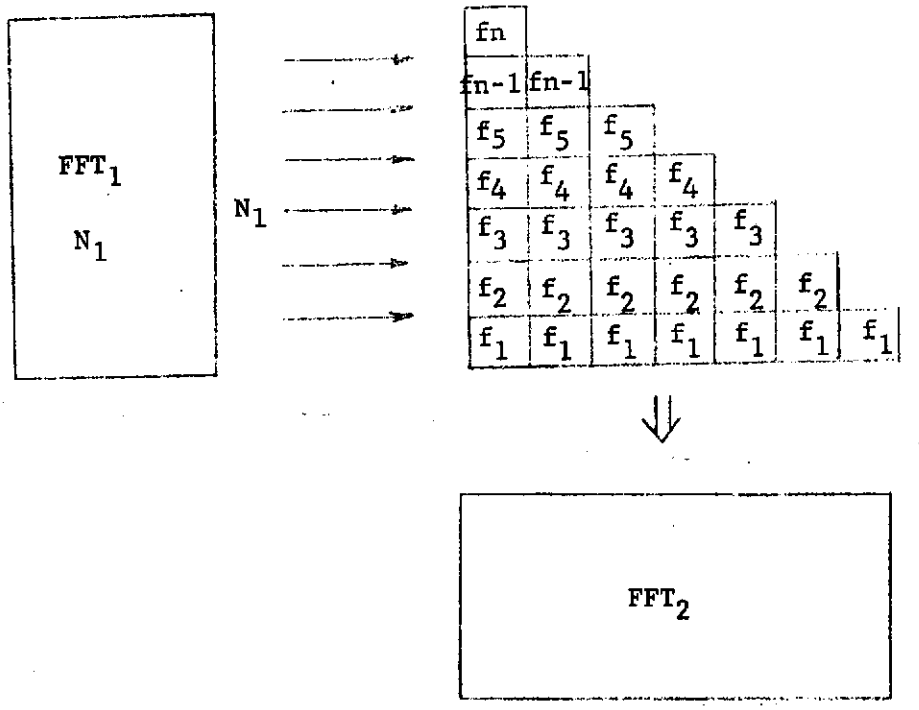

Figure 5.2.4-10. Triangular Memory

When N_2 samples for the first filter have been collected, FFT_2 resolves the filter to the final resolution. At the next output of FFT_1, N_2 outputs of f_2 become available and only 1 point for the new f_1 filter need be saved. Thus, at any one time, only N_2 points for one coarse filter need be stored.

5.2.5 Detailed Processor Design

5.2.5.1 Introduction

Various processor designs have been studied and optimized for accomplishing the azimuth compression task. Two separate configurations are considered: one for the L-band system and one for the X-band. A proposed best design for each system is outlined in the following sections. In general, the L-band configuration requires more memory and processing capacity than the X-band, since it requires about five times the time-bandwidth-product (TBW).

5.2.5.2 Hardware Requirements

The processor requirements are shown in section 5.2.2, Table 5.2.2-2. The machine must be capable of processing the collected data to an azimuth resolution of 30 meters minimum, at 1/12th of the real time data rate. For the L-band option, a maximum time-bandwidth product (TBW) of 182 is required. For the X-band option, a highest TBW is 35. It is desired to provide maximum multilook capability in both range and azimuth consistent with the resolution requirements and bandwidth limitations of the system. The processor must also provide for the clutter tracking function, gain compensation, azimuth reference function generation, as well as general timing and control functions. Finally, the processor must interface properly with the input and output tape recorders.

5.2.5.3 Processor Design, L-Band

Considerably more processing capability is required for the L-band option than the X-band, due to the longer wavelength and, hence, higher time bandwidth product. It is for such high TBWs that the two-stage

FFT algorithm becomes more efficient, primarily in the area of memory requirements, than the "line-by-line" correlator. For this reason, two-stage FFT processing, as shown in the block diagram, Figure 5.2.5-1, will be implemented if both X and L-band options are to be required. If only X-band were to be considered, the situation would be quite different, and the line-by-line correlator should prove to be the simpler approach.

The two-stage FFT correlator first multiplies the target data by a dechirp (function) to eliminate the linear FM component present on all the targets. The result is then filtered in two stages to separate different azimuth points by virtue of their frequency offset from the reference frequency. The first stage filters the spectrum into coarse frequency bands. Samples of each filter are stored in an intermediate memory until enough samples of each filter are available to do a second FFT. The second FFT separates the targets contained in each beam of the first FFT, to provide the final resolution.

A block diagram of the two-stage processor for the L-band system is shown in Figure 5.2.5-1. Data is stripped off the tape and formatted by the relatively small tape buffer into 10 bit words (s + 4, I and Q). The word rate out of this buffer is 708 KHz, which is 1/12th of the real time word rate (or $\frac{1}{(12)(10)}$ of the serial, real time bit rate). Data first goes to the range multilook circuitry which can provide 1, 2, or 3 looks in range to match the azimuth resolution options. Multilook is accomplished merely by performing a running sum of two or three adjacent range cells. Two more bits are added to each word size to accommodate this summation without saturation.

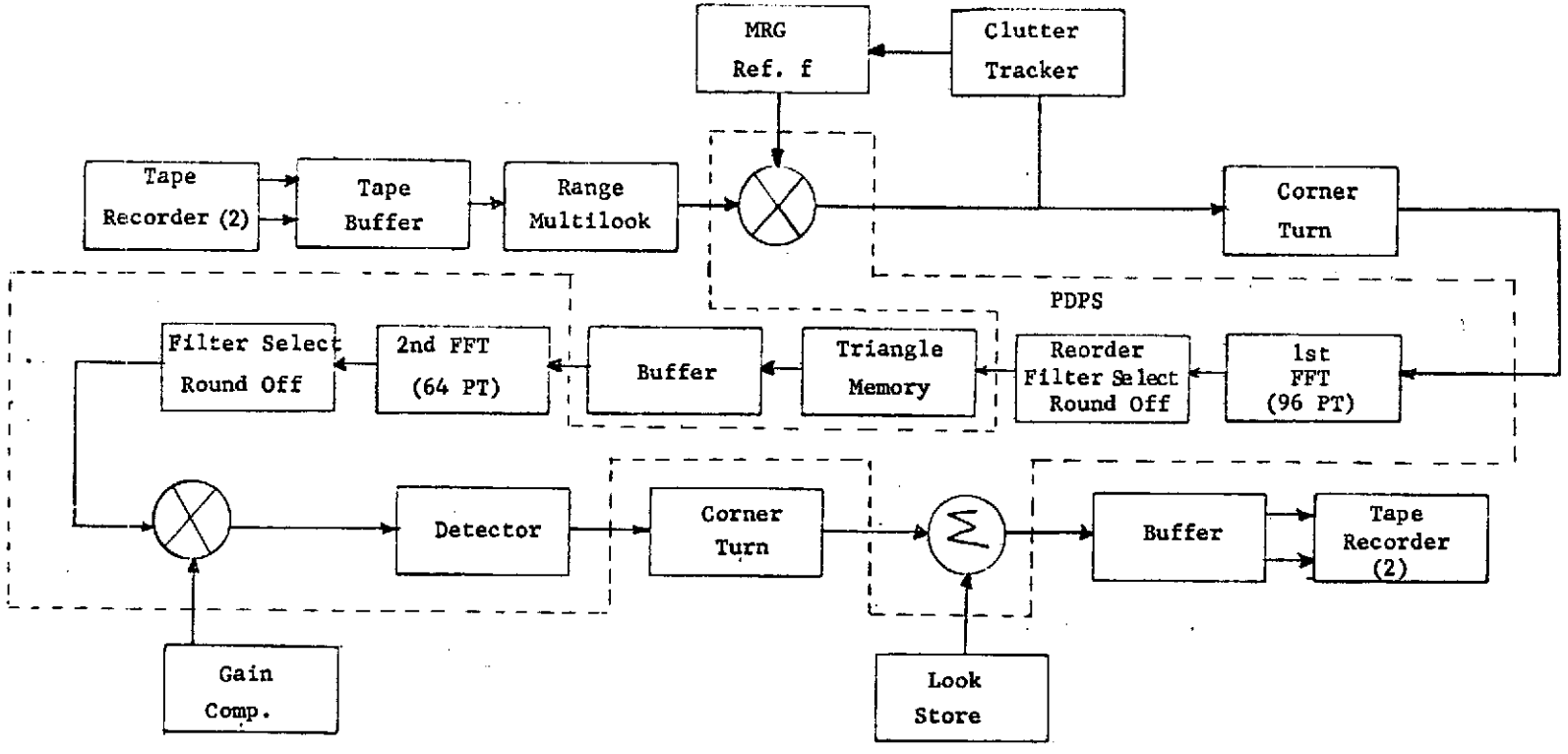

Figure 5.2.5-1. SSAR L-Band Processor

From the range multilook, the data is multiplied (mixed) by a complex azimuth reference function generated in the Map Reference Generator (MRG), which is detailed later. The mixer output goes to the processor and also to the clutter track loop via a Zero Frequency Discriminator (ZFD). This loop is closed through a low pass filter mechanized in the computer, to the MRG reference function. The purpose of this loop is to keep the clutter spectrum centered in the sampling interval.

A "corner turn" memory is required prior to the first FFT to get the range-sequential data sequential in azimuth, which is necessary in order to do an FFT. The corner turn is mechanized (see Figure 5.2.5-2) such that data is read into 1/5th of the memory in one direction, while it is being read out of the other 4/5ths in an orthogonal (azimuth) direction, at four times the input rate. This is required in order to do the 75% overlapping of first stage FFTs. While N_1 points are being processed in the FFT, $\frac{N_1}{4}$ new points are being collected and being stored in 1/5th of the memory. Before the next FFT is performed, the output commutator is moved so that the new data and 3/4ths of the old data will be utilized as the next N_1 points to the FFT. In this way, the memory is fully utilized all the time yet requires only (5/4) N_1 points of storage, the storage required is:

$$\text{C.T. Storage} = \frac{5}{4} N_1 N_B N_R$$

where N_1 = the number of points required for the first stage FFT

N_B = the number of bits per complex word

N_R = the number of range cells

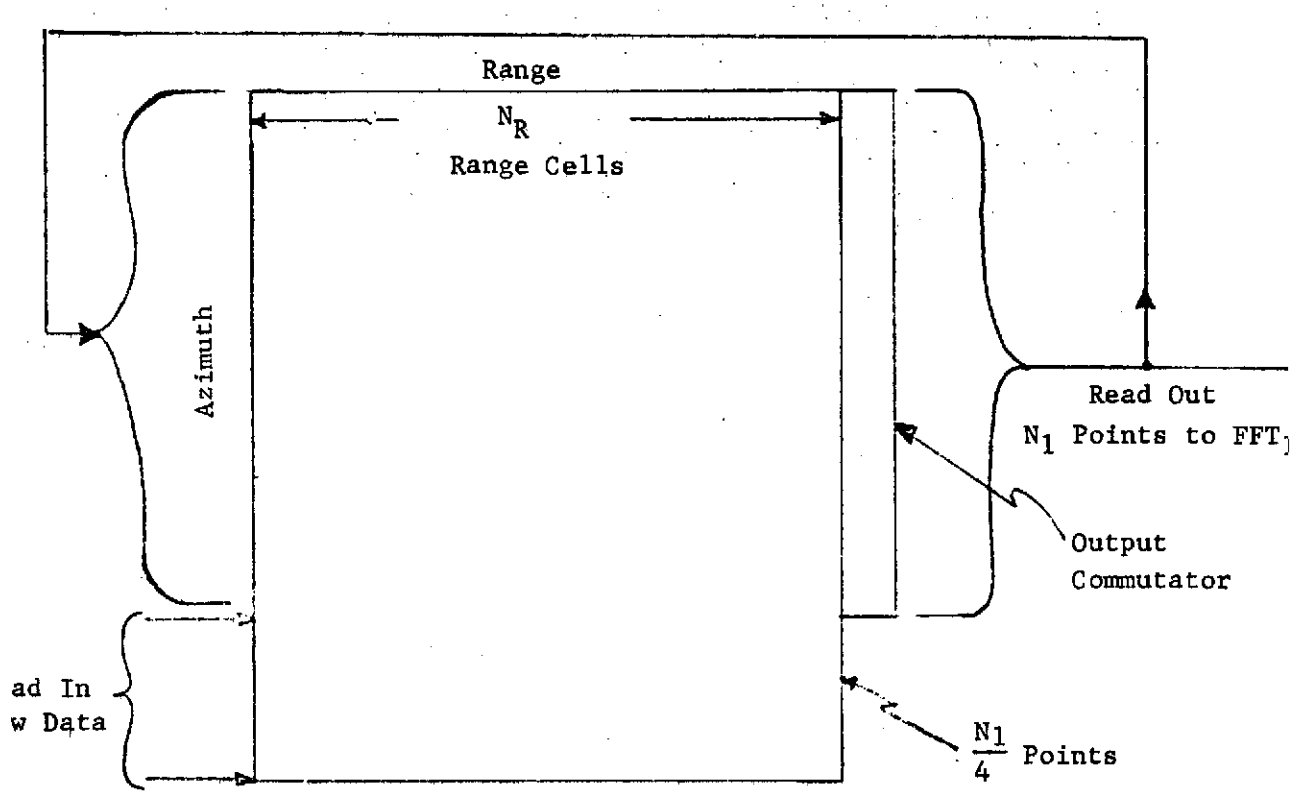

- Write across, read down
- Read out rate is 4 times read in rate
- Memory contains 5/4 of points required for 1st FFT (N_1)
- Shift output and input down 1/4 of memory after every FFT_1

Figure 5.2.5-2. Corner Turn Buffer

It will be shown that $N_1 = 96$ is optimal; thus we have:

$$\text{C.T. Storage} = \frac{5}{4}\,(96)(14)(2084) =$$

$$= 3,\,501,\,120 \text{ bits}$$

Next, we turn our attention to the FFTs. Each output filter must have a bandwidth sufficiently small to provide the required azimuth separation of targets (resolution). The bandwidth required to do this is:

$$BW = \frac{1}{T_{coh}} = \frac{1}{.514 \text{ sec}} = 1.945 \text{ Hz.}$$

Each coherent integration time (T_{coh}), the processor must synthesize filters of this bandwidth across the input sampling spectrum (the radar prf). Thus, we need $\frac{prf}{BW} = \frac{3000 \text{ Hz}}{.514 \text{ Hz}} = 1542$ filters. For two stage processing, the number of effective filters is given by $\frac{N_1 N_2}{4}$, where N_1 is the number of points in the first FFT (FFT_1), and N_2 the number in FFT_2 ($\frac{N_1}{3}$ filters are retained from the first stage and $\frac{3}{4} N_2$ from the second). Equating these quantities gives:

$$\frac{N_1 N_2}{4} = 1542$$

$$N_2 = \frac{6168}{N_1}$$

Actually, N_2 must be mechanized to be the next larger power of 2 ($N_2 = 2^n$). N_1 is constrained to be a number given by $(3)(2^m)$, where m and n are integers. Obviously, many configurations are possible by trading off N_1 against N_2. Six such configurations were computed for their total memory requirements. The results are plotted in Figure 5.2.5-3, and values of $N_1 = 96$ and $N_2 = 64$ were selected as requiring minimum memory.

The major memory component is the so-called "triangle", or intermediate memory. It stores the saved filters from FFT_1 until the required number of samples for the second stage are available. The

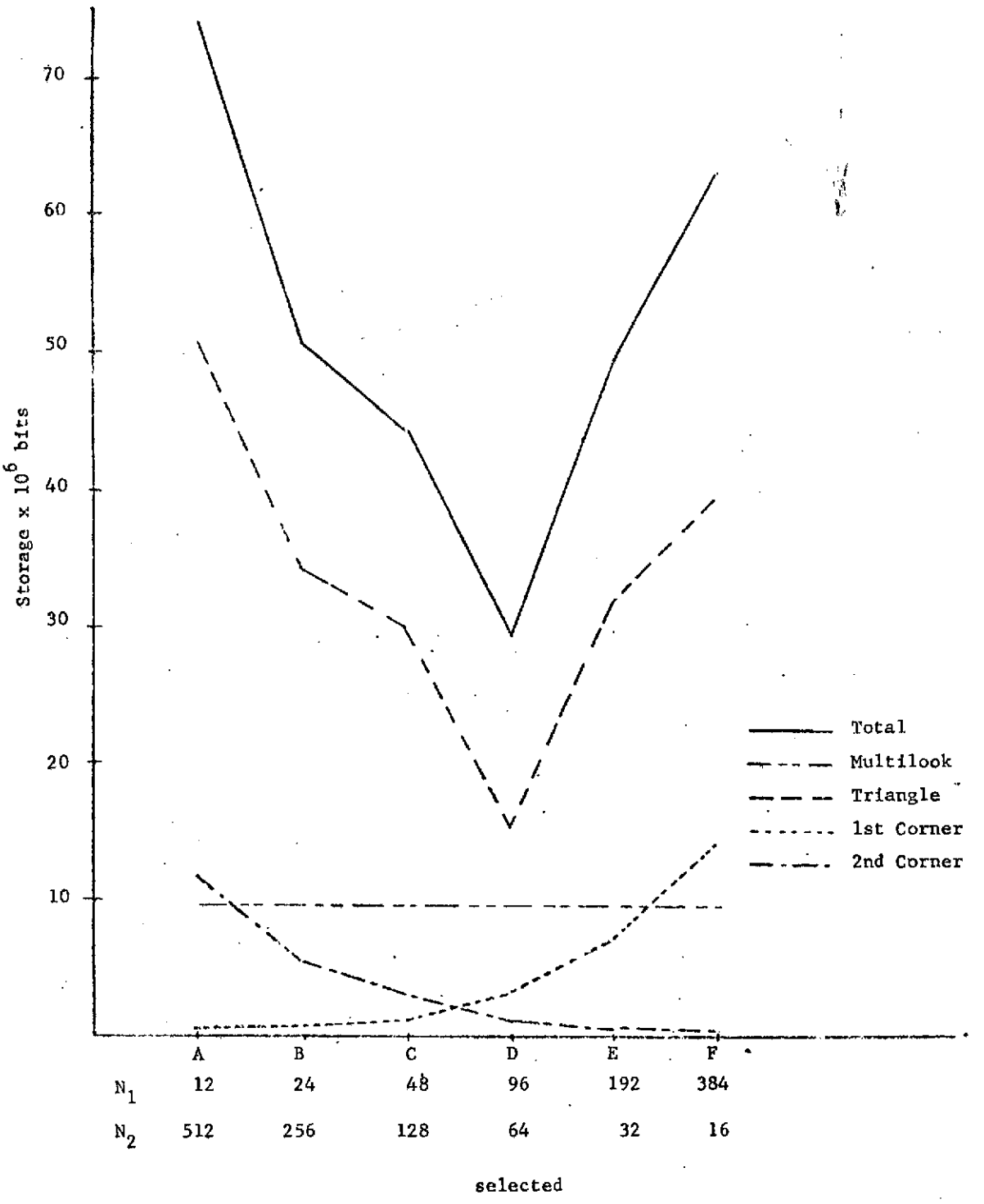

Figure 5.2.5-3. L-Band Processor Memory Requirements

filters kept from the first stage are only those required to cover the SAR bandwidth, which is 3 x 355 = 1065 Hz, where 3 is the number of independent looks and 355 the SAR bandwidth required to obtain 30 meter resolution. This is $\frac{1065}{3000}$ = .356 of the first stage filters. For the mechanization selected, this is .356 $(\frac{N_1}{3})$ = .356 $(\frac{96}{3})$ = 11.4, so 12 filters are saved. The number required for the second stage FFT is $N_2 = \frac{6168}{N_1} = \frac{6168}{96}$ = 64.3, so a 64 point FFT will be mechanized. Thus, the triangle memory must have a shape of 12 x 64, resulting in a face area of 228 (see Figure 5.2.5-4). The required storage is:

$$\begin{aligned} \text{Triangle Storage} &= 2 \times N_B \times N_R \times \text{Area} \\ &= 2(16)\ (2084)\ (228) \\ &= 15,\ 204,\ 864 \end{aligned}$$

(Two triangles are required to do the 50% overlapping in the second FFT; the bit increase through FFT_1 is limited to s + 7).

After the second FFT, 48 of the 64 filters are retained as being non-redundant, reducing the effective data rate to $(\frac{48}{64})$ (708) = 531 KHz. A gain compensation function is performed followed by detection. Next, the data must go through another corner turn to become sequential in range again, in order to be compatible with the film recorder and display. This corner turn is double buffered and operates on 48 filters at a time. The storage required is:

$$\begin{aligned} \text{C. T. Storage} &= (2)(N_B)(N_R)(3/4\ N_2) \\ &= 2(8)(2084)(48) \\ &= 1,\ 600,\ 512 \end{aligned}$$

Again, word size increases through FFT_2 are limited to s + 7 bits each, and since detection has already occurred, only real words need be

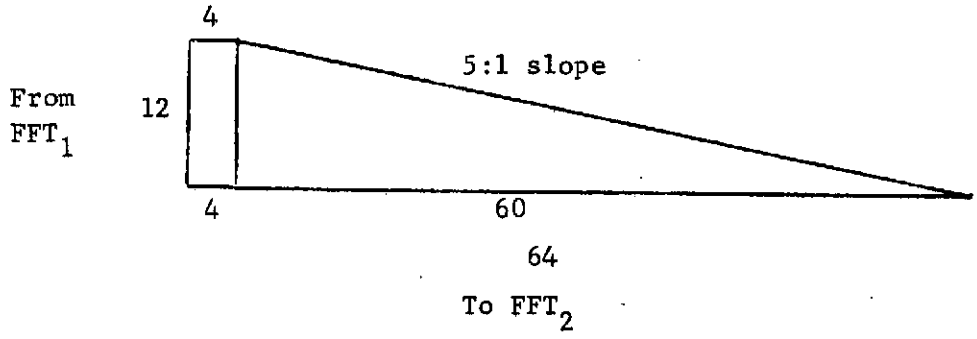

Face Area = (12)(4) + (5 + 4 + 3 + 2 + 1)(12) = 228

Figure 5.2.5-4. Triangle Memory

handled by the corner turn.

Finally, a multilook adder and storage are required. For this particular L-band case, there are three independent and two overlapped looks. The FFT outputs are grouped into three azimuth chunks each integration time (T_{coh}). As shown in Figure 5.2.5-5, each chunk is added into its accumulator until all five "looks" have been summed. Each third will be completed and "dumped" at a different time. The memory requirements for the look storage are:

$$\text{Look Storage} = K \left(\frac{N_1 N_2}{4}\right) (N_B) (N_R)$$

where K = fraction of filters kept from FFT_1

$$\text{storage} = \frac{3}{8} \left[\frac{(96)(64)}{4}\right](2084)(8)$$

$$= 9{,}603{,}072 \text{ bits}$$

This yields a total processor memory requirement of 29,909,568 bits. The other modes of the L-band option have lower resolution requirements but a higher number of looks; in other words, the total processed bandwidth remains about the same. Therefore, the total memory requirements will not be any larger.

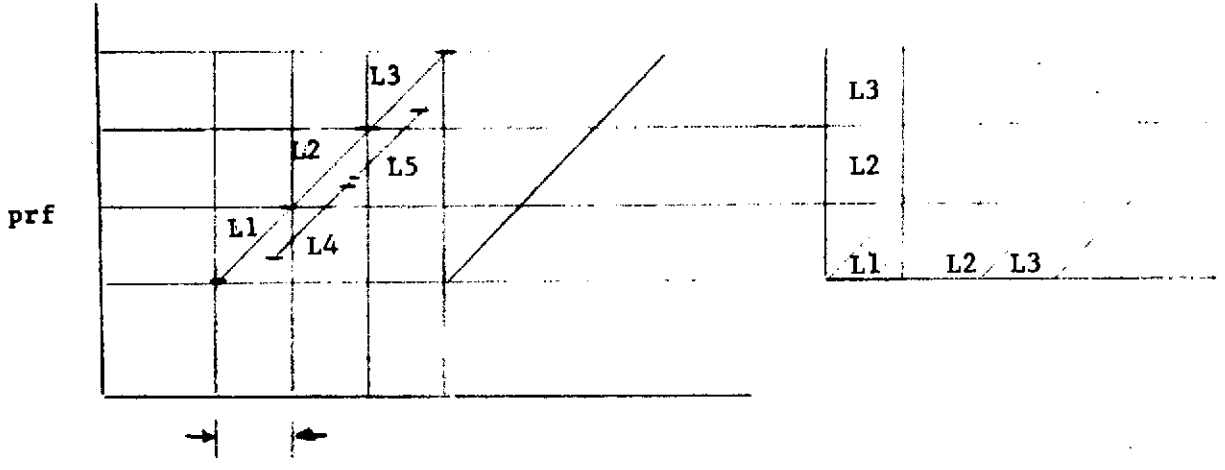

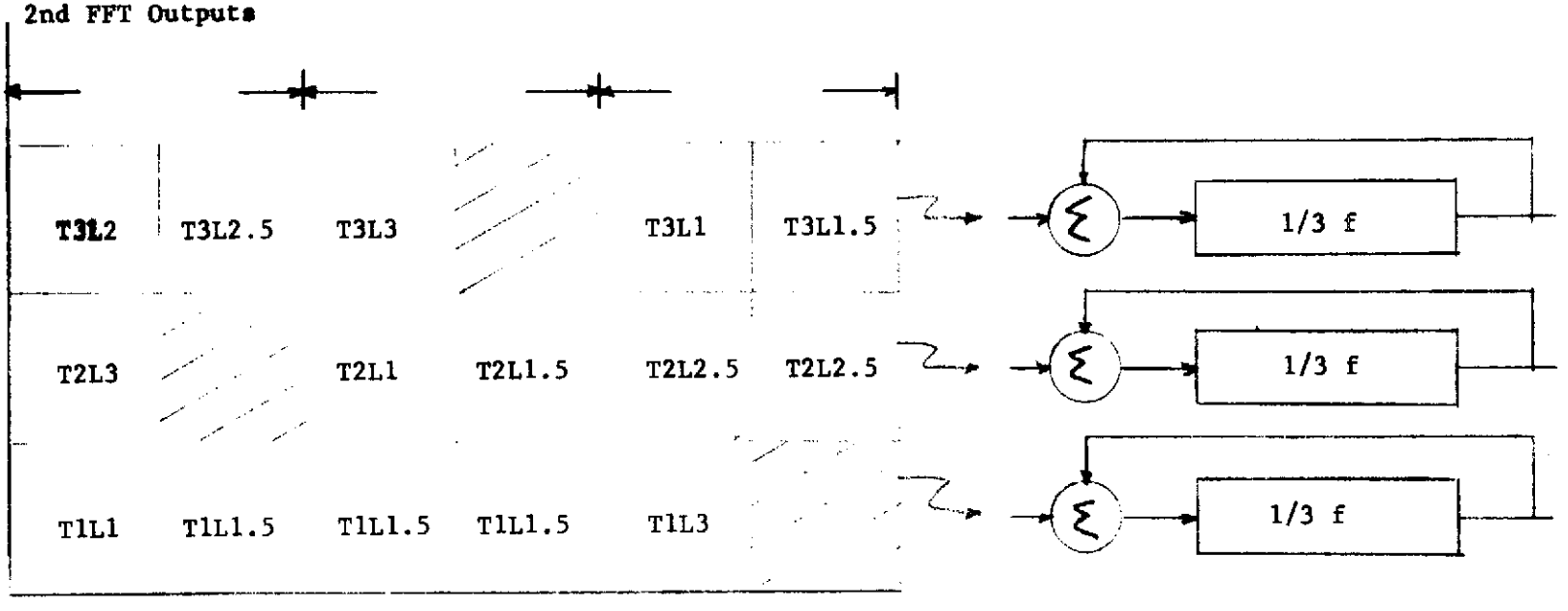

Figure 5.2.5-5. Multilook L-Band

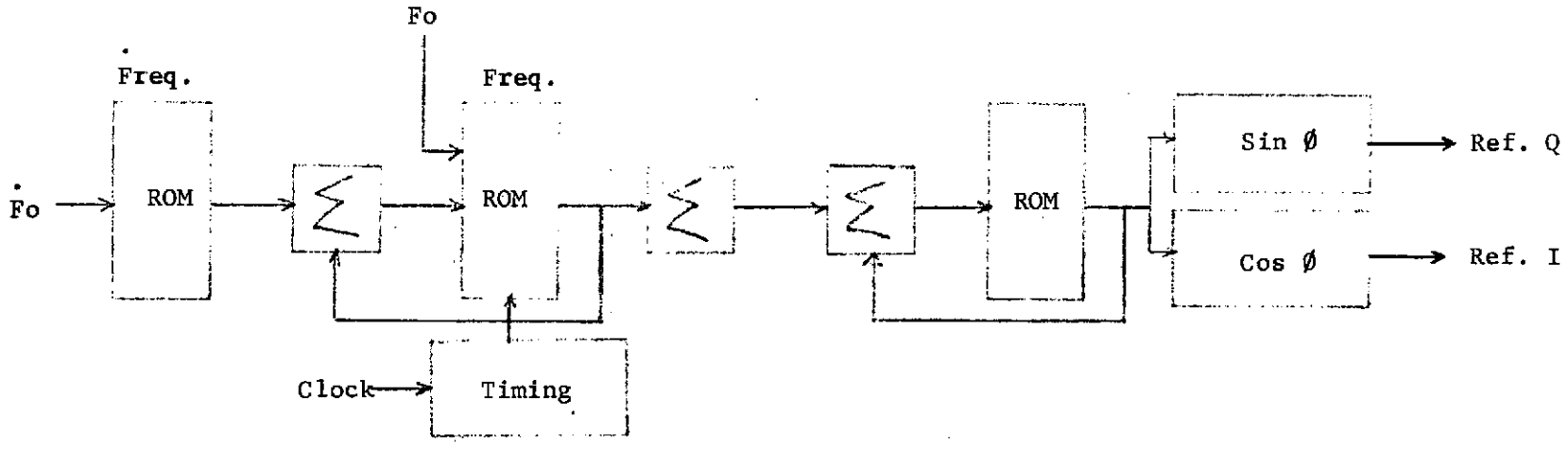

Figure 5.2.5-6. Map Reference Generator

A key component of the processor is the Map Reference Generator. This is a piece of specialized hardware (see Figure 5.2.5-6) which generates the linear FM reference signal. This is done by integrating a constant, $\dot{F}$ each IPP to produce a linearly increasing parameter called F (frequency). F is itself integrated to generate a parabolic phase function, which synthesizes the sine and cosine waves directly using ROM look-up tables. The F parameter may be modified by addition of the offset frequency from the clutter track loop.

5.2.5.4 Processor Design, X-Band

Since the X-band system has a relatively low Time Bandwidth Product of 35, two design approaches are feasible. One is the two-stage FFT batch processor similar to the one proposed for the L-band system. The other is a straightforward line-by-line correlator. The two approaches are compared and the line-by-line is shown to be more desirable.

A block diagram of an X-band, two-stage processor is shown in Figure 5.2.5-7. It is similar to the L-band processor, except that 48 and 32 points were selected for the first and second FFTs respectively. This gives an effective number of filters across the prf of $\frac{N_1 N_2}{4} = 384$. Since the maximum prf is 4 KHz, this yields $\frac{4000 \text{ Hz}}{384} = 10.4$ Hz per filter, which is consistent with the 0.1 second integration time specified for this mode. The FFT sizes selected minimize the total memory requirement, as shown on the graph in Figure 5.2.5-8, to 15,354,912 bits. The triangle memory for this case must store $.473 \left(\frac{N_1}{3}\right) = 8$ first stage filters ($.473 = \frac{4(355)}{3000}$, where 355 is the SAR bandwidth per look, 4 the number of independent looks, and 3000 the

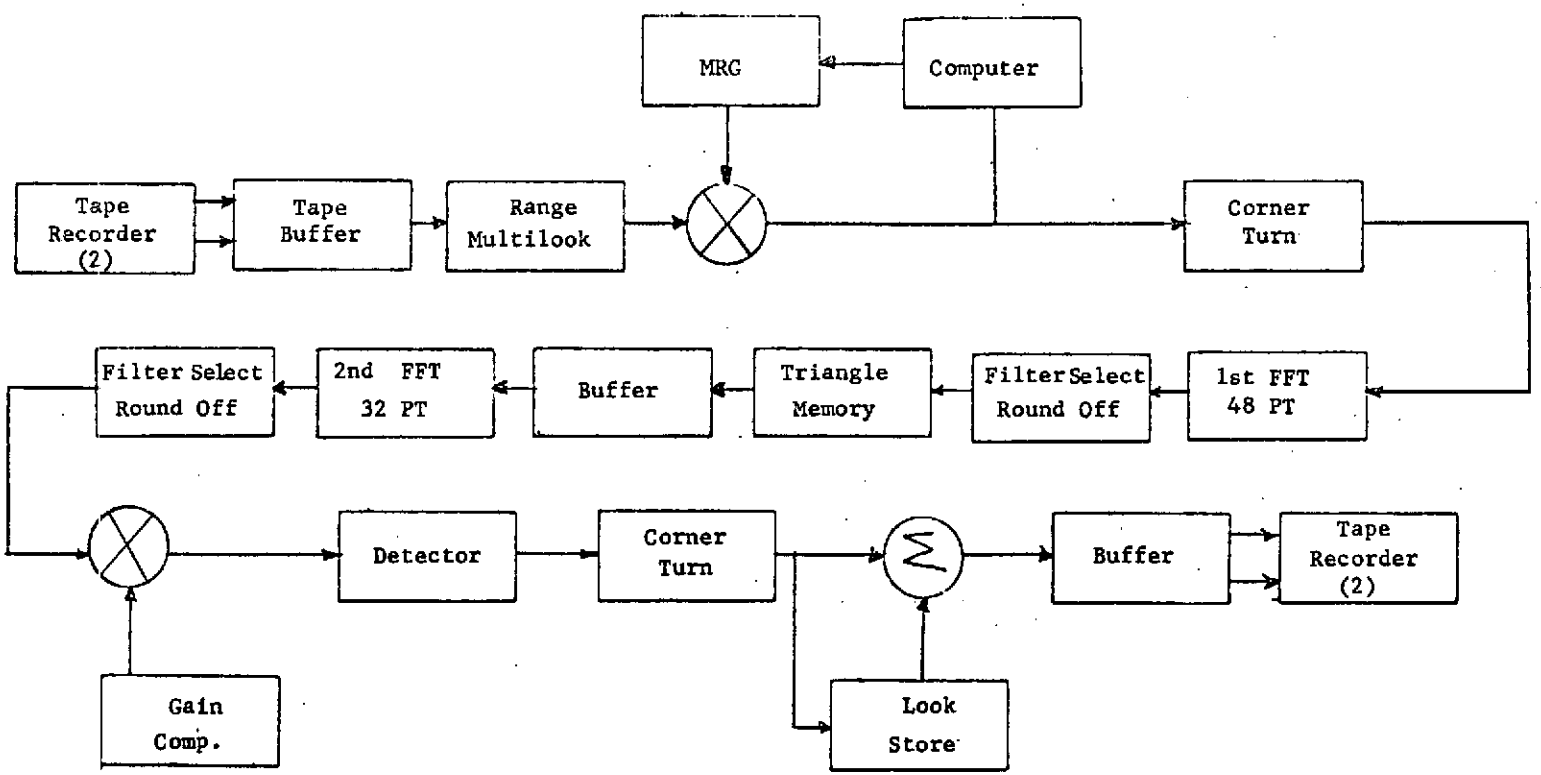

Figure 5.2.5-7. SSAR X-Band Processor

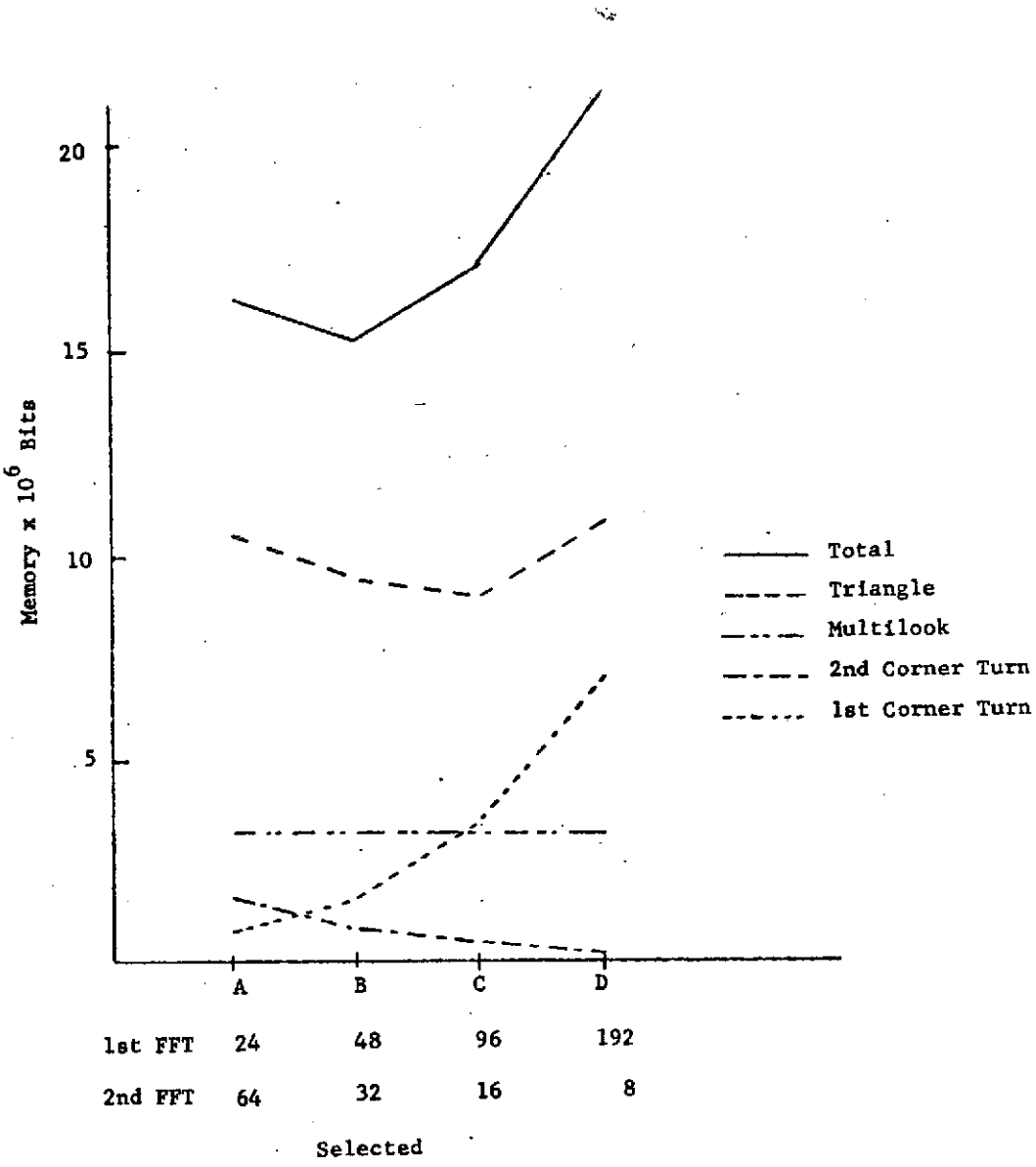

Figure 5.2.5-8. Memory Tradeoff for X-Band

minimum prf). The face area of an 8 x 32 triangle is 144, so the storage is (area)$(N_B)(N_R)$ = 9,603,072 bits, where N_B is held to 16.

The corner turn memories are computed as in the previous section. The first corner turn requires $(\frac{5}{4})(N_1)(N_B)(N_R)$ = 1,750,560 bits; the output corner turn requires $(2)(N_B)(N_R)(\frac{3}{4}\ N_2)$ = 800,256 bits. The look storage is $K\ (\frac{N_1 N_2}{4})\ (N_B)(N_R) = 1/2\ (\frac{(48)(32)}{4})(8)(2084)$ = 3,201,024. This makes the total processor memory requirements 15,354,912 bits.

The second approach to an X-band processor would be the line-by-line correlator, shown in Figure 5.2.5-9. Here, the tape unpacking and range multilook are accomplished as before. The correlator, however, is mechanized to provide a separate linear FM reference function for every target. Since the TBW is 35, 35 references are required per look, and there are seven independent looks. Thus, 7 x 35 = 245 targets must be correlated simultaneously. For the other X-band modes, TBW is less, but the number of looks is higher, so this product remains about constant. It is this product that determines the number of "channels" which must be mechanized, where each channel consists of a reference function complex multiply followed by an accumulator. The accumulator integrates the target for the required integration time (T_{coh}), and then "dumps" the result through the detection circuits to the output tape. No corner turn buffers are required since the data is handled sequentially in range.

A practical implementation of the above requires a combination of serial and parallel multiplexing of the memory in order to minimize arithmetic hardware (by time sharing them among serial channels).

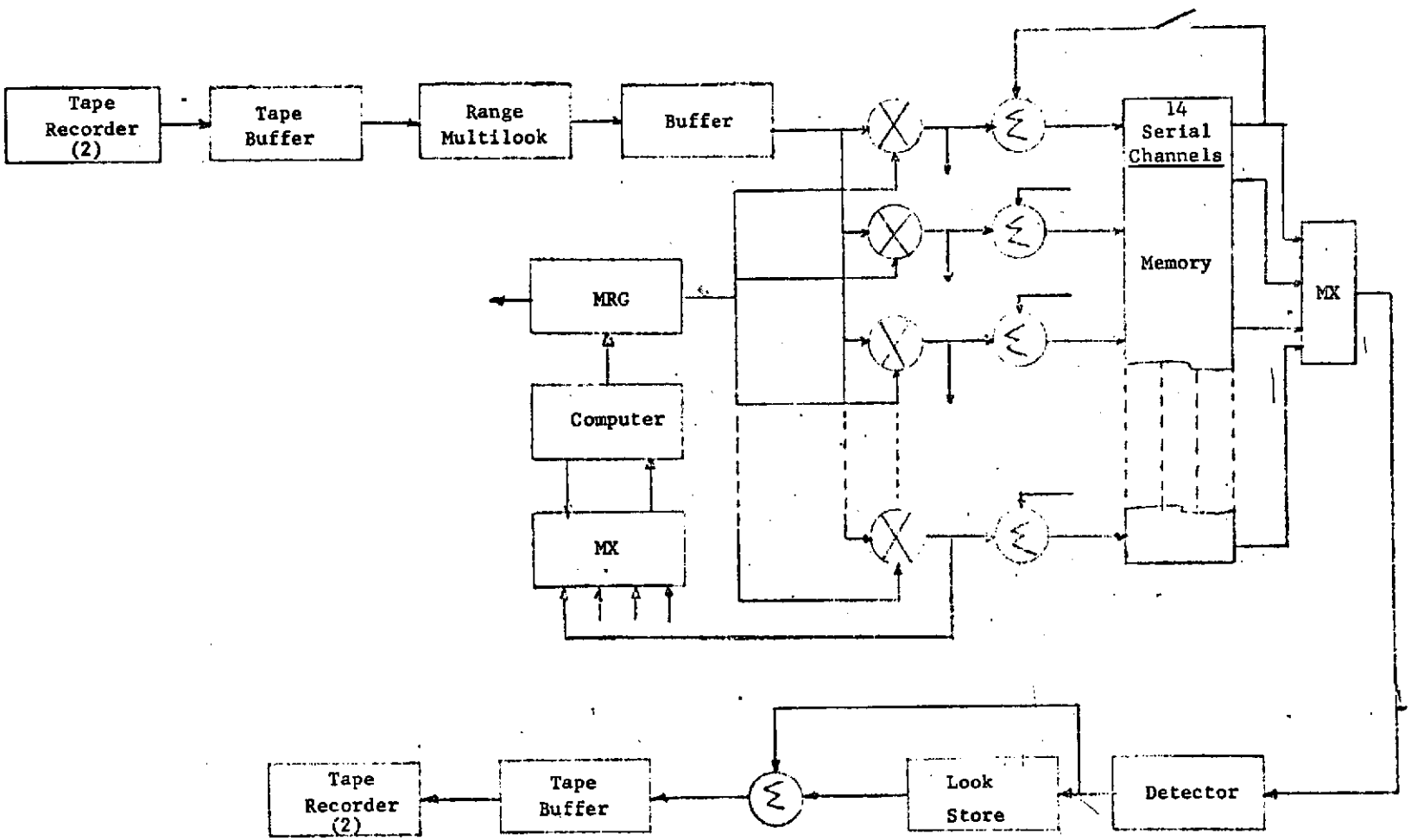

Figure 5.2.5-9. Line-By-Line Correlator

Parallel multiplexing is required when the serial data rates exceed practical hardware speeds. A mechanization was selected of 18 parallel channels, each with its own arithmetic hardware, and each containing 14 serial channels. Thus, 14 x 18 = 252 channels are available, where 7 x 35 = 245 are required. The 14 serial channels require a 14:1 data rate increase to 14 x 708 = 9.92 MHz, which is within an arbitrarily selected 10 MHz hardware limit. A speed-up buffer is constructed to accomplish this. It stores 2084 range cells each IPP in one-half of its memory, while the other half reads out the previous IPP's data 14 times and at 14 times the rate. The memory required to do this is:

$$\begin{aligned} \text{S.O. Memory} &= (2)(N_R)(N_B) \\ &= (2)(2084)(14) \\ &= 58{,}352 \text{ bits} \end{aligned}$$

The amount of correlator memory required is simply:

$$\begin{aligned} \text{Cor. Memory} &= (N_C)(N_R)(N_B) \\ &= (252)(2084)(16) \\ &= 8{,}402{,}688 \text{ bits} \end{aligned}$$

where N_C is the number of mechanized correlator channels and N_B is held to $2(s + 7)$ by a round off.

Following the detection, a multilook accumulator is required. Each dumped target from the correlator must be stored until all other "looks" of that target have been added to it. The number of independent (non-overlapped) targets that must be stored is 4 x 35 = 140, since there are four independent looks in this mode. Thus, the memory required is:

$$\begin{aligned} \text{M.L. Memory} &= (4)(35)(N_R)(N_B) \\ &= (4)(35)(2084)(8) \\ &= 2{,}334{,}080 \text{ bits} \end{aligned}$$

The total memory requirements (see Table 5.2.5-1) are thus, 10,795,120 bits, about 2/3 of the two-stage FFT design. This, coupled

Table 5.2.5-1 Comparison of X-Band Options For Memory Requirements

Line-By-Line Correlator		Two-Stage FFT, Best Design	
Memory Unit	# Bits	Memory Unit	# Bits
		1st Corner Turn	1,750,560
Speed Up Buffer	58,352	Triangle	9,603,072
Correlator Memory	8,402,688	2nd Corner Turn	800,256
Look Store	2,334,080	Look Store	3,201,024
TOTAL	10,795,120	TOTAL	15,354,912

with the greater simplicity inherent in the more straightforward line-by-line approach, leads to its strong recommendation for accomplishing the X-band option.

5.2.5.5 PDSP Processing

The programmable digital signal processor is a fast processor capable of carrying out complex multiplications of the form A x B $\pm$ C. It is, therefore, possible to program it to carry out such functions as FFT, weighting, recursive filtering as well as many other commonly used functions. Thus, the main advantages of such a unit is its speed (10 MHz) and flexibility. For the given processing task, the PDSP was utilized for functions which are suitable for its present design. More specifically, base 2 FFT was carried out with the aid of the PDSP while base 3 FFT was done with hardware. To optimize on the speed of the processing external buffers were used throughout the processing chain. The PDSP was used to carry out FFT_2, weighting, complex and real multiply and detection.

To estimate the number of PDSP units needed to carry out the processing of each option, the aperture time was computed and the total number of computations (in clock pulses) relative to a given aperture time. This, in turn, was converted into ideal PDSP units which then were assumed to be 80% efficient, thus, yielding a nominal figure for the number of PDSP units utilized. The true optimal utilization of the PDSP calls for detail design which is beyond the scope of this study, therefore, only rough estimates are derived based on the most strict constraints. With no regard to optimized processing overlays and iterative priorities, computations were carried out for an ideal processor. Ideal processor was defined as a 10 MHz unit which is able to carry out all computations in a given time aperture. Assuming 80% efficiency of such a unit, the nominal number of PDSP units was computed.

The basic macro instructions utilized in each of the processing chains were: FFT (base two Fast Fourier Transform), Move (move data out of memory - for FFT only), CMPY (complex multiply), RMPY (real multiply), DET (detection - $\sqrt{I^2 + Q^2}$).

Timing in clock pulses was based on the following equations:

$$\text{FFT + MOVE} = \left(\left(\frac{N}{2} \times NSB + 3\right)(NS + 1)\right) NB$$

$$\text{CMPY} = (N \times NSB + 3)\, NB$$

$$\text{EMPY} = \left(\frac{N}{2} \times NSB + 3\right) NB$$

$$\text{DET} = (N \times NSB + 3)\, NB$$

where N = number of data points

NS = number of stages (base 2)

NB = number of blocks

NSB = number of subblocks

The modified system diagram is shown in Figure 5.2.5-10 while a tabulation of the PDSP utilization is given in Table 5.2.5-2.

Table 5.2.5-2 PDSP Utilization

Function	MACRO	Time (in clocks)	Aperture (in clocks)	Ideal PDSP (units)
Ref. Multiply	CMPLY	50088	960000	.052175
Weighting	RMPLY	100035	960000	.10423
1st FFT_2	FFT	135198	960000	.140831
2nd FFT_2	FFT	315462	2560000	.123227
Gain Correct	RMPLY	33930	2560000	.01325
Detect	DET	67338	2560000	.026304
			Σ =	.46

Nominal number of PDSP units = 1.2 (ideal # of PDSP)

Nominal # of PDSP = 1.2 (.46) = .552 $\Rightarrow$ 1

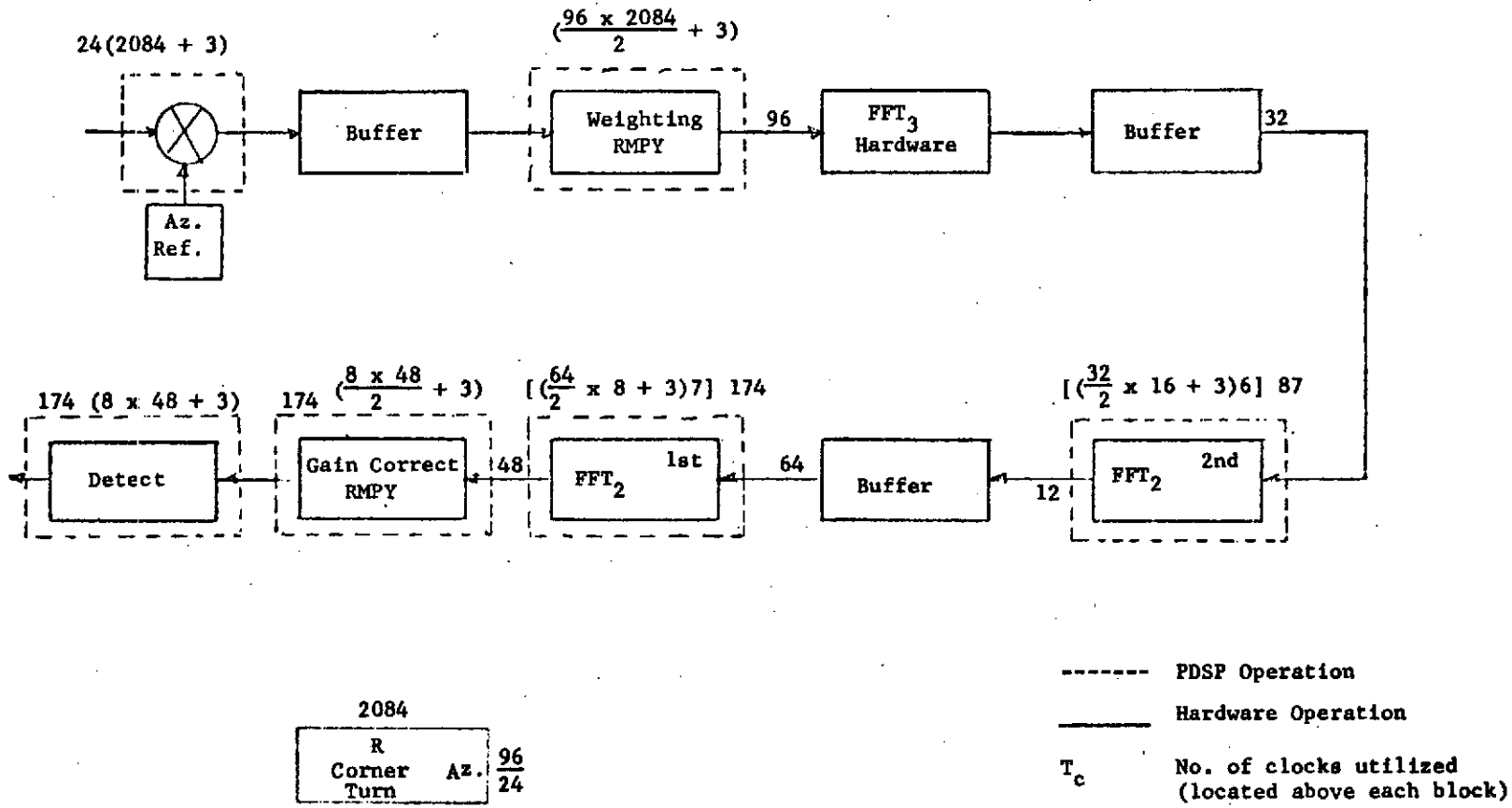

Figure 5.2.5-10. PDSP Processing

5.3 Radar Calibration

The equipment calibration of concern is that of ascertaining exactly what the radar gains and transmitted power are so that the receiver power and, hence, the ground reflectivity may be determined at any given time. As receiver gain varies with AGC, it is desirable to have a near real time calibration. This is achieved using a continuous comparison technique with a known fraction of the transmitted signal injected into the receiver such that the receiver-transmitted power ratio is determined. Absolute (and relatively inaccurate) independent measuments are then replaced with comparative measurements.

A calibrated density wedge appears on the film continuously reflecting actual system conditions at that time commensurate with accompanying map data. The precise time location and amplitude of the calibration pulse allows automatic reflectivity calculation to be made by the computer/processor upon map coordinate designation as well as direct visual density comparison. The use of corner reflectors of known cross sectional areas would provide occasional supplementary near absolute calibration checks.

5.3.1 Reflectivity Determination

5.3.1.1 Introduction

The reflectivity or backscatter coefficient is basically determined by comparing the received with transmitted power; rougher terrain tends to return more power than smoother terrain. Detailed examination of the measurement indicates a variety of ground geometric and radar parametric factors must be accurately known in order to make a determination.

Examination of the equation for the reflectivity or backscatter coefficient indicates areas of concern. Then, equations are derived in Appendix C and are given below.

$$\sigma^{o} = \left(\frac{P_{rn}}{P_a}\right) \frac{4(4\pi)^3 R^3}{G^2 \lambda^3 c} \sin \phi_i$$

$$= \left(\frac{P_{rn}}{P_a}\right) \frac{4(4\pi)^3 R^3}{G^2 \lambda^3 c} \tan \phi_i$$

These equations are a short form of the precise detailed form which would be used in actual backscatter calculation;[1,2] however, they serve to indicate the salient parameters and as a basis for discussion.

5.3.1.2 Radar Parametric Factors

The first term in the equation $\left(\frac{P_{rn}}{P_a}\right)$ is the ratio of the received to average transmitted power. Determination of this ratio directly results in less error than measuring the received and average power independently and then determining the ratio. A typical technique, further discussed in section 5.3.2, involves injecting a precisely known fraction of the transmitted power into the receiver. This power is then operated on in precisely the same way as the received power by the elements in the signal processing path, thus, eliminating error-prone independent measurements.

---

[1] AN/APQ-97 Radar Calibration Design Study (Conf.), April 1971, United States Army, Engineer Topographic Laboratories, Fort Belvoir, Virginia. Prepared by Westinghouse Defense & Space Center, Baltimore, Md.

[2] Radar Handbook; Ground Echo, Chapter 25, Richard K. Moore, University of Kansas, McGraw-Hill, 1970.

Actually, a calibrated series of different fractional power RF pulses derived from the transmitter are injected into the receiver during dead time. The dynamic range of these pulses will be about 60 dB in 2.0 dB steps. This allows any processing non-linearities to be "calibrated out". This calibrated density wedge repeatedly appearing on the map films allows direct visual comparison between map film densities and wedge densities, thus, determining the power ratio. Possible observer measurement inaccuracies may be eliminated by direct digital correlator "read out" upon designation of the desired area. More specific details of the injection technique are given in section 5.3.2.

As seen from the backscatter equations, the antenna gain (G) is an important parameter in the measurement. The antenna pattern in azimuth and especially elevation and perhaps in other than the cardinal planes should be known. It must be determined that antenna sidelobe contributions to the map area under examination are negligible. The patterns should also be known accurately such that precise gain to the map examination area is known.

Other factors in the equations for backscatter and reflectivity are wavelength (λ), velocity of light (c) and range (R); all of which are known.

5.3.1.3 Geometric Factors

Knowledge of the antenna pattern may not in itself obviate gain pattern errors. This problem is somewhat aggrivated by the relatively narrow elevation patterns (for the X-band systems) compared to the swath width. Swath edge gain is roughly 5 dB less than swath center

gain. For known ground slopes, the precise angular deviation from boresight and, therefore, the gain commensurate with specific swath coordinates can be determined. This geometry is illustrated in Figure 5.3.1-1.

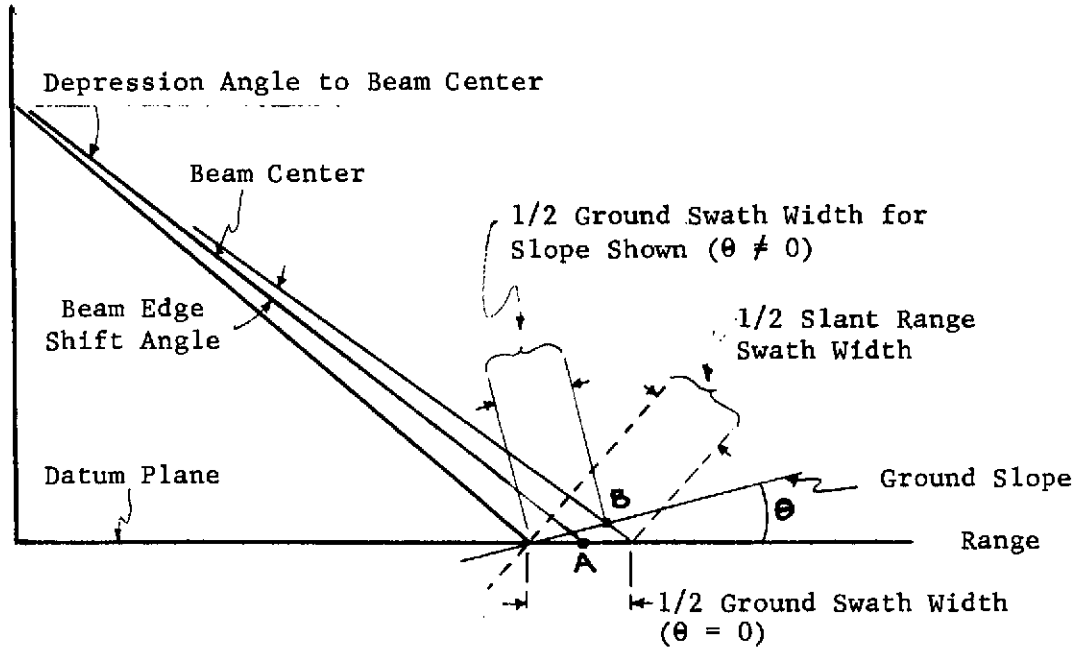

Figure 5.3.1-1. Beam Edge Shift

The radar determines relative range in radial distances from the antenna or, in effect, operates in slant range coordinates. The slant range swath width is basically set for a known depression angle to obtain a given ground range assuming no ground slope. Thus, swath width edge intercepts the ground at point "A" in Figure 5.3.1-1 for zero slope. If there is some slope of angle 0, then the beam edge shifts to point B where the antenna gain to B is different than A. These effects are not negligible as discussed in Appendix D. The impact is that backscatter measurements mode at beam edge as compared to beam center for the X-band systems are somewhat in error unless

ground slope is known or near zero. This problem is not significant for the L-band system due to the wider (five times) elevation beam pattern.

Examination of the equation in section 5.3.1.1 shows the backscatter and reflectivity coefficient are functions of the sine and tangent of the incident angle respectively. Calculations have been made ignoring these functions due to lack of incidence angle knowledge.

The ground slope angle can be determined using several techniques. (Knowledge of ground slope is sufficient for determining incidence angle since beam center depression angle is known; see Appendix D). Slope can be determined from the imagery itself provided relatively defined geographic features such as peaks and valleys are present. Then, using the effects of layover or foreshortening and shadowing, slope determinations can be made.[1] Another technique is the use of contour map. Over much of the areas for which accurate backscatter is to be determined such as agricultural land, accurate maps are available from which the ground slope can be determined.[2]

5.3.2 Calibration Technique

A calibrated series of pulses over a 60 dB range each decreasing in magnitude by about 2 dB are generated. These pulses are derived

---

[1] Geologic Evaluation of Radar Imagery from Darien Province, Panama, Harold C. McDonald - CRES TM-133-6, Univ. of Kansas Center for Research.

[2] AN/APQ-97 Radar Calibration Design Study (Conf.), April 1971, United States Army, Engineer Topographic Laboratories, Fort Belvoir, Virginia. Prepared by Westinghouse Defense and Space Center, Baltimore, Maryland.

from the transmitted output power and are injected into the receiver front ends excluding only the antenna, circulator, receiver protector and some waveguide. The antenna gain patterns are measured accurately while the other measured element losses are relatively small and stable. These calibration pulses pass through the entire radar/processor system, are treated in much the same manner as the ground received signals, ultimately appearing on the output or map film. These calibration pulses may be compared in density with the map imagery. As the attenuation of each pulse between transmitter and receiver is known, the fractional received to transmitter power may be determined for equi-density pulses. Thus, a stable, accurate calibration technique is available.

Continuous system monitoring of such parameters as transmitter power, receiver gain via the AGC voltage as well as other parameters will be monitored and transferred to the ground and recorded along with the data. This will provide a measure of general system status as well as an independent verification of reflectivity calculations.

The front end injection functional block diagram is shown in Figure 5.3.2-1. A sample of the transmitter pulse is taken through directional couplers injected into both horizontal and vertical polarization receive channels. The injected power is such that it exceeds straight leak-through by at least 20 dB and still is treated linearly by the LNA, mixer and IF preamp. The pulse is then injected into a multitap surface wave delay line. The taps are designed such that a series of pulses each 2 dB less than the preceding and 200 ns apart as shown in Figure 5.3.2-2 (a) are generated.

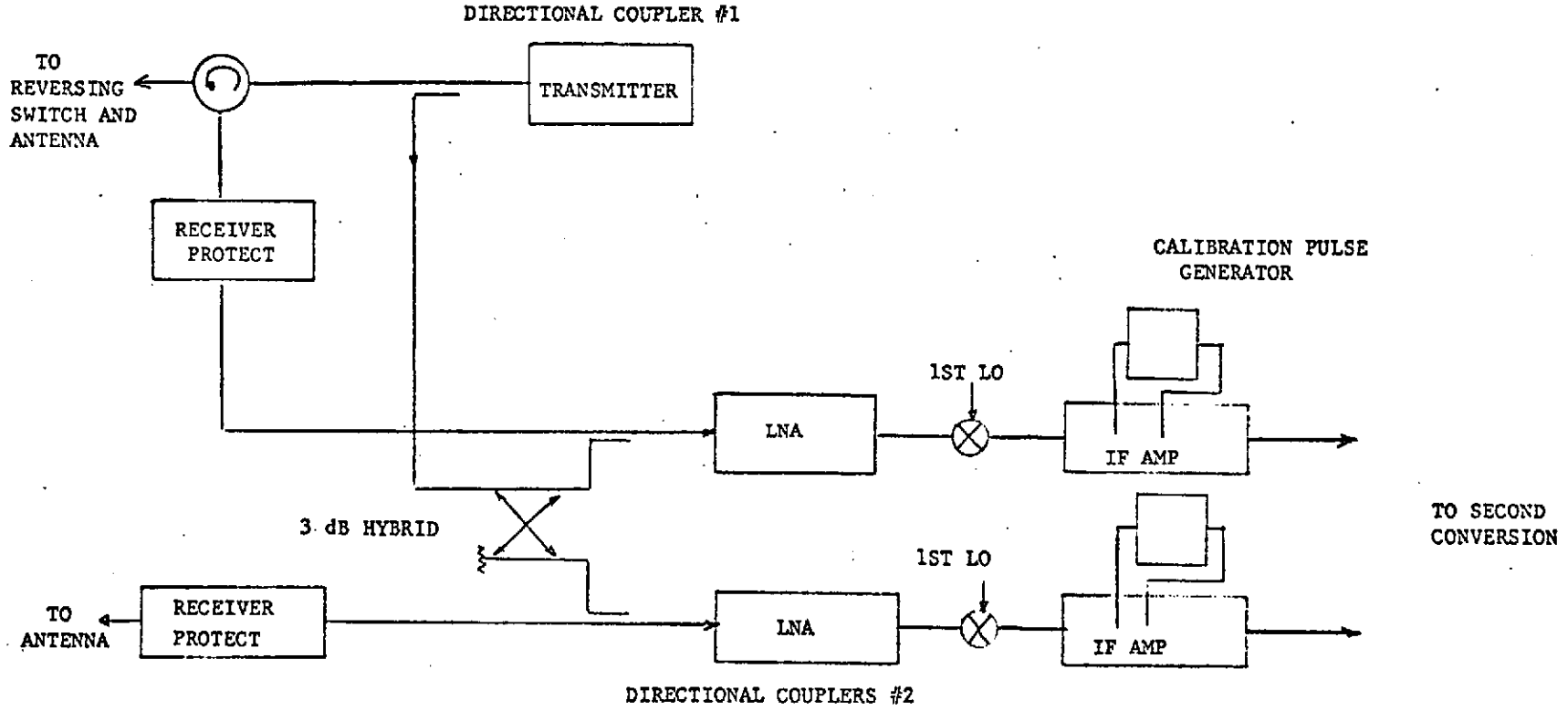

Figure 5.3.2-1. Calibration Signal Injection

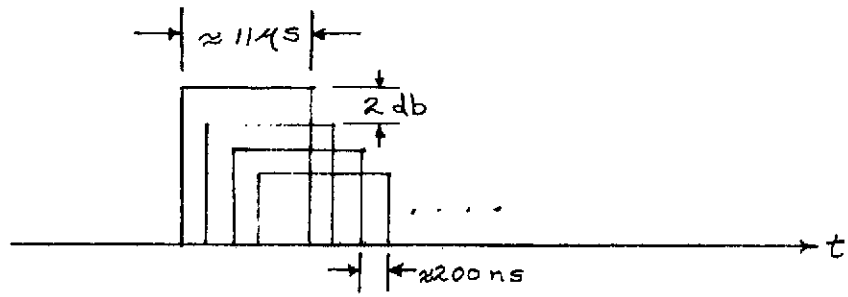

(a) Receiver Input, Expanded

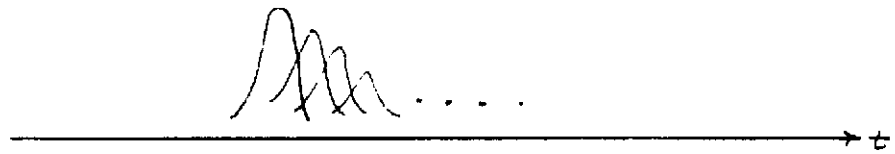

(b) Receiver Output, Compressed

Figure 5.3.2-2. Calibration Pulses

Figure 5.3.2-2(a) and (b) show the relative amplitude and suggested spacing.

The pulses are passed through the receiver just after the transmitter pulse and before the beginning of the swath width. The spacing is about two range cells. The attenuation is 2 dB/step over at least a 24 dB dynamic range. Then, pulses are laid out on the film forming continuous bands on either the near or far range side of the map film. The intrinsic non-linearities of the film as well as any in the receiver are taken into account since both calibration pulses and target histories pass through the same path. A microdenitometer can then be used to directly compare calibration bands with mapped targets.

As no azimuth phase history is included in the RF signal phase, the digital correlator phase, but not amplitude weighting, is removed for the calibration pulses only such that proper azimuth integration can occur.

Input signal strength variance over the nominal 60 dB AGC range can be introduced in one of two ways: (1) generate and process 30 or more pulses over the 60 dB range or (2) process three groups of 12 pulses each in a repetitive fashion. These two possible sequences are shown in Figure 5.3.2-3. Sequence (1) requires more time from transmitter "main bang" pulse at t_o and pulse accuracy of last 12 pulse may not be sufficient. This is because in the repetitive delay line technique, while simple and reliable, the accuracy of each pulse depends on each preceding pulse. Sequence (2) only requires accuracy be carried over 12 pulses since a separate three-step attenuator is used to get the three groups. Less time is required from t_o to start of the swath width. Each clump is generated for an integration time with blanking and coding to separate and identify each clump. A separate step attenuator is necessary, however.

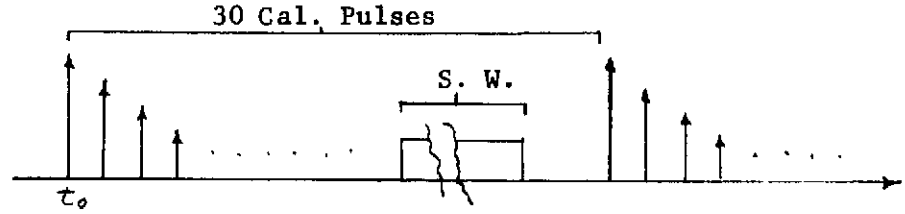

(a) Calibration Sequence (1)

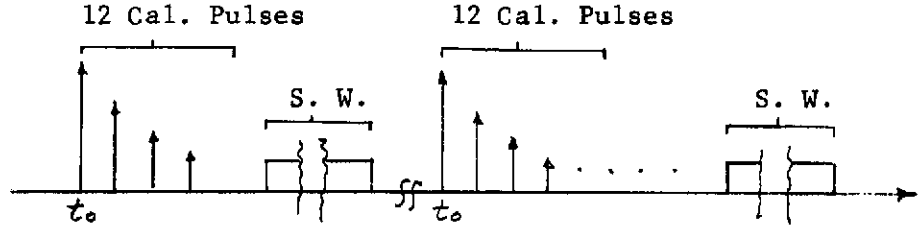

(b) Calibration Sequence (2)

Figure 5.3.2-3. Possible Calibration Sequences

In each case, a near continuous calibrated density wedge is

available to be placed on a map film for direct visual densitometric comparison or for usage in digital computer subroutines in the course of doing automatic reflectivity calculations.

5.3.2.1 Calibration Power Levels

Typically, the dynamic calibration pulse range should bracket the expected return signal level or from γ = +15 to -35 dB, a range of 50 dB, Calculation of the front end received to transmitter power ratio commensurate with these γs will then allow the desirable attenuation to be calculated. Approximate calculations for the X-band system are shown.

$$\frac{P_r}{P_t} = \frac{G^2 \lambda^2 \sigma}{(4\pi)^3 R^4}$$

where P_r = received per pulse power at LNA input

P_t = transmitted per pulse power

G = antenna gain = 44 dB

λ = wavelength = .03m = -15.22 dBm

R = Slant range = 951 Kms = +59.8 dBm

σ = $\sin \theta \, r_a \, r_g$

where γ = reflectivity coefficient

θ = depression angle = 60^o

r_a = compressed azimuth resolution

r_g = compressed ground range resolution

This equation for received power involving the compressed resolution cell as opposed to the uncompressed cell (real beam width X expanded pulse width) is used because of the way the correlator treats the calibration signal. The calibration pulses have no azimuth phase

history so to permit correlation like that from the ground, the correlation reference will be set to zero during the calibration pulse interval. Since all the calibration power will fall in one azimuth, channel equivalent compressed ground cell power should be used. One difference to be noted is that the calibration pulses do not have the antenna pattern weighting over the aperture, however, this may automatically be taken care of in the correlator/computer through knowledge of the antenna pattern scaling.

Now

$$r_a = 30m$$

$$r_r = 30m$$

so for the maximum power requirement $\gamma = +15$ dB

$$\sigma = (31.5)(\sin 60^o)\ (30m)(30m)$$

$$\sigma = 24500m^2 \Rightarrow 43.9\ dBm^2$$

so

$G^2 = 2 \times 44$ dB	88 dB	
$\lambda^2 = 2 \times (-15.2\ dBm^2)$		$-30.4\ dBm^2$
=	$+43.9\ dBm^2$	
$(4\pi)^3$ =		-33.0 dB
R^4 =		$-238\ dBm^4$
	+131.9	-301.4
		131.9
		-169.5 dB

The first pulse should be approximately -169.5 dB below the transmitte and receiver input. The calibration signal injection functional block diagram is shown in Figure 5.3.2-1. The RF directional couplers introduce 88 dB of attenuation (44 dB each coupler). This provides

sufficient isolation so as to insignficantly affect transmitter output power or receiver noise figure. The remaining 81.5 dB of attenuation is placed in the IF calibration pulse generated path. The IF calibration circuitry is made extremely gain stable. This circuitry is further described in section 5.3.2.2.

5.3.2.2 Calibration Pulse Generator

The calibration circuit required must be capable of delaying the linear FM expanded pulse in 30 successive 0.2 usec increments while attenuating each successively delayed pulse by 2 dB. The 2 dB drop in amplitude for each 0.2 usec time interval represents the rate of decrease of target amplitude with increasing time. It is necessary that both the 2 dB step and 0.2 usec interval be accurately represented for registration and calibration purposes. Because of the high accuracy, reliability and temperature stability, this requirement necessitates a surface wave device mechanization. Briefly, a surface wave device consists of an interdigitated metal structure on the surface of piezoelectric crystal substrate such as quartz. Since the information carrying waves travel on the substrate surface, they are easily sampled and controlled by this interdigitated metal structure. A sketch of the delay device is shown in Figure 5.3.2-4. It consists of an input transducer of overlapping or interdigitated metal structures and an array of output interdigitated metal transducers. The center of each succeeding output transducer is 0.2 usec greater in time delay from the input transducer and has an overlap reduction giving 2 dB greater loss. Because photolithographic techniques are very accurate, the delay and overlap requirements can be easily and reproducibly met.

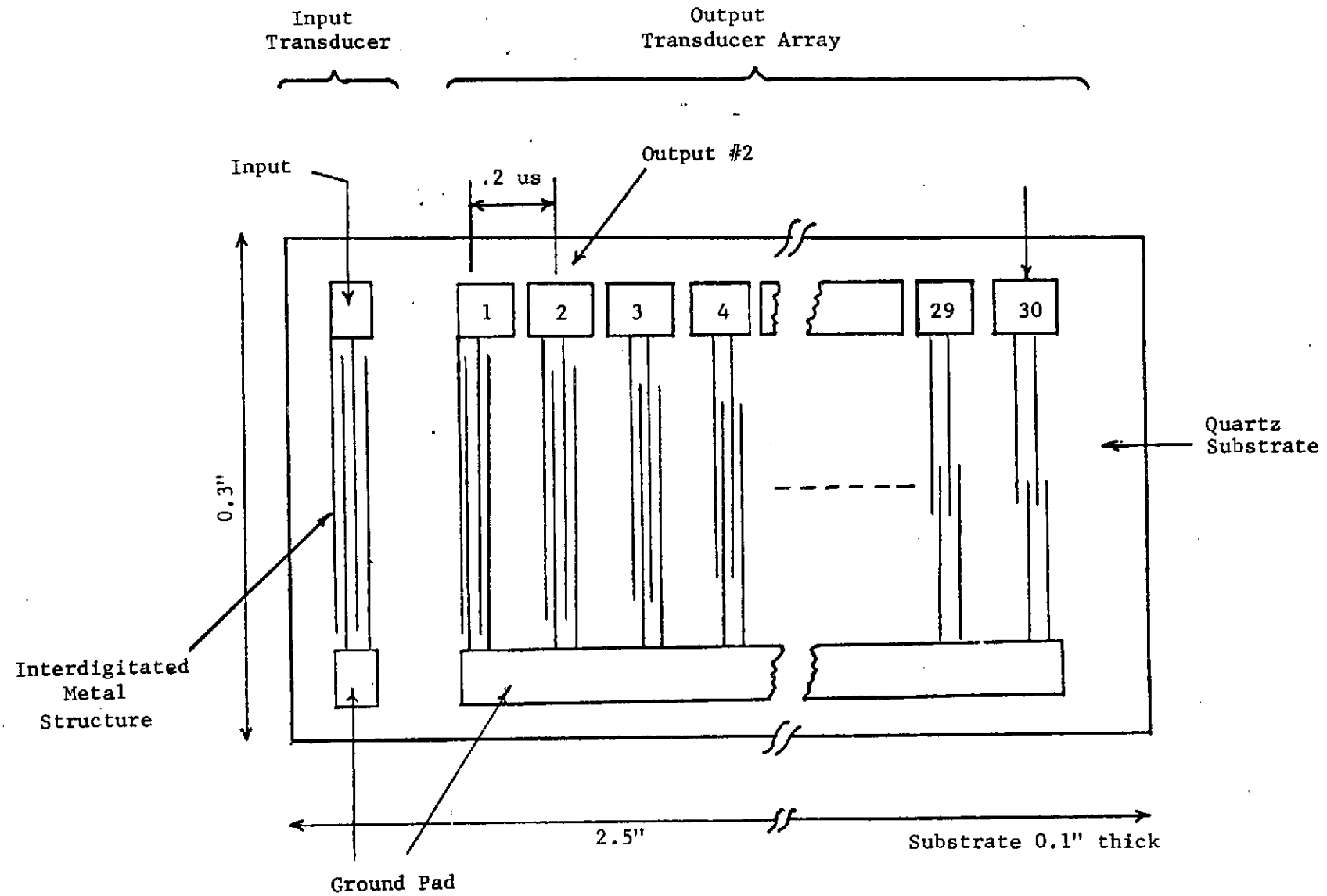

Figure 5.3.2-4. Delay Device

Westinghouse has demonstrated in-house capabilities well in excess of those required here on similar devices.

Figure 5.3.2-5 shows a block diagram of the calibration pulse generator circuit. It consists of an input drive amplifier, surface wave delay device (Figure 5.3.2-4) and output transducer summation network. The input drive amplifier raises the signal level sufficiently to drive the delay device. Care is taken in the design to preserve phase and amplitude linearity over the signal dynamic range and to have sufficient gain stability. In general, amplifiers with these bandwidth and drive requirements have phase linearity of $\pm 0.1^{o}$ and amplitude flatness of 0.2 dB. The output summation network is used for two purposes; it sums the delayed samples into a continuous pulse train and simultaneously creates isolation between output transducers. It consists of a series resistance (R_i) from each transducer connected to a low input impedance recovery amplifier. Isolation between output transducers is obtained by allowing each to have a relatively high insertion loss on the order of 50 dB and the use of the resistive summation network with 30 dB of isolation. The resultant cumulative isolation between output transducers is then on the order of 130 dB, which is more than sufficient. The recovery amplifier is a simple common base stage designed to have low noise figure (2 dB) and good gain stability. Due to the large number of resistances (30), the summation network and output amplifier would incorporate microelectronic techniques to reduce the size and weight. The delay line device itself would be mounted in a standard flat pack and hermetically sealed.

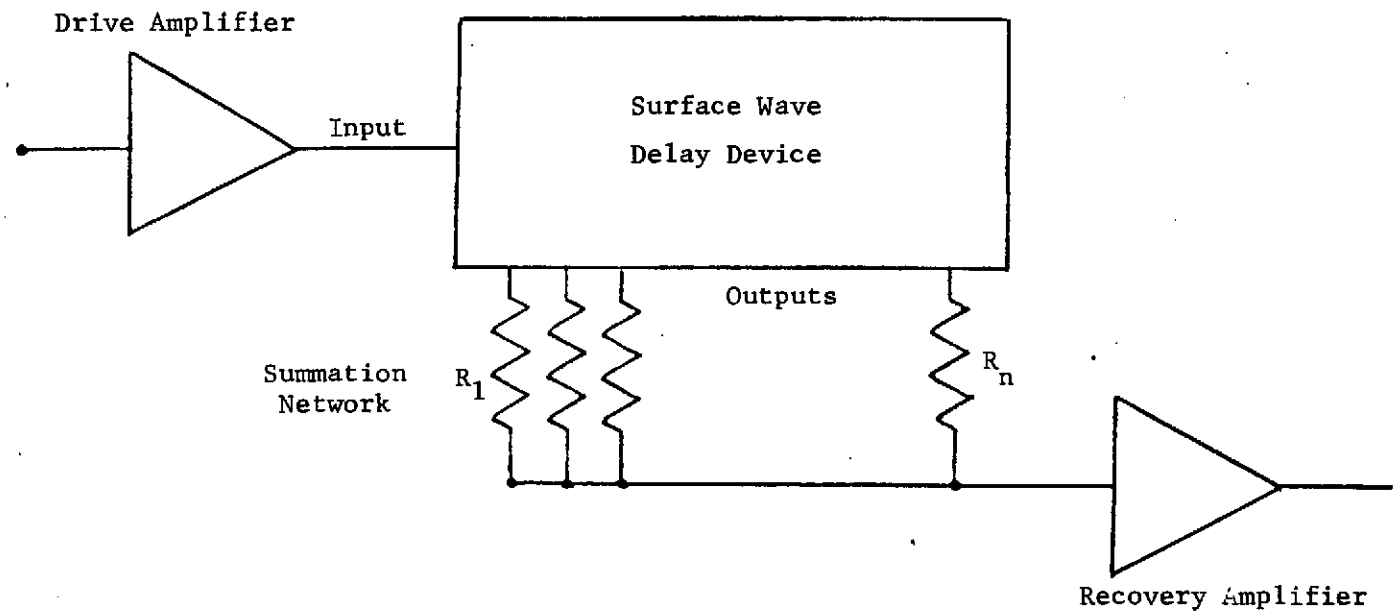

Figure 5.3.2-5. Calibration Pulse Generator

5.3.2.3 Calibration/System Interface Requirements

The techniques previously discussed require a minimum of system interfacing as the calibration pulses are carried right along with the data, thus, being subject to the same system conditions as the data. The physical interfaces are shown in Figure 5.3.2-1 where three directional couplers are used to extract a portion of the "main bang" and then reinject the attenuated version into each of the receiver channels and repetitive pulse generator.

Since the calibration pulses are always present, no turn on or off commands are necessary. As previously mentioned, technique one requires some 17 us of time prior to the start of each swath width for the calibration interval while technique two requires a 14 us calibration interval. Coding pulses are required to identify density groups. These are injected in the multiplexer. The data rate impact requirement is negligible as the calibration pulses amount to some 30 samples compared to some 1300 in the swath width.

APPENDIX A

DERIVATION OF BACKSCATTER EQUATION

1. Basic Equation

The received radar power can be determined from equation [1]:

$$P_r = \frac{P_t G^2 \lambda^2 \sigma}{(4\pi)^3 R^4} \qquad [1]$$

where P_r = per pulse received power

P_t = peak transmitted power

G = antenna gain (one way)

λ = wavelength

σ = effective cross-sectional area

R = range

The correlated received power from a SAR scatter area is the weighted sum of a number of pulses n where:

$$n = T_i f_r = \frac{\lambda R}{2 r_a v} f_r \qquad [2]$$

where T_i = integration time

f_r = repetitive rate

v = s/c velocity

r_a = ground azimuth resolution

Then the received integrated power becomes

$$Pr_n = P_r n = \frac{P_t G^2 \lambda^2 \sigma}{(4\pi)^3 R^4} \frac{\lambda R}{2 v r_a} f_r$$

$$Pr_n = \frac{P_t G^2 \lambda^3}{2(4\pi)^3 r R^3} \frac{f_r}{r_a} \sigma \qquad [3]$$

Uniform weighting was assumed for the sake of brevity. The precise formulation would result in a series using the actual weighting values.

Now

$$\sigma = \sigma^0 Ag = \sigma^0 r_a \frac{r_{rs}}{\sin \phi_i} \qquad [4]$$

and $\sigma^0 = \gamma \cos \phi_i$

where Ag = ground cross-sectional area

r_{rs} = slant range resolution cell

ϕ_i = ground incidence angle

σ^0 = backscatter coefficient

The incidence angle is shown in Figure A-1.

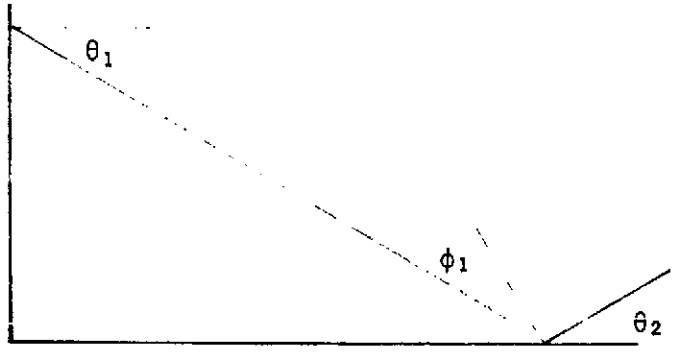

Figure A-1. Important Angles in Backscatter Determination

Note that incidence angle is only equal to the complement of the depression angle for no terrain slope ($\theta_2 = 0$).

Now

$$r_{rs} = c\tau/2 \qquad [5]$$

where τ = transmitted pulse width

c = velocity of light

The use of equations [4] and [5] in [3] results in

$$Pr_n = \frac{P_t G^2 \lambda^3}{2(4\pi)^3 R^3} \frac{f_r}{r_a} \frac{r_a c\tau}{2 \sin \phi_i} \sigma^0$$

$$= \frac{P_a G^2 \lambda^3 c}{4(4\pi)^3 R^3} \frac{\sigma^0}{\sin \phi_i} \qquad [6]$$

where $P_a = P_t f_r \tau$ = average power [7]

Now

$$\sigma^0 = \left(\frac{Pr_n}{P_a}\right) \frac{4(4\pi)^3 R^3}{G^2 \lambda^3 c} \sin \phi_i \qquad [8]$$

which is a short form equation for determining the backscatter coefficient. The reflectivity coefficient may be determined as

$$\gamma = \left(\frac{Pr_n}{P_a}\right) \frac{4(4\pi)^3 R^3}{G^2 \lambda^3 c} \tan \phi_i \qquad [9]$$

APPENDIX B

CALCULATION OF SIGNAL AND NOISE LEVELS IN RADARS USING PULSE COMPRESSION AND SYNTHETIC APERTURE

IF Signal and Noise Power

The basic radar range equation may be used to calculate the instantaneous per pulse IF signal level:

$$S_{IF} = \frac{P_{pk}\, G^2\, \lambda^2\, \sigma}{(4\pi)^3\, LR^4} \qquad [1]$$

where P_{pk} = peak transmitter power

G = antenna gain

λ = wavelength

L = system losses

R = slant range

σ = target cross-sectional area

For area targets, where σ is the reflective cross-sectional area,

$$\sigma = \frac{cT}{2} R\, \beta\, \gamma\, \tan\, \phi \equiv \sigma_u \qquad [2]$$

where T = transmitted (expanded) pulsewidth

c = velocity of light

β = antenna 3 dB azimuth beamwidth

γ = backscatter coefficient

ϕ = aspect angle = antenna depression angle (flat earth)

σ_u = uncompressed cross-sectional area

For a flat earth[1],

$$\tan \phi = \frac{H}{\sqrt{R^2 - H^2}} = \frac{H}{R} \cdot \frac{1}{\sqrt{1 - (H/R)^2}} \qquad [3]$$

where H = spacecraft altitude

The instantaneous per pulse IF area target power is thus

$$C_{IF} = \frac{P_{pk} G^2 \lambda^2 cT \beta \gamma H}{2(4\pi)^3 LR^4 \sqrt{1 - (H/R)^2}} \qquad [4]$$

The IF noise power is

$$N = kT_o B_{IF} \overline{NF} \qquad [5]$$

where kT_o = -174.4 dBm

B_{IF} = IF bandwidth

$\overline{NF}$ = noise figure

Combining [1], [4] and [5], the IF S/N and C/N values become:

$$S/N_{IF} = \frac{P_{pk} G^2 \lambda^2 \sigma}{(4\pi)^3 kT_o B_{IF} \overline{NF} LR^4} \qquad [6]$$

$$C/N_{IF} = \frac{P_{pk} G^2 \lambda^2 cT \beta \gamma H}{2(4\pi)^3 kT_o B_{IF} \overline{NF} LR^4 \sqrt{1 - (H/R)^2}} \qquad [7]$$

---

1. The flat earth approximation was used in deriving these equations. In satellite usage, range and aspect angle would be calculated for spherical earth. The conclusions reached here are valid for flat and spherical earth.

Range Compression

Range pulse compression increases peak signal power by the pulse compression ratio. To a first approximation this compression ratio equals the signal time-bandwidth product, $T\Delta F$, where ΔF equals $1/\tau$ and τ is the compressed pulsewidth. Hence, the pulse compression ratio equals T/τ.

In the case of area targets, the peak signal power is increased by T/τ, but the cross-sectional area σ is reduced in the range dimension by the same T/τ compression ratio:

$$\sigma_{\substack{\text{post range}\\ \text{compression}}} = \left(\frac{cT}{2} R \beta \gamma \tan \phi\right) \left(\frac{\tau}{T}\right) \qquad [8]$$

$$= \frac{c\tau}{2} R \beta \gamma \tan \phi$$

The net result is that post compression area target power is left unchanged from IF area target power.

From [1],

$$S_{\substack{\text{post range}\\ \text{compression}}} = \frac{T}{\tau} S_{IF}$$

$$= \frac{(T/\tau) P_{pk} G^2 \lambda^2 \sigma}{(4\pi)^3 L R^4} \qquad [9]$$

From [4],

$$C_{\substack{\text{post range}\\ \text{compression}}} = \frac{(T/\tau) P_{pk} G^2 \lambda^2 c\tau \beta \gamma H}{2(4\pi)^3 L R^4 \sqrt{1 - (H/R)^2}}$$

$$= C_{IF} \qquad [10]$$

Since the noise power is not correlated during compression,

$$N_{\substack{\text{post range}\\ \text{compression}}} = N_{IF}$$

$$= k T_o B_{IF} \overline{NF} \qquad [11]$$

Hence,

$$S/N_{\substack{\text{post range}\\ \text{compression}}} = \frac{(T/\tau)\ P_{pk}\ G^2\ \lambda^2\ \sigma}{(4\pi)^3\ kT_o\ B_{IF}\ \overline{NF}\ LR^4}$$

$$= (T/\tau)\ S/N_{IF} \qquad [12]$$

$$C/N_{\substack{\text{post range}\\ \text{compression}}} = \frac{(T/\tau)\ P_{pk}\ G^2\ \lambda^2\ c\tau\ \beta\ \gamma\ H}{2(4\pi)^3\ kT_o\ B_{IF}\ \overline{NF}\ LR^4\sqrt{1 - (H/R)^2}}$$

$$= C/N_{IF} \qquad [13]$$

From [9] and [10],

$$S/C_{\substack{\text{post range}\\ \text{compression}}} = \left(\frac{T}{\tau}\right) S/C_{IF} \qquad [14]$$

Pulse compression thus increases both S/N_{IF} and S/C_{IF} values by the compression ratio T/τ.

The fact that pulse compression does not alter the area target power may be visualized in the following manner. In the IF, area target pulses are T seconds long and of power P_{pk}. Consecutive pulses are separated in time by $\frac{1}{B_{IF}} = \tau$, the compressed pulsewidth. Hence, at any given instant, T/τ pulses of power P_{pk} overlap, making the net instantaneous power proportional to $P_{pk}\ (T/\tau)$. Compression increases the power by T/τ but compresses the expanded pulses into contiguous pulses τ long. The compressed pulses are thus non-overlapping, with each having power proportional to $P_{pk}\ (T/\tau)$.

Azimuth Compression

The same results as found above may be derived for synthetic aperture azimuth compression. The azimuth compression ratio equals the signal time-bandwidth product:

$$ACR = T_{INT}\,\Delta F \qquad [15]$$

where T_{INT} = integration time

$$= \frac{L_{INT}}{V_{s/c}}$$

$$\Delta F = \frac{2V_{s/c}^{2}}{\lambda R} \cdot T_{INT}$$

$$\left[\frac{2V_{s/c}^{2}}{\lambda R} = \frac{df}{dt} = \text{time rate of change in target doppler frequency as spacecraft flies past target}\right]$$

$V_{s/c}$ = spacecraft velocity

L_{INT} = synthetic antenna aperture formed by integration

ACR = azimuth pulse compression

Thus,

$$ACR = \frac{2V_{s/c}^{2}}{\lambda R} T_{INT}^{2} = \frac{2\,L_{INT}}{\lambda R} L_{INT} \qquad [16]$$

The compressed azimuth resolution, r_{az}, formed by the synthetic beam is

$$r_{az} = R\,\theta_{syn}$$

$$= R\,\frac{\lambda}{2\,L_{INT}} \qquad [17]$$

Hence,

$$ACR = \frac{L_{INT}}{r_{az}} \qquad [18]$$

Peak signal powers for both point target and area target signals are increased by this azimuth compression ratio.

From [17], the maximum resolution that the system can produce is achieved when

$$L_{INT} = R\beta = \text{maximum synthetic aperture that can be formed}$$

and is
$$r_{az} = \frac{\lambda R}{2L_{INT}} = \frac{\lambda}{2\beta}$$

$$= \frac{D}{2} \qquad [19]$$

where $\beta = \frac{\lambda}{D}$

D = antenna aperture

Mechanizing $L_{INT} = R\beta$ is referred to as processing the full aperture. When azimuth resolution requirements are relaxed from the maximum value of [19], the processor need process only a fraction $\frac{L_{INT}}{R\beta}$ of the full aperture to yield

$$r_{az} = \frac{D}{2} \frac{R\beta}{L_{INT}} \qquad [20]$$

where $L_{INT} = V_{s/c} T_{INT} < R\beta$ (see [15])

When the full aperture is processed, the doppler bandwidth in the processor is

$$\Delta F_D = 2 \cdot \frac{V_{s/c}}{\lambda} \sin \frac{\beta}{2}$$

$$= \frac{2 V_{s/c}}{\lambda} \beta, \quad \frac{\beta}{2} << 1 \qquad [21]$$

and the spatial frequency bandwidth is

$$\Delta F_S = \frac{\Delta F_D}{V_{s/c}} = \frac{2\beta}{\lambda} \qquad [22]$$

When a fraction $L_{INT}/R\beta$ of the full aperture is processed, and

$$\Delta F_S' = \frac{2\beta'}{\lambda}$$

where $\beta' = \frac{L_{INT}}{R}$

The processor thus need process a fraction

$$\frac{\Delta F_S'}{\Delta F_S} = \frac{2\beta'/\lambda}{2\beta/\lambda} = \frac{L_{INT}}{R\beta} \qquad [23]$$

of the total available spatial frequency bandwidth. The processor will utilize filters that pass only the necessary bandwidth to achieve the required resolution [20]. A fraction $L_{INT}/R\beta$ of the area target power is thus passed by the processor filter. The effective azimuth dimension of the area target cell, [2], hence becomes

$$R\beta \left[\frac{L_{INT}}{R\beta}\right] = L_{INT} \qquad [24]$$

As in the case of range compression, the area target cross-sectional area is compressed in the azimuth dimension by the azimuth compression ratio, L_{INT}/r_{AZ}. The post compression clutter cross-sectional area thus becomes, from [8] and [24],

$$\sigma = r_R \, R\beta \, \gamma \tan\phi \left[\frac{L_{INT}}{R\beta}\right] \left[\frac{r_{AZ}}{L_{INT}}\right]$$

$$= r_R \, r_{AZ} \, \gamma \tan\phi \equiv \sigma_c \qquad [25]$$

where $r_R = \frac{c\tau}{2}$ = range resolution

As was discussed for range compression, the IF signal consisted of overlapping pulses, each of length T, where consecutive pulses were separated by τ. Compression altered this to a series of contiguous, non-overlapping pulses, each of length τ. This situation exists in azimuth exactly as in range. Consecutive "pulses" of length L_{INT} and power P_{pk} are separated by r_{AZ}. (Consecutive "pulses" are, of course, separated by $\frac{V_{s/c}}{PRF}$. This work is based on the assumption that $r_{AZ} \geq \frac{V_{s/c}}{PRF}$.) In range the separation τ was determined from the receiver bandwidth $B_{IF} = 1/\tau$; in azimuth the separation r_{AZ} is determined from the processor spatial frequency bandwidth $\Delta F_S = 1/r_{AZ}$. The azimuth compressed "pulses" are then contiguous, non-overlapping "pulses" of length r_{AZ} and power $P_{pk}\left[\frac{L_{INT}}{r_{AZ}}\right]$. The analogy with range compression is thus complete.

The post compression (PC) area target power is, from [18], [24], and [25],

$$C_{PC} = C_{IF}\left[\frac{L_{INT}}{r_{AZ}}\right]\left[\frac{r_{AZ}}{L_{INT}}\right]\left[\frac{L_{INT}}{R\beta}\right]$$

$$= C_{IF}\left[\frac{L_{INT}}{R\beta}\right] \qquad [26]$$

$$= \frac{P_{pk}\, G^2\, \lambda^2\, cT\, \beta\, H\, \gamma}{2(4\pi)^3\, LR^4\, \sqrt{1 - (H/R)^2}}\left[\frac{L_{INT}}{r_{AZ}}\right]\left[\frac{r_{AZ}}{L_{INT}}\right]\left[\frac{L_{INT}}{R\beta}\right]$$

If the factor $(\frac{T}{\tau})$ $(\frac{\tau}{T})$ is added to include the effects of range compression,

$$C_{PC} = \frac{P_{pk}\, G^2\, \lambda^2\, r_R\, r_{AZ}\, \gamma \tan\phi}{(4\pi)^3\, L\, R^4}\left[\frac{T}{\tau}\right]\left[\frac{L_{INT}}{r_{AZ}}\right]$$

where $\tan \phi = \frac{H}{R} \frac{1}{\sqrt{1 - (H/R)^2}}$ from [3]

$$r_R = \frac{c\tau}{2} \qquad \text{from [25]}$$

If $\sigma_c \equiv$ compressed cross-sectional area

$$= r_R \, r_{AZ} \, \gamma \tan \phi \qquad [27]$$

then

$$C_{PC} = \frac{P_{pk} \, G^2 \, \lambda^2 \, \sigma_c}{(4\pi)^3 \, L \, R^4} \left[\frac{T}{\tau}\right] \left[\frac{L_{INT}}{r_{AZ}}\right] \qquad [28]$$

From this,

$$C_{PC} \propto \frac{1}{R^4 \sqrt{1 - (H/R)^2}}$$

since

$$\sigma_c \propto \tan \phi \propto \frac{1}{R \sqrt{1 - (H/R)^2}}$$

and

$$L_{INT}/r_{AZ} \propto R$$

The post compression point target signal power is, from [9] and [18],

$$S_{PC} = S_{IF} \left[\frac{T}{\tau}\right] \left[\frac{L_{INT}}{r_{AZ}}\right]$$

$$= \frac{P_{pk} \, G^2 \, \lambda^2 \, \sigma}{(4\pi)^3 \, L \, R^4} \left[\frac{T}{\tau}\right] \left[\frac{L_{INT}}{r_{AZ}}\right] \qquad [29]$$

From this,

$$S_{PC} \propto \frac{1}{R^3}$$

since $L_{INT}/r_{AZ} \propto R$

Noise, as in the case of range compression, does not correlate with anything, and its power is not increased by azimuth compression. The processor filter discussed above does, however, reduce the noise bandwidth. From [15], the processor doppler bandwidth must be

$$\Delta F_D = \frac{2\ V_{s/c}^{\ 2}}{\lambda R}\ T_{INT}$$

$$= \frac{2V_{s/c}^{\ 2}}{\lambda R}\ \frac{L_{INT}}{V_{a/c}}$$

and, since

$$r_{AZ} = \frac{\lambda R}{2\ L_{INT}}$$

then

$$\Delta F_D = \frac{V_{s/c}}{r_{AZ}} \qquad [30]$$

The processor thus reduces noise bandwidth by a factor of

$$\frac{\Delta F_D}{f_r} = \frac{V_{s/c}}{f_r}\ \frac{1}{r_{AZ}} \qquad [31]$$

and, from [11]

$$N_{PC} = N_{IF}\ \frac{V_{s/c}}{f_r}\ \frac{1}{r_{AZ}}$$

$$= k\ T_o\ \overline{NF}\ \left[B_{IF}\ \frac{V_{s/c}}{f_r}\ \frac{1}{r_{AZ}}\right] \qquad [32]$$

Final Results

The results of equations [28], [29], and [32] indicate that range and azimuth compression leaves the IF area target power unchanged except for the $L_{INT}/R\beta$ loss, increases point target signal power by the product of the range and azimuth compression ratios, and reduces noise power by narrowing the noise bandwidth.

The post compression area target/noise ratio becomes, from [28] and [32],

$$C/N_{PC} = \frac{P_{pk}\, G^2\, \lambda^2\, \sigma_c}{(4\pi)^3\, kT_o\, B_{IF}\, \overline{NF}\, L\, R^4}\ \frac{T}{\tau}\ \frac{L_{INT}}{r_{AZ}}\ \frac{f_r}{\Delta F_D}$$

From [15] and [18],

$$\frac{L_{INT}}{r_{AZ}} = T_{INT}\, \Delta F_D$$

and since

$$P_{AVE} = P_{pk}\, T\, f_r$$

$$B_{IF} = \frac{1}{\tau}$$

then

$$C/N_{PC} = \frac{P_{AVE}\, G^2\, \lambda^2\, \sigma_c}{(4\pi)^3\, kT_o\, \overline{NF}\, L\, R^4}\, T_{INT}$$

The integration time T_{INT} is

$$T_{INT} = \frac{1}{\Delta f_{CORR}} \qquad [33]$$

where Δf_{CORR} is the processor bandwidth formed by integration. (It is not

the bandwidth of the processor filter, ΔF_D.) The net result is

$$C/N_{PC} = \frac{P_{AVE}\ G^2\ \lambda^2\ \sigma_c}{(4\pi)^3\ kT_o\ \Delta f_{CORR}\ \overline{NF}\ L\ R^4} \qquad [34]$$

where $\sigma_c = r_R\ r_{AZ}\ \gamma\ \tan\ \phi$

This result is often derived by stating that IF area target/noise is

$$C/N_{IF} = \frac{P_{pk}\ G^2\ \lambda^2\ \sigma_c}{(4\pi)^3\ kT_o\ B_{IF}\ \overline{NF}\ L\ R^4}$$

where the return is considered to be that from a point target of cross-sectional area σ_c, which is the compressed cross-sectional area. This quantity is then multiplied by the number of pulses coherently integrated, $T_{INT}\ f_r$, and by the range compression ratio, T/τ. This results in

$$C/N_{PC} = \frac{P_{pk}\ G^2\ \lambda^2\ \sigma_c}{(4\pi)^3\ kT_o\ B_{IF}\ \overline{NF}\ L\ R^4}\ \frac{T}{\tau}\ T_{INT}\ f_r$$

Using $P_{AVE} = P_{pk}\ T\ f_r$

$B_{IF} = 1/\tau$

$\Delta f_{CORR} = 1/T_{INT}$

the result becomes

$$C/N_{PC} = \frac{P_{AVE}\ G^2\ \lambda^2\ \sigma_c}{(4\pi)^3\ kT_o\ \Delta f_{CORR}\ \overline{NF}\ L\ R^4}$$

which is identical to [34]. The result [34] can be further reduced by noting that

$$\Delta f_{CORR} = \frac{1}{T_{INT}} = \frac{V_{s/c}}{L_{INT}}$$

and that $$L_{INT} = \frac{\lambda R}{2 r_{AZ}}$$

Thus,

$$C/N_{PC} = \frac{P_{AVE}\ G^2\ \lambda^3\ r_R\ \gamma\ H}{2(4\pi)^3\ kT_o\ \overline{NF}\ L\ V_{a/c}\ R^4\ \sqrt{1 - (H/R)^2}}$$

The post compression signal/noise ratio becomes, from [29] and [32],

$$S/N_{PC} = \frac{P_{pk}\ G^2\ \lambda^2\ \sigma}{(4\pi)^3\ kT_o\ B_{IF}\ \overline{NF}\ L\ R^4} \left[\frac{T}{\tau}\right] \left[\frac{L_{INT}}{r_{AZ}}\right] \frac{f_r}{\Delta F_D}$$

Again using

$$\frac{L_{INT}}{r_{AZ}} = T_{INT}\ \Delta F_D$$

$$P_{AVE} = P_{pk}\ T\ f_r$$

$$B_{IF} = 1/\tau$$

$$T_{INT} = \frac{1}{\Delta f_{CORR}}$$

the final result becomes

$$S/N_{PC} = \frac{P_{AVE}\ G^2\ \lambda^2\ \sigma}{(4\pi)^3\ kT_o\ \Delta f_{CORR}\ \overline{NF}\ L\ R^4} \qquad [36]$$

and, with

$$\Delta f_{CORR} = \frac{2\ V_{s/c}\ r_{AZ}}{\lambda R}$$

$$S/N_{PC} = \frac{P_{AVE}\ G^2\ \lambda^2\ \sigma}{2(4\pi)^3\ kT_o\ V_{s/c}\ r_{AZ}\ \overline{NF}\ L\ R^3} \qquad [37]$$

As was the case in area target/noise, [36] may be derived by multiplying S/N_{IF}, [6], by the range compression ratio T/τ and by the number of pulses coherently integrated, $T_{INT}\ f_r$:

$$S/N_{PC} = \frac{P_{pk}\ G^2\ \lambda^2\ \sigma}{(4\pi)^3\ kT_o\ B_{IF}\ \overline{NF}\ L\ R^4}\ \frac{T}{\tau}\ T_{INT}\ f_r$$

$$= \frac{P_{AVE}\ G^2\ \lambda^2\ \sigma}{(4\pi)^3\ kT_o\ \Delta f_{CORR}\ \overline{NF}\ L\ R^4}$$

which is identical to [36].

In comparing the C/N_{PC} and S/N_{PC} equations, note that [34] for C/N and [36] for S/N are of identical form. The only difference is the cross-sectional area σ: a constant value is used for S/N and a variable value $r_R\ r_{AZ}\ \gamma\ \tan\phi$ is used for C/N. Also, whereas C/N is proportional to $1/R^4$ $(H/R << 1)$[1], S/N is proportional to $1/R^3$ for a constant r_{AZ}. If r_{AZ} is proportional to range, then S/N will be proportional to $1/R^4$ again. Finally, range and azimuth compression increases the S/C_{IF} ratio by the product of the range and azimuth compression ratios (and by the loss factor $L_{INT}/R\beta$).

---

1. C/N is proportional to $1/R^3$ when the equation includes a factor of $\tan\phi$; see Appendix D.

APPENDIX C

DERIVATION OF BACKSCATTER EQUATION

Basic Equation

The received radar power can be determined from equation [1]:

$$P_r = \frac{P_t G^2 \lambda^2 \sigma}{(4\pi)^3 R^4} \qquad [1]$$

where P_r = per pulse received power

P_t = peak transmitted power

G = antenna gain (one way)

λ = wavelength

σ = effective cross-sectional area

R = range

The correlated received power from a SAR scatter area is the weighted sum of a number of pulses n where

$$n = T_i f_r = \frac{\lambda R}{2 r v_a} f_r \qquad [2]$$

where T_i = integration time

f_r = repetitive rate

v = s/c velocity

r_a = ground azimuth resolution

Then the received integrated power becomes

$$Pr_n = P_r\, n = \frac{P_t\, G^2\, \lambda^2\, \sigma}{(4\pi)^3\, R^4}\ \frac{\lambda R}{2vr_a}\ f_r$$

$$Pr_n = \frac{P_t\, G^2\, \lambda^3}{2(4\pi)^3\, R^3}\ \frac{f_r}{r_a}\ \sigma \qquad [3]$$

Uniform weighting was assumed for the sake of brevity. The precise formulation would result in a series using the actual weighting values.

Now,

$$\sigma = \sigma^0\ Ag = \sigma^0\ r_a\ \frac{v_{rs}}{\sin \phi_i} \qquad [4]$$

and $$\sigma^0 = \gamma \cos \phi_i$$

where Ag = ground cross-sectional area

r_{rs} = slant range resolution cell

ϕ_i = ground incidence angle

σ^0 = backscatter coefficient

The incidence angle is shown in Figure C-1.

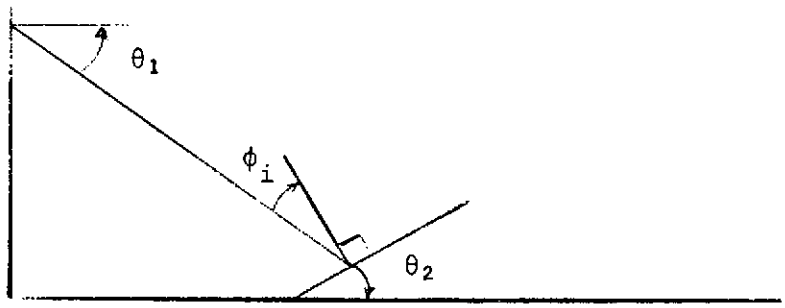

Figure C-1. Important Angles in Backscatter Determination

Note that incidence angle is only equal to the complement of the depression angle for no terrain slope ($\theta_2 = 0$).

Now

$$r_{rs} = \frac{c\tau}{2} \qquad [5]$$

where τ = transmitted pulse width

c = velocity of light

The use of equations [4] and [5] in [3] results in

$$Pr_n = \frac{P_t G^2 \lambda^3}{2(4\pi)^3 R^3} \frac{f_r}{r_a} \frac{r_a c\tau}{2 \sin \phi_i} \sigma^0$$

$$= \frac{P_a G^2 \lambda^2 c}{4(4\pi)^3 R^3} \frac{\sigma^0}{\sin \phi_i} \qquad [6]$$

where $P_a = P_t f_r \tau$ = average power [7]

Now

$$\sigma^0 = \left(\frac{Pr_n}{P_a}\right) \frac{4(4\pi)^3 R^3}{G^2 \lambda^3 c} \sin \phi_i \qquad [8]$$

which is a short form equation for determining the backscatter coefficient. The reflectivity coefficient may be determined as

$$\gamma = \left(\frac{Pr_n}{P_a}\right) \frac{4(4\pi)^3 R^3}{G^2 \lambda^3 c} \tan \phi_i \qquad [9]$$

APPENDIX D

SIGNAL/NOISE AND DEPRESSION ANGLE RELATIONSHIPS

SSAR Signal-to-Noise

The system specifications call for a specific ground range resolution, r_{rg}. Various system tradeoffs have resulted in different depression angles. As it happens, an increase in depression angle results in an increase in IF or receiver bandwidth, but does not (for a fixed average power) result in loss of S/N due to the increase in IF bandwidth.

Point Targets

There are several ways to derive the S/N relationship for a SAR in terms of average power; one is shown below.

$$\left(\frac{S}{N}\right)_{\text{per pulse}} = \frac{P_{pk}\, G^2\, \lambda^2\, \sigma}{(4\pi)^3\, FKT\, B_{IF}\, R^4} \qquad [1]$$

where B_{IF} = IF bandwidth

and the other parameters need not be defined as they are in common usage. Now the net S/N after processing is improved by the number of pulses integrated, n. So,

$$\frac{S}{N} = \left(\frac{S}{N}\right)_{\text{per pulse}} n \qquad [2]$$

where n = number of pulses integrated = $T_i\, f_r$

T_i = integration time

f_r = PRF

and $P_{avg} = P_{pk}\, d = P_{pk}\, \tau\, f_r$

Equation [1] becomes

$$\frac{S}{N} = \frac{P_{avg}\, G^2\, \lambda^2\, \sigma}{(4\pi)^3\, FKT\, R^4} \cdot \frac{T_i\, f_r}{\tau\, f_r\, B_{IF}}$$

and since

$$\tau \simeq \frac{1}{B_{IF}}$$

$$T_i \simeq \frac{1}{\Delta f_o}$$

where Δf_o = correlator bandwidth

so

$$\frac{S}{N} = \frac{P_{avg}\, G^2\, \lambda^2\, \sigma}{(4\pi)^3\, FKT\, R^4} \cdot \frac{1}{\Delta f_o} \qquad [3]$$

Therefore, regardless of the IF BW, as long as correlator bandwidth and average power are held constant, S/N does not change.[1] If the number of integrated pulses (n) is constant, then according to Equation [2], $(S/N)_{per\ pulse}$ is constant and so peak power is directly proportional to IF bandwidth.

An alternate derivation of integrated signal-to-noise using a SAR system with pulse compression

$$\frac{S}{N} \propto \frac{P_{pk}}{B_{IF}} \cdot ACR \cdot RCR \qquad [4]$$

---

1. For a constant σ; i.e., a point target.

where ACR = azimuth compression ratio = $\frac{f_r}{\Delta f_o}$

RCR = range compression ratio = $\frac{\tau_u}{\tau_c}$

τ_u = uncompressed pulse width

τ_c = compressed pulse width

Then,

$$\frac{S}{N} \propto \frac{P_{pk}}{B_{IF}} \cdot \frac{f_r}{\Delta f_o} \frac{\tau_u}{\tau_c} \qquad [5]$$

since $B_{IF} \simeq \frac{1}{\tau_c}$

$$\frac{S}{N} \propto \frac{P_{pk} f_r \tau_u}{\Delta f_o} = \frac{P_{pk} d}{\Delta f_o} = \frac{P_{avg}}{\Delta f_o} \qquad [6]$$

Again, since Equation [6] is independent of IF bandwidth, Equation [4] is also, and for a constant ACR, RCR must be directly proportional to IF bandwidth.

Area Targets

Since for clutter (area targets as opposed to discrete point targets)

$$\sigma_c = A \sigma_o = r_{rg} r_a \gamma \sin \phi \qquad [7]$$

where r_{rg} = ground range = $\frac{r_s}{\cos \phi}$ [8]

as shown in Figure D-1.

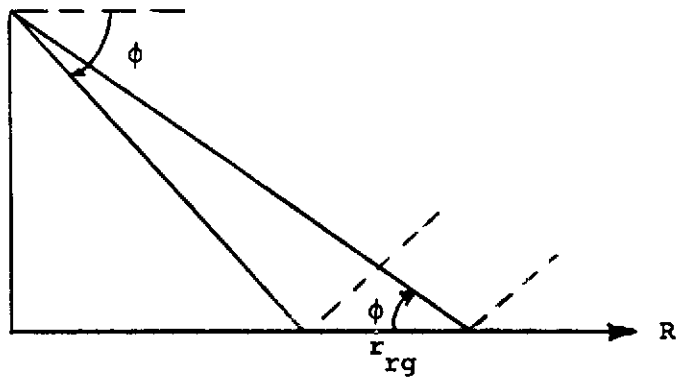

Figure D-1. Slant Range/Ground Range Relationship

or $$\sigma_c = r_{rs}\, r_a\, \gamma \tan \phi \qquad [9]$$

Substituting Equation [7] into [6]:

$$\frac{C}{N} = \frac{P_{avg}\, G^2\, (\lambda^2)\, r_{rg}\, r_a\, \gamma \sin \phi}{(4\pi)^3\, FKT\, R^4\, \Delta f_o} \qquad [10]$$

Substituting Equation [9] into [6]:

$$\frac{C}{N} = \frac{P_{avg}\, G^2\, \lambda^2\, r_{rs}\, r_a\, \gamma \tan \phi}{(4\pi)^3\, FKT\, R^4\, \Delta f_o} \qquad [11]$$

Now

$$r_{rs} = \frac{c\tau}{2} = \frac{c}{2B_{IF}} \qquad [12]$$

Then Equation [11] becomes

$$\frac{C}{N} = \frac{P_{avg}\, G^2\, \lambda^2\, \gamma \tan \phi\, c}{2(4\pi)^3\, FKT\, R^3\, 2v\, B_{IF}} \qquad [13]$$

where $$T_i = \frac{1}{\Delta f_o} = \frac{R\lambda}{2v\, r_a} \qquad [14]$$

was used.

It would appear that for a constant ground range resolution r_{rg}, r_s must get smaller as the depression angle increases (Equation [8]), thus causing an increase in IF bandwidth (Equation [12]) and decrease in C/N. This is not quite true since B_{IF} is a function of ϕ, so combining Equations [8] and [12] results in

$$B_{IF} = \frac{c}{2r_{rg} \cos \phi} \qquad [15]$$

and substituting Equation [15] into [13]

$$\frac{C}{N} = \frac{P_{avg} G^2 \lambda^2 \gamma r_{rg} \sin \phi}{(4\pi)^3 FKT R^3 2v} \qquad [16]$$

Equation [16] indicates that for an increase in depression angle the direct increase in C/N is due to the change in sin ϕ for a constant ground range resolution r_{rg}. Incidentally, the slant range resolution pulse width and IF bandwidth may decrease and increase respectively due to a depression angle change, but this does not directly cause a change in C/N. This can also be seen in Equation [10] which only involves ground range and Δf_o which is a function of azimuth resolution. Also, as previously mentioned, a constant ground range resolution requirement may result in a shorter pulse width and wider IF bandwidth; however, the critical tradeoff exists in the area of A/D capability, not S/N.

A fairly complete set of equations for discrete and area target power at various stages of processing along with signal-to-noise ratios are derived in Appendix B.

APPENDIX E

GAIN VARIATION OVER SLOPED EARTH

This appendix calculates the effects on imagery of a sloping earth terrain. In the nominal situation, the earth is assumed to be spherical, as in Figure E-1. Then, antenna peak gain is directed at a given depression angle, nominally 60°, and the receiver on/off gating is adjusted to accept signals returning from ranges between R_1 and R_2. A certain swath on the ground is then illuminated and is contained within a given antenna beamwidth, nominally ± 20 mr for the X-band systems proposed here.

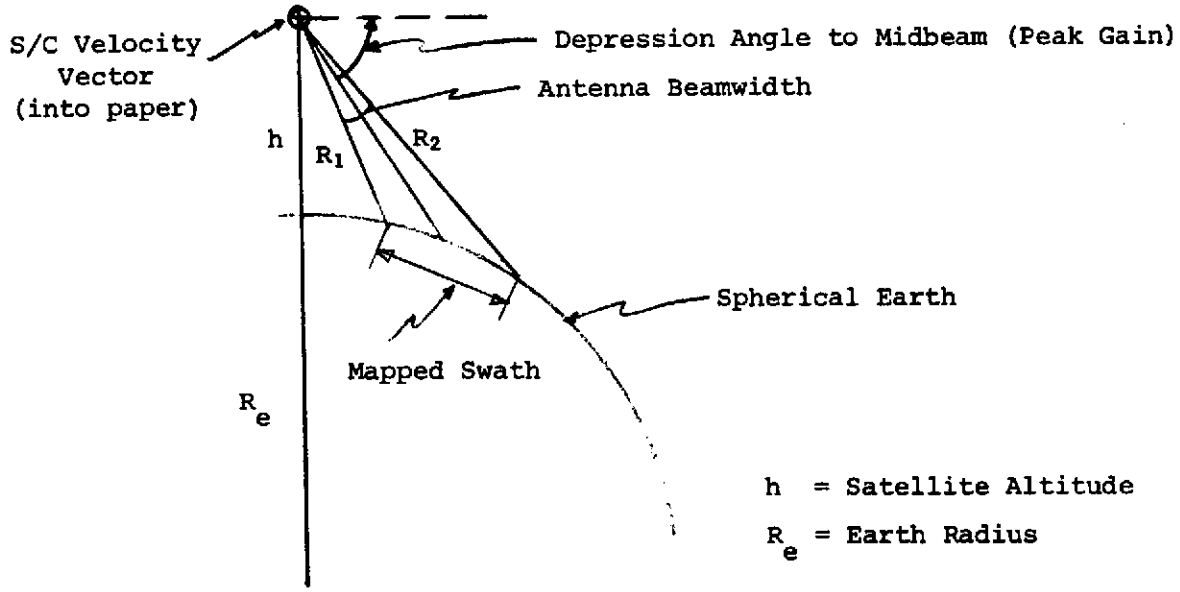

Figure E-1. Nominal Spherical Earth Geometry

The antenna gain variation over the ground swath is then known and can be taken into account in various measurements, such as backscatter coefficient measurements. If, however, the earth is not spherical over the swath being illuminated, the antenna gain variation over the swath will change. For example, Figure E-2 except that an elevation slope has been introduced over part of the swath. Here, the earth is still spherical from the near swath edge to mid-swath, but it is flat from the swath center on, inclined at an angle X with respect to a line tangent to the earth at mid-swath. In practice, this would correspond to gently rising terrain. The receiver on/off

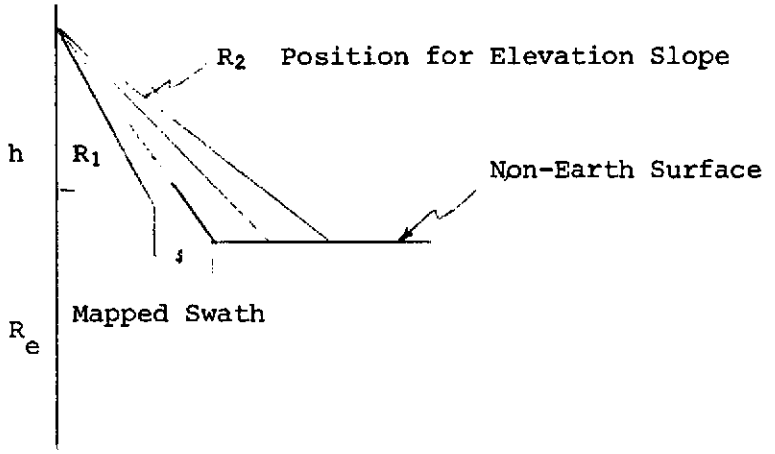

Figure E-2

gating remains adjusted to accept signals returning from ranges between R_1 and R_2, as in Figure E-1. Range R_1 still defines the same near swath edge as in Figure E-1, since the earth remains spherical in this region. Range R_1, however, due to the changed earth shape, now intercepts the earth at a point farther from mid-swath than it did in Figure E-1. The beamwidth 0 between mid-swath range R_0 and range R_2 is now greater than 20 mr, and

the antenna gain variation over this swath section is altered from what it was for the spherical earth case of Figure E-1. Map measurements requiring detailed knowledge of the antenna gain variations over the swath would then be in error.

These effects have been studied for the geometry of Figure E-2. Slant ranges for the spherical earth are calculated as in Figure E-3 as follows:

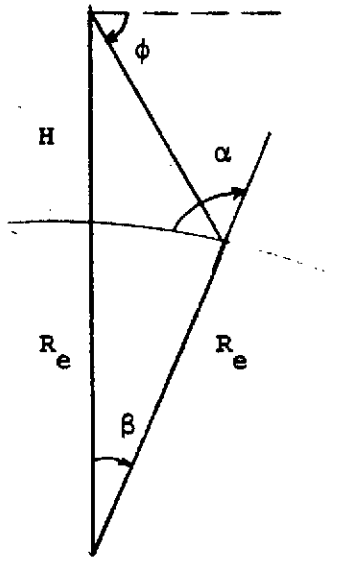

Figure E-3. Spherical Earth Range Calculation

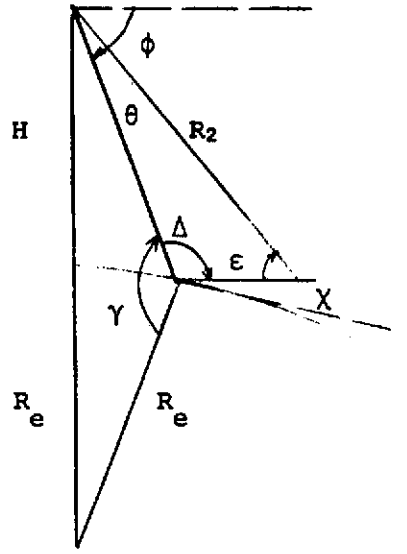

Figure E-4. Distorted Earth Angle Calculation

$$\frac{\sin}{H + R_e} = \frac{\cos \phi}{R_e}$$

$$\sin = (1 + H/R_e) \cos \phi$$

$$\beta = \alpha - (\frac{\pi}{2} - \phi)$$

$$R_x = R \sin \beta / \cos \phi$$

The half-beamwidth ϕ between mid-swath range R_0 and range R_2 is calculated as in Figure E-4 as follows:

$$\Delta = 2\pi - \gamma - \frac{\pi}{2} - \chi$$

$$\frac{\sin G}{R_1} = \frac{\sin \Delta}{R_2}$$

$$\phi = \pi - \varepsilon - \Delta$$

Results of these calculations appear in Table E-1. Since the slope is assumed to extend over the entire half-swath (~20 km), slopes of 5° are considered greater than those that would be encountered in practice. The beamwidth variations correspond to swath edge antenna gain differences of 2-3 dB from the spherical earth gains.

This example is, of course, only one of the deviations from a spherical earth that can cause antenna gain variations over the swath. It is, however, representative of the effects encountered.

TABLE E-1

ANGLE ERROR FOR DISTORTED EARTH
[0 - 20] mr

INCLINATION ANGLE χ	DEPRESSION ANGLE ϕ		
	45°	60°	75°
1°	1 mr	1 mr	1 mr
2°	2	2	3
3°	2	2	4
4°	3	3	6
5°	4	4	8
6°	5	5	10
7°	6	6	13
8°	7	7	16
9°	8	8	19
10°	9	10	23

APPENDIX F

AZIMUTH AMBIGUITY CALCULATION

A key design requirement is the range and azimuth ambiguity level. The following discussion will briefly discuss attaining a specified azimuth ambiguity level commensurate with other system constraints.

Many clutter elements are illuminated by an antenna looking broadside to the line of flight. The antenna beamwidth

$$\beta \cong \frac{\lambda}{d}$$

where λ = wavelength

d = real aperture

provides illumination for the elements within this beamwidth; thus, the doppler spectrum becomes

$$\Delta f = \frac{2v}{d} \beta_a = \frac{2v}{\lambda} \frac{\lambda}{d} = \frac{2v}{d}$$

as shown in Figure F-1(a).

Considering the CW return clutter process as some time function f(t) and then impulsing it with some periodic sampling or pulsing functions s(t), the resultant function is

$$f_o(t) = f(t)\ s(t)$$

or in the frequency domain

$$F_o(w) = F(w) * S(w)$$

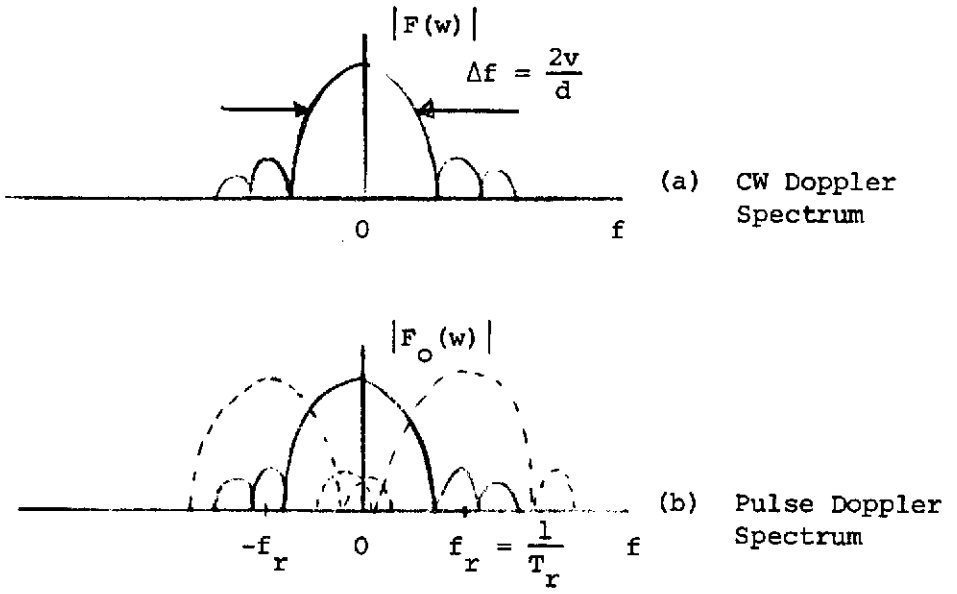

Figure F-1. Spectra

This spectra is shown in Figure F-1(b). The convolution (sampling) process produces overlapping microstructure spectra each of "width" Δf and separated by the sampling (PRF) frequency.

Note that if the antenna pattern were rectangular, then the subtended scatterers would provide doppler information lying with a rectangular spectrum of width

$$\Delta f = \frac{2v}{d}$$

The sampled spectra would overlap when

$$f_r = \frac{2v}{d}$$

which in a crude sense is a limiting PRF condition. Alternately, two pulses are transmitted for movement of one real aperture length along

the flight path. So,

$$2v\ T_r = 2\ \frac{v}{f_r} = 2\ \frac{v}{2v}\ d = d$$

It is well known that for a sidelooking synthetic aperture radar

$$r_a = \frac{R\lambda}{2v\ T_i}$$

where r_a = azimuth resolution

R = offset slant range

T_i = integration time

Note that if the entire real beamwidth is used to form the synthetic aperture

$$T_i = \frac{R\beta}{v} = \frac{R\lambda}{vd}$$

and

$$r_a = \frac{R\lambda}{2v\ T_i} = \frac{R_\lambda}{2v\ R_\lambda}\ vd = \frac{d}{2}$$

and the limiting resolution in half the real aperture. It is also known the frequency time slope is

$$\left| \frac{\Delta f}{\Delta t} \right| = \frac{2v^2}{R\lambda}$$

The portion of the spectrum utilized (for reasonably high TBP) is

$$\Delta f \cong \left| \frac{\Delta f}{\Delta T} \right| T_i = \frac{2v^2}{R\lambda}\ \ \frac{R_\lambda}{2v\ r_a} = \frac{v}{r_a}$$

That is, if one is interested in obtaining a specified resolution r_a, one must process bandwidth Δf. The equations are for uniform spectra and the

-4 dB point on the compressed result. Weighting, of course, decreases the resolution. Note also if the entire PRF interval is processed (assuming uniform spectra) and the entire spectrum were just filled

$$r_a = \frac{v}{\Delta f} = \frac{v}{f_r} = \frac{v}{2v/d} = \frac{d}{2}$$

So, if the entire spectrum is utilized ($\Delta f = f_r$), again the limiting resolution occurs.

The equation $\Delta f = \frac{v}{r_a}$ is essential in realistic system design since one of the primary constraints on system design is the azimuth ambiguities which occur when adjacent PRF spectra are within the processed bandwidths. The designer then directly trades off ambiguity level for processed bandwidth (Figure F-2).

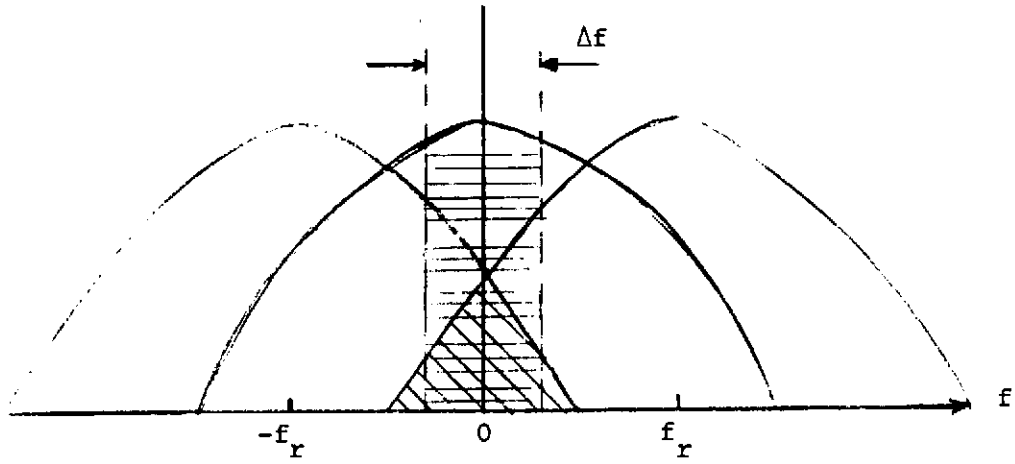

Figure F-2. Processed Bandwidth

Further, such a graph indicates directly the multilook concept in that for a given ambiguity level the processed bandwidth Δf may be subdivided into several smaller bandwidths of poorer resolution.

It should be apparent that working with rectangular spectra and limiting case resolutions and PRF's does not take into account realistic spectra shape and simply does not allow actual ambiguities to be calculated and realistic design tradeoffs to be made.

Azimuth Ambiguity Evaluation

In this section the actual azimuth ambiguity level for the X-band only radar system will be calculated.

The radar doppler spectrum is drawn in Figure F-3. The spectral amplitude is, of course, just the antenna azimuth pattern interpreted for the s/c velocity of 7.6 Km/sec. with a 13.5 ft. unweighted azimuth antenna aperture. Since the aperture is unweighted, peak sidelobe level is 26 dB below peak mainlobe. Also sketched in Figure F-3 is one of the ambiguous doppler spectra that appear at multiples of the PRF. A PRF of 4.0 KHz is used here; note that this centers the ambiguous doppler spectrum such that a null appears near the center of the processed bandwidth. A processed bandwidth of 1.8 KHz is also indicated in Figure F-3. This bandwidth is adequate to process nine azimuth looks[1].

---

1. Note that for multilook operation the vehicle should move far enough to give uncorrelated looks at the target. For a correlation time τ_c commensurate with the clutter bandwidth Δf

$$\tau_c \simeq \frac{1}{\Delta f} = \frac{d}{2v}$$

The flight distance during this time is

$$v\tau_c = \frac{vd}{2v} = \frac{d}{2}$$

so the antenna must move at least one-half the real aperture for more than one look.

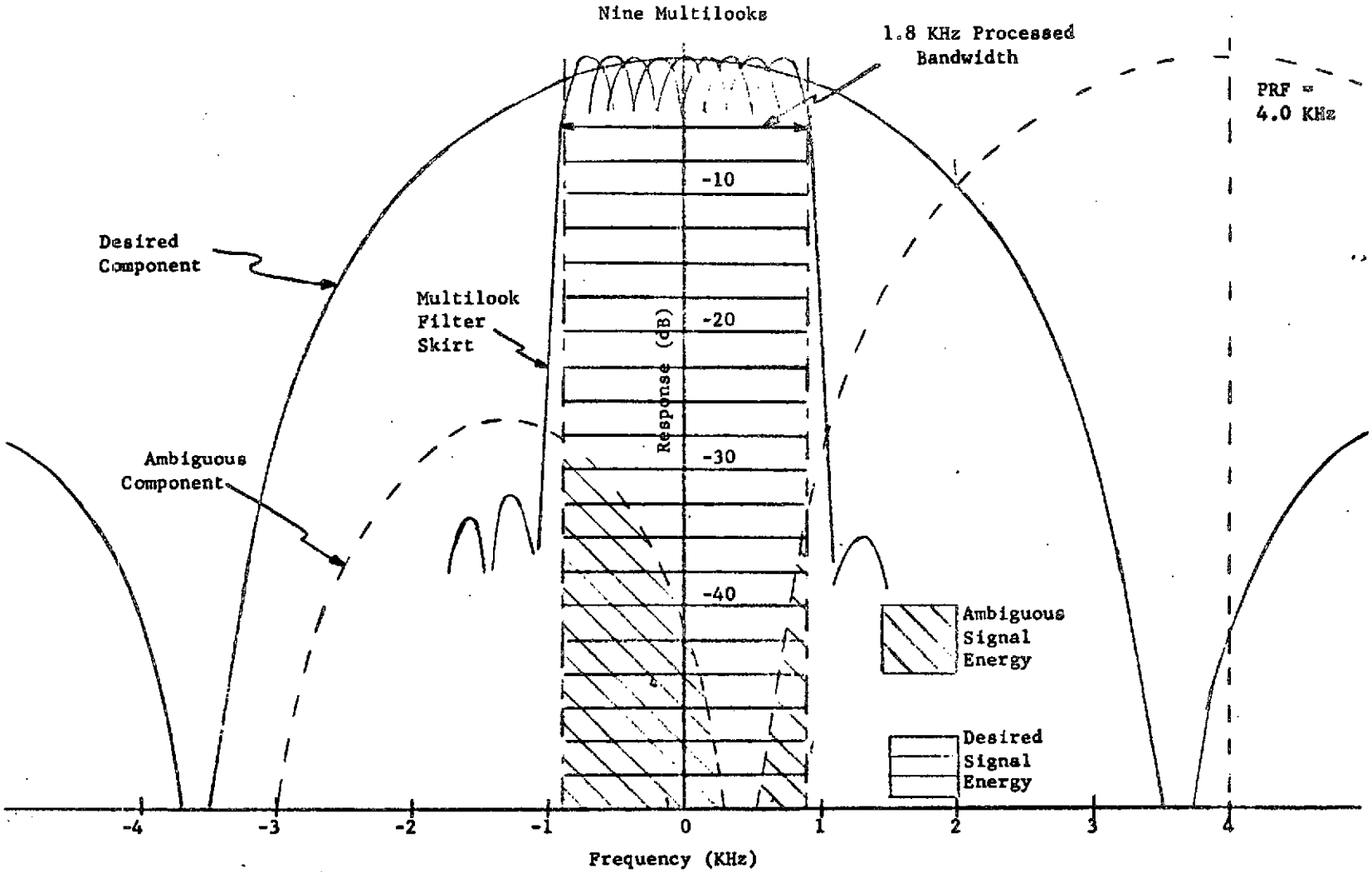

Figure F-3. Doppler Spectrum

Some of the ambiguous doppler spectrum lies within the processed bandwidth. The azimuth ambiguity level is the ratio of the total spectral energy of the ambiguous signal contained within the processed bandwidth to the total spectral energy of the desired signal contained within the processed bandwidth. These energies are found, of course, by integrating the spectral densities of Figure F-3 over the processed bandwidth. Placing the null of the ambiguous spectrum near the center of the processed bandwidth helps minimize the azimuth ambiguity level. When this integration is carried out, the resulting ratio is -30 dB. The passband is, of course, not square as is shown in Figure F-3, but is defined by the frequency response of the multilook filters. The positions of the nine multilook filters are sketched in Figure F-3, and the actual response of one (the one with the worst ambiguity level) is sketched in also.

Summary

Using the equation $\Delta f = \frac{v}{r_a}$ results in processed bandwidth

$$\Delta f = \frac{7600 \text{ m/s}}{30\text{m}} = 252 \text{ Hz}$$

allowing 40% for resolution degradation due to weighting

$$\Delta f_a \cong (1.4)\ (252) \cong 350 \text{ Hz}$$

For five spectrally contiguous multilooks the spectrum required is

$$\Delta f_T = 5\ \Delta f_a \cong 1750 \text{ Hz}$$

as directed in Figure F-3.

NOTE: The processing bandwidth design equation used is $\Delta f = \frac{v}{r_a}$, not the limiting case equation $\Delta f = \frac{2v}{d}$ and

$$\frac{v}{r_a} < \frac{2v}{d} = \frac{2(7600\ m/s)}{(4.12m)} = 3700\ Hz$$

$$1750\ Hz < 3700\ Hz$$

APPENDIX G

ANTENNA SWITCHING

Configuration 1 utilizes a high reliability waveguide switch. The precise implementation of said switch is subject to some question. Mechanical switches of this type have been space qualified for Skylab; however, the potential reliability improvement of a solid state configuration is desirable.

Desirable electrical and mechanical characteristics are given in the table below.

RF SWITCH CHARACTERISTICS	
P_{peak}	~ 5 KW
P_{avg}	~ 150 W
Frequency	9.5 GHz
Loss	< -.1 dB
Bandwidth	$\geq$ 100 MHz
Isolation	$\geq$ 26 dB
Weight	$\leq$ 2.5 lbs.
Power	$\leq$ 3 W

A solid state candidate is shown in Figure G-1.

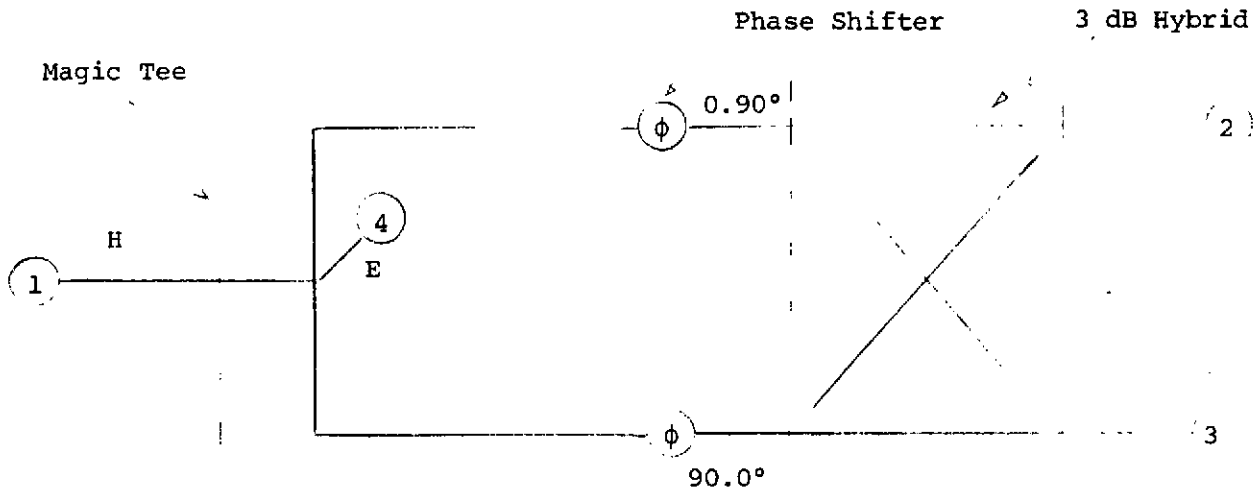

(a) Four Port Solid State Microwave Switch

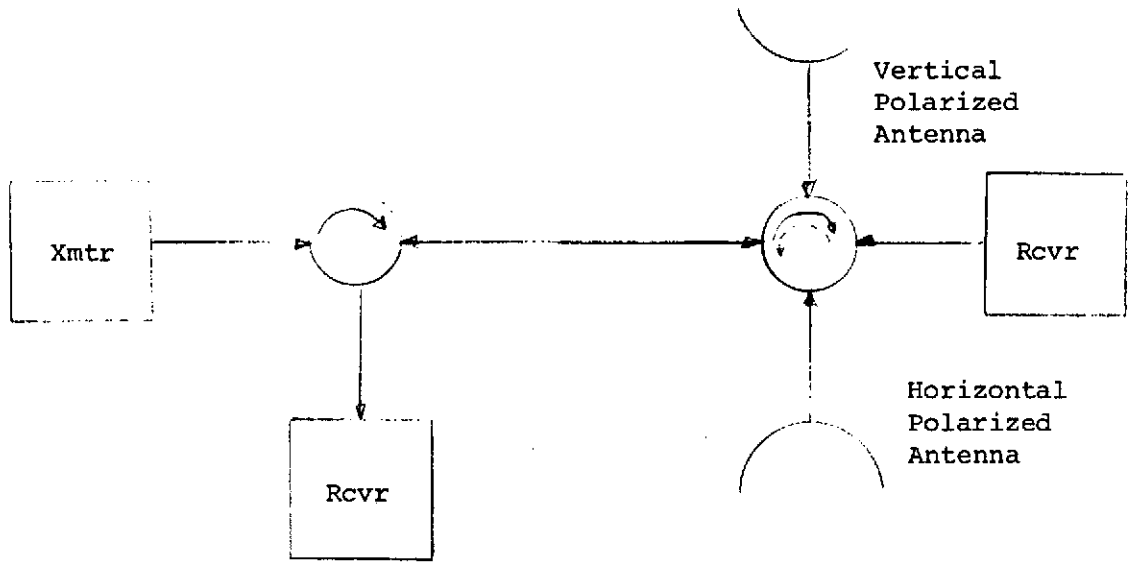

(b) System Configuration

Figure G-1. Four Port Switch Utilizing Ferrite Phase Shifters

The switch shown in (a) when embedded in the system configuration of (b) has the desired power transfer properties. That is, depending upon the state of the quadrature phase shifters, the transmit power is sent to either of the H or V antenna and upon return is assigned to the appropriate receiver channel.

The microwave phase shifters are ferrite devices whose state is dependent upon an established EM field direction generated by a solenoid coil. A change in current direction produces a change in the intrinsic ferrite field state and causes a quadrature phase shift of the applied X band field.

This configuration can meet all of the specifications of the table except Loss; the best obtainable is a two-way loss of .6 dB which exceeds the requirement by some .4 dB; however, the potential reliability may considerably exceed a mechanical switch.

It is not an off-the-shelf item and some relatively low risk development is involved.

APPENDIX H

LOCKING DEVICE WEIGHT

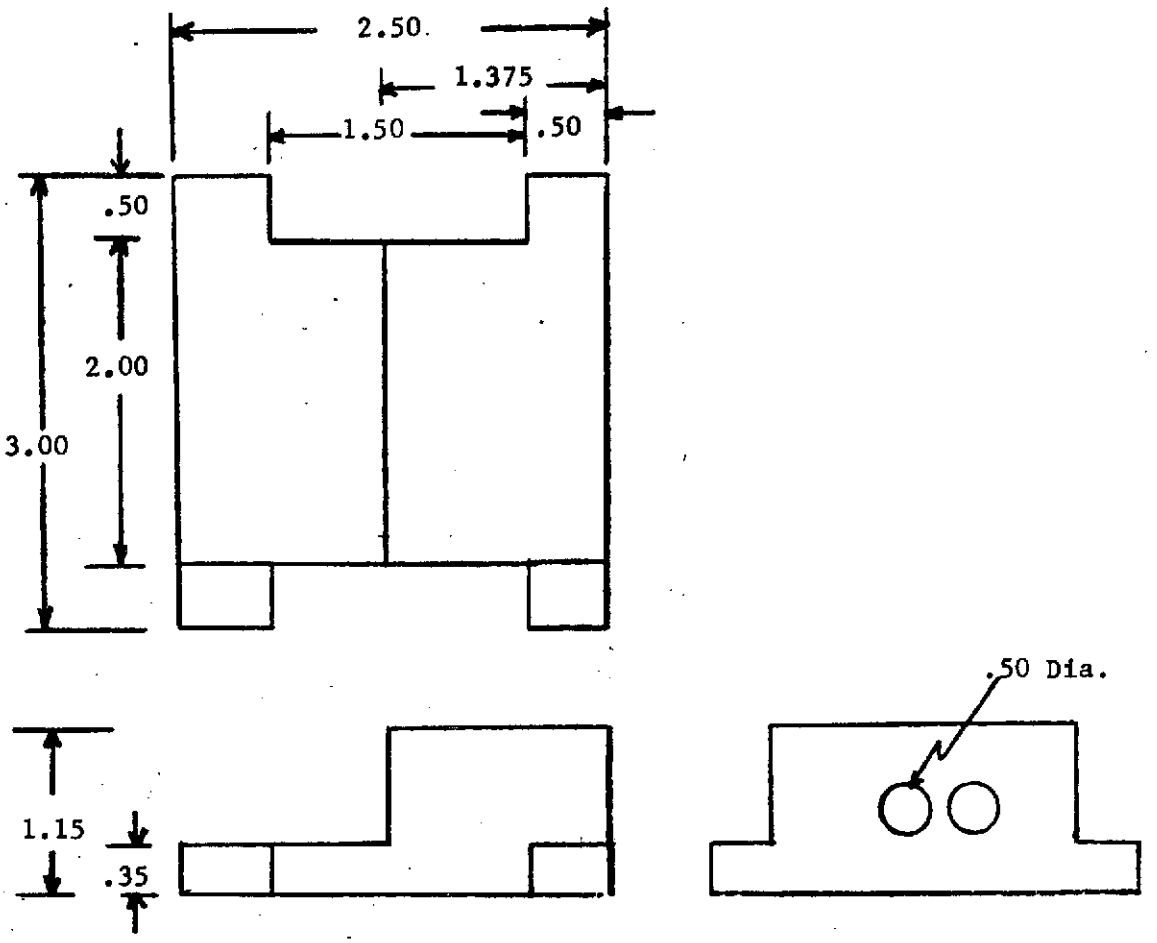

Volume

$V = (2.50 \times 3.00 \times .35) - (1.50 \times .50 \times .35 \times 2) + [(1.15 - .35) \times 2.0 \times 1.375] - [(\pi/4)\ (.5)^2\ (1.375)\ (2)] = 2.625 - .525 + 2.200 - .539$

$V = 3.760\ in^3$

Weight Al = .1 (3.76) = .376 lb.

APPENDIX J

HINGE STRESS CALCULATIONS

Configuration 1

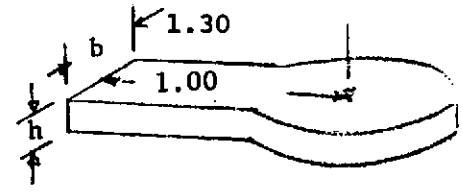

b = .60

Cl Weight Reflector and Hinge = 45

Force = 20 x 45 = 900

Distance to Pivot = 1.30

M = Moment = 1.30 x 900 = 1170

I = Moment of Inertia = $\frac{b\ h^3}{12} = \frac{.60\ h^7}{12} = .05\ h^3$

$y = h/2$

With SST: Stress Allowable = 80,000 psi = $\frac{M\ y}{I}$

Solving for h:

$$80{,}000 = \frac{1170\ (h/2)}{.05\ h^3}$$

$h^2 = .1463$

h = .382 h x Safety Factor = .382 x 1.25 = .478

2 hinges .239" will be satisfactory.

With 6061-T6 Al: Stress Allowable = 35,000 psi = $\frac{M\ y}{I}$

Solving for h:

$$35{,}000 = \frac{1170\ (h/2)}{.05\ h^3}$$

$h^2 = .334$

$h = .578$ h x Safety Factor = .578 x 1.25 = .723

2 hinges .362" will be satisfactory.

Configuration 2

Weight = 85

Force = 20 x 85 = 1700

Moment = 1.3 x 1700 = 2210

With SST: Stress Allowable = 80,000 psi = $\frac{M\ y}{I}$

$$80{,}000 = \frac{2210\ (h/2)}{.05\ h^3}$$

$h^2 = .276$

$h = .526$ h x Safety Factor = .526 x 1.25 = .657

2 hinges .329"
or } will be satisfactory.
3 hinges .219"

With Al: Stress Allowable = 35,000 psi = $\frac{M\ y}{I}$

$$35{,}000 = \frac{2210\ (h/2)}{.05\ h^3}$$

$h^2 = .631$

$h = .795$ h x Safety Factor = .795 x 1.25 = .993

2 hinges .496"
or } will be satisfactory.
3 hinges .331"

Use 3 hinge configuration to agree with 3 post configuration from Hinge Post Calculations.

APPENDIX K

HINGE POST STRESS CALCULATIONS

ASSUME: 20G loading
Cantilevered beam for post
Safety factor of 1.25 based on yield
Loading at centerline of pivot
Equal loading of hinges

Configuration 1:

Antenna and hardware weight = 92 lbs.

Force = 20 x 92 = 1840 lbs.

Distance to pivot = 1.00 in. (Distance necessary to stow feed and reflector)

M = Moment = 1840 x 1.00 = 1840 in-lb.

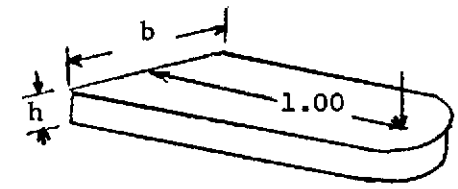

I = Moment of inertia = $\frac{b\ h^3}{12}$

(Assume b = 1.375 min.)

$I = \frac{1.375\ h^3}{12} = .1146\ h^3$

$y = h/2$

With SST: Stress Allowable = 80,000 psi = $\frac{M\ y}{I}$

Solving for h:

$$80{,}000 = \frac{(1840)\ (h/2)}{.1146\ h^3}$$

$h^2 = .1004$

$h = .3168$ h x Safety Factor = .3168 x 1.25 = .396

2 hinges .200" thick will be satisfactory.

With 6061 - T6 Al: Stress allowable = 35,000 psi = $\frac{M\ y}{I}$

Solving for h:

$$35{,}000 = \frac{(1840)\ (h/2)}{.1146\ h^3}$$

$$h^2 = .2294$$

$h = .4789$ h x Safety Factor = .4789 x 1.25 = .599

2 hinges .300" thick will be satisfactory.

Configuration 2:

Antenna and hardware weight = 174 lbs.

Force = 20 x 174 = 3480

Distance to pivot = 2.50 in. (Distance necessary to stow feed and reflector)

M = Moment = 3480 x 2.50 = 8700

I = Moment of inertia = $\frac{b\ h^3}{12}$

(Assume b = 1.375" min.)

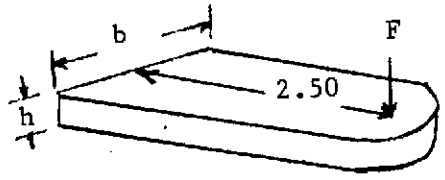

$$I = \frac{1.375\ h^3}{12} = .1146$$

y = h/2

With SST: Stress allowable = 80,000 psi = $\frac{M\ y}{I}$

Solving for h:

$$80{,}000 = \frac{(8700)\ (h/2)}{.1146\ h^3}$$

$$h^2 = .4745$$

$h = .6888$ h x Safety Factor = .6888 x 1.25 = .861

2 hinges .431" thick
3 hinges .287" thick } will be satisfactory.

With 6061 - T6 Al: Stress allowable = 35,000 psi = $\frac{M\ y}{I}$

Solving for h:

$$35{,}000 = \frac{(8700)\ (h/2)}{.1146\ h^3}$$

$$h^2 = 1.0845$$

$$h = 1.0414$$

h x Safety Factor = 1.0414 x 1.25 = 1.302

2 hinges .651" thick
3 hinges .434" thick } will be satisfactory.
4 hinges .326" thick

APPENDIX L

WEIGHT CALCULATIONS FOR HINGE

Configuration 1:

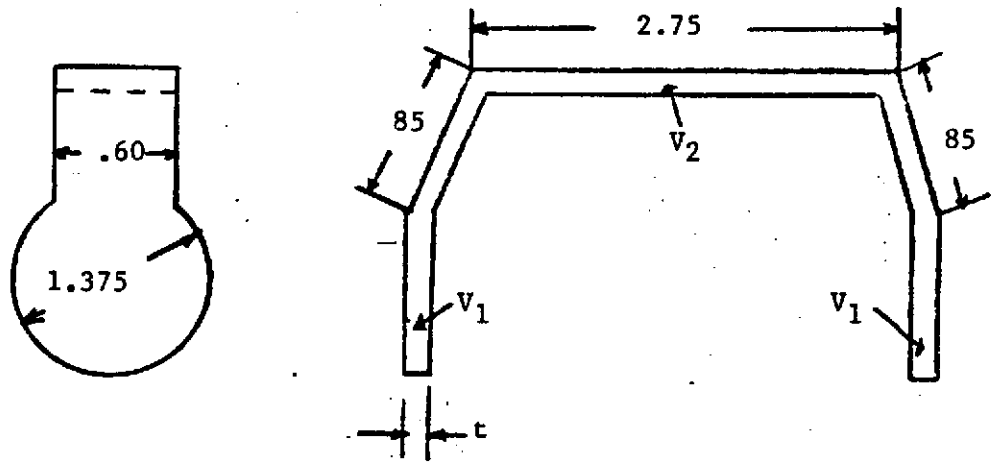

For SST t = .239

$$V_1 = \frac{\pi\ (1.375)^2}{4}\ (.239) = .355$$

$$V_2 = (.85 + .85 + 2.75)\ (.60)\ (.239) = .638$$

Weight = .28 $(V_1 + V_2)$ = .28 (.355 + .638) = .278 lb.

For Alum. t = .362

$$V_1 = \frac{\pi\ (1.375)^2}{4}\ (.362) = .538$$

$$V_2 = (.85 + .85 + 2.75)\ (.60)\ (.362) = .967$$

Weight = .1 $(V_1 + V_2)$ = .1 (.538 + .967) = .151 lb.

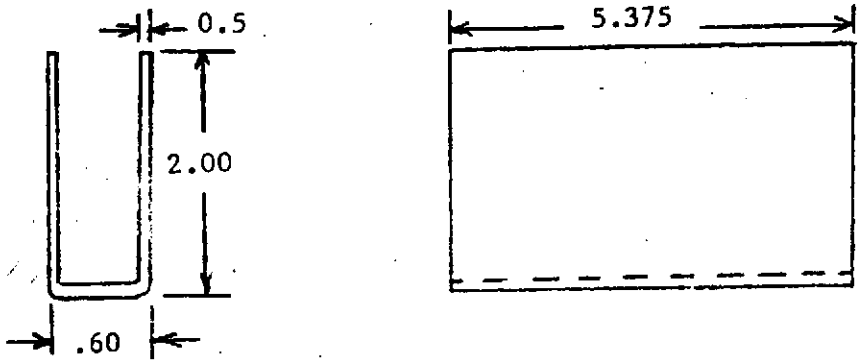

V = (2.00 + 2.00 + .60) (.05) (5.375) = 1.236

Weight (Al) = .1 (1.236) = .124 lb.

Weight (SST) = .28 (1.236) = .346 lb.

Total Weight, 2 hinges:

Al = .550 lb. ← Use for minimum weight

SST = 1.248 lb.

Configuration 2:

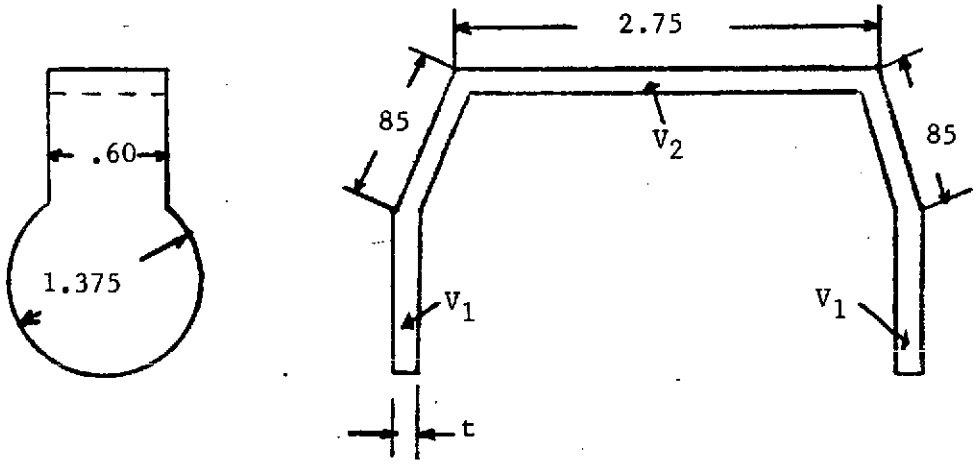

For SST t = .219

$$V_1 = \frac{\pi\ (1.375^2)\ (.219)}{4} = .325$$

V_2 = (.85 + .85 + 2.75) (.60) (.219) = .585

Weight = .28 (V_1 + V_2) = .28 (.325 + .585) = .255 lb.

For Al t = .331

V_1 = (π/4) (1.375) (.331) = .492

V_2 = (.85 + .85 + 2.75) (.60) (.331) = .884

Weight = .1 (.492 + .884) = .138 lb.

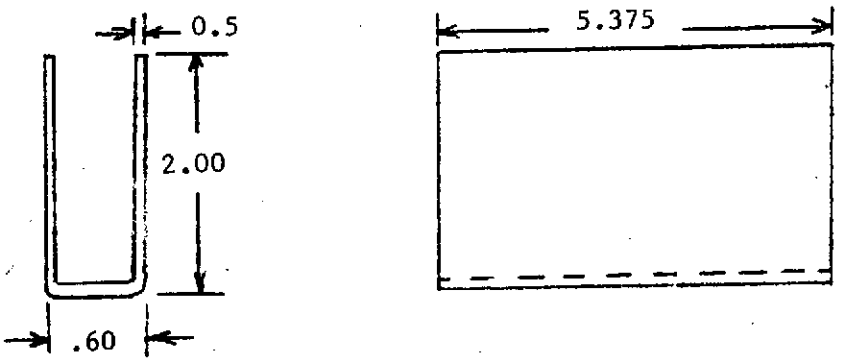

V = (2.00 + 2.00 + .60) (.05) (5.375) =

Weight (Al) = .1 (1.236) = .124 lb.

Weight (SST) = .3 (1.236) = .346 lb.

Total Weight, 3 hinges:

Al = .786 lb. ← Use for minimum weight

SST = 1.803 lb.

APPENDIX M

WEIGHT CALCULATIONS FOR HINGE POSTS

Configuration 1:

2 hinges

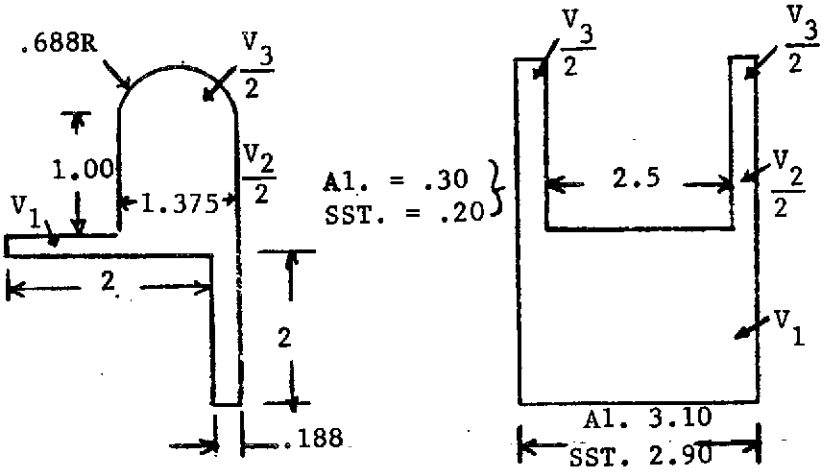

Al: $V_1 = (2.188)\ (.188)\ (3.10) + (2.0)\ (.188)\ (3.10) = 2.441$

SST: $V_1 = (2.188)\ (.188)\ (2.90) + (2.0)\ (.188)\ (2.90) = 2.283$

Al: $V_2 = 2\ (.30)\ (1.00)\ (1.375) = .825$

SST: $V_2 = 2\ (.20)\ (1.00)\ (1.375) = .550$

Al: $V_3 = \pi\ (.688^2)\ (.30) = .446$

SST: $V_3 = \pi\ (.688^2)\ (.20) = .297$

Weight = $(V_1 + V_2 + V_3)$ (density)

Al: $(2.441 + .825 + .446)\ (.1) = .371$ lb.

SST: $(2.283 + .550 + .297)\ (.28) = .876$ lb.

For 2 hinges:

Al = 2 x .371 = .742 lb. ← Use for minimum weight

SST = 2 x .876 = 1.753 lb.

Configuration 2:

3 hinges

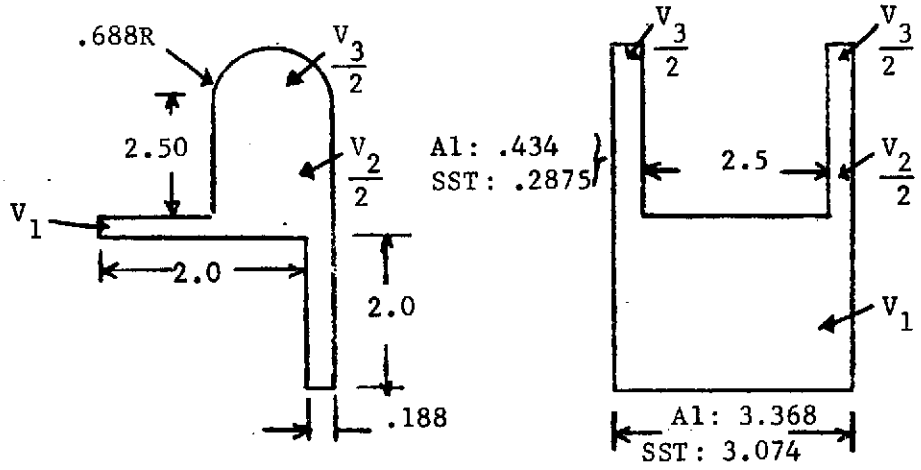

Al: $V_1 = (2.188)\ (.188)\ (3.368) + (2.00)\ (.188)\ (3.368) = 2.652$

SST: $V_1 = (2.188)\ (.188)\ (3.074) + (2.00)\ (.188)\ (3.074) = 2.420$

Al: $V_2 = 2\ (.434)\ (2.50)\ (1.375) = 2.984$

SST: $V_2 = 2\ (.287)\ (2.50)\ (1.375) = 1.973$

Al: $V_3 = \pi\ (.688^2)\ (.434) = .645$

SST: $V_3 = \pi\ (.688^2)\ (.287) = .427$

Weight = $(V_1 + V_2 + V_3)$ density

Al: $(2.652 + 2.984 + .645)\ (.1) = .628$ lbs./hinge

SST: $(2.420 + 1.973 + .427)\ (.28) = 1.344$ lbs./hinge

For 3 hinges:

Al = 1.884 lbs. ← Use for minimum weight

SST = 4.032 lbs.

APPENDIX N

HONEYCOMB STRUCTURE STRESS CALCULATIONS

REFERENCES: Design Handbook for Honeycomb Structures by Hexcel, Oct. 1967.
Mechanical Properties of Hexcel Honeycomb Materials by Hexcel, Aug. 1972.

Configuration #1:

$$P = \frac{20 \times \text{Weight}}{\text{Area}} = \frac{20 \times 140}{682} = 4.11 \frac{\text{lb}}{\text{in}^2}$$

1. Maximum Bending Moment

$M = \beta\, p\, b^2$ $\qquad \beta = .077$ (for b/a = .71)

$M = (.077)\ (4.11)\ (22^2)$

$M = 153.17$ in-lb/in

2. Selecting Materials and Establishing Allowable Stresses

Top Facing: 3003 Al (Heat Transfer)	Bottom Facing: 5052 Al (Strength)
$F_f = F_{cy} = 25{,}000$ psi cycle	$F_f = F_{cy} = 37{,}000$ psi
$E_f = 10 \times 10^6$	$E_f = 10 \times 10^6$
$\omega_f = .1$ lb/in^3	$\omega_f = .1$ lb/in^3
$\lambda = .1 - \mu^2 = .89$ ($\mu = .33$)	$\lambda = .89$ ($\mu = .33$)

Core 3/16 - 5052 - .0015 honeycomb

$\omega_c = 4.4$ lb/f^3 $= 2.55 \times 10^{-3}$ lb/in^3

$G_{ca} = 30{,}000$

$G_{cb} = 68{,}000$

$F_s = 215$ psi

$F_c = 250$ psi

$\omega_{fail} = .1$ lb/in^3

$E_{fail} = 10 \times 10^6$ psi

3. Determine Facing Thickness (Using Stress Minimum)

$$t = \sqrt{\frac{\omega_c M}{2 \omega_f E_f}} = \sqrt{\frac{(.00255)(153.17)}{(2)(.1)(25{,}000)}} = \sqrt{7.812 \times 10^{-5}}$$

$t = .00838$

Make $t_1 = .188$ for thermal reasons

$t_2 = .012$ for strength

4. Determining Core Thickness

$$t_c = \sqrt{\frac{2 \omega_f M}{\omega_c F_f}} = \sqrt{\frac{(2)(.1)(153.17)}{(.00255)(25{,}000)}} = \sqrt{4.805 \times 10^{-1}}$$

$t_c = .693$ in

Increase to .700 in.

5. Evaluating Parameter V

$$V = \frac{\pi^2 E_{f_1} t_1 E_{f_2} t_2 t_c}{\lambda (E_{f_1} t_1 + E_{f_2} t_2) b^2 G_{c_2}}$$

$$V = \frac{\pi^2 (10 \times 10^6)(.188)(10 \times 10^6)(.012)(.700)}{(.89)[(10 \times 10^6)(.188) + (10 \times 10^6)(.012)](22^2)(30{,}000)}$$

$$V = \frac{1.559 \times 10^{12}}{2.584 \times 10^{11}}$$

$$V = .0603$$

6. From Charts VI-6 and VI-8 for b/a = .71

$C_2 = .44$

$C_3 = .17$

Maximum bending moments:

$$M_a = \frac{16\ p\ b^2}{K^4} (C_3 + \mu\ C_2) = \frac{16\ (4.11)\ (22^2)}{\pi^4}\ (.17 + .33\ [.44])$$

$$M_a = 326.744\ (.3152) = 102.99\ \frac{\text{in-lb}}{\text{in}}$$

$$M_b = 326.744\ (.44 + .33\ [.17])$$

$$M_b = 162.10\ \frac{\text{in-lb}}{\text{in}}$$

7. Stress in Upper and Lower Plates

$$S_{a\ \text{upper}} = \frac{M_a}{(t)\ (r_1 + r_2)} = \frac{102.99}{(.188)\ (.8)}$$

$$S_{a\ \text{upper}} = 684.77 \text{ psi}$$

$$S_{a\ \text{lower}} = \frac{102.99}{(.012)\ (.8)} = 10{,}728.13 \text{ psi}$$

$$S_{b\ \text{upper}} = \frac{162.10}{(.188)\ (.8)} = 1077.79 \text{ psi}$$

$$S_{b\ \text{lower}} = \frac{162.10}{(.012)\ (.8)} = 16{,}885.42 \text{ psi}$$

8. Calculating Maximum Shear Loads

$$S_b = \frac{16\ p\ b}{\pi^3} C_5 \qquad C_5 = .82 \text{ from VI-12}$$

$$S_b = \frac{(16)\ (4.11)\ (22)}{\pi^3}\ (.82)$$

$$S_b = 38.26 \text{ psi}$$

$$S_a = 46.659\ C_4 \qquad C_4 = .70 \text{ from VI-12}$$

$$S_a = 32.66 \text{ psi}$$

9. Evaluating Shear Stresses

$$f_{sa} = \frac{2\ S_a}{d + t_c} = \frac{2\ (32.66)}{.90 + .70} \qquad d = .188 + .012 + .70 = .90$$

$$f_{sa} = 40.825 \text{ psi}$$

$$f_{sb} = \frac{2\ S_b}{d + t_c} = \frac{2\ (38.26)}{.90 + .70} = 47.825 \text{ psi}$$

10. Panel Deflection

$$\delta = \frac{16\ p\ b^4\ C_1}{\tau^6\ D}$$

$$D = \frac{E_{f1}\ b_1\ E_{f2}\ t_2\ h^2}{E_{f_1}\ b_1\ \lambda_2 + E_{f2}\ t_2\ \lambda_1}$$

$$D = \frac{(10 \times 10^6)\ (.188)\ (10 \times 10^6)\ (.012)\ (.8^2)}{(10 \times 10^6)\ (.188)\ (.89) + (10 \times 10^6)\ (.012)\ (.89)}$$

$$D = 81{,}114.6 \text{ in-lb}$$

From Chart VI-3 $\qquad C_1 = .50$

$$\delta = \frac{16\ (4.11)\ (22^2)\ (.50)}{\pi^6\ (81{,}114.6)}$$

$$\delta = .0987 \text{ in. at center}$$

Configuration #2:

Load $p = 20 \times \frac{175}{931} = 3.76$ psi

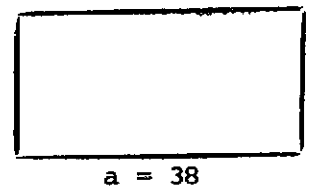

1. Maximum Bending Moment

$M = \beta p b^2$ $\beta = .08$ (for $b/a = .64$)

$M = (.08)\ (3.76)\ (24.5^2)$

$M = 180.55 \frac{\text{in.-lb.}}{\text{in.}}$

2. Select Materials and Establish Allowable Stresses

Top Facing: 3003 Al

$F_f = F_{cy} = 25{,}000$ psi yield

$E_f = 10 \times 10^6$ psi

$\omega_f = .1$ lb./in.^{3}

$\lambda = .89$ ($\mu = .33$)

Bottom Facing: 5052 Al

$F_y = F_{cy} = 37{,}000$ psi

$E_f = 10 \times 10^6$

$\omega_f = .1$ lb./in.^{3}

$\lambda = .89$ ($\mu = .33$)

Core 3/16 - 5052 - .0015

$\omega_c = 4.4$ lb./f $= 2.55 \times 10^{-3}$ lb./in.^{3}

$G_{ca} = 30{,}000$

$G_{cb} = 68{,}000$

$F_s = 215$ psi

$F_c = 250$ psi

$\omega_{fail} = .1$ lb./in.^{3}

$E_{fail} = 10 \times 10^6$ psi

3. Determine Facing Thickness (Using Stress Minimum)

$$t = \sqrt{\frac{\omega_c M}{2 \omega_f F_f}} = \sqrt{\frac{(.00255)\ (180.55)}{(2)\ (.1)\ (25{,}000)}} = \sqrt{.0000921}$$

$t = .0096$

Make $t_2 = .012$ Use 5052 wall for strength

$t_1 = .188$ For thermal reasons

4. Determine Core Thickness

$$t_c = \sqrt{\frac{2\ f\ M}{c\ F_f}} = \sqrt{\frac{(2)\ (.1)\ (180.55)}{(.00255)\ (25{,}000)}} = \sqrt{.5664}$$

$t_c = .7526$

5. Evaluating Parameter V

$$V = \frac{\pi^2\ E_{f_2}\ t_2\ E_{f_1}\ t_1\ t_c}{d\ (E_{f_2}\ t_2 + E_{f_1}\ t_1)\ b^2\ G_{ca}}$$

$$V = \frac{\pi^2\ (10 \times 10^6)\ (.012)\ (10 \times 10^6)\ (.188)\ (.900)}{(.89)\ [(10 \times 10^6)\ (.012) + (10 \times 10^6)\ (.188)]\ (24.5^2)\ (30{,}000)}$$

$$V = \frac{2.003924 \times 10^{12}}{3.205335 \times 10^{13}}$$

$V = .0625$

6. From Charts VI-6 and VI-8 Pick Constant C_2 and C_3

$C_2 = .50$

$C_3 = .15$

Maximum bending moments:

$$M_a = \frac{16\ p\ b^2}{\pi^4}\ (C_3 + \mu\ C_2) = \frac{16\ (3.76)\ (24.5^2)}{\pi^4}\ (.15 + [.33]\ [.50])$$

$$M_a = 116.78\ \frac{\text{in.-lb.}}{\text{in.}}$$ Moment across width

$$M_b = \frac{16\ p\ b^2}{\pi^4}\ (.50 + .33\ [.15]) =$$

$$M_b = 203.71\ \frac{\text{in.-lb.}}{\text{in.}}$$

7. Stress in Upper and Lower Plates

$$S_{a\ \text{upper}} = \frac{M_a}{(t_1)\ (r_1 + r_2)} = \frac{116.78}{(.188)\ (1.0)} = 621.17\ \text{psi}$$

$$S_{a\ \text{lower}} = \frac{116.78}{(.012)\ (1.0)} = 9731.67\ \text{psi}$$

$$S_{a\ \text{upper}} = \frac{203.71}{(.188)\ (1.0)} = 1083.56\ \text{psi}$$

$$S_{b\ \text{lower}} = \frac{203.71}{(.012)\ (1.0)} = 16{,}975.83\ \text{psi}$$ (well below allowable 37,000 psi yield for 5052)

8. Calculating Maximum Shear Loads

$$S_b = \frac{16\ p\ b}{\pi^3}\ C_5$$ $C_5 = .70$ from VI-12

$$S_b = \frac{(16)\ (3.76)\ (24.5)\ (.70)}{\pi^3}$$

$S_b = 33.275$ lb./in. shear load on side b

$$S_a = \frac{16\ p\ b}{\pi^3}\ C_4$$ $C_4 = .85$ from VI-12

$$S_a = \frac{(16)\ (3.76)\ (24.5)\ (.85)}{\pi^3}$$

S_a = 40.406 lb./in. shear load on side a

9. Evaluating Shear Stresses

$$f_{sa} = \frac{2\ S_a}{d + t_c} \qquad d = .188 + .012 + .900 = 1.100$$

$$f_{sa} = \frac{2\ (40.406)}{1.100 + .900} = 40.406 \text{ psi}$$

$$f_{sb} = \frac{2\ S_b}{d + t_c}$$

$$f_{sb} = \frac{2\ (33.275)}{1.100 + .900} = 33.275 \text{ psi}$$

10. Panel Deflection

$$\delta = \frac{16\ p\ b^4\ C_1}{\pi^6\ D}$$

$$D = \frac{E_{f1}\ t_1\ E_{f_2}\ t_2\ h^2}{E_{f_1}\ t_1\ \lambda_2 + E_{f_2}\ t_2\ \lambda_1} \qquad h = \text{distance between facing centroids}$$

$$D = \frac{(10 \times 10^6)\ (.188)\ (10 \times 10^6)\ (.012)\ (1.0^2)}{(10 \times 10^6)\ (.188)\ (.84) + (10 \times 10^6)\ (.012)\ (.89)} = \frac{2.256 \times 10^{11}}{1.780 \times 10^6}$$

D = 126,741 in.-lb.

From Chart VI-3, C = 0.5

$$\delta = \frac{16\ (3.76)\ (24.5^4)\ (.5)}{\pi^6\ (126{,}741)} = .089 \text{ in.}$$